Thermodynamic aspects of processive enzymatic degradation of recalcitrant polysaccharides

Termodynamiske aspekter ved den prosessive enzymatiske degraderingen av vanskelig nedbrytbare polysakkarider

Philosophiae Doctor (PhD) Thesis

Anne Grethe Hamre

Department of Chemistry, Biotechnology and Food Science
Faculty of Veterinary Medicine and Bioscience
Norwegian University of Life Sciences

Ås 2015

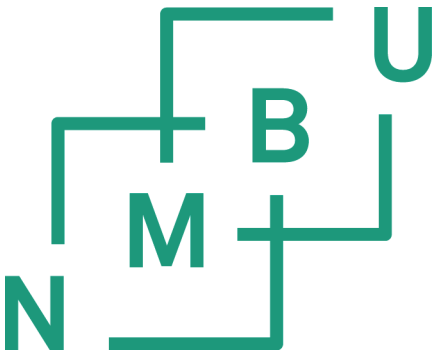

Thesis number 2015:46

ISSN 1894-6402

ISBN 978-82-575-1289-7

Tell me your secrets and ask me your questions
Oh let's go back to the start
Running in circles, coming in tails
Heads on a science apart

Nobody said it was easy
It's such a shame for us to part
Nobody said it was easy
No one ever said it would be this hard
Oh, take me back to the start.

The Scientist – Coldplay

Table of Contents

Acknowledgements

The work presented in this thesis was carried out during the period 2011-2015 in the Bio-organic research group, Department of Chemistry, Biotechnology and Food Science (IKBM) at The Norwegian University of Life Sciences (NMBU). The work was funded by the Research Council of Norway, grant number 209335/F20, and IKBM.

First of all, I would like to express my gratitude to my supervisor Professor **Morten Sørlie**. Thank you for believing in me and giving me the opportunity to be a PhD student in your group. Although being a PhD-student is a rollercoaster, and not quick and easy, I have never regretted doing a PhD. Your knowledge, indomitable optimism, and well of new ideas have inspired me since I was a master's student. For some reason you understand when my brain is too cloudy and a pep-talk to set a new course is needed.

Secondly, I would like to thank my co-supervisors Dr. **Anne Line Filtvedt**, Dr. **Øyvind L. Busk**, and Dr. **Geir Mathiesen**. Especially **Geir** deserves thanks for helping me, as a chemist, perform molecular biology.

Our collaborators abroad should also be mentioned. Thanks to Associate Professor **Priit Väljamäe** at the University of Tartu for sharing his expertise in the field of processivity. I also thank Assistant Professor **Christina M. Payne** and PhD-student **Suvamay Jana** at University of Kentucky's Department of Chemical and Materials Engineering for conducting the molecular dynamics simulations and sharing their thoughts about binding free energy and processivity. I really appreciate the effort you have put in, especially in the last few months.

Of course all other co-authors also deserve a thank you for their respective contributions. I would like to highlight the hard working master's students whose work has been a great help. So, thank you **Hanne**, **Silje**, **Nicole**, **Matilde**, and **Daniel**. You can be proud of yourselves.

To all my past and present colleagues in the "chemistry hall"; thanks for being so positive and helpful, thus creating such a good working environment. Special thanks go to fellow PhD-student **Kristine B. Eide** for being a great motivator, "partner in crime" and of course for proofreading this thesis.

Thanks to the PEP-group headed by Professor **Vincent Eijsink** for hosting the 1st floorers in an already crowded lab.

I would also like to express my gratitude to my family and friends for your love and support. You know who you are. Last, but by no means least; thank you **David**! Thank you for being you, for listening to never-stopping monologues about enzymes, students, and papers, thank you for putting me back on the ground when the PhD rollercoaster is throwing me around, and thank you for making me think about other things taking me with you to see the world. You have an excellent way of coping with a scientist!

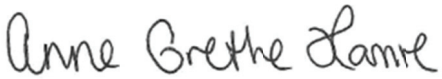

Ås, 21. April 2015

Abbreviations

AAs	Auxiliary activities
Ala	Alanine
Asp	Aspartate
Asn	Asparagine
CAZy	Carbohydrate-Active EnZYmes
ChiA	Chitinase A
ChiB	Chitinase B
ChiC	Chitinase C
CBP21	Chitin binding protein 21
CHOS	Chito-oligosaccharide
CBM	Carbohydrate binding module
EDTA	Ethylenediaminetetraacetic acid
FEP/λ-REMD	Free energy perturbation with replica exchange molecular dynamics
GHs	Glycoside hydrolases
GlcN	*N*-glucosamine
GlcNAc	*N*-acetyl glucosamine
Glu	Glutamine
His	Histidine
ITC	Isothermal titration calorimetry

k_{cat}	Rate constant
k_{cat}^{app}	Apparent k_{cat}
k_{off}	Dissociation constant
k_{off}	Association constant
LPMOs	Lytic polysaccharide monooxygenases
MD	Molecular dynamics
NMR	Nuclear magnetic resonance
P_{app}	Apparent processivity
Phe	Phenylalanine
P_{intr}	Intrinsic processivity
RMSF	Root mean square fluctuation
Ser	Serine
S. marcescens	*Serratia marcescens*
TI	Thermodynamic integration
T. reesei	*Trichoderma reesei*
Tyr	Tyrosine
Å	Ångstrøm

List of publications

This thesis is based upon studies presented in the following, appended papers:

Paper I

Activation of enzymatic chitin degradation by a lytic polysaccharide monooxygenase

Anne Grethe Hamre, Kristine B. Eide, Hanne H. Wold, and Morten Sørlie, *Carbohydr. Res.* **2015**, 407, 166-169.

Paper II

Enzyme processivity changes with the extent of recalcitrant polysaccharide degradation

Anne Grethe Hamre, Silje B. Lorentzen, Priit Väljamäe, and Morten Sørlie, *FEBS Lett.*, **2014**, 588, 4620-4624.

Paper III

Thermodynamic relationships with processivity in *Serratia marcescens* family 18 chitinases

Anne Grethe Hamre, Suvamay Jana, Matilde Mengkrog Holen, Geir Mathiesen, Priit Väljamäe, Christina M. Payne, and Morten Sørlie, *Submitted to J. Phys. Chem. B,* **2015**.

Paper IV

Processivity, substrate positioning and binding; the role of polar residues in a family 18 glycoside hydrolase

Anne Grethe Hamre, Suvamay Jana, Nicole K. Reppert, Christina M. Payne, and Morten Sørlie, *Submitted to J. Biol. Chem.,* **2015**.

Paper V

Aromatic-mediated carbohydrate recognition in processive *Serratia marcescens* chitinases

Suvamay Jana, Anne Grethe Hamre, Patricia Wildberger, Matilde Mengkrog Holen, Vincent G. H. Eijsink, Gregg T. Beckham, Morten Sørlie, and Christina M. Payne, *Manuscript*.

Paper VI

The directionality of processive enzymes acting on recalcitrant polysaccharides is reflected in the kinetic signatures of oligomer degradation

Anne Grethe Hamre, Daniel Schaupp, Vincent G. H. Eijsink, and Morten Sørlie, *Resubmitted to FEBS Lett.* **2015**.

Papers not included in the thesis:

Using SILAC proteomics to investigate the effect of the mycotoxin, alternariol, in the human H295R steroidogenesis model

Shewit Kalayou, Anne Grethe Hamre, Doreen Ndossi, Lisa Connolly, Morten Sørlie, Erik Ropstad, and Steven Verhaegen, *Cell Biol. Toxicol.* **2014**, 30, 361-376

Forming a loop on substrate binding for a processive glycoside hydrolase; thermodynamic signatures

Suvamay Jana, Anne Grethe Hamre, Emil Ebbestad Frøberg, Morten Sørlie, and Christina M. Payne, *Manuscript in preparation*.

Abstract

Carbohydrates play diverse, essential roles in all known organisms. These include roles in storage and structure as well as specific signaling roles. One carbohydrate can be linked to other carbohydrates or functional groups, through glycosidic linkages. The hydrolysis of these linkages is catalyzed by glycoside hydrolases (GHs), which have specific functions in carbohydrates' degradation. They may have endo-activity, cleaving the polymer chains at random positions, or exo-activity, preferentially cleaving from either the reducing or non-reducing end of the substrate. These features may be accompanied by either processive or non-processive action. Processive enzymes hydrolyze a series of glycosidic linkages along the same polymer chain before dissociation.

The non-soluble polysaccharides chitin and cellulose are the two most abundant biopolymers in nature, with estimated production rates of 100 billion and one trillion tons per year, respectively. Chitin consists of chains of β-1,4-linked *N*-acetyl-glucosamine (GlcNAc) units while cellulose is composed of β-1,4-linked glucose units. In both cases successive units are rotated 180 ° relative to each other, thus the structural unit is a disaccharide. Despite the vast amounts produced, they do not accumulate in nature because specialized GHs, namely chitinases and cellulases, depolymerize them. The chitinolytic machinery of the Gram-negative soil bacterium *Serratia marcescens* has often been used as a model system for enzymatic degradation of recalcitrant polysaccharides. It consists of two processive exo-chitinases (Chitinase A (ChiA) and Chitinase B (ChiB)), one non-processive endo-acting chitinase (Chitinase C (ChiC), an *N*-acetyl-hexosaminidase, and an accessory lytic polysaccharide monooxygenase (LPMO) called CBP21.

The overall goal of the work described in this thesis was to gain a deeper understanding of how substrates bind to chitinases, thereby improving understanding of how recalcitrant polysaccharides are efficiently degraded. To obtain such understanding, the main objectives were to determine the energetic and kinetic contributions of wild type enzymes and key residues in substrate binding. The work involved six specific studies that are described in detail in appended papers, designated **Paper I-VI**.

In the first two papers, the chitinolytic machinery of *Serratia marcescens* is introduced. **Paper I** presents apparent catalytic rate constants for degradation of two forms of β-chitin

by ChiA, ChiB and ChiC, alone and together with CBP21. The presence of CBP21 boosted initial rates of ChiA-and ChiB activity 6- and 9- fold, respectively, but had no effect on ChiC activity. **Paper II** shows that apparent processivity (P^{app}) decreases with increases in the degree of chitin degradation. The use of initial P^{app} values is recommended, and they were determined to be 30.1 ± 1.5, 24.3 ± 2.0, and 14.3 ± 1.4 for ChiA, ChiB, and ChiC, respectively. P^{app} also correlates with efficiency: the most processive enzyme is also the most efficient chitin degrader.

In the second part of this dissertation, apparent processivity for wild type enzymes (**Paper III**) and specific polar and aromatic residues (**Paper IV** and **V**, respectively) were compared to free energy change. In addition, three dynamic hallmarks that are qualitatively related to processivity were addressed both experimentally by isothermal titration calorimetry (ITC) and theoretically by molecular dynamics (MD) simulations. All three papers show that the processive ability of GHs is directly linked to free energy change. Moreover, **Paper III** shows that ChiA is significantly more desolvated than ChiB and ChiC upon binding to hexa-*N*-acetyl glucosamine, $(GlcNAc)_6$, and that the conformational entropy is unfavorable for ChiA and ChiC while it is "neutral" for ChiB. In **Paper IV**, the potential roles of polar residues in substrate binding were investigated by examining two residues situated in substrate binding subsites of the exo-processive chitinase ChiA. ChiA-T276A was found to have dramatically lower processivity and free energy change than ChiA-WT (P^{app} = 17.1 ± 0.4 vs. 30.1 ± 1.5 and ΔG_r° = −10.5 ± 0.1 vs. – 8.3 ± 0.1 for binding to allosamidin) and ChiA-R172A. ChiA-R172A reduced the recognition and positioning of the substrate in the active site. ChiA and ChiB are complementary, working processively in opposite directions: ChiA towards the non-reducing end and ChiB towards the reducing end. The contribution of aromatic residues in the active sites of these enzymes has previously demonstrated importance for both processivity and positioning of the substrate in the active site. **Paper V** presents relative changes in binding free energy ($\Delta\Delta G$) for six aromatic residues in ChiA and ChiB. Most of them showed unfavorable changes, indicating that they affect processivity, in accordance with previous processivity measurements.

Finally, **Paper VI** examines the kinetics of substrate degradation of the aromatic residues situated in subsite +1 and +2 in both ChiA and ChiB. The results show that the tailoring of the enzymes to opposite directionalities is reflected in the kinetic parameters K_m and k_{cat}. K_m increases for mutants of both enzymes, k_{cat} increases for ChiB mutants and

decreases for ChiA mutants. This is likely due to differences in the importance of k_3, the rate of product release.

Sammendrag

Karbohydrater spiller viktige roller for livet på jorden og er essensiell i alle kjente organismer. Dette inkluderer spesifikke roller i signalisering, samt for lagring og struktur. Karbohydrater bindes til hverandre eller funksjonelle grupper via glykosidbindinger. Hydrolysen av disse bindingene katalyseres av Glykosidhydrolaser (GHer) som har spesifikke funksjoner i degradering av karbohydrater. De kan kutte polymerkjeden tilfeldig ved å være endoaktive, eller de kan ha en preferanse for enten den reduserende eller ikke-reduserende enden av substratet ved å være exoaktive. Disse egenskapene kan bli ledsaget av prosessiv eller ikke-prosessiv virkemåte. Prosessive enzymer hydrolyserer en rekke glykosidbindinger langs den samme polymerkjeden før de dissosierer.

De uløselige polysakkaridene kitin og cellulose er de to biopolymerene med høyest årlig produksjon i naturen. Det produseres henholdsvis 100 milliarder og 1 billion tonn kitin og cellulose. Kitin består av kjeder med β-1,4 linkede *N*-acetylglukosaminenheter (GlcNAc), mens cellulose er bygget opp av β-1,4 linkede glukoseenheter. I begge tilfeller er de etterfølgende enhetene rotert 180 ° i forhold til hverandre slik at den minste strukturelle enheten er et disakkarid. På tross av de store mengdene som produseres akkumuleres ikke kitin og cellulose i naturen fordi spesialiserte GHer, kitinaser og cellulaser, bryter de ned. Det kitinolytiske maskineriet til den Gram-negative jordbakterien *Serratia marcescens* har ofte blitt benyttet som modellsystem for den enzymatiske degraderingen av vanskelig nedbrytbare polysakkarider. Maskineriet består av to prosessive eksokitinaser (Kitinase A (ChiA) og Kitinase B (ChiB)), en ikke-prosessiv endokitinase (Kitinase C (ChiC)), en kitobiase og et hjelpeprotein i form av en lytisk polysakkarid monooksygenase (LPMO) ved navn CBP21.

Det overordnede målet for arbeidet som er beskrevet i denne avhandlingen er å oppnå en dypere forståelse for hvordan substrat binder til kitinaser. Dermed forbedres forståelsen av hvordan vanskelig nedbrytbare polysakkarider effektivt degraderes. For å oppnå denne forståelsen har hovedfokuset i denne avhandlingen vært å bestemme energetiske og kinetiske bidrag som villtype enzymer og nøkkelresiduer har på substratbinding. Arbeidet har involvert seks spesifikke studier som er beskrevet i detalj i vedlagte artikler, benevnt **Artikkel I-VI**.

I de første to artiklene introduseres det kitinolytiske maskineriet til *Serratia marcescens*. **Artikkel I** viser observerte katalytiske hastighetskonstanter for degraderingen av to former for β-kitin med ChiA, ChiB and ChiC, alene og sammen med CBP21. Med CBP21 tilstede økte de initielle hastighetene henholdsvis 6 og 9 ganger for eksoaktive ChiA og ChiB, mens ingen effekt ble vist for ChiC. **Artikkel II** viser at observert prosessivitet (P^{app}) synker med økende grad av kitindegradering. Det anbefales derfor å bruke initielle P^{app} verdier, og de ble bestemt til å være 30.1 ± 1.5, 24.3 ± 2.0 og 14.3 ± 1.4 for henholdsvis ChiA, ChiB, og ChiC. P^{app} viser seg å korrelere med effektivitet. Det mest prosessive enzymet er mest effektiv til å degradere kitin.

I del to av denne avhandlingen ble observert prosessivitet for villtype enzymene (**Artikkel III**) og spesifikke polare og aromatiske residuer (henholdsvis **Artikkel IV** og **V**) sammenlignet med endring i frienergien. I tillegg ble tre dynamiske karakteristikker som er kvalitativt relatert til prosessivitet studert både eksperimentelt ved bruk av isoterm titreringskalorimetri (ITC) og teoretisk ved bruk av molekylære dynamikksimuleringer (MD). Alle de tre artiklene viser at GHers prosessive evne er direkte knyttet til endring i frienergi. Videre viser **Artikkel III** at ChiA er signifikant mer desolvatisert enn ChiB og ChiC ved binding til heksa-*N*-acetyl glukosamin, $(GlcNAc)_6$, og at konformasjonsentropien er ugunstig for ChiA og ChiC, mens den er «nøytral» for ChiB. I **Artikkel IV** ble potensielle roller for polare residuer i substratbinding undersøkt ved å studere to residuer i substratbindende subseter i ChiA. ChiA-T276A har drastisk reduserte P^{app} og $\Delta G_r°$ verdier sammenlignet med ChiA-WT (P^{app} = 17.1 ± 0.4 vs. 30.1 ± 1.5 og $\Delta G_r° = -10.5 \pm 0.1$ vs. –8.3 ± 0.1 for binding til allosamidin) og ChiA-R172A. ChiA-R172A reduserer gjenkjennelsen og posisjoneringen av substratet inn i det aktive setet. ChiA og ChiB er komplementære og degraderer kitin i motsatt retning. ChiA degraderer mot den ikke-reduserende enden, mens ChiB degraderer mot den reduserende enden. Bidraget fra aromatiske residuer i de aktive setene til disse enzymene har tidligere vist seg å være viktige både for prosessivitet og substratposisjonering. **Artikkel V** viser relative endringer i bindingsfrienergi ($\Delta\Delta G$) for seks aromatiske residuer i ChiA og ChiB. De fleste viser ugunstige endringer, noe som antyder at disse har større innvirkning på prosessivitet. Dette stemmer overens med tidligere prosessivitetsmålinger.

Til slutt presenterer **Artikkel VI** en kinetisk studie av de aromatiske residuene lokalisert i subsete +1 og +2 i ChiA og ChiB. Resultatene viser at enzymenes direksjonalitet er reflektert i de kinetiske parameterene K_m and k_{cat}. K_m øker for mutantene i både ChiA og

ChiB, k_{cat} øker for ChiB mutantene og synker for ChiA mutantene. Dette skyldes sannsynligvis at k_3, dissosiasjonskonstanten, har ulik betydning i de to enzymene.

1. Introduction

Carbohydrates, in the form of mono-, di-, oligo-, and poly-saccharides, are compounds with the stoichiometric formula $(CH_2O)_n$ or derivatives of such compounds. They have wide stereochemical variations due to the extreme heterogeneity of monosaccharide structures, intersugar linkages and the fact that myriads of molecules can be glycosylated (e.g. proteins, lipids, and nucleic acids). For example, a reducing hexasaccharide has over 10^{12} possible isomers (Laine 1994).

Around two-thirds of the carbon in the biosphere is in the form of carbohydrates, which play diverse, essential roles in all known organisms (Sinnott 1990). Living organisms use oligo- and poly-saccharides for a multitude of biological functions, from storage and structure to specific signaling roles (Cerqueira et al. 2012). Conversion of recalcitrant biopolymers, such as cellulose, to easily fermentable compounds like glucose is also of increasing economic interest (Himmel et al. 2007). Cellulose is the most abundant biopolymer with an annual production of one trillion tons (Kim et al. 2006).

Glycosidic linkages are covalent bonds joining one carbohydrate to another carbohydrate or functional group. These linkages are extremely stable, with half-lives of approximately 5 million years in cellulose (Wolfenden et al. 1998). Despite this and the vast amounts of carbohydrates produced annually, they do not accumulate in nature because efficient catalytic systems for both creating and cleaving glycosidic linkages, consisting of various specialized enzymes known as Carbohydrate-Active enZymes (CAZymes), have evolved (Henrissat 1991). To elucidate how these enzymes work, it is important to study the interactions between carbohydrates and proteins. This thesis is based upon contributions to such efforts, involving kinetic and thermodynamic investigations of the enzymatic hydrolysis of the polysaccharide chitin, its soluble analogue chitosan, and chito-oligosaccharides using calorimetric, mass spectrometric, chromatographic, and molecular dynamics simulation techniques.

1.1 Chitin and chitosan

Chitin is a natural, linear polysaccharide that consists of chains of β-1,4 linked *N*-acetyl-glucosamine (GlcNAc) units, successively rotated 180° relative to each other, as shown in Figure 1 (Rinaudo 2006). It is the second most abundant biopolymer in nature, with 100 billion tons being produced annually (Tharanathan & Kittur 2003).

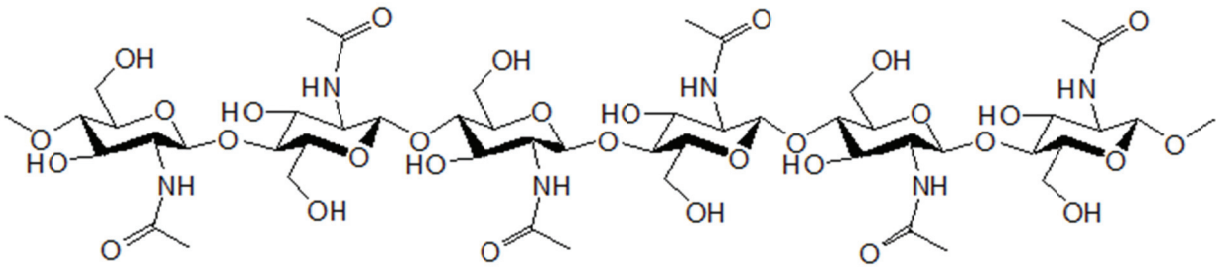

Figure 1: Chitin consists of β-1,4 linked *N*-acetyl-glucosamine units.

In its native state, chitin is crystalline. Two crystalline forms, named α and β, are definitely recognized. A third form, the γ-form, has been discussed, but is probably just an α-variant (Rinaudo 2006). Chitin chains are generally organized in sheets, where they are tightly bound together by a number of intra-sheet hydrogen bonds contributing to the insolubility of chitin in common solvents (Harish Prashanth & Tharanathan 2007). α-chitin contains two antiparallel molecules per unit cell, while β-chitin only has one and is therefore composed of molecules in a parallel arrangement (Blackwell 1969; Minke & Blackwell 1978; Saito et al. 2000). The antiparallel orientation of the polymer chains in α-chitin allows formation of high numbers of hydrogen bonds, resulting in tight packing of the polymeric strands and high stability of the crystalline structure (Minke & Blackwell 1978; Sikorski et al. 2009). The tight packing excludes the presence of water. In β-chitin, however, the parallel orientation of the polymer strands allows the presence of up to two water molecules per *N*-acetyl-glucosamine unit, making this form less recalcitrant (Kobayashi et al. 2010; Sawada et al. 2012). α-chitin is by far the most abundant form and is found in numerous biological systems, e.g. fungal and yeast cell walls, insect cuticles, and both tendons and shells of krill, lobsters, and crabs. β-chitin is rarer and is typically found in squid pens,

spines of some diatoms and various tube worms. The main commercial sources of chitin are crab and shrimp shells (Rinaudo 2006).

Chitosan is a heterologous de-*N*-acetylated analog of chitin consisting of linear β-1,4-linked *N*-glucosamine (**D**, GlcN) and *N*-acetyl-glucosamine units (**A**) (Figure 2). Unlike chitin, chitosan is soluble in dilute aqueous acid solutions (Hackman 1954; Sannan et al. 1976). The name chitosan refers to a number of chitin derivatives, which are mostly described by the fraction of *N*-acetylated units (F_A), the degree of polymerization (DP) or the molecular weight distribution (PD for polydispersity). These factors determine the properties of the polymer (Vårum et al. 1991a; Vårum et al. 1991b).

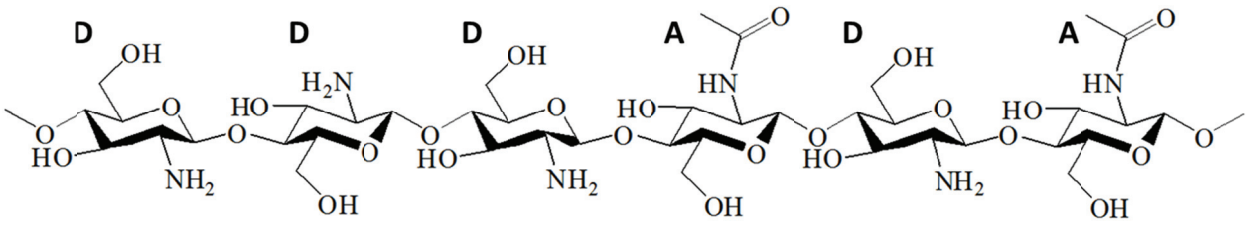

Figure 2: Chitosan consists of randomly distributed β-1,4 linked *N*-acetyl-glucosamine (A) and glucosamine units (D).

Chitin and chitosan in both their native and modified forms are used for diverse purposes, for instance in food, biotechnology, material science, gene therapy, drug and pharmaceutical applications (Figure 3) (Aam et al. 2010; Harish Prashanth & Tharanathan 2007). Hydrolysis of chitin and chitosan generates hetero chito-oligosaccharides (CHOS), which also have several interesting medicinal properties e.g. facilitation of bone-tissue formation (Ratanavaraporn et al. 2009), gene therapy (Köping-Höggård et al. 2003), inhibition of angiogenesis (Wu et al. 2012), and inhibition of adhesion of pathogens to human cells (Quintero-Villegas et al. 2013; Rhoades et al. 2006).

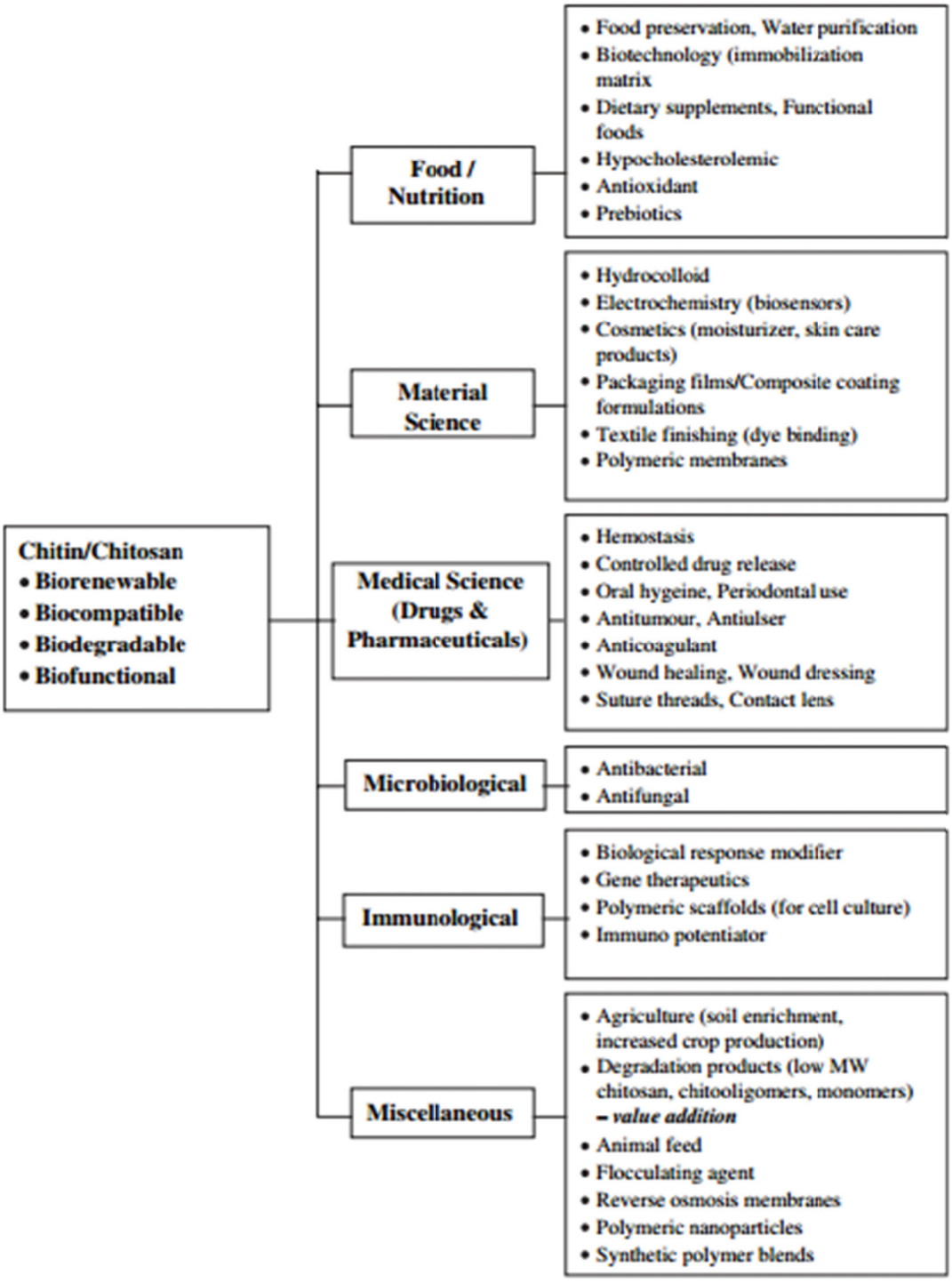

Figure 3: Current and potential applications of chitin and chitosan (Harish Prashanth & Tharanathan 2007).

1.2 Glycoside hydrolases (GHs)

Glycoside hydrolases are key enzymes in carbohydrate metabolism, as they catalyze the hydrolysis of glycosidic bonds between carbohydrates or between carbohydrates and non-carbohydrate moieties in glycosides, glycans and glycoconjugates (www.cazy.org; Lombard et al. 2014). Thus, these enzymes play essential roles in myriads of biological processes. They also have commercial importance. For instance, cellulases and xylanases can be used to produce sugars from pretreated biomass substrates, which can then be fermented to produce ethanol and butanol as renewable alternatives to gasoline (Wilson 2009). Furthermore, some have implications for human health. Notably, the GH endohexosaminidase D produced by *Streptococcus pneumonia* contributes to the virulence of the organism by taking part in the deglycosylation of IgG antibodies (Abbott et al. 2009), while the human chitinase, acidic mammalian chitinase, is induced and heavily over-expressed in asthmatic tissue during T_H2 inflammation (Zhu et al. 2004). The last two examples show that glycosidase inhibitors may have great therapeutic potential.

1.2.1 Classification

Carbohydrate active enzymes were originally classified using the IUB Enzyme Nomenclature based on recommendations from the International Union of Biochemistry and Molecular Biology (IUBMB). According to this system, each enzyme is given an Enzyme Commission (EC) number that is based on substrate specificity and the type of reaction catalyzed. The EC-number of GHs is 3.2.1.x, where the first three digits indicate enzymes hydrolyzing *O*-glycosyl linkages and the x indicates the substrates and molecular mechanisms (IUBMB 1992). This classification system does not necessarily reflect the structural features of the classified enzymes and is therefore not very suitable for enzymes showing broad specificity, especially when they act on several substrates (Henrissat 1991; Henrissat & Davies 1997).

Based on the assumption that there is a direct relationship between sequence and folding similarities, Bernard Henrissat and co-workers initiated efforts to compare the primary sequences of glycoside hydrolases. The work led to the introduction of a new classification system, based upon amino acid sequence similarities, and establishment of the Carbohydrate

Active EnZYmes (CAZY) database, in which the enzymes are classified into different families (Henrissat 1991). Today, glycosyltransferases, polysaccharide lyases, carbohydrate esterases, and a group of redox enzymes named auxiliary activities (AAs) are also classified by the same classification system (www.cazy.org; Lombard et al. 2014). The CAZY database has been available on the web, at www.cazy.org, since 1998 (Cantarel et al. 2009). The development of the classification system and ongoing efforts to improve it have been reported in several scientific papers. At the time of the last publication, sequence information for almost 340 000 CAZymes had been compiled and over 330 families defined (Lombard et al. 2014).

1.2.2 Mechanisms

Glycosidic bonds are enzymatically hydrolyzed via general acid catalysis that requires two essential residues: a proton donor and a nucleophile/base. There are two possible results of the hydrolysis, either inversion or retention of the configuration at the C1 anomeric oxygen (Koshland 1953; Sinnott 1990). Both mechanisms involve an oxacarbenium-ion-like transition state (Rye & Withers 2000).

An inverting glycosidase typically uses a catalytic acid and a catalytic base residue located approximately 10 Å apart. The reaction occurs via a single-displacement mechanism (Figure 4) where the glycosidic oxygen is protonated by the catalytic acid. At the same time the catalytic base removes a proton from a water molecule. This is accompanied by a nucleophilic attack of the water molecule on the anomeric carbon yielding a product with opposite stereochemistry (Davies & Henrissat 1995; Rye & Withers 2000; Vuong & Wilson 2010).

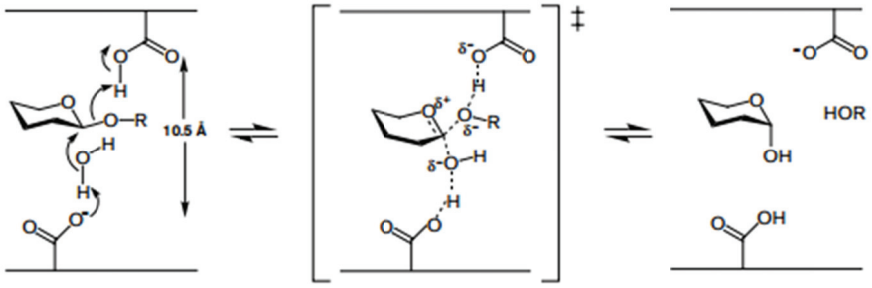

Figure 4: General catalytic mechanism of inverting glycoside hydrolases (Rye & Withers 2000).

The retaining glycoside hydrolases use a general acid/base catalyst and a nucleophile placed approximately 5.5 Å from each other, and the reaction proceeds via a double displacement mechanism (Figure 5) (Davies & Henrissat 1995; Rye & Withers 2000; Vuong & Wilson 2010). The catalyst acts first as an acid, donating a proton to the glycosyl oxygen. Concomitantly the nucleophile forms a covalent intermediate. In the next step, the deprotonated acid/base acts as a general base, receiving a proton from a water molecule. The activated water molecule then carries out a nucleophilic attack on the nucleophilic intermediate created in the first step, resulting in retention of the stereochemistry at the anomeric center.

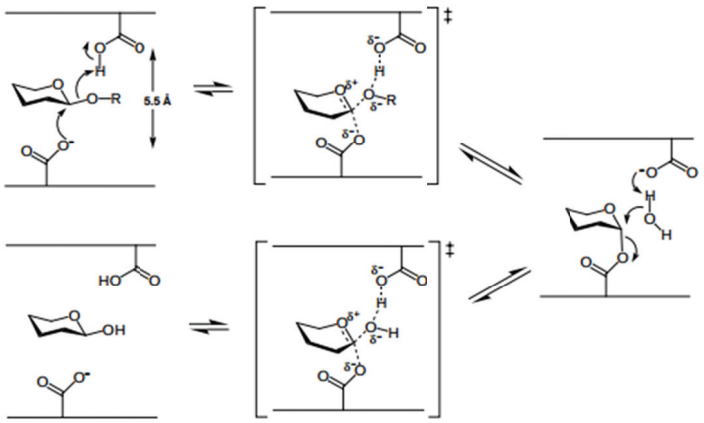

Figure 5: General catalytic mechanism of retaining glycoside hydrolases (Rye & Withers 2000).

1.2.3 Structure

Most glycoside hydrolases are multi-domain enzymes consisting of a catalytic domain linked to one or more non-catalytic domains, mainly carbohydrate-binding domains (CBMs). The CBMs promote the association of the enzymes with their substrates, whereas the catalysis occurs in the active site of the catalytic domain. The topology of the active sites is divided into three classes, often described as pocket, cleft and tunnel (Figure 6) (Davies & Henrissat 1995).

Enzymes that specifically attack chain ends act mostly on substrates with a large number of available chain ends and their active site is often located within a pocket. Thus, they are not efficient degraders of fibrous substrates such as cellulose (Davies & Henrissat 1995). The depth and shape of the pocket reflects the number of subsites that participate in substrate binding and release (Davies et al. 1997). The clefts are open structures, allowing binding at random sites of substrate polymers, and are mostly present in endo-acting enzymes. Tunnel topology allows polysaccharide chains to be threaded through the active sites, thereby increasing the ability of enzymes to catalyze numerous hydrolytic events without releasing the substrate. This feature is especially useful when the substrate has few exposed chain ends (Davies & Henrissat 1995). It also forms the basis for processivity, a key factor for efficient enzymatic degradation of insoluble substrates.

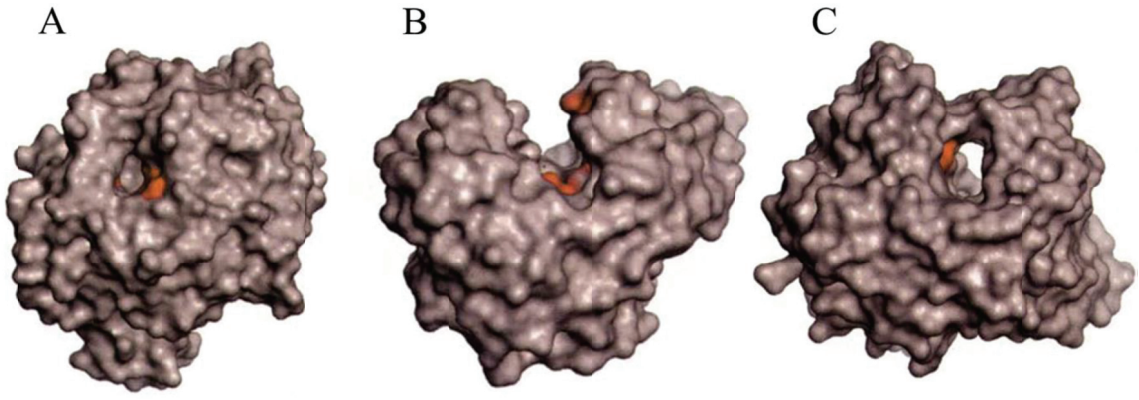

Figure 6: Active site topology of glycoside hydrolases (Davies & Henrissat 1995). A, Pocket; B, Cleft; C, Tunnel.

1.2.4 Modes of action

Carbohydrates can be efficiently degraded through the synergistic action of enzyme cocktails consisting of mixtures of GHs and accessory enzymes. The GHs have different modes of action, including random cleavage (endo mode) of the polymer chain and cleavage from either the reducing or non-reducing chain end (exo mode). Both endo- and exo-enzymes may have either processive or non-processive action (Davies & Henrissat 1995).

1.2.4.1 Processivity

Processivity is the ability of an enzyme to remain attached to a substrate between successive hydrolytic reactions (Davies & Henrissat 1995; Rouvinen et al. 1990). For glycoside hydrolases, processivity is crucial due to the large free energy penalties incurred when enzymes depolymerize crystalline substrates. Calculations show that the penalty is 5.6 kcal/mol per chitobiose unit and 5.4 kcal/mol per cellobiose unit (Beckham & Crowley 2011; Beckham et al. 2011). This emphasizes the importance of an enzyme staying attached to the polymer.

Structural data from enzymes obtained from various model organisms indicate that the degree of processivity is related to the structure of the catalytic domain. Processive enzymes possess long tunnels or deep clefts in their active site. Non-processive enzymes have shallower clefts and are thought to act in endo mode on disordered regions of the polymer crystals (Divne et al. 1994; Rouvinen et al. 1990). However, non-processive enzymes also have the ability to catalyze more than one cleavage per enzyme-substrate association, because they may remain loosely associated with the substrate (Divne et al. 1998; Varrot et al. 2003).

Processive enzymes often have highly conserved aromatic residues in their active site, which directly interact with sugar rings of the substrate. Notably, tryptophans provide a flexible hydrophobic sheath that the substrate can slide along (Divne et al. 1998; Varrot et al. 2003). However, this “stickiness” of the enzyme leads to a low dissociation rate, k_{off}, which reduces the catalytic efficiency for easily diffusible, soluble substrates (Harjunpää et al. 1996; Jalak & Väljamäe 2010). It is shown that removal of specific aromats convert processive enzymes to be non-processive as well as reducing the activity towards crystalline

substrates drastically. Removal of the active site loop forming the tunnel in processive enzymes can also make them non-processive (Horn et al. 2006a; von Ossowski et al. 2003; Zakariassen et al. 2009; Zhou et al. 2004). Other structural and dynamic variations, unrelated to the presence of aromatic residues, can also contribute to differences in processivity (Payne et al. 2012).

Measuring and quantifying processivity is important in order to gain insights into the structural base, molecular mechanisms, and biotechnological implications of the enzymes of interest. Unfortunately, this is highly challenging for several reasons. Firstly, it is not easy to perform straightforward biochemical analyses of insoluble substrates (Horn et al. 2012a). Secondly, it is difficult to measure processivity in systems that exhibit biphasic kinetics (Beckham et al. 2014). However, several methods have been developed to assess the processive ability of GHs, termed apparent processivity (P^{app}), quantitatively. The formal mathematical definition of P^{app} is the number of catalytic events an enzyme performs divided by the number of times the enzyme acquires a chain end (Horn et al. 2012a). However, in practice, P^{app} can be regarded as the actual processive ability of an enzyme acting on a particular substrate under a given set of conditions (Beckham et al. 2014). As indicated, P^{app} is highly dependent on the substrate (Horn et al. 2012a). This is due to the differences in accessibility of chain ends, structural heterogeneities and steric obstacles (Kurasin & Väljamäe 2011), which may lead to traffic jams of unproductively bound enzymes (Igarashi et al. 2011). Variations in substrate can also contribute to reductions in enzyme processivity observed with increases in the extent of polysaccharide degradation (**Paper II**). Removing obstacles, increasing the number of lanes, entrances, and exits by pretreatment of the substrate, and using synergistic enzyme cocktails can improve the efficiency of hydrolysis (Igarashi et al. 2011).

Unlike apparent processivity, which is dependent on the substrate, intrinsic processivity (P^{Intr}) is the average number of successive catalytic events before dissociation of an "ideal" substrate, and is thus the upper limit of apparent processivity. P^{Intr} is approximated by dividing the catalytic rate constant k_{cat} by the dissociation rate coefficient k_{off}. This equation implies that the probability of dissociation from the substrate is extremely low, and k_{off} is thus rate-limiting (Beckham et al. 2014; Horn et al. 2012a; Kurasin & Väljamäe 2011; Lucius et al. 2003). For the cellobiohydrolase Cel7A from *Trichoderma reesei* P^{Intr} is reportedly ~ 4000 when interacting with reduced bacterial cellulose (which has a high degree of polymerization) (Kurasin & Väljamäe 2011).

There are several standard approaches for measuring processivity. Many of these methods exploit the fact that each productive binding of a processive enzyme to a polymeric substrate leads to the production of at most one product with an odd number of sugars (primarily tri- or monomeric). All other products from the same initial association are dimers. The ratio between even and odd numbered products can therefore be used as an indication of the degree of processivity. This method is based on simple chromatographic analysis, but several potential pitfalls need to be taken into consideration. Uncertainties about the initial binding mode, and thus the initial product profile, as well as the formation of soluble, intermediate products can interfere with the results (Horn et al. 2012a). The ratio between numbers of soluble and insoluble reducing ends can also be used as a measure of P^{app}. Processive enzymes create high numbers of soluble reducing ends since each initial cut is followed by the production of soluble dimers, but also non-processive endo enzymes do this. Soluble and non-soluble reducing ends can be separated and analyzed using relatively standard analytical methods (Beckham et al. 2014; Horn et al. 2012a). The described methods have yielded processivity values up to 25 (**Paper II**; (Horn et al. 2012a; Kurasin & Väljamäe 2011)).

To overcome limitations of the methods discussed, new techniques based on substrate labeling have been developed by studying cellulases acting on cellulose. One of these, the single-hit method also exploits the fact that processive enzymes produce more soluble than non-soluble reducing ends. By working at low enzyme to substrate ratios and low degrees of degradation, the risk of enzymes hitting the same chain twice is minimized. Original reducing ends are labeled before the enzymatic reaction while reducing ends generated in the reaction are labeled afterwards. Soluble reducing groups are measured by absorbance-based methods while fluorescence is used for the insoluble ends (Kurasin & Väljamäe 2011). P^{app} can also be determined by using single-turnover conditions. Shortly after adding the enzyme to a solution containing a uniformly ^{14}C-labeled substrate, non-labeled substrate is added. Each bound enzyme can only perform one processive run on the labeled substrate under such conditions. The average number of ^{14}C-cellobiose units released during a single run, which equals P^{app}, is measured. (Jalak & Väljamäe 2010; Velleste et al. 2010). Values from both single-hit and single-turnover experiments are quite similar, indicating that the two methods have similar validity (Horn et al. 2012a).

In recent years, computational results obtained by modeling and molecular dynamics have provided useful information for understanding processivity. Three dynamic

characteristics are qualitatively related to the experimentally measured processivity: i) the degree of ligand solvation, ii) the magnitude of average atomic fluctuation of the ligand as a function of binding site, and iii) the magnitude of overall fluctuations of key catalytic site residues (Payne et al. 2012). These characteristics have led to the hypothesis that ligand binding free energy ($\Delta G_b°$) is related to the degree of processivity through the thermodynamics of chemical equilibrium (Equation 1) and that this can be calculated theoretically (Payne et al. 2013).

$$\Delta G_b° / RT = \ln (P^{Intr} * k_{on} / k_{cat}) \qquad \text{Equation 1}$$

where R is the universal gas constant, T is the temperature in Kelvin, P^{Intr} is the intrinsic processivity, k_{on} is the association rate coefficient, and k_{cat} is the catalytic rate coefficient. This relationship implies that the more strongly an enzyme binds to the substrate the more processive it is.

1.2.5 Auxiliary activities

Plant cell walls have very complex structures, consisting of cellulose, hemicellulose, pectin, and lignin among other. The carbohydrates form a complex matrix composed of crystalline and insoluble cellulose fibers together with soluble carbohydrates (Gilbert 2010; Levasseur et al. 2013). Lignin, the main non-carbohydrate component, forms an intricate network of phenolic compounds that provide a hard, hydrophobic and insoluble barrier (Levasseur et al. 2013; Vanholme et al. 2010). The degradation of the plant cell wall constituents was initially believed to be performed by two different systems; a hydrolytic system breaking down the carbohydrates and an oxidative ligninolytic system depolymerizing lignin (Levasseur et al. 2013).

The auxiliary activities (AA) class of enzymes has recently replaced the class of carbohydrate binding modules (CBMs) in the CAZy database (Cantarel et al. 2009; Levasseur et al. 2013). It includes families of lytic polysaccharide monooxygenases (LPMOs) and families of redox enzymes involved in lignin breakdown. To be included in the AA class, an enzyme must be able to help other CAZymes gain access to carbohydrate constituents of plant cell walls. The AA enzymes are not limited to single catalytic reaction mechanisms or specific substrates. The introduction of this class has permitted complete

description of the main contributors to plant cell wall degradation. Initially, 10 families and subfamilies of three of the families were included (Levasseur et al. 2013). In January 2015 the class comprised 13 families (www.cazy.org).

The LPMOs are classified in families AA9, AA10, AA11, and AA13. The first two families consisting of LPMOs that were described are AA9 and AA10. They consist mostly of fungal and bacterial members, respectively (Horn et al. 2012b; Levasseur et al. 2013). Members of both families have a flat substrate binding surface containing a diagnostic conserved arrangement of the N-terminal amino group and two histidines that can jointly bind a metal ion (Aachmann et al. 2012; Karkehabadi et al. 2008; Quinlan et al. 2011). Members of AA9 were originally thought to be non-catalytic CBMs that facilitate the binding and degradation of insoluble substrates. They can appear in enzymes as independent non-catalytic carbohydrate-binding proteins or as separate domains. Work by Vaaje-Kolstad and coworkers in 2005 showed that CBP21, a family 10 AA enzyme, produced by the soil bacterium *Serratia marcescens* and known to bind β-chitin, can disrupt the crystalline structure of this substrate and thus dramatically increase chitinase efficiency (Suzuki et al. 1998; Vaaje-Kolstad et al. 2005a). Vaaje-Kolstad and coworkers subsequently demonstrated that the same protein is an oxidative enzyme that cleaves polysaccharide chains in crystalline chitin via both a hydrolytic step and an oxidative step (Vaaje-Kolstad et al. 2010). This generates two new chain ends on the crystalline surface: a normal non-reducing end and an oxidized reducing end being an aldonic acid. Molecular oxygen has been shown to participate in the reaction, and addition of external electron donors increases the activity of CBP21. The same properties are shared by a cellulase (CelS2) from *Streptomyces coelicolor* comprising an AA10 and a cellulose binding domain (CBM2) (Forsberg et al. 2011) as well as in a AA9 enzyme (*Pc*GH61D) from the fungus *Phanerochaete chrysosporium* (Westereng et al. 2011). Furthermore, these enzymes are dependent on metal ions, preferably copper (Aachmann et al. 2012; Quinlan et al. 2011; Vaaje-Kolstad et al. 2012; Westereng et al. 2011).

1.3 The chitinolytic machinery of Serratia marcescens

Chitin is degraded by chitinases (EC 3.2.1.14), which belong to glycoside hydrolase family 18 (www.cazy.org; (IUBMB 1992; Lombard et al. 2014)). Enzymes with chitinolytic activity are present in a wide spectrum of microorganisms. The Gram-negative soil bacterium *Serratia marcescens* is regarded as the most efficient chitin degrader and has a highly evolved enzymatic machinery (Monreal & Reese 1969). In 1986 Fuchs and co-workers purified five chitinolytic enzymes produced by this bacterium, namely the exo-processsive Chitinase A (ChiA) and Chitinase B (ChiB), the nonprocessive endo-active Chitinase C1 (ChiC1) and Chitinase C2 (ChiC2), and the surface active LPMO Chitin Binding Protein 21 (CBP21) (Figure 7) (Fuchs et al. 1986; Igarashi et al. 2014; Monreal & Reese 1969; Vaaje-Kolstad et al. 2013). In addition, an *N*-acetyl-hexosaminidase that converts dimers produced by ChiA, ChiB, and ChiC to monomeric *N*-acetylglucosamine units has been discovered (Figure 7) (Kless et al. 1989; Tews et al. 1996).

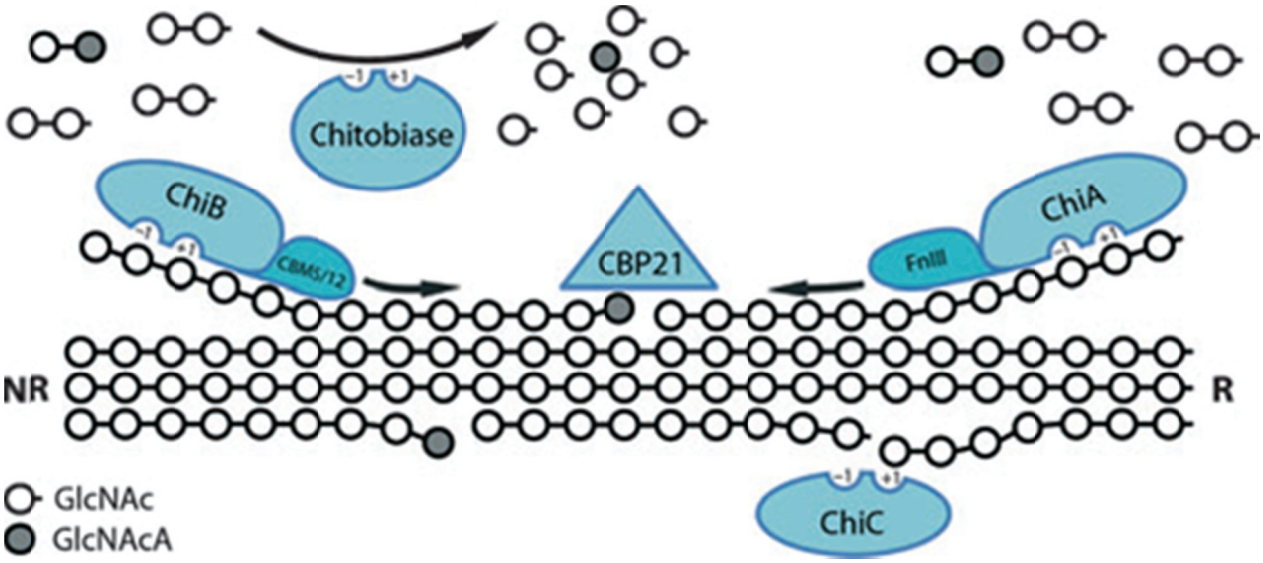

Figure 7: Schematic diagram of the chitinolytic machinery of *Serratia marcescens* (Vaaje-Kolstad et al. 2013).

1.3.1 The GH18 chitinases ChiA, ChiB, and ChiC

Serratia marcescens produces, as mentioned, three GH18 chitinases, namely ChiA, ChiB, and ChiC. The catalytic domains of these enzymes have a $(\beta/\alpha)_8$ TIM barrel fold with important catalytic residues located in β-strand 4. These catalytic residues form a conserved, diagnostic DXDXE motif with the catalytic acid located at the end of the barrel. Another highly conserved residue, a serine, is part of an additional diagnostic motif, the SXGG motif (Suzuki et al. 1999; Terwisscha van Scheltinga et al. 1996).

The first bacterial or fungal GH18 chitinase structure solved was that of ChiA (Figure 8). It is a multi-modular enzyme with a catalytic module coupled to an N-terminal chitin-binding module with a fibronectin (FnIII)-like fold. In addition, a small, inserted α + β domain consisting of 75 amino acid residues is found between strand B7 and helix A7 (Perrakis et al. 1994). The inserted domain looks like a bump, and extends the height of one of the sides of the deep catalytic cleft, contributing to the formation of a tunnel-like active site (Perrakis et al. 1994; Zees et al. 2009). ChiB is also multi-modular, but instead of the FnIII-like fold it has a C-terminal CBM5 chitin-binding module (Figure 8). The catalytic domain has a fold similar to that of ChiA, including a tightly associated α + β domain. In ChiB this domain provides a flexible loop near the active site. ChiB has also a support loop that ChiA lacks, which interacts with the chitin-binding module (van Aalten et al. 2000).

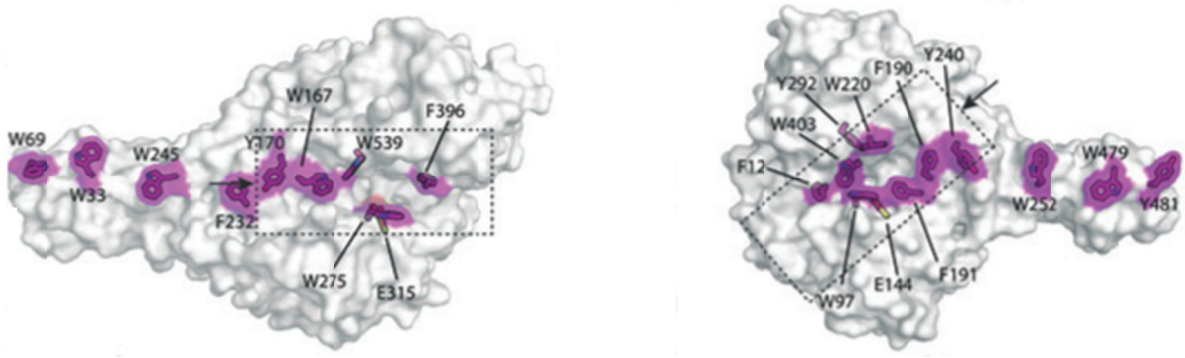

Figure 8: Crystal structures of the exo-processive chitinases ChiA (left) and ChiB (right) from *Serratia marcescens* (Vaaje-Kolstad et al. 2013). The aromatic amino acids that interact with the substrate through stacking interactions are highlighted in magenta.

Comparison of the crystal structures of ChiA and ChiB shows that their chitin-binding domains are located on the non-reducing and reducing sides of the substrate-binding cleft, respectively (van Aalten et al. 2000). Thus it is assumed that ChiA and ChiB degrade chitin chains in opposite directions in the exo-mode (van Aalten et al. 2000). This has been experimentally proven by both labelling and high speed-atomic force microscopy (HS-AFM) scanning (Hult et al. 2005; Igarashi et al. 2014). Due to the opposite directionalities, they have synergistic effects on chitin degradation rates (Brurberg et al. 1996). No such effects are seen with regard to processivity (**Paper II**). Although ChiA and ChiB mainly work in the exo-mode, they have some endo-activity towards the soluble substrate chitosan (Sikorski et al. 2006). ChiA also shows some endo-activity towards insoluble substrates, possibly due to its relatively open active-site cleft, which is a typical characteristic of endo-acting enzymes (Brurberg et al. 1996; Davies & Henrissat 1995; Perrakis et al. 1994; Sikorski et al. 2006). In ChiB, the roof over the active site cleft is partially closed, creating a more tunnel-like catalytic cleft, which is an important feature for exo-enzymes (Davies & Henrissat 1995; van Aalten et al. 2000).

The catalytic clefts in both ChiA and ChiB are covered with a path of aromatic residues that continues over the surface of the chitin binding domain, and interacts with the substrate through hydrophobic stacking interactions with the pyranose rings (Perrakis et al. 1994; van Aalten et al. 2000). Although ChiA and ChiB do not have a typically tunnel-shaped active site, they have been shown to act processively (Horn et al. 2006b; Horn et al. 2006c; Sikorski et al. 2006; Sørbotten et al. 2005). This is probably due to the path of aromatic residues, which promotes sliding of the substrate through the active site between each catalytic cycle (Breyer & Matthews 2001; Varrot et al. 2003).

ChiC, also referred to as ChiC1, tends to be cleaved by endogenous proteases, yielding ChiC2, a form consisting solely of the catalytic domain (Gal et al. 1998; Suzuki et al. 1999; Synstad et al. 2008). Sequence information implies that ChiC1 is composed of two chitin-binding modules: a C-terminal FnIII module coupled to a downstream CBM12 chitin-binding module (Suzuki et al. 1999). The structure of the catalytic domain, recently solved by Payne et al. and shown in Figure 9, confirms previously presumed features, such as the lack of the small $\alpha + \beta$ domain found in ChiA and ChiB, thus explaining the shallow substrate-binding cleft (Payne et al. 2012; Synstad et al. 2008). The shallow cleft resembles that of the plant endo-chitinase hevamine (Terwisscha van Scheltinga et al. 1995). Several experimental studies suggest that ChiC has endo-activity, since the enzyme is less active

towards oligomeric substrates and more active towards complex polymeric substrates than processive exo-chitinases (Horn et al. 2006b; Suzuki et al. 2002; Synstad et al. 2008). The shallow substrate binding cleft of ChiC and the lack of surface-exposed aromatic residues in the FnIII domain imply that ChiC is non-processive (Vaaje-Kolstad et al. 2013). Experimental studies have confirmed this (Horn et al. 2006b; Sikorski et al. 2006). Synergistic effects between ChiA and ChiC on the hydrolysis of both powdered and crystalline chitin have been observed, but not between ChiB and ChiC (Suzuki et al. 2002). In the chitinolytic machinery of *S. marcescens*, ChiC complements ChiA and ChiB by supplying the exo-enzymes with new reducing and non-reducing chain ends (Brurberg et al. 1996; Suzuki et al. 2002).

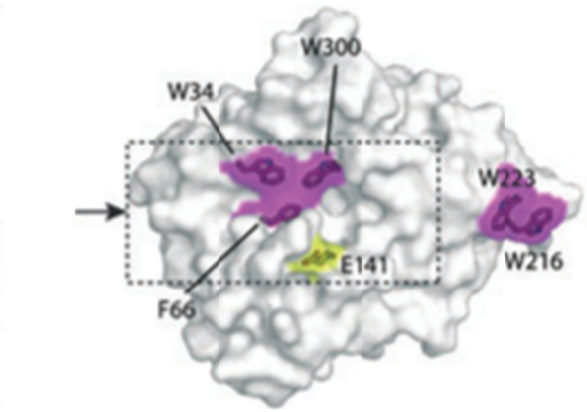

Figure 9: Crystal structure of the non-processive endo-chitinase ChiC2 from *Serratia marcescens* (Vaaje-Kolstad et al. 2013). The aromatic amino acids that interact with the substrate through stacking interactions are highlighted in magenta and the catalytic acid in yellow.

1.3.1.1 Substrate-assisted mechanism

The structures of ChiA from *S. marcescens* and hevamine, an endo-chitinase from the plant *Hevea brasiliensis,* were the first two GH18 structures to be studied (Perrakis et al. 1994; Terwisscha van Scheltinga et al. 1994). Both enzymes were found to act via a retaining acid catalysis mechanism, which was therefore suggested to be a general property of GH18 chitinases (Perrakis et al. 1994; Terwisscha van Scheltinga et al. 1995). However,

a deviation from other glycoside hydrolase families was noted, as they lacked the normal arrangement of the two carboxylic acids in the catalytic center (Perrakis et al. 1994; Terwisscha van Scheltinga et al. 1994). An explanation for this deviation was found when hevamine was studied in complex with the pseudotrisaccharide allosamidin (Terwisscha van Scheltinga et al. 1995), a specific inhibitor of GH18 chitinases (Sakuda et al. 1986). Allosamidin contains an allosamizoline group that binds in subsite −1 of the hevamine-allosamidin complex. It was therefore suggested that allosamidin mimics the reaction intermediate in which a positive charge at C1 is stabilized intramolecularly by the carbonylic O-atom of the *N*-acetyl group at C2. Thus, the nucleophile missing from the structure is provided by the substrate itself (Terwisscha van Scheltinga et al. 1995), and hence this specific mechanism is called substrate-assisted. As a result, Family 18 chitinases have an absolute preference for acetylated units in subsite −1 (Tews et al. 1997). Anchimeric assistance from the C2 *N*-acetyl group on the −1 sugar leads to the formation of a covalent oxazolinium intermediate (Tews et al. 1997). Molecular dynamics simulations show that the hydrolysis mechanism used by GH18 chitinases involves distortion of the −1 sugar ring from the relaxed $^{4}C_{1}$ chair conformation to a skewed $^{1,4}B$ boat conformation, which is necessary for creation of the oxazolinium intermediate (Brameld & Goddard 1998; Papanikolau et al. 2001; van Aalten et al. 2001). The transition from a $^{4}C_{1}$ chair conformation to the skewed $^{1,4}B$ boat conformation, is highly energy demanding, requiring ~ 8 kcal/mol (Biarnes et al. 2007).

The substrate-assisted mechanism (Figure 10) of ChiB from *S. marcescens* has been studied in detail using extensive mutagenic, crystallographic, and computational approaches (Synstad et al. 2004; Vaaje-Kolstad et al. 2004; van Aalten et al. 2001). It has been described in detail by Synstad and co-workers (Synstad et al. 2004). The conserved DXDXE motif (Asp^{140}-Glu^{144}), Ser^{93} in the diagnostic motif SXGG, and the conserved residues Tyr^{10}, Tyr^{214} and Asp/Asn^{215} are all important residues in the catalysis. In the free enzyme, Asp^{142} is found in the 'down' position sharing a proton with Asp^{140}. Upon substrate binding, protonated Asp^{142} rotates to the 'up' position losing its hydrogen bond to Asp^{140}. In the 'up' position it interacts with Glu^{144} and the *N*-acetyl nitrogen of the −1 sugar, having one hydrogen bond to each. Concomitantly, Ser^{93} and Tyr^{10} are adjusted to stabilize the charge on Asp^{140} as well as filling the cavity left behind by Asp^{142}. The adjustments cause both residues to act as donors in strong hydrogen bonds with Asp^{140}, thus compensating for the negative charge of the latter. The interaction between Asp^{140} and the *N*-acetyl group fixes

the −1 sugar in the distorted skewed boat conformation, but Tyr^{214} and Asp^{215} are also involved in stabilization of this complex. Tyr^{214} interacts with the *N*-acetyl group while Asp^{215} accepts a hydrogen bond from the O6 hydroxyl (Synstad et al. 2004; Vaaje-Kolstad et al. 2004; van Aalten et al. 2000).

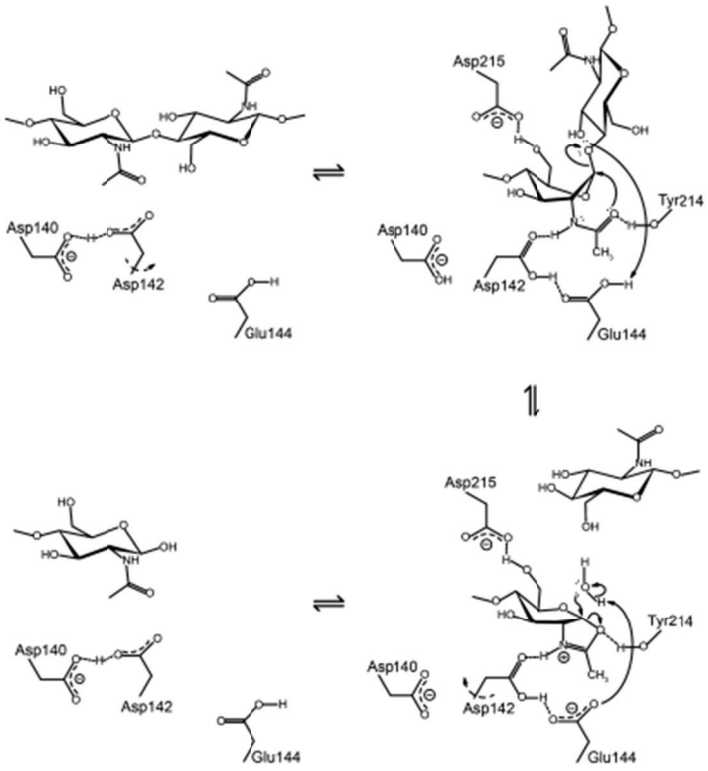

Figure 10: The substrate-assisted mechanism used by GH family 18 chitinases (Vaaje-Kolstad et al. 2013).

1.3.1.2 Processivity in GH18 chitinases

When measuring the processivity of chitinases, general methods described in section 1.2.4.1 are applied, but often with some specific modifications or considerations. As previously mentioned, successive sugar units in chitin chains are rotated 180° relative to each other, and the catalysis is substrate-assisted requiring an acetylated sugar unit in subsite −1 (Rinaudo 2006; Terwisscha van Scheltinga et al. 1995; Tews et al. 1997; van Aalten et al. 2001). Thus, the sliding of the chitin polymer through the active site results in

productive binding only for alternate sugars. The products of processive degradation are therefore disaccharides (Horn et al. 2006b). Chitinases also bind unproductively to chitosans if the sugar bound in subsite −1 is deacetylated. This feature can be exploited when measuring processivity, both quantitatively and qualitatively.

Processivity is often qualitatively analyzed using chitosans with a random distribution of acetylated units. The degradation products are analyzed by size-exclusion chromatography. A dominance of even-numbered products in the early stages of the reaction is indicative of processivity, while non-processive enzymes produce equal amounts of odd- and even-numbered oligomers (Sikorski et al. 2006; Sørbotten et al. 2005). Processivity can be quantitatively analyzed using chitosan and a capillary viscometer to monitor relative viscosity, which is sensitive to changes in the high molecular fraction of the substrate, reflecting the number of initial endo-cuts. In addition, it is necessary to determine the total amount of reducing chain ends created in the enzymatic reaction. By comparing these two parameters, a value for processivity is obtained (Horn & Eijsink 2004; Sikorski et al. 2006). As for general processivity measurements, absolute values must be handled with great care. The processivity values are likely to be underestimated as the likelihood of full enzyme-substrate dissociation is expected to increase with increases in the length of the 'sliding path' (Horn et al. 2012a).

Processivity studies of the chitinolytic machinery of *S. marcescens*, mainly performed on chitosan, have revealed fundamental aspects with regard to the contributions of aromatic residues in ChiA (Zakariassen et al. 2009) and ChiB (Horn et al. 2006a). As previously described, the substrate-binding clefts of processive enzymes are lined with aromatic residues that make the enzyme slide and stay attached to the substrate, due to hydrophobic stacking interactions (Divne et al. 1998; Katouno et al. 2004; Uchiyama et al. 2001; Varrot et al. 2003). Processivity is nearly abolished by single-point mutations of such residues in substrate-binding subsites (− subsites in ChiA and + subsites in ChiB). Important residues in this regard are W^{167} (subsite −3) in ChiA and W^{97} and W^{220} (subsite +1 and +2) in ChiB (Horn et al. 2006a; Zakariassen et al. 2009).

1.3.2 The AA10 LPMO CBP21

CBP21 is the fifth chitinolytic enzyme produced by *S. marcescens*. When it was first cloned and characterized it was found to have strong affinity for β-chitin, but no enzymatic activity was detected (Suzuki et al. 1998). In 2005, the crystal structure of CBP21 was solved, showing it to be a monomeric enzyme consisting of two β-sheets stabilized by two disulfide bridges (Figure 11). Hence, the enzyme has a compact, distorted β-sandwich architecture with a hydrophobic core including several conserved aromatic acids, especially tryptophan residues. The binding surface is flat and covered by a number of conserved, mostly polar residues. Six of these are known to be important for substrate binding (Vaaje-Kolstad et al. 2005b) as confirmed by recent nuclear magnetic resonance (NMR) analyses (Aachmann et al. 2012).

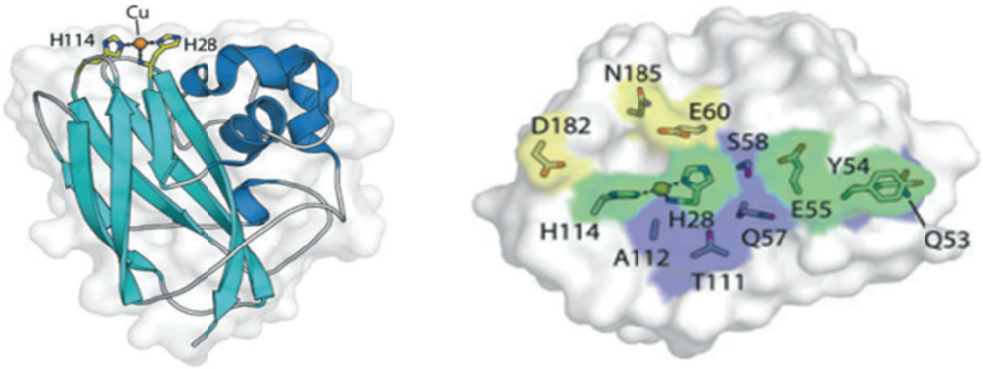

Figure 11: Crystal structure of CBP21 (Vaaje-Kolstad et al. 2013). Left: The N-terminal amino group and the side chains of His^{28} and His^{114} (yellow colored carbon atoms) bind a metal ion (golden sphere). Right: Residues known to be involved in chitin binding from mutagenesis experiments, NMR analyses, or both are colored yellow, blue and green, respectively.

One of the first studies on CBP21 showed that it can boost the degradation of chitin by chitinases (Vaaje-Kolstad et al. 2005a). The mechanism, described in 2010, indicated that CBP21 can depolymerize chitin chains in the presence of an external electron donor and molecular oxygen. Accordingly, the presence of the electron donor ascorbic acid significantly increases the chitinase efficiency. The introduction of chain breaks and negative charges by CBP21 leads to a disruption of the crystal packing, thereby providing

new attachment points for chitinases and enhancing substrate accessibility (Vaaje-Kolstad et al. 2010). Synergism between CBP21 and each of the individual *S. marcescens* chitinases has been established, suggesting that CBP21 has a fundamentally different role from the chitinases (Vaaje-Kolstad et al. 2005a).

The NMR structure of CBP21 shows that the imidazole side chain and two conserved histidine residues constitute a copper-binding site. Thus, CBP21 is copper-dependent. One of these histidine residues (His^{114}) is strictly conserved in the N-terminal (Aachmann et al. 2012). This explains why addition of the metal ion chelator ethylendiaminetetraacetic acid (EDTA) or mutation of the metal-binding residue His114 inactivates the enzyme (Vaaje-Kolstad et al. 2005a; Vaaje-Kolstad et al. 2010).

In the reaction mechanism catalyzed by CBP21, one regular non-reducing chain end and one oxidized chain end are formed (Figure 12). The oxidized chain end appears as an aldonic acid in the solution, including two carboxylic oxygen atoms of which are derived from molecular oxygen and water (Vaaje-Kolstad et al. 2010). It has also been shown that CBP21 binds Cu^{+} more strongly than Cu^{2+}, implying that it can protect reduced copper ions from oxidation (Aachmann et al. 2012). This is consistent with the conception that molecular oxygen tends to bind copper in its reduced monovalent state, in accordance with a catalytic mechanism proposed for a GH61 type LPMO. Upon oxygen binding, an electron is transferred from Cu^{+} to O_2, generating a superoxo intermediate that may initiate the reaction by abstracting a hydrogen from the substrate (Figure 12) (Aachmann et al. 2012; Phillips et al. 2011; Que & Tolman 2008).

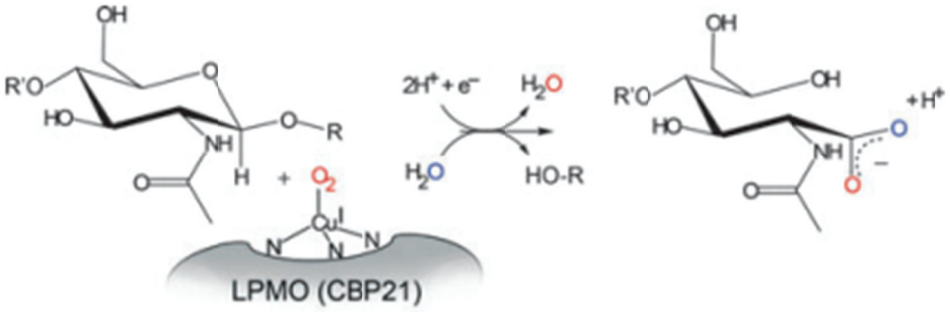

Figure 12: The reaction mechanism used by CBP21 (Aachmann et al. 2012).

1.4 Thermodynamics of protein-ligand interactions

The thermodynamic parameters of binding interactions are crucial factors to elucidate in order to understand biomolecular recognition, and thus play important roles in modern drug design. To describe the forces involved in molecular associations, information about the changes in all thermodynamic parameters is needed, including the heat capacity change and the free energy, enthalpy, and entropy of binding.

1.4.1 The association constant (K_a) and binding free energy ($\Delta G°$)

A typical reaction between a protein (P) and a ligand (L) can be described as:

$$P + L \underset{K_d}{\overset{K_a}{\leftrightarrow}} PL$$ Equation 2

where K_a and K_d are the association and dissociation constants, respectively. The association constant can be expressed through the standard Gibbs free-energy change ($\Delta G°$):

$$\Delta G° = -RT\ln K_a = RT\ln K_d$$ Equation 3

where R is the gas constant (8.314472 J mol^{-1} K^{-1}) and T is the temperature (Kelvin). $\Delta G°$ determines the spontaneity of a biomolecular binding equilibrium. In other words, it describes a key variable: the binding affinity between the ligand and enzyme. More negative values mean a more favorable reaction and higher binding affinity. The change in free energy has both enthalpic ($\Delta H°$) and entropic ($\Delta S°$) contributions, as described by the following equation:

$$\Delta G° = \Delta H° - T\Delta S°$$ Equation 4

Many combinations of $\Delta H°$ and $\Delta S°$ values can elicit the same free energy and thus the same binding affinity. Entropic and enthalpic contributions in biological systems often vary considerably, but in a compensatory manner (Cooper et al. 2001), i.e favorable changes in binding enthalpy are compensated by opposite changes in entropy, and vice versa. This so-called entropy-enthalpy compensation leads to relatively small variations in the free energy, especially in aqueous systems where non-covalent interactions dominate. In such systems,

the enthalpy-entropy compensation also appears to be a consequence of perturbing the many weak intermolecular interactions (Dunitz 1995).

1.4.2 Binding enthalpy ($\Delta H_r°$)

The simplest way of regarding the physical meaning of binding enthalpy in a protein-ligand interaction is that it represents the changes in non-covalent bond energy that occur during the interaction. The measured enthalpy change must be the result of the formation and breaking of many individual bonds, since bonds are unlikely to be formed without any being broken. The reaction enthalpy change ($\Delta H_r°$) of a binding reflects the changes in weak interactions, such as electrostatic-electrostatic interactions, hydrogen bonding, and dipole-dipole interactions when the two components change from being free solvated species to one solvated complex (Perozzo et al. 2004).

1.4.3 Binding entropy ($\Delta S_r°$)

The entropic term in protein-ligand interactions can be viewed as the sum of translational, solvation, and conformational entropic changes, as expressed in Equation 5 (Baker & Murphy 1997).

$$\Delta S_r° = \Delta S_{mix}° + \Delta S_{solv}° + \Delta S_{conf}° \qquad \text{Equation 5}$$

At temperatures close to 385 K, the entropy of solvation is estimated to be close to zero, and the change in heat capacity ($\Delta C_{p,r}$) can be related to the solvation entropy change ($\Delta S_{solv}°$) of the binding reaction at t = 30 °C, as described by Equation 6 (Baker & Murphy 1997; Baldwin 1986; Murphy et al. 1990; Murphy 1994).

$$\Delta S_{solv}° = \Delta C_{p,r}° \ln(303K/385K) \qquad \text{Equation 6}$$

The solvation entropy change originates from the release of water molecules as the active site and the ligand undergo complete or partial desolvation upon binding (Freire 2004). The direct interactions that occur, in combination with the lost solvation interactions, determine if the binding is favorable, neutral, or unfavorable (Li & Lazaridis 2005). Binding energies

of water molecules have been mapped in water-protein and water-ligand interactions showing that the energies are dependent on where the water molecule is bound. They are reportedly, –0.38 kcal/mol and −0.04 kcal/mol for water molecules bound in the first and second hydration shell around the protein, respectively, and −0.45 kcal/mol, –0.55 kcal/mol, and –0.56 kcal/mol for water molecules bound in the active site, in a cavity and buried, respectively (Amadasi et al. 2006). The binding energy of a water molecule coupling protein and ligand is particularly beneficial, −1.13 kcal/mol (Amadasi et al. 2006). The release of a highly ordered water molecule may generate a favorable entropy change, of up to 7 cal/K mol (Dunitz 1994).

Furthermore, the entropy of translation ($\Delta S_{mix}°$) can be calculated as a cratic term, a statistical correction, that reflects mixing of solute and solvent molecules and the changes in translational/rotational degrees of freedom, as expressed by Equation 7 (Baker & Murphy 1997).

$$\Delta S_{mix}° = R\ln(1/55.5\text{K}) \qquad \text{Equation 7}$$

where R is the gas constant (8.314472 J mol^{-1} K^{-1}), and $\Delta S_{mix}°$ is consequently estimated to be –8 cal/K mol.

Changes in conformational entropy originate from changes in conformational freedom for both the ligand and protein. The changes are usually unfavorable since binding leads to loss of conformational freedom for both molecules (Freire 2004). $\Delta S_{conf}°$ can be calculated from Equation 5 using experimentally determined $\Delta S_r°$ values, and $\Delta S_{mix}°$ and $\Delta S_{solv}°$ values calculated from Equation 6 and 7.

1.4.4 Change in heat capacity (ΔC_p)

Heat capacity is defined as the amount of energy that is required to increase the temperature of a substance by one degree Kelvin. In a biomolecular reaction, the change in heat capacity, $\Delta C_{p,r}°$, is defined as the temperature dependency of the enthalpy change as described in Equation 8.

$$\Delta C_{p,r} = \left(\frac{\partial \Delta H_r^\circ}{\partial T} \right)$$ Equation 8

where $\Delta H_r°$ is the change in reaction enthalpy and T is the temperature in Kelvin. It can also be defined with respect to entropy change (Equation 9):

$$\Delta C_{p,r} = \left(\frac{\partial \Delta S_r^\circ}{\partial \ln T} \right)$$ Equation 9

The dependencies between $\Delta C_{p,r}°$ and temperature may be either weak or strong, but in narrow physiological temperature ranges they are often hard to observe (Perozzo et al. 2004). Originally, Walter Kauzmann hypothesized that significant changes in heat capacity displayed by macromolecular systems are largely associated with hydrophobic interactions (Kauzmann 1959). However, this concept has been subsequently questioned, and it has been proposed that significant $\Delta C_{p,r}°$ changes are to be expected for any macromolecular process that involves several cooperative weak interactions (Cooper 2005). A negative value of $\Delta C_{p,r}°$ indicates that $\Delta H°$ is more negative when the temperature increases, meaning an increase in bond formation at higher temperatures (Holdgate 2001). Liquids are more disordered than solids and have additional translational and rotational degrees of freedom, thus they can absorb more heat energy leading to a positive $\Delta C_{p,r}°$ (Cooper 2005).

1.5 Isothermal titration calorimetry (ITC)

Isothermal titration calorimetry (ITC) is one of the main calorimetric techniques applied when studying binding of ligands to biological macromolecules. By using this method the energy associated with a chemical reaction is measured. In a single experiment, it is possible to measure the association constant (K_a), stoichiometry (n), free energy ($\Delta G°$), enthalpy ($\Delta H°$) and entropy ($\Delta S°$) of the binding (Holdgate 2001; Perozzo et al. 2004; Wiseman et al. 1989).

An ITC instrument consists of two identical cells, a reference cell and a sample cell, composed of a highly efficient thermal conducting material surrounded by an adiabatic jacket (Figure 13). The most commonly used ITC instruments are based on cell feedback, where sensitive thermopile circuits detect temperature differences between the two cells as well as between the cells and the jacket. Heaters located on the cells and the jacket are activated when necessary to maintain identical and stable temperatures in all components (Pierce et al. 1999).

A typical ITC-experiment is performed by placing one of the reactants (protein) in the sample cell with a long syringe. The other reactant (ligand) is then titrated, stepwise, via an injection syringe attached to a teflon paddle with a stirring motor to ensure proper mixing during the whole experiment (Leavitt & Freire 2001; Pierce et al. 1999). It is important for both the ligand and the protein to be in exactly the same buffer, which must be thoroughly degassed prior to use. This is to avoid problems due to mismatched buffers and air bubbles. The reference cell contains none of the reactants, only buffer or water (Holdgate 2001; Pierce et al. 1999). Firstly, constant power is applied to the reference cell directing the feedback circuit to activate the sample cell's heater. This represents the baseline. When the titration is started and the ligand and protein react, a certain amount of heat will either be released or absorbed, depending on whether the reaction is endothermic or exothermic. The difference in temperature between the sample cell and reference cell is detected by the calorimeter. Exothermic reactions lead to a decrease in the feedback power while endothermic reactions lead to an increase. The measured signal is the amount of power needed to maintain the constant temperature difference between the reaction and the reference cell, yielding what is called an ITC thermogram (Figure 13). By integrating the deflections from baseline with respect to time, the heat released or absorbed is obtained. The heat is proportional to the fraction of bound ligand (Holdgate 2001; Perozzo et al. 2004;

Pierce et al. 1999). Furthermore, the experimental data are often presented as a plot where the heat detected in each titration is plotted versus the molar ratio of ligand and receptor concentration (Figure 13). An appropriate binding model can be fitted to these data in order to obtain the values of interest (Perozzo et al. 2004).

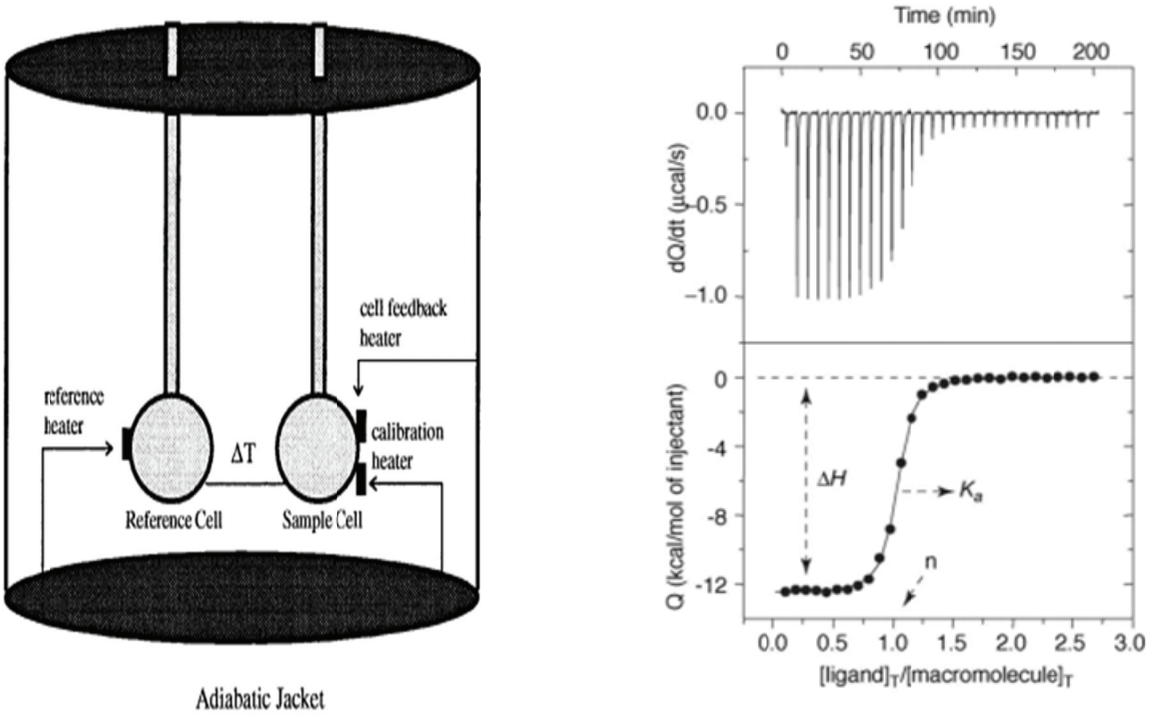

Figure 13: Left: Schematic diagram of an ITC instrument (Pierce et al. 1999). Right: The upper panel shows a typical ITC thermogram while the lower panel shows a typical binding isotherm and how ΔH, K_a, and n are found (Freire 2004).

The observed heat includes not only the heat of interest (the heat of binding), but also the heat of dilution of the protein, the heat of dilution of the ligand, and the heat of mixing. It is therefore important to correct for the unwanted heat effects. Both the heat of dilution of the protein and the heat of mixing are usually negligibly small. The heat of dilution of the ligand is always larger because the starting concentration in the sample cell is zero, and must therefore be removed from the overall heat measured. This can be done by subtracting a linear regression through the last few points of the titration. This is regarded as an approximation for the dilution and mixing heats (Holdgate 2001).

The shape of the isotherm obtained from an ITC experiment depends on what is called the *c*-value (Figure 14), which can be calculated by multiplying K_a by the protein concentration and the stoichiometry of the reaction. An exact estimate of K was originally thought to require a *c*-value between 10 and 1000 (Wiseman et al. 1989), but it is possible to work with low-affinity systems if suitable precautions are taken (Turnbull & Daranas 2003). It is important to use a sufficient portion of the binding isotherm for analysis. This can be obtained by ensuring there is a high ligand to protein molar ratio at the end of the titration, accurate knowledge of the concentrations of both the ligand and the receptor, an adequate signal-to-noise ratio and known stoichiometry. However, large *c*-values prohibit determination of K_a since there are too few data points near equivalence (Pierce et al. 1999).

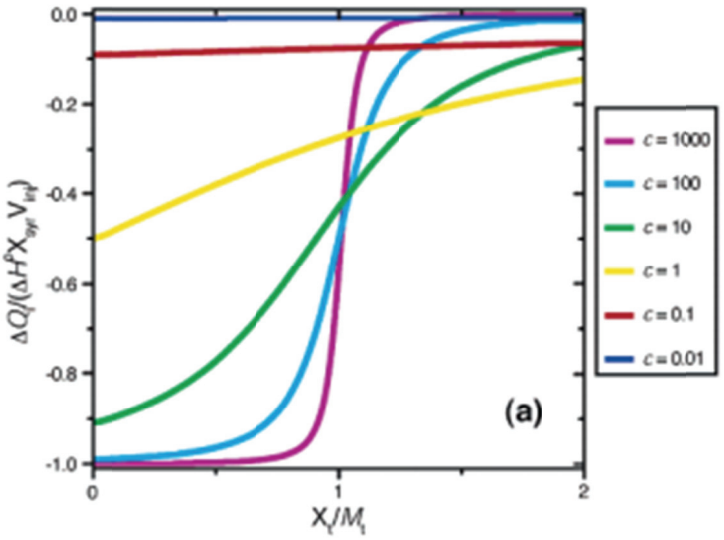

Figure 14: The shape of the ITC isotherm is dependent on the *c*-value (Turnbull & Daranas 2003).

2. Outline

The studies this thesis is based upon were part of a wider project exploring the mechanisms whereby substrate and inhibitors bind to the chitinases of GH family 18. To efficiently degrade the complex and frequently recalcitrant polysaccharide architecture, microorganisms have evolved synergistic cocktails of GHs and accessory enzymes, each of which has a specific function in the degradation. Endo-acting enzymes randomly cleave the polymer chains, whereas exo-acting enzymes preferentially act from either reducing or non-reducing ends. Both endo- and exo-mechanisms can be combined with processive action, meaning that the enzyme hydrolyzes a series of glycosidic linkages along the same polymer chain, producing dimeric products, before dissociation.

To understand how GHs effectively break down recalcitrant polysaccharides, the contributions of each enzyme and their residues must be investigated. In this thesis, the main objective has been to determine the energetic and kinetic contributions of key residues in substrate binding. In this context, the focal topics are processivity, binding strength, stability, positioning, and directionality. The already well-studied chitinolytic machinery of the Gram-negative soil bacterium *Serratia marcescens* has been used in degradation and binding studies of both natural and non-natural substrates to investigate their mechanisms. Both experimental (calorimetry, chromatography and mass spectrometry) and theoretical (molecular dynamics (MD) simulations) approaches have been applied.

In **Paper I** and **Paper II**, the chitinolytic machinery of *Serratia marcescens* is introduced. **Paper I** assessed the rate-enhancing effect of the accessory protein CBP21 by determining apparent catalytic rate constants for two forms of β-chitin degradation by ChiA, ChiB, and ChiC alone and together with CBP21. In **Paper II**, we wanted to further develop a method for measuring processivity by investigating possible correlations between the degree of chitin conversion, apparent processivity, and efficiency. Three dynamic hallmarks have been proposed to be qualitatively related to experimental measurements of processivity: i) the degree of ligand solvation, ii) the magnitude of average atomic fluctuation of the ligand as a function of binding site, and iii) the magnitude of overall fluctuations of key catalytic site residues. The theoretical intrinsic processivity also hypothetically correlates with the binding strength between enzyme and ligand. In section two of this thesis, containing **Paper III** to **Paper V**, these characteristics were addressed

using both experimental and computational approaches (ITC and MD simulations, respectively). In **Paper III** we show results obtained for the wild type enzymes ChiA, ChiB, and ChiC, while **Paper IV** and **Paper V** address functions of specific polar and aromatic residues.

More specifically, in **Paper IV** we explored potential roles of polar residues as such residues have been little investigated. Residues of the exo-processive ChiA were investigated with regard to processivity, binding strength, and substrate positioning. In **Paper V**, we sought to obtain foundations for a general theory on the role of aromatic residues in all processive glycoside hydrolases as this action follows a general mechanism. Residues of both ChiA and ChiB were investigated. These enzymes have opposite directionalities, with ChiA moving from the reducing end and ChiB from the non-reducing end. The mechanisms underlying the different directionalities of ChiA and ChiB were investigated in **Paper VI** by kinetic characterization (k_{cat} and K_m) of the aromatic residues in subsites +1 and +2 to see if the different directionalities are reflected in these parameters.

3. Results and discussion

Chitin is a β-1,4-linked polymer of *N*-acetylglucosamine (GlcNAc) units. It is the second most abundant biopolymer in nature, and hence has enormous biological and economic importance. Microorganisms have evolved potent, synergistic cocktails of GHs and other accessory enzymes that can efficiently degrade carbohydrate polymer chains. Chitin turnover is catalyzed by GHs called chitinases, which can act from both the reducing and non-reducing ends, as well as in an endo mode. The presence of enzymes with different degrees of processivity is also of great importance. The chitinolytic machinery of the soil bacterium *S. marcescens* is often used as a model system for enzymatic degradation of recalcitrant polysaccharides. It has been investigated in detail, but still there are many unresolved questions. The first three papers in this thesis focus on the wild type chitinolytic enzymes produced by *S. marcescens*: ChiA, ChiB, ChiC, and CBP21.

ChiA is a reducing end-specific processive chitinase that moves towards the non-reducing end as the substrate is hydrolyzed. ChiB is a non-reducing end-specific processive chitinase acting towards the reducing end (Horn et al. 2006a; Hult et al. 2005; Igarashi et al. 2014; Perrakis et al. 1994; van Aalten et al. 2000; Zakariassen et al. 2009) while ChiC is a non-processive, endo-acting enzyme (Horn et al. 2006b). CBP21 is an LPMO of AA family 10. The recent discovery of the LPMOs is an important contribution to our understanding of enzymatic degradation of recalcitrant polysaccharides (Levasseur et al. 2013; Phillips et al. 2011; Quinlan et al. 2011; Vaaje-Kolstad et al. 2010). LPMOs exhibit complementary activities to GHs as they induce chain breaks in polysaccharide chains comprising the crystalline material. One of the first studies of CBP21 showed that this enzyme can boost the activity of ChiA, ChiB, and ChiC (Vaaje-Kolstad et al. 2005a). A later, groundbreaking study by Vaaje-Kolstad *et. al* showed that it had an even more pronounced effect when a reducing agent was added (Vaaje-Kolstad et al. 2010). In yet another study, α-chitin substrates of varying particle size and crystallinity were degraded with *S. marcescens* chitinases alone and together with CBP21. ChiB and ChiC activity was clearly boosted by the presence of CBP21, and most strongly when they were degrading the most crystalline substrates. However, ChiA was not generally affected, although a weak effect was seen on its activity with the most crystalline substrates. The results are consistent with the

hypotheses that LPMOs mainly attack crystalline areas of the insoluble substrates and that this crystallinity inhibits many GHs.

The boosting effect of LPMOs had previously only been examined qualitatively. In **Paper I**, we therefore examined the initial rate enhancing effect of CBP21 on its related chitinases. Apparent k_{cat} (k_{cat}^{app}) values were determined for ChiA, ChiB, and ChiC alone and together with CBP21, while degrading 3 μm particulate β-chitin. Samples were collected at regular time intervals, and product formation was monitored by HPLC. In substrate-saturated conditions, the initial rates correspond to V_{max}. From initial rates k_{cat}^{app} values were determined to be $1.7 \pm 0.1 s^{-1}$, $1.7 \pm 0.1\ s^{-1}$, and $1.2 \pm 0.1\ s^{-1}$ for ChiA, ChiB, and ChiC, respectively. Adding CBP21 induced 6- and 9- fold increases in k_{cat}^{app} for the two exo-active chitinases ChiA and ChiB, up to $11.1 \pm 1.5\ s^{-1}$ and $13.9 \pm 1.4\ s^{-1}$, respectively. However, adding CBP21 to the endo-active chitinase ChiC had little or no effect on its k_{cat}^{app} ($0.9 \pm 0.1\ s^{-1}$). These results clearly show a rate enhancing effect of CBP21 on ChiA and ChiB. Previously, it was shown that the addition of CBP21 also boosts the activity of ChiA, ChiB, and ChiC when added during the reaction, having a "rescuing effect" on the chitinases (Vaaje-Kolstad et al. 2005a). Thus the presence of an LPMO also helps in removing obstacles on the substrate, creating longer obstacle-free paths. However, the results shown in **Paper I** partially conflict with conclusions of Vaaje-Kolstad et al. and Nakagawa et al. (Nakagawa et al. 2013; Vaaje-Kolstad et al. 2010). It has been suggested that LPMOs create new chain ends, thereby generating new attack points on the recalcitrant polysaccharides (Vaaje-Kolstad et al. 2010). In contrast, our finding that only endo-active ChiC was unaffected implies that there are sufficient attack points for the enzyme and thus CBP21 is redundant. This can be explained by the substrate saturating conditions that were used. The substrate to enzyme ratio was significantly lower in the study by Vaaje-Kolstad and co-workers. The non-existing effect of ChiA on α-chitin was explained by different possible target regions. In that respect it is worth noting that α-chitin consists of more tightly packed chitin chains than β-chitin (Blackwell 1969; Minke & Blackwell 1978).

As already mentioned, many polymer active enzymes act in a processive manner. This means that they bind individual polymer chains in long tunnels or deep clefts and hydrolyze a series of glycosidic linkages along the same chain before they dissociate (Davies & Henrissat 1995; Rouvinen et al. 1990). Intrinsic processivity (P^{Intr}) is the theoretical potential for processive ability, typically in the range of 1000. However, the actual processive ability observed in experiments is more than a magnitude lower. This is defined

as apparent processivity (P^{app}) and varies, depending on both the substrate and conditions (Cruys-Bagger et al. 2013; Horn et al. 2012a; Kurasin & Väljamäe 2011). Real substrates often contain structural heterogeneities or steric obstacles that influence the probability of dissociation. Such steric obstacles may include aggregates of microcrystals, entangled structures, or bound non-substrate substances. Consequently, it has been hypothesized that P^{app} is limited by the average length of the obstacle-free path on the substrate (Cruys-Bagger et al. 2013; Jalak & Väljamäe 2010; Kurasin & Väljamäe 2011). Thus, processive runs are generally halted long before the enzyme randomly dissociates from the strand and P^{app} deviates from P^{Intr}. When enzymes encounter an obstacle on the substrate they get stuck and cause so-called traffic jams due to the low dissociation constants (k_{off}) of processive cellulases (Igarashi et al. 2011; Shang et al. 2013). k_{off} is therefore rate-limiting, preventing enzyme recruitment, and as an overall result slowing the rate of polymer degradation (Cruys-Bagger et al. 2013; Jalak & Väljamäe 2010). It is also worth noting that for chitinases, k_{on} seems to be rate limiting (Kuusk et al. 2015; Zakariassen et al. 2010).

In **Paper II**, P^{app} values for ChiA, ChiB, ChiC, and the ChiB mutant W97A were assessed by determining $[(GlcNAc)_2]/[GlcNAc]$ ratios by HPLC, and comparing the ratios to degrees of chitin conversion. The results showed that P^{app} values continuously declined in assays with the exo-enzymes ChiA and ChiB. Thus, as the substrate becomes increasingly depolymerized, the data suggest that it also becomes more recalcitrant. Shorter obstacle-free paths are therefore likely to be present, as previously discussed for cellulose hydrolysis (Cruys-Bagger et al. 2013; Jalak & Väljamäe 2010; Kurasin & Väljamäe 2011), thus affecting P^{app}. The diminishing trend for P^{app} was less clear for ChiC and ChiB-W97A. It seems that endo-active enzymes, such as ChiC, are less dependent on processivity and that their mode of catalysis is controlled more by substrate accessibility. In the light of these results, we strongly urge the use of initial P^{app} values. Initial degradation rates show that ChiA and ChiB are the two most processive chitinases ($P^{app} = 30.1 \pm 1.5$ and $P^{app} = 24.3 \pm 2.0$, respectively). As expected, the non-processive ChiC and ChiB-W97A show significantly lower ratios than ChiA and ChiB ($P^{app} = 14.3 \pm 1.4$ and $P^{app} = 11.0 \pm 1.8$, respectively).

When measuring apparent processivity, several potential pitfalls must be taken into consideration, as discussed in the Introduction (section 1.2.4.1). When using the $[(GlcNAc)_2]/[GlcNAc]$ method in particular, one must take special care as there are no *a priori* reasons to assume that the first cleavage exclusively yields an odd numbered

oligosaccharide. Different enzymes can have different preferences for the orientation of the chain end relative to the polymer surface and different probabilities of endo-mode initiation. The formation of soluble intermediate products may also interfere with the results (Horn et al. 2012a). However, our results are consistent with recent estimates from a HS-AFM study showing that half-lives of processivity were 21 and 13 for ChiA and ChiB, respectively (Igarashi et al. 2014). These values can be converted to processivity values by dividing by ln2 (Nakamura et al. 2014) leading to processivity values of 30.3 and 18.8, respectively.

Furthermore, the results presented in **Paper II** show a correlation between P^{app} and efficiency. ChiA, ChiB, and ChiC degraded chitin to extents of approximately 75, 45, and 30 %, respectively. Thus, the more degraded the chitin is, the more processive the enzyme. This is in line with previous indications that this correlation may be generally valid for many enzyme-substrate systems. In this context, it is worth noting that enzymes with reduced activity towards chitin can experience a strong increase in their activity towards water-soluble chitosan (Horn et al. 2006a; Zakariassen et al. 2009). The efficiencies presented in **Paper II** conflict with findings of a previous comparative study of ChiA, ChiB, and ChiC suggesting that ChiA and ChiC have the ability to degrade chitin completely, although some polymeric substrate remained after degradation with ChiB (Horn et al. 2006c). The apparent discrepancy is likely due to the use of different β-chitin variants, leading to varying lengths of obstacle-free paths on the substrate and differences in the formation of traffic jams. In **Paper II**, 180 μm microparticulate β-chitin was used, while Horn and co-workers used 3 μm microparticulate β-chitin. To investigate synergistic effects, effects of different combinations of chitinases on P^{app} and degree of degradation were examined. P^{app} did not increase, but diminished to an intermediate state between values recorded for the individual enzymes, but the degree of degradation increased to nearly 100 % for all tested combinations.

Finally, P_{app} was also determined for ChiA acting on α-chitin, yielding a value of 14.2 ± 0.5. This is significantly lower than the value determined for β-chitin (30.1 ± 1.5). A general finding from **Paper I** and **Paper II** is that it is important to report the exact specifications of the substrate used. Different substrates and substrate to enzyme ratios yield different results. It must also be emphasized that the processed substrates used in such research are different from the substrates the chitinolytic enzymes encounter in nature.

Paper I and **Paper II** revealed differences among the chitinases with regard to activation, efficiency and processivity. Processivity has previously been shown to be related to the topology of the active sites of the enzymes (Davies & Henrissat 1995). In this respect: ChiA has a relatively open active site cleft, a typical feature of endo-acting enzymes (Davies & Henrissat 1995; Perrakis et al. 1994); ChiB has a partially closed active site cleft, leading to a more tunnel-like active site topology that is frequently observed in exo-acting enzymes (Davies & Henrissat 1995; van Aalten et al. 2000); and ChiC has a shallow substrate binding cleft (Payne et al. 2012). We therefore hypothesized that the innate differences between the chitinases will be reflected in their thermodynamic signatures upon substrate binding. This hypothesis, and the suggestion from a recent computational study that ligand binding free energy and the degree of processivity are positively correlated (Equation 1) (Payne et al. 2013), were tested in **Paper III.**

In **Paper III**, both computational and experimental approaches were used to determine changes in free energy, enthalpy, and entropy upon substrate binding and the molecular-level contributions to these parameters. Free energy changes ($\Delta G°$) of binding hexa-*N*-acetylglucosamine, $(GlcNAc)_6$, to ChiA, ChiB, and ChiC were determined using ITC and free energy perturbation with Hamiltonian replica exchange molecular dynamics (FEP/λ-REMD) (Deng & Roux 2006; Jiang et al. 2009; Jiang & Roux 2010). The $\Delta G°$ values were compared to P_{app} values presented in **Paper II**. As mentioned, initial P^{app} values were determined to be 30.1 ± 1.5, 24.3 ± 2.0, and 14.3 ± 1.4 for ChiA, ChiB, and ChiC respectively. The hypothesized correspondence between less favorable binding free energy changes ($\Delta G°_b$) and low processive ability was indeed observed using the FEP/λ-REMD measurements. $\Delta G°_b$ is most beneficial for ChiA (−16.7 ± 1.4 kcal/mol), followed by ChiB (−15.2 ± 1.3 kcal/mol), while the value for the less processive ChiC is substantially less favorable (−9.6 ± 1.6 kcal/mol).

However, ITC data are not necessarily consistent with the data obtained from FEP/λ-REMD simulations. The two methods only yielded the same free energy change for ChiC ($\Delta G_r° = -9.7 \pm 0.1$ kcal/mol and $\Delta G°_b = -9.6 \pm 1.6$ kcal/mol, respectively). ChiA and ChiB bind the hexamer with approximately the same affinity, −8.7 ± 0.1 kcal/mol and −9.3 ± 0.1 kcal/mol, respectively. Given the accuracy of the ChiC data, there are probably physical issues regarding ChiA and ChiB rather than computational errors. In all FEP/λ-REMD simulations, $(GlcNAc)_6$ was first docked so that it covered four substrate-binding and two

substrate-releasing subsites (subsite −2 to +4 for ChiB and subsite −4 to + 2 for ChiA and ChiC). It has been proposed that ChiB has a 80 % preference for such binding, while $(GlcNAc)_6$ will occupy subsite −3 to +3 in 20 % of the scenarios (Horn et al. 2006c). Binding preferences have not been determined for $(GlcNAc)_6$ in ChiA, but $(GlcNAc)_5$ binding analyses indicate that there is powerful substrate affinity in subsite +3 (unpublished results; (Horn et al. 2006c; Norberg et al. 2011). FEP/λ-REMD simulations were therefore also performed for the −3 to +3 scenario, giving $\Delta G°_b$ values of −13.4 ± 1.9 kcal/mol and −6.2 ± 1.5 kcal/mol for ChiA and ChiB, respectively. These values are closer to the experimental values indicating both that ITC provides a mean value for all the different binding modes and that experimental conditions during ITC measurements may bias the results. In order to assess the free energy change the enzymes must be catalytically inactivated, thus they may not bind the hexamer in the same way as the wild-type enzymes during productive binding. Furthermore, two stages are observed in an enzyme reaction. The substrate binds reversibly to the enzyme, forming what is called a Michaelis complex before the enzyme catalyzes the chemical step and releases the product. The Michaelis complex is surely formed in a FEP/λ-REMD simulation, but in an ITC experiment the degree to which the complex is formed is uncertain. A Stoddart diagram shows the possible conformational routes that might be followed by a pyranoside ring as it moves from one conformation to another (Figure 15, left panel) (Stoddart 1971). Based on this diagram, Biarnes and co-workers have computed a free energy landscape for glucopyranose ring conformations based on β-D-glucopyranose. These diagrams show approximate energetic barriers for transitions from one conformation to another (Biarnes et al. 2007). The *N*-acetyl glucosamine unit situated in subsite −1 changes from the relaxed $^4C_1$ chair conformation to a distorted boat conformation prior to hydrolysis (Brameld & Goddard 1998). The energetic barrier corresponds to a value of ~ 8 kcal/mol, but the energy landscapes show that some of the possible conformational routes chitinases pass through have even higher energetic barriers, in the range of 10-15 kcal/mol (Biarnes et al. 2007). Thus, even small deviations in the Michaelis-complex are likely to influence the binding free energy values strongly.

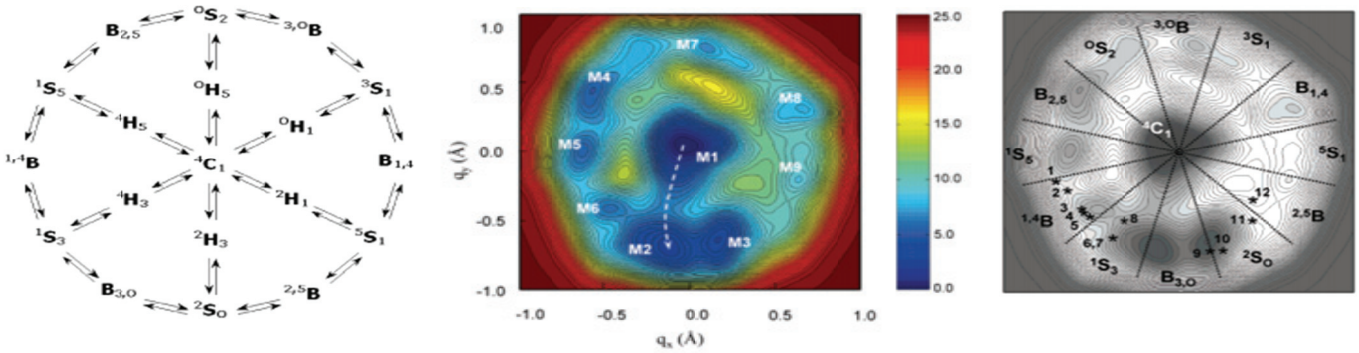

Figure 15: Left: Stoddart's diagram (Stoddart 1971). The *N*-acetyl glucosamine unit positioned in subsite −1 of GH18 chitinases changes from $^{4}C_{1}$ to $^{1,4}B$ before hydrolysis. Middle: Computed free energy landscape of β-D-glucopyranose with respect to ring distortion. Energy values are given in kcal/mol (Biarnes et al. 2007). Right: Distribution of the conformations on the computed free energy surface. ChiA and ChiB are marked 1 and 2, respectively (Biarnes et al. 2007).

In **Paper III** we also addressed the solvation and conformational entropy of ChiA, ChiB, and ChiC. Solvation entropy is the change in entropy due to solvation of water molecules upon ligand binding. Water is a versatile component that is often present at interfaces of biomolecular complexes. It is adaptable to its surroundings as it can act both as a hydrogen bond donor and acceptor having few steric limitations on bond formation. Binding between biomolecules is usually accompanied by the displacement of bound water molecules from the binding sites and formation of direct interactions (Ladbury 1996). The combination of direct interactions that occur and the solvation interactions lost will determine if the binding is favorable, neutral, or unfavorable (Li & Lazaridis 2005). A water molecule located at a protein-ligand interface can make a favorable contribution to binding affinity and also increase the stability of the complex. The entropic cost of trapping water molecules is assumed to be large, and an interface with no space between the interacting protein and the ligand will have a higher binding affinity, K_d, than if the gap is full of water. In some cases, however, the enthalpy gained from the formation of extra water-mediated hydrogen bonds is greater than the entropic penalty incurred by immobilizing the water involved (Ladbury 1996; Li & Lazaridis 2005). The binding free energy of a bound water molecule depends on where it is located, but internal and external water molecules appear to interact with proteins almost equally. However, a water molecule coupling a protein and

ligand is particularly beneficial, with a value of −1.13 kcal/mol. Here, the energetic contributions are shared equally between the protein and ligand (Amadasi et al. 2006).

The change of solvation entropy ($\Delta S_{solv}°$) was determined for the three chitinases through the temperature dependency of $\Delta H_r°$ (Equation 8) and the relationship to the change in heat capacity (Equation 6). The results show that ChiA is significantly more desolvated than ChiB and ChiC upon binding to $(GlcNAc)_6$, having a $\Delta S_{solv}°$ of −17.5 kcal/mol compared to −11.5 kcal/mol for the latter two. In 2012, Payne et al. proposed that there are correlations between processivity and three dynamic features of the catalytic domain, one of which is a positive correlation with solvation (Payne et al. 2012). MD simulations of active site solvation supported the experimental estimates insofar that they showed ChiA to be the most desolvated chitinase upon binding to $(GlcNAc)_6$. Moreover, the MD simulations showed that ChiB is less desolvated than ChiA, but more desolvated than ChiC, in accordance with the P^{app} values already discussed (**Paper II**).

The thermodynamic characterization of the binding of the three chitinases to the family 18 inhibitor allosamidin, which binds from subsite –3 to −1 (Papanikolau et al. 2003; van Aalten et al. 2001), has previously been performed (Baban et al. 2010; Cederkvist et al. 2007). With simplification, the solvation entropy change for binding to the positive subsites can be obtained by subtracting the solvation entropy change associated with allosamidin binding from the solvation entropy change associated with $(GlcNAc)_6$ binding. The results suggest that ChiA is most desolvated in positive subsites, ChiC in negative subsites while the contribution from positive and negative subsites is equal in ChiB (Figure 16). Studies on ChiA have shown that it has a powerful substrate affinity in subsite +3 (unpublished results; (Horn et al. 2006c; Norberg et al. 2011). The crystal structure of ChiA is more open towards the solvent in subsite +3 than, for example, in subsite −3, possibly explaining why ChiA is more desolvated in positive subsites. It is important to underline that these results are simplifications. A beneficial change in the solvation entropy may also be caused by release of entropically constrained water molecules and not necessarily reflect the number of water molecule released on the surface of the protein.

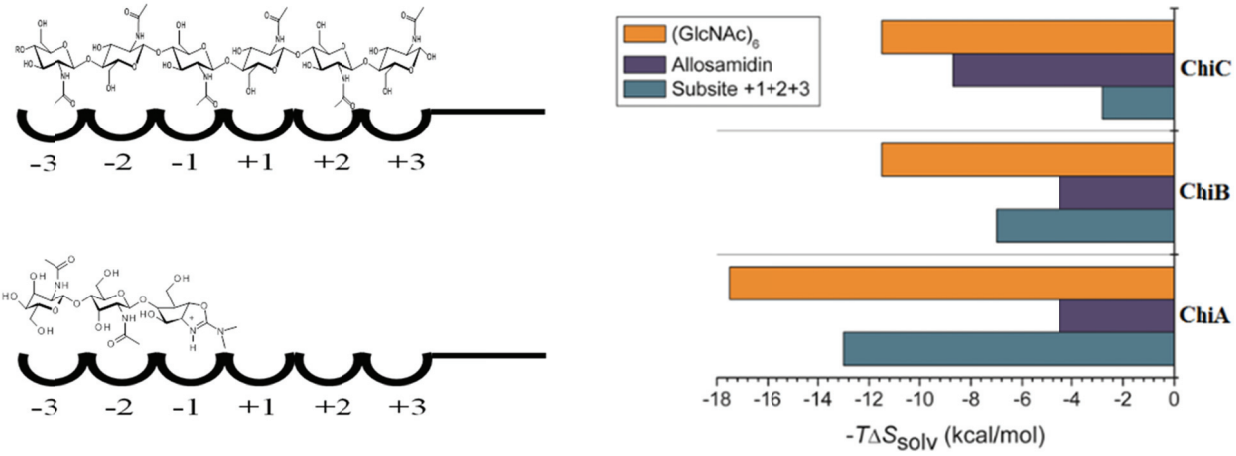

Figure 16: Left: Chemical structures of $(GlcNAc)_6$ (top) and allosamidin (bottom) aligned in their respective subsites. Right: Schematic representation of $-T\Delta S_{solv}°_{(GlcNAc)6}$ (cyan), $-T\Delta S_{solv}°_{allosamidin}$ (blue), and $-T\Delta S_{solv}°_{subsite\ +1,+2,+3}$ (orange) for ChiA, ChiB, and ChiC.

The conformational entropy relates to changes in conformational freedom for both the ligand and protein. It is usually unfavorable since binding leads to loss of conformational freedom for both molecules (Freire 2004). The relationship between $\Delta S_r°$, $\Delta S_{mix}°$, $\Delta S_{conf}°$, and $\Delta S_{solv}°$ described in equation 5 shows that the conformational entropy is unfavorable for ChiA and ChiC (10.9 kcal/mol and 7.2 kcal/mol respectively) while it is more or less neutral for ChiB (−0.1 kcal/mol). Root Mean Square Fluctuations (RMSFs) of the proteins over the course of 250-ns MD simulations revealed that conformational freedom in the protein structure upon ligand binding correlated well with the experimental observations for ChiA and ChiB. ChiA is rigidified upon binding, corresponding to the unfavorable ΔS_{conf}, while the flexibility of ChiB with the ligand bound from −3 to +3 is only very slightly affected. The relationship of ChiC's flexibility to conformational entropy contributions is not as obvious as for ChiA and ChiB. In general, longer ligands, e.g. $(GlcNAc)_6$ are more flexible than shorter ligands (e.g. allosamidin) and are more likely to lock proteins upon binding due to the higher number of interaction contacts. Accordingly, the results show that $-T\Delta S_{solv}$ is 9 ± 1 kcal/mol higher when binding to $(GlcNAc)_6$ than when binding to allosamidin, for all three chitinases.

Paper III shows that theoretical and experimental data mostly correlate, although they do not always give identical values. Therefore, we sought to extend knowledge of the free energy changes and their correlation with processivity by investigating contributions of key polar and aromatic residues in the exo-processive chitinases ChiA and ChiB. Although they have been little studied, polar residues are also important for carbohydrate-protein interactions due to their ability to form hydrogen bonds. A sugar-hydroxyl group, for example, may potentially be involved in as many as three hydrogen bonds; one as a donor and two as an acceptor (Vyas 1991). Compared to the hydrophobic stacking interactions, involving aromatic residues, hydrogen bonds are more specific and have smaller interaction surfaces. Processivity is therefore thought to be facilitated by the hydrophobic stacking interactions since they reduce the sliding energy of the polymers and function as flexible and fluid-like sheaths that the polymers can slide along (Divne et al. 1998; Varrot et al. 2003).

In 1997, Meyer and Schulz showed that a combination of hydrogen bonding and hydrophobic interactions contribute to the total energy profile of a maltooligosaccharide – maltoporin model. The total energy profile is smooth, promoting processivity since the rather high energy barriers are reduced. The energy profiling also showed that the energy minima of the aromatic stacking interactions tend to compensate for the maxima of the polar interactions (Meyer & Schulz 1997) underlining the importance of both interaction forms.

In a later study, Varrot et al. solved five high-resolution structures of the *Humicola insolens* Cel6A in complex with non-hydrolysable thio-oligosaccharides, and explored that the enzyme must tolerate intermediate states of non-productive binding during a processive run (Varrot et al. 2003). Subsite −1 is highly optimized for productive binding and must be able to accommodate both faces of the pyranoside rings. In addition, the crystal structures revealed a third binding mode, intermediate between the former two. Further investigation of the binding modes identified interactions involved, and how sliding might occur in a processive mechanism. The productive binding mode involves a large number of hydrogen bonds between the ligand and protein, whereas the non-productive binding modes are mostly facilitated by indirect hydrogen bonding and complex networks of solvent-mediated interactions. Productive binding to subsite −1 involves three direct hydrogen bonds, compared to only one in the non-productive binding mode. The structures also showed that the tryptophan residues in the substrate binding cleft can tilt, thus being flexible and able to align with the sugar rings in both binding modes.

The studies by Meyer, Varrot and their respective colleagues showed that both aromatic and polar residues play important roles in the catalytic hydrolysis of *O*-glycosidic linkages. To elucidate the potential and probable roles of polar residues in our focal chitinolytic system the crystal structure of ChiA in complex with $(GlcNAc)_6$ was studied (pdb code 1EHN, Figure 17) (Perrakis et al. 1994). It revealed several important intermolecular interactions between substrate and enzyme in the substrate binding subsites −2, −3, and −4. The aromatic residue Trp^{167} situated in subsite −3 has previously been shown to be crucial for binding and positioning of a polymeric substrate as well as in processive hydrolysis (Norberg et al. 2011; Zakariassen et al. 2009). Thus, roles of two of the polar residues involved in the intermolecular interactions, Arg^{172} and Thr^{276}, were examined in **Paper IV** (Figure 17).

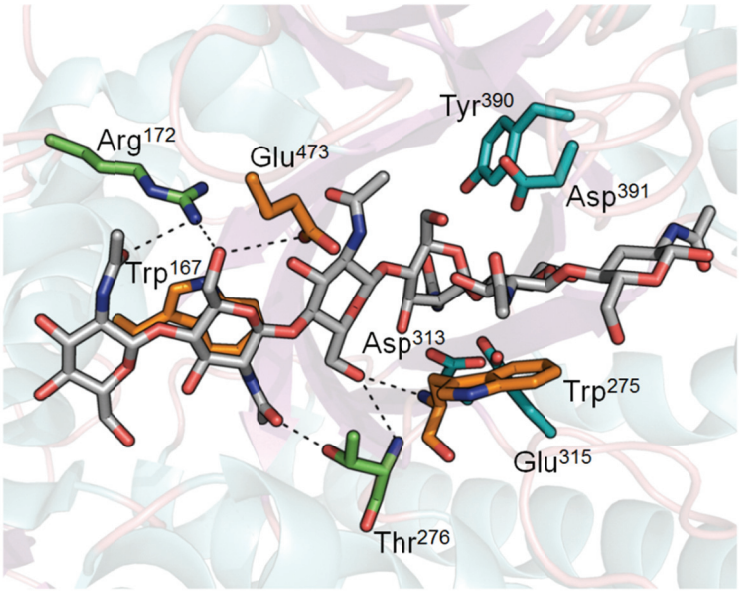

Figure 17: Crystal structure of the active site of ChiA in the presence of $(GlcNAc)_6$. Highlighted in green are the two residues investigated in this study (Thr^{276} and Arg^{172}). Other important substrate binding residues (Trp^{167}, Glu^{473}, Asp^{313} and Glu^{315}) are highlighted in orange while product-binding residues (Trp^{275}, Tyr^{390} and Asp^{391}) are shown in cyan.

First the relationship described in Equation 1 and investigated in **Paper III** was further examined. The free energy change for the soluble substrate $(GlcNAc)_6$ and the well-known

inhibitor allosamidin, and the degrees of processivity of ChiA-WT, ChiA-R172A, and ChiA-T276A were determined by ITC and the [$(GlcNAc)_2$]/[GlcNAc] ratio (**Paper II**), respectively. Catalytically inactivated enzymes must be used when $(GlcNAc)_6$ is the ligand while the system is perturbed less when using allosamidin in combination with catalytically active enzymes. The results show that the initial P_{app} value for ChiA-R172A is only slightly reduced compared to ChiA-WT (P^{app} = 25.9 ± 0.9 and 30.1 ± 1.5, respectively), while the reduction is more substantially for ChiA-T276A (P^{app} = 17.1 ± 0.4). Examination of free energy changes shows a correlation between P_{app} and binding strength. The free energy change is significantly reduced towards both $(GlcNac)_6$ and allosamidin for the less processive ChiA-T276A, and the reduction is largest for allosamidin binding.

Moreover, computational analyses (molecular dynamics simulations) support the conclusion that ChiA-WT and ChiA-R172A behave similarly, while ChiA-T276A is clearly different. Three characteristic measurements of active site dynamics were determined from 250-ns MD simulations of the three enzymes: the RMSF of the bound $(GlcNAc)_6$ ligand, the RMSF of the protein catalytic center, and the −1 pyranose ring pucker amplitude. Each of these measurements indirectly reflects binding affinity. As expected, the results show that enzymes with more flexible/dynamic active sites have lower binding affinity and processive ability. Both the RMSF of the ligand and the catalytic center have previously been hypothesized to be "hallmarks" of processivity (Payne et al. 2012), but the cited study focused only on general differences between processive and non-processive chitinases. In **Paper IV** we show that the observed relationship between active site dynamics and processive ability is also applicable to mutants of the same enzyme.

In addition to the reduction in free energy change for ChiA-T276A compared to ChiA-WT, a significant, larger reduction in the enthalpy change was detected and, again, the reduction was larger for allosamidin than for $(GlcNAc)_6$ binding. The changes in $\Delta H_r°$ reflect changes in weak interactions (i.e. hydrogen bonds, electrostatic and polar interactions) between the ligand and the enzyme compared to those with the solvent. An enthalpy-entropy compensation, where removal of a strong binding interaction may allow for a gain in entropy through greater flexibility of the protein backbone, negates full conversion of the reduced enthalpy change into a free energy change (Cooper et al. 2001).

In accordance with the results presented in **Paper II** we found that the degree of processivity correlates with the extent of chitin degradation. ChiA-WT and ChiA-R172A

have a higher initial degree of processivity than ChiA-T276A and are also more efficient degraders of β-chitin. Under our experimental conditions, 75, 50, and 20 % of the added β-chitin was degraded by ChiA-WT, ChiA-R172A, and ChiA-T276A, respectively.

A possible role for Arg^{172} was revealed by determination of the sequences of deacetylated and acetylated sugar moieties in the products of chitosan hydrolysis. As previously seen for the subsite −3 mutant ChiA-W167A (Norberg et al. 2011), ChiA-R172A has no strong preferences for acetylated/deacetylated units except for the absolute preference for an acetylated unit in subsite −1. In contrast, both the wild type and ChiA-T276A have clear preferences for acetylated units in subsites −1, −2, −4 and −1, −3, and −4, respectively. These findings suggest that Arg^{172} participates in the recognition and positioning of the substrate in the active site and that Thr^{276} does not determine the location of acetyl groups along the cleft.

Paper IV provides both experimental evidence and simulation results showing that polar residues can play a key role in processivity. Many of the aromatic residues lining the active sites in glycoside hydrolases have previously been studied. In **Paper V** and **Paper VI**, roles of specific residues that are important for both processivity and directionality in ChiA and ChiB were addressed. These enzymes are complementary, acting processively in opposite directions (Hult et al. 2005; Igarashi et al. 2014). More specifically, effects of four mutations in substrate binding subsites (ChiA-W167A (−3), ChiB-W97A (+1), ChiB-W220A (+2), and ChiB-F190A (+3)) and two in product releasing subsites (ChiA-W275A (+1) and ChiA-F396A (+2)) were investigated (Figure 19).

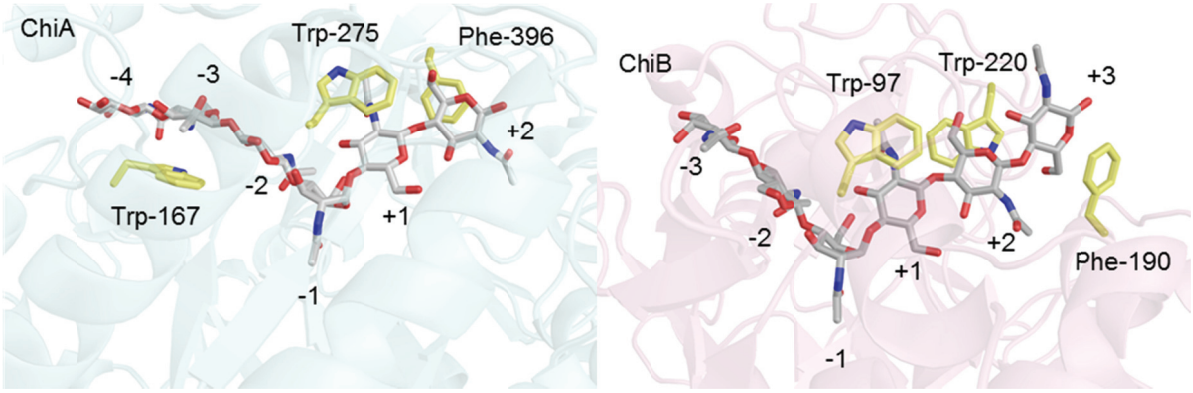

Figure 19: The catalytic active sites of ChiA (left) and ChiB (right), from subsites −4 to +2 and subsites −3 to +3, respectively. The $(GlcNAc)_6$ ligand is shown in stick with grey carbons. The aromatic residues are shown in stick with yellow carbons.

Cellulose, β-1,4 linked D-glucopyranose, is also degraded by GHs. The only difference between chitin and cellulose is the *N*-acetyl group in chitin (Figure 18). In chains of both compounds sugar units are successively rotated 180° relative to each other so the smallest structural unit is a disaccharide (Gardner & Blackwell 1975).

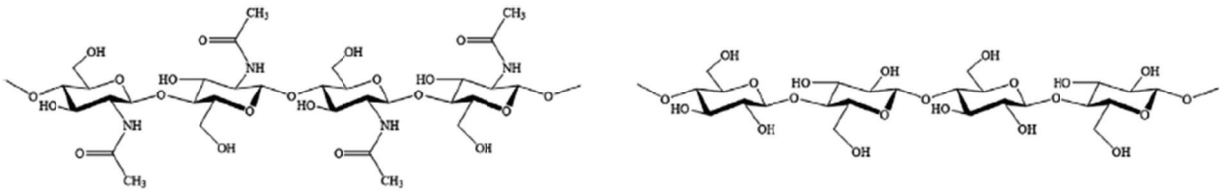

Figure 18: The chemical structure of chitin and cellulose (left and right, respectively).

Interestingly, cellulose-degrading enzymes are classified into a total of 21 GH families, mostly families 5, 6, 7, 8, 9, 12, 44, 45, and 48 (Lee 2013; Lombard et al. 2014). However, chitinases are only found in two families: GH families 18 and 19 (Lombard et al. 2014). Families 7 and 48 contain processive exocellulases moving from the reducing end, and all use the retaining mechanism. Processive exocellulases moving in the opposite direction are found in family 6, using the inverting mechanism (Barr et al. 1996; Lombard et al. 2014; Wilson & Kostylev 2012). Some processive endo-cellulases belonging to families 5 and 9

have recently been discovered (Sakon et al. 1997; Watson et al. 2009). In contrast, all GH18 enzymes use the same retaining substrate-assisted mechanism, but differ in several aspects of their mode of action (Terwisscha van Scheltinga et al. 1995; Tews et al. 1997; van Aalten et al. 2001). This family contains both endo- and exo active enzymes, both processive and non-processive enzymes, and enzymes with different directionalities of processivity (Horn et al. 2006a; Hult et al. 2005; Igarashi et al. 2014; Vaaje-Kolstad et al. 2013; Zakariassen et al. 2009). There are also differences between chitinases and cellulases with regard to their catalytic domains. A common feature of all chitinases is a catalytic domain consisting of a $(\beta/\alpha)_8$ TIM barrel fold with important catalytic residues and two conserved diagnostic motifs (Suzuki et al. 1999; Terwisscha van Scheltinga et al. 1996). In contrast, cellulases have a large variety of folds, i.e. the TIM-barrel, βαβ-barrel, β-sandwich and α-helix circular array (Himmel et al. 1997).

It is of great interest to unravel and explain the large differences between cellulases and chitinases as their substrates are fairly similar. Thus, in **Paper V** we explored the relationships between the aromatic residues, processivity, and free energy changes, using the complementary enzymes ChiA and ChiB as model system. The intention was to define the roles of each residue and in a long term perspective obtain foundations for a general interaction mechanism across various carbohydrate active enzyme families. Previous work has shown that ChiA-W167A, ChiA-W275A, ChiA-F396A, ChiB-W97A, and ChiB-W220A have reduced degrees of processivity with crystalline chitin, relative to the respective WT enzymes. They have also reduced activity towards chitin, but increased activity towards chitosan (Horn et al. 2006a; Zakariassen et al. 2009). The reduction in processivity is largest for residues situated in substrate-binding subsites. Unpublished, initial P_{app} values determined by measuring the initial $[(GlcNAc)_2]/[GlcNAc]$ ratio (**Paper II**) show no effect on processivity for ChiB-F190A (23.5 ± 2.0 versus 24.3 ± 2.0 for ChiB-WT).

In **Paper V**, the free energy changes for the six aromatic residues were obtained experimentally from ITC and computationally from thermodynamic integration (TI). For direct comparison with computational results, free energy changes relative to wild-type, $\Delta\Delta G_{ITC}$, was determined by subtracting the free energy change of binding $(GlcNAc)_6$ to the wild-type from the free energy change of binding $(GlcNAc)_6$ to the mutant. The experimental and computational $\Delta\Delta G$ values are generally well aligned within the capabilities of each technique. As discussed for **Paper III**, we expect that the discrepancies

observed are due to location and binding conformation of $(GlcNAc)_6$ rather than errors in either method.

In both ChiA and ChiB, four residues have been implicated as participants in the substrate assisted catalytic mechanism (Asp^{313}, Glu^{315}, Tyr^{390}, and Asp^{391} in ChiA and Asp^{142}, Glu^{144}, Asp^{215}, and Tyr^{214} in ChiB) (Aronson et al. 2006; Brameld & Goddard 1998; Tews et al. 1997; van Aalten et al. 2001). Flexibility of the catalytic center, as measured by the RMSF of the catalytic tetrad may, as already mentioned, be associated with reduced substrate chain association (k_{on}) and likely reduced processivity (Payne et al. 2012). RMSF is a measure of the degree to which the ligand fluctuates about an average position. Higher values correspond to a higher degree of freedom. The RMSFs of carbohydrate ligands bound in the active sites of GHs have also been linked to the processive function of these enzymes (Payne et al. 2012). Thus, RMSFs were determined for the $(GlcNAc)_6$ ligand bound to the wild type enzymes and the six alanine mutants.

In ChiA, the free energy changes of ChiA-W167A and ChiA-W275A are quite unfavorable, suggesting these residues play important roles in tight binding. This is also illustrated by enhanced flexibility of their respective active sites and the flexibility of the $(GlcNAc)_6$-ligand across the cleft. Trp^{167} is largely responsible for maintaining the shape of the substrate-side of the ChiA-cleft. Replacing Trp with Ala reduces the ligand contact with the protein, and the normally strained ligand relaxes into the newly opened protein space to maintain protein interactions. In ChiA-W275A, the catalytic residues fluctuate significantly, indicating $(GlcNAc)_6$ is no longer productively bound. As Trp^{275} occupies an important position in product-binding subsite +1, it can also be implicated that it has a role in product stability. The $\Delta\Delta G$ value for ChiA-F396A is almost negligible and the mutation has relatively little effect on the dynamics of either the protein or the ligand, implying that it has little or no role in ligand binding. This is consistent with an slight reduction in processivity for this residue (Zakariassen et al. 2009).

Relative free energy changes are quite unfavorable for ChiB-W97A and ChiB-W220A, suggesting they are key residues in tight binding, enabling the enzyme to remain attached to the crystalline substrate throughout processive action. This is in line with the hypothesis that increased binding affinity correlates with increased processivity (Payne et al. 2013) and that substrate-side tight binding may have the highest impact on processive ability (Igarashi et al. 2014). In contrast to ChiA-W167A and ChiA-W275A, RMSFs for ChiB-W97A and

ChiB-W220A show localized ligand destabilization, mainly increasing the flexibility of substrate-binding subsites +2 and +3. The catalytic tetrad fluctuates more than in ChiB-WT. These findings correlate with the previously discussed dynamic hallmarks of processivity (Payne et al. 2012). Further, it seems that ChiB-F190A only has a minor role in ligand binding since the $\Delta\Delta G$-value is almost negligible. However, this mutant has the same effects on RMSFs as the other ChiB-mutants. Phe^{190} and Trp^{220} are localized on opposite sides of the active site cleft, sandwiching the ligand. This affords the ligand stability in the ChiB cleft. By studying the local dynamics of these residues to the +3 pyranose ring **Paper V** shows that removal of Phe^{190} enhances the interactions between the pyranose ring and Trp^{220}. It is also seen that when Phe^{190} is mutated to alanine, the ligand fluctuates in subsite +3, but the proximity of the +3 sugar to Trp^{220} is increased. We suggest that Phe^{190} might have a role in substrate recruitment, but multiple sequence alignment shows, surprisingly, that Phe^{190} is not a conserved residue, in contrast to Trp^{97} and Trp^{220}. Thus it is likely that ChiB has not developed a function requiring a bulky, hydrophobic residue in this position.

Overall, the results show that the residues near the entrance (ChiB-F190) or the exit (ChiA-F396) do not seem to affect binding affinity and processivity. In Cel6A from *T. reesei,* however, the pattern seems to be opposite, although both ChiB and *T. reesei* Cel6A are non-reducing end specific processive GHs. The ChiB-F190-like residue Trp^{272} at the catalytic cleft entrance in Cel6A negates activity on insoluble cellulosic substrates when mutated to alanine (Payne et al. 2011). Further, the results show that aromatic residues close to the catalytic center maintain hydrophobic π-stacking interactions with $(GlcNAc)_6$ and hence play a significant role in binding affinity and processivity. The reducing end-specific processive *T.reesei* cellobiohydrolase Cel7A-W367A and the non-processive *T.reesei* cellobiohydrolase Cel7B-W329A both situated in subsite +1 show the same unfavorable relative free energy change (Taylor et al. 2013) as ChiA-W275A. Finally, the results provided in **Paper V** show that aromatic residues may behave differently in different GHs even if they have similar positions. Thus, the free energy change alone is not sufficient to generalize the role of aromatic residues.

Overall, **Paper III** to **V** show positive correlations between processivity and free energy change of both wild type chitinases and variants with mutations of key polar and aromatic residues, thus confirming the hypothesis by Payne et al. (Payne et al. 2013). Along with this hypothesis, three dynamic hallmarks of processivity were suggested; i) the degree of ligand solvation, ii) the magnitude of average atomic fluctuation of the ligand as a function of

binding site, and iii) the magnitude of overall fluctuations of key catalytic site residues (Payne et al. 2012). These hallmarks have been shown using a combination of theoretical and experimental approaches or by computational methods alone, to be applicable to a real system of glycoside hydrolases, namely the chitinolytic machinery of *S. marcescens*.

As previously discussed, the residues located in subsites +1 and +2 in ChiA and ChiB serve different roles. In ChiA, they are product-binding while in ChiB they are substrate-binding (Hult et al. 2005; Igarashi et al. 2014). Being close to the catalytic acid, mutations of these residues are likely to affect the catalytic reaction. K_m and k_{cat} values were determined for ChiA-W275A (+1) and ChiA-F396A (+2) in **Paper VI** using $(GlcNAc)_4$ as a substrate. Further, the mutants were compared to the previously obtained values for ChiA-WT, ChiB-WT, ChiB-W97A (+1), and ChiB-W220A (+2) (Krokeide et al. 2007). The kinetic data show that the wild type enzymes have similar K_m and k_{cat} values, while the four mutations have clear effects. K_m values increased for both enzymes, but more strongly in ChiB (W97A and W220A caused 200-fold and 18-fold increases, respectively) than in ChiA (W275A and F396A caused 17-fold and 2.3-fold increases, respectively). Furthermore, k_{cat} of ChiB mutants also increased (W97A and W220A from 28 s^{-1} to 126 s^{-1} and 45 s^{-1}, respectively), but decreased in ChiA (W275A and F396A from 33 s^{-1} to 8 s^{-1} and 13 s^{-1}, respectively).

ChiA-W275A is an interesting mutant, showing the largest difference between experimental and computational $\Delta\Delta G$ values in **Paper V**. Furthermore, it is the only enzyme that displays substrate inhibition, necessitating the use of an adapted Michaelis-Menten equation (Equation 10) instead of straightforward Michaelis-Menten kinetics (Equation 11) when measuring K_m and k_{cat} in **Paper VI**. As already mentioned, the energetic barrier of changing from the relaxed C_1 chair conformation to a distorted boat conformation prior to hydrolysis corresponds to a value of ~ 8 kcal/mol (Brameld & Goddard 1998). When the tryptophan is removed in the case of W275A, sufficient binding energy is probably not available to overcome this free energy penalty. Other non-productive binding modes may thus be prominent. Two $(GlcNAc)_4$ molecules may bind either side of the catalytic acid, causing substrate inhibition, in the same manner as previously observed for chitotriose thiazolines in ChiA (Macdonald et al. 2010). Here, one molecule bound from subsite −3 to −1 and one in subsite +1 and +2 with the third unit being distorted in the solvent. By the use of Equation 10, the substrate inhibition constant, K_i, was calculated to be 25 μM for ChiA-W275A.

$$v_0 = V_{max} \frac{[S]}{K_m + \left(1 + \frac{[S]}{K_i}\right)[S]}$$ Equation 10

$$v_0 = V_{max} \frac{[S]}{K_m + [S]}$$ Equation 11

Product release should be considered as a potentially rate-limiting factor when analyzing the catalytic properties of polysaccharide degrading enzymes, as exemplified by product inhibition issues encountered in the industrial saccharification of cellulose (Teugjas & Väljamäe 2013). The equations for such Michaelis-Menten kinetics are described in Equation 12-14 (Fersht 1999). Upon mutation, removal of aromatic side chains likely reduces the substrate association rate (k_1) and increases both the substrate dissociation rate (k_{-1}) and the rate of product release (k_3) (Equation 12). All these factors may contribute to the observed increases in K_m (Equation 13).

$$E + S \underset{k_{-1}}{\overset{k_1}{\rightleftarrows}} E\text{-}S \xrightarrow{k_2} E\text{-}P \xrightarrow{k_3} E + P$$ Equation 12

$$K_m = \frac{k_3}{k_2 + k_3} \cdot \frac{k_2 + k_{-1}}{k_1}$$ Equation 13

$$k_{cat} = \frac{k_2 k_3}{k_2 + k_3}$$ Equation 14

The catalytic centers of ChiA and ChiB are highly similar. The mutational effects on k_2 should therefore be similar for the two enzymes, implying that changes in k_{cat} must be caused by differences in k_3 (Equation 14). k_{cat} is reduced in ChiA apparently due to a negative effect on k_2 that is not compensated by an increase in k_3. It is thus likely that the positive subsites in ChiA are optimized for rapid release of dimeric products hence effects on k_3 are not noticeable. In ChiB the presumably similar effect on k_2 is compensated for, leading to an increase in k_{cat} implying that k_3 is rate-limiting and the positive subsites optimized for staying attached to the substrate. Comparison of the structures of ChiA and

ChiB in complex with substrate (Papanikolau et al. 2001; van Aalten et al. 2001) shows that subsites +1 and +2 are narrower in ChiB, possibly explaining why product release is more restricted and rate-limiting in ChiB than in ChiA. In conclusion, **Paper VI** shows that the tailoring of the enzymes to opposite directionalities is reflected in the kinetics of $(GlcNAc)_4$ degradation.

4. Concluding remarks

The main objective of the work this thesis is based upon was to obtain a better understanding of how substrates bind to family 18 chitinases in order to improve the understanding of how recalcitrant polysaccharides are effectively degraded. The energetic and kinetic contributions of wild type enzymes and their key residues were investigated. We show that availability of a complete chitinolytic machinery is important in this respect as it can be used to address several key features of the different enzymes.

It has been proposed that the degree of ligand solvation, the magnitude of average atomic fluctuation of the ligand as a function of binding site, and the magnitude of overall fluctuations of key catalytic site residues are dynamic hallmarks that qualitatively relate to experimentally measured processivity. In addition, the theoretical intrinsic processivity has been hypothesized to correlate with the free energy change of the binding between the enzymes and their ligands. Both simulation and experimental results presented in this thesis confirm these hypothesized relationships. Furthermore, the results provide the first indications of the importance of polar residues in substrate binding and processivity of glycoside hydrolases.

5. References

Aachmann, F. L., Sørlie, M., Skjåk-Bræk, G., Eijsink, V. G. & Vaaje-Kolstad, G. (2012). NMR structure of a lytic polysaccharide monooxygenase provides insight into copper binding, protein dynamics, and substrate interactions. *Proc. Natl. Acad. Sci. USA*, 109 (46): 18779-84.

Aam, B. B., Heggset, E. B., Norberg, A. L., Sørlie, M., Vårum, K. M. & Eijsink, V. G. (2010). Production of chitooligosaccharides and their potential applications in medicine. *Mar. Drugs*, 8 (5): 1482-517.

Abbott, D. W., Macauley, M. S., Vocadlo, D. J. & Boraston, A. B. (2009). *Streptococcus pneumoniae* endohexosaminidase D, structural and mechanistic insight into substrate-assisted catalysis in family 85 glycoside hydrolases. *J. Biol. Chem.*, 284 (17): 11676-89.

Amadasi, A., Spyrakis, F., Cozzini, P., Abraham, D. J., Kellogg, G. E. & Mozzarelli, A. (2006). Mapping the energetics of water-protein and water-ligand interactions with the "natural" HINT forcefield: predictive tools for characterizing the roles of water in biomolecules. *J. Mol. Biol.*, 358 (1): 289-309.

Aronson, N. N., Halloran, B. A., Alexeyev, M. F., Zhou, X. E., Wang, Y., Meehan, E. J. & Chen, L. (2006). Mutation of a conserved tryptophan in the chitin-binding cleft of *Serratia marcescens* chitinase A enhances transglycosylation. *Biosci. Biotech. Biochem.*, 70 (1): 243-51.

Baban, J., Fjeld, S., Sakuda, S., Eijsink, V. G. H. & Sørlie, M. (2010). The roles of three *Serratia marcescens* chitinases in chitin conversion are reflected in different thermodynamic signatures of allosamidin binding. *J. Phys. Chem. B*, 114 (18): 6144-6149.

Baker, B. M. & Murphy, K. P. (1997). Dissecting the energetics of a protein-protein interaction: the binding of ovomucoid third domain to elastase. *J. Mol. Biol.*, 268 (2): 557-69.

Baldwin, R. L. (1986). Temperature dependence of the hydrophobic interaction in protein folding. *Proc. Natl. Acad. Sci. USA*, 83 (21): 8069-72.

Barr, B. K., Hsieh, Y. L., Ganem, B. & Wilson, D. B. (1996). Identification of two functionally different classes of exocellulases. *Biochemistry*, 35 (2): 586-92.

Beckham, G. T. & Crowley, M. F. (2011). Examination of the alpha-chitin structure and decrystallization thermodynamics at the nanoscale. *J. Phys. Chem. B*, 115 (15): 4516-22.

Beckham, G. T., Matthews, J. F., Peters, B., Bomble, Y. J., Himmel, M. E. & Crowley, M. F. (2011). Molecular-level origins of biomass recalcitrance: decrystallization free energies for four common cellulose polymorphs. *J. Phys. Chem. B*, 115 (14): 4118-27.

Beckham, G. T., Ståhlberg, J., Knott, B. C., Himmel, M. E., Crowley, M. F., Sandgren, M., Sørlie, M. & Payne, C. M. (2014). Towards a molecular-level theory of carbohydrate processivity in glycoside hydrolases. *Curr. Opin. Biotechnol.*, 27C: 96-106.

Biarnes, X., Ardevol, A., Planas, A., Rovira, C., Laio, A. & Parrinello, M. (2007). The conformational free energy landscape of beta-D-glucopyranose. Implications for substrate preactivation in beta-glucoside hydrolases. *J. Am. Chem. Soc.*, 129 (35): 10686-93.

Blackwell, J. (1969). Structure of β-chitin or parallel chain systems of poly-β-(1-4)-*N*-acetyl-D-glucosamine. *Biopolymers*, 7 (3): 281-98.

Brameld, K. A. & Goddard, W. A. (1998). Substrate distortion to a boat conformation at subsite −1 is critical in the mechanism of family 18 chitinases. *J. Am. Chem. Soc.*, 120 (15): 3571-3580.

Breyer, W. A. & Matthews, B. W. (2001). A structural basis for processivity. *Protein Sci.*, 10 (9): 1699-711.

Brurberg, M. B., Nes, I. F. & Eijsink, V. G. (1996). Comparative studies of chitinases A and B from *Serratia marcescens*. *Microbiology*, 142 (Pt 7): 1581-9.

Cantarel, B. L., Coutinho, P. M., Rancurel, C., Bernard, T., Lombard, V. & Henrissat, B. (2009). The Carbohydrate-Active EnZymes database (CAZy): an expert resource for Glycogenomics. *Nucleic Acids Res.*, 37 (Database issue): D233-8.

Cederkvist, F. H., Saua, S. F., Karlsen, V., Sakuda, S., Eijsink, V. G. & Sørlie, M. (2007). Thermodynamic analysis of allosamidin binding to a family 18 chitinase. *Biochemistry*, 46 (43): 12347-54.

Cerqueira, N., Brás , N., Ramos, M. J. & Fernandes, P. A. (2012). Glycosidases – a mechanistic overview, carbohydrates - comprehensive studies on glycobiology and glycotechnology. I: Chang, P. C.-F. (red.).

Cooper, A., Johnson, C. M., Lakey, J. H. & Nöllmann, M. (2001). Heat does not come in different colours: entropy-enthalpy compensation, free energy windows, quantum confinement, pressure perturbation calorimetry, solvation and the multiple causes of heat capacity effects in biomolecular interactions. *Biophys. Chem.*, 93 (2-3): 215-30.

Cooper, A. (2005). Heat capacity effects in protein folding and ligand binding: a re-evaluation of the role of water in biomolecular thermodynamics. *Biophys. Chem.*, 115 (2-3): 89-97.

Cruys-Bagger, N., Tatsumi, H., Ren, G. R., Borch, K. & Westh, P. (2013). Transient kinetics and rate-limiting steps for the processive cellobiohydrolase Cel7A: effects of substrate structure and carbohydrate binding domain. *Biochemistry*, 52 (49): 8938-48.

Davies, G. & Henrissat, B. (1995). Structures and mechanisms of glycosyl hydrolases. *Structure*, 3 (9): 853-9.

Davies, G. J., Wilson, K. S. & Henrissat, B. (1997). Nomenclature for sugar-binding subsites in glycosyl hydrolases. *Biochem. J.*, 321 (Pt 2): 557-9.

Deng, Y. Q. & Roux, B. (2006). Calculation of standard binding free energies: Aromatic molecules in the T4 lysozyme L99A mutant. *J. Chem. Theory Comput.*, 2 (5): 1255-1273.

Divne, C., Ståhlberg, J., Reinikainen, T., Ruohonen, L., Pettersson, G., Knowles, J. K., Teeri, T. T. & Jones, T. A. (1994). The three-dimensional crystal structure of the catalytic core of cellobiohydrolase I from *Trichoderma reesei*. *Science*, 265 (5171): 524-8.

Divne, C., Ståhlberg, J., Teeri, T. T. & Jones, T. A. (1998). High-resolution crystal structures reveal how a cellulose chain is bound in the 50 A long tunnel of cellobiohydrolase I from *Trichoderma reesei*. *J. Mol. Biol.*, 275 (2): 309-25.

Dunitz, J. D. (1994). The entropic cost of bound water in crystals and biomolecules. *Science*, 264 (5159): 670.

Dunitz, J. D. (1995). Win some, lose some: enthalpy-entropy compensation in weak intermolecular interactions. *Chem. Biol.*, 2 (11): 709-12.

Fersht, A. (1999). *Structure and mechanism in protein science: a guide to enzyme catalysis and protein folding*. New York: Freeman.

Forsberg, Z., Vaaje-Kolstad, G., Westereng, B., Bunæs, A. C., Stenstrøm, Y., MacKenzie, A., Sørlie, M., Horn, S. J. & Eijsink, V. G. (2011). Cleavage of cellulose by a CBM33 protein. *Protein Sci.*, 20 (9): 1479-83.

Freire, E. (2004). Isothermal titration calorimetry: controlling binding forces in lead optimization. *Drug Discov. Today Technol.*, 1 (3): 295-9.

Fuchs, R. L., McPherson, S. A. & Drahos, D. J. (1986). Cloning of a *Serratia marcescens* gene encoding chitinase. *Appl. Environ. Microbiol.*, 51 (3): 504-9.

Gal, S. W., Choi, J. Y., Kim, C. Y., Cheong, Y. H., Choi, Y. J., Lee, S. Y., Bahk, J. D. & Cho, M. J. (1998). Cloning of the 52-kDa chitinase gene from *Serratia marcescens* KCTC2172 and its proteolytic cleavage into an active 35-kDa enzyme. *FEMS Microbiol. Lett.*, 160 (1): 151-8.

Gardner, K. H. & Blackwell, J. (1975). Refinement of the structure of β-chitin. *Biopolymers*, 14 (8): 1581-95.

Gilbert, H. J. (2010). The biochemistry and structural biology of plant cell wall deconstruction. *Plant Physiol.*, 153 (2): 444-55.

Hackman, R. H. (1954). Studies on chitin. I. Enzymic degradation of chitin and chitin esters. *Aust. J. Biol. Sci.*, 7 (2): 168-78.

Harish Prashanth, K. V. & Tharanathan, R. N. (2007). Chitin/chitosan: modifications and their unlimited application potential—an overview. *Trends Food Sci. Tech.*, 18 (3): 117-131.

Harjunpää, V., Teleman, A., Koivula, A., Ruohonen, L., Teeri, T. T., Teleman, O. & Drakenberg, T. (1996). Cello-oligosaccharide hydrolysis by cellobiohydrolase II from *Trichoderma reesei.* Association and rate constants derived from an analysis of progress curves. *Eur. J. Biochem.*, 240 (3): 584-91.

Henrissat, B. (1991). A classification of glycosyl hydrolases based on amino acid sequence similarities. *Biochem. J.*, 280 (Pt 2): 309-16.

Henrissat, B. & Davies, G. (1997). Structural and sequence-based classification of glycoside hydrolases. *Curr. Opin. Struct. Biol.*, 7 (5): 637-44.

Himmel, M. E., Karplus, P. A., Sakon, J., Adney, W. S., Baker, J. O. & Thomas, S. R. (1997). Polysaccharide hydrolase folds diversity of structure and convergence of function. *Appl. Biochem. Biotechnol.*, 63-65: 315-25.

Himmel, M. E., Ding, S. Y., Johnson, D. K., Adney, W. S., Nimlos, M. R., Brady, J. W. & Foust, T. D. (2007). Biomass recalcitrance: engineering plants and enzymes for biofuels production. *Science*, 315 (5813): 804-7.

Holdgate, G. A. (2001). Making cool drugs hot: isothermal titration calorimetry as a tool to study binding energetics. *BioTechniques*, 31 (1): 164-6, 168, 170 passim.

Horn, S. J. & Eijsink, V. G. H. (2004). A reliable reducing end assay for chito-oligosaccharides. *Carbohydr. Polym.*, 56 (1): 35-39.

Horn, S. J., Sikorski, P., Cederkvist, J. B., Vaaje-Kolstad, G., Sørlie, M., Synstad, B., Vriend, G., Vårum, K. M. & Eijsink, V. G. (2006a). Costs and benefits of processivity in enzymatic degradation of recalcitrant polysaccharides. *Proc. Natl. Acad. Sci. USA*, 103 (48): 18089-94.

Horn, S. J., Sørbotten, A., Synstad, B., Sikorski, P., Sørlie, M., Vårum, K. M. & Eijsink, V. G. (2006b). Endo/exo mechanism and processivity of family 18 chitinases produced by *Serratia marcescens*. *FEBS J.*, 273 (3): 491-503.

Horn, S. J., Sørlie, M., Vaaje-Kolstad, G., Norberg, A. L., Synstad, B., Vårum, K. M. & Eijsink, V. G. H. (2006c). Comparative studies of chitinases A, B and C from *Serratia marcescens*. *Biocatal. Biotransform.*, 24 (1-2): 39-53.

Horn, S. J., Sørlie, M., Vårum, K. M., Väljamäe, P. & Eijsink, V. G. (2012a). Measuring processivity. *Methods Enzymol.*, 510: 69-95.

Horn, S. J., Vaaje-Kolstad, G., Westereng, B. & Eijsink, V. G. H. (2012b). Novel enzymes for the degradation of cellulose. *Biotechnol. Biofuels*, 5.

Hult, E. L., Katouno, F., Uchiyama, T., Watanabe, T. & Sugiyama, J. (2005). Molecular directionality in crystalline β-chitin: hydrolysis by chitinases A and B from *Serratia marcescens* 2170. *Biochem. J.*, 388 (Pt 3): 851-6.

Igarashi, K., Uchihashi, T., Koivula, A., Wada, M., Kimura, S., Okamoto, T., Penttila, M., Ando, T. & Samejima, M. (2011). Traffic jams reduce hydrolytic efficiency of cellulase on cellulose surface. *Science*, 333 (6047): 1279-1282.

Igarashi, K., Uchihashi, T., Uchiyama, T., Sugimoto, H., Wada, M., Suzuki, K., Sakuda, S., Ando, T., Watanabe, T. & Samejima, M. (2014). Two-way traffic of glycoside hydrolase family 18 processive chitinases on crystalline chitin. *Nat. Commun.*, 5: 3975.

IUBMB. (1992). *Enzyme nomenclature 1992: recommendations of the Nomenclature Committee of the International Union of Biochemistry and Molecular Biology on the nomenclature and classification of enzymes*. San Diego: Academic Press.

Jalak, J. & Väljamäe, P. (2010). Mechanism of initial rapid rate retardation in cellobiohydrolase catalyzed cellulose hydrolysis. *Biotechnol. Bioeng.*, 106 (6): 871-83.

Jiang, W., Hodoscek, M. & Roux, B. (2009). Computation of absolute hydration and binding free nergy with Free Energy Perturbation Distributed Replica-Exchange Molecular Dynamics (FEP/REMD). *J. Chem. Theory Comput.*, 5 (10): 2583-2588.

Jiang, W. & Roux, B. (2010). Free Energy Perturbation Hamiltonian Replica-Exchange Molecular Dynamics (FEP/H-REMD) for absolute ligand binding free energy calculations. *J. Chem. Theory Comput.*, 6 (9): 2559-2565.

Karkehabadi, S., Hansson, H., Kim, S., Piens, K., Mitchinson, C. & Sandgren, M. (2008). The first structure of a glycoside hydrolase family 61 member, Cel61B from *Hypocrea jecorina*, at 1.6 Å resolution. *J. Mol. Biol.*, 383 (1): 144-54.

Katouno, F., Taguchi, M., Sakurai, K., Uchiyama, T., Nikaidou, N., Nonaka, T., Sugiyama, J. & Watanabe, T. (2004). Importance of exposed aromatic residues in chitinase B from *Serratia marcescens* 2170 for crystalline chitin hydrolysis. *J. Biochem.*, 136 (2): 163-8.

Kauzmann, W. (1959). Some factors in the interpretation of protein denaturation. *Adv. Protein Chem.*, 14: 1-63.

Kim, J., Yun, S. & Ounaies, Z. (2006). Discovery of cellulose as a smart material. *Macromolecules*, 39 (16): 4202-4206.

Kless, H., Sitrit, Y., Chet, I. & Oppenheim, A. B. (1989). Cloning of the gene coding for chitobiase of *Serratia Marcescens*. *Mol. Gen. Genet.*, 217 (2-3): 471-473.

Kobayashi, K., Kimura, S., Togawa, E. & Wada, M. (2010). Crystal transition between hydrate and anhydrous β-chitin monitored by synchrotron X-ray fiber diffraction. *Carbohydr. Polym.*, 79 (4): 882-889.

Koshland, D. E. (1953). Stereochemistry and the mechanism of enzymatic reactions. *Biol. Rev. of the Camb. Philos. Soc.*, 28 (4): 416-436.

Krokeide, I. M., Synstad, B., Gåseidnes, S., Horn, S. J., Eijsink, V. G. & Sørlie, M. (2007). Natural substrate assay for chitinases using high-performance liquid chromatography: a comparison with existing assays. *Anal. Biochem.*, 363 (1): 128-34.

Kurasin, M. & Väljamäe, P. (2011). Processivity of cellobiohydrolases is limited by the substrate. *J. Biol. Chem.*, 286 (1): 169-77.

Kuusk, S., Sørlie, M. & Väljamäe, P. (2015). The predominant molecular state of bound enzyme determines the strength and type of product inhibition in the hydrolysis of recalcitrant polysaccharides by processive enzymes. *J. Biol. Chem.*

Köping-Höggård, M., Mel'nikova, Y. S., Vårum, K. M., Lindman, B. & Artursson, P. (2003). Relationship between the physical shape and the efficiency of oligomeric chitosan as a gene delivery system in vitro and in vivo. *J. Gene Med.*, 5 (2): 130-41.

Ladbury, J. E. (1996). Just add water! The effect of water on the specificity of protein-ligand binding sites and its potential application to drug design. *Chem. Biol.*, 3 (12): 973-80.

Laine, R. A. (1994). A calculation of all possible oligosaccharide isomers both branched and linear yields 1.05 x 10(12) structures for a reducing hexasaccharide: the isomer barrier to development of single-method saccharide sequencing or synthesis systems. *Glycobiology*, 4 (6): 759-67.

Leavitt, S. & Freire, E. (2001). Direct measurement of protein binding energetics by isothermal titration calorimetry. *Curr. Opin. Struct. Biol.*, 11 (5): 560-6.

Lee, J. W. (2013). *Advanced Biofuels and Bioproducts*. New York, NY: Springer New York.

Levasseur, A., Drula, E., Lombard, V., Coutinho, P. M. & Henrissat, B. (2013). Expansion of the enzymatic repertoire of the CAZy database to integrate auxiliary redox enzymes. *Biotechnol. Biofuels*, 6 (1): 41.

Li, Z. & Lazaridis, T. (2005). The effect of water displacement on binding thermodynamics: concanavalin A. *J. Phys. Chem. B*, 109 (1): 662-70.

Lombard, V., Golaconda Ramulu, H., Drula, E., Coutinho, P. M. & Henrissat, B. (2014). The carbohydrate-active enzymes database (CAZy) in 2013. *Nucleic Acids Res.*, 42 (Database issue): D490-5.

Lucius, A. L., Maluf, N. K., Fischer, C. J. & Lohman, T. M. (2003). General methods for analysis of sequential "n-step" kinetic mechanisms: application to single turnover kinetics of helicase-catalyzed DNA unwinding. *Biophys. J.*, 85 (4): 2224-39.

Macdonald, J. M., Tarling, C. A., Taylor, E. J., Dennis, R. J., Myers, D. S., Knapp, S., Davies, G. J. & Withers, S. G. (2010). Chitinase inhibition by chitobiose and chitotriose thiazolines. *Angew Chem Int Ed Engl*, 49 (14): 2599-602.

Meyer, J. E. & Schulz, G. E. (1997). Energy profile of maltooligosaccharide permeation through maltoporin as derived from the structure and from a statistical analysis of saccharide-protein interactions. *Protein Sci.*, 6 (5): 1084-91.

Minke, R. & Blackwell, J. (1978). The structure of α-chitin. *J. Mol. Biol.*, 120 (2): 167-81.

Monreal, J. & Reese, E. T. (1969). The chitinase of *Serratia marcescens*. *Can. J. Microbiol.*, 15 (7): 689-96.

Murphy, K. P., Privalov, P. L. & Gill, S. J. (1990). Common features of protein unfolding and dissolution of hydrophobic compounds. *Science*, 247 (4942): 559-61.

Murphy, K. P. (1994). Hydration and convergence temperatures - on the use and interpretation of correlation plots. *Biophys. Chem.*, 51 (2-3): 311-326.

Nakagawa, Y. S., Eijsink, V. G., Totani, K. & Vaaje-Kolstad, G. (2013). Conversion of α-chitin substrates with varying particle size and crystallinity reveals substrate preferences of the chitinases and lytic polysaccharide monooxygenase of *Serratia marcescens*. *J. Agric. Food Chem.*, 61 (46): 11061-6.

Nakamura, A., Watanabe, H., Ishida, T., Uchihashi, T., Wada, M., Ando, T., Igarashi, K. & Samejima, M. (2014). Trade-off between processivity and hydrolytic velocity of cellobiohydrolases at the surface of crystalline cellulose. *J. Am. Chem. Soc.*, 136 (12): 4584-4592.

Norberg, A. L., Dybvik, A. I., Zakariassen, H., Mormann, M., Peter-Katalinic, J., Eijsink, V. G. & Sørlie, M. (2011). Substrate positioning in chitinase A, a processive chito-biohydrolase from *Serratia marcescens*. *FEBS Lett.*, 585 (14): 2339-44.

Papanikolau, Y., Prag, G., Tavlas, G., Vorgias, C. E., Oppenheim, A. B. & Petratos, K. (2001). High resolution structural analyses of mutant chitinase A complexes with substrates provide new insight into the mechanism of catalysis. *Biochemistry*, 40 (38): 11338-43.

Papanikolau, Y., Tavlas, G., Vorgias, C. E. & Petratos, K. (2003). De novo purification scheme and crystallization conditions yield high-resolution structures of chitinase A and its complex with the inhibitor allosamidin. *Acta Crystallogr.* , 59 (Pt 2): 400-3.

Payne, C. M., Bomble, Y. J., Taylor, C. B., McCabe, C., Himmel, M. E., Crowley, M. F. & Beckham, G. T. (2011). Multiple functions of aromatic-carbohydrate interactions in a processive cellulase examined with molecular simulation. *J. Biol. Chem.*, 286 (47): 41028-35.

Payne, C. M., Baban, J., Horn, S. J., Backe, P. H., Arvai, A. S., Dalhus, B., Bjørås, M., Eijsink, V. G., Sørlie, M., Beckham, G. T., et al. (2012). Hallmarks of processivity in glycoside hydrolases from crystallographic and computational studies of the *Serratia marcescens* chitinases. *J. Biol. Chem.*, 287 (43): 36322-30.

Payne, C. M., Jiang, W., Shirts, M. R., Himmel, M. E., Crowley, M. F. & Beckham, G. T. (2013). Glycoside hydrolase processivity is directly related to oligosaccharide binding free energy. *J. Am. Chem. Soc.*, 135 (50): 18831-9.

Perozzo, R., Folkers, G. & Scapozza, L. (2004). Thermodynamics of protein-ligand interactions: history, presence, and future aspects. *J. Recept. Signal Transduction Res.*, 24 (1-2): 1-52.

Perrakis, A., Tews, I., Dauter, Z., Oppenheim, A. B., Chet, I., Wilson, K. S. & Vorgias, C. E. (1994). Crystal structure of a bacterial chitinase at 2.3 Å resolution. *Structure*, 2 (12): 1169-80.

Phillips, C. M., Beeson, W. T., Cate, J. H. & Marletta, M. A. (2011). Cellobiose dehydrogenase and a copper-dependent polysaccharide monooxygenase potentiate cellulose degradation by *Neurospora crassa*. *ACS Chem. Biol.*, 6 (12): 1399-406.

Pierce, M. M., Raman, C. S. & Nall, B. T. (1999). Isothermal titration calorimetry of protein-protein interactions. *Methods*, 19 (2): 213-21.

Que, L., Jr. & Tolman, W. B. (2008). Biologically inspired oxidation catalysis. *Nature*, 455 (7211): 333-40.

Quinlan, R. J., Sweeney, M. D., Lo Leggio, L., Otten, H., Poulsen, J. C., Johansen, K. S., Krogh, K. B., Jørgensen, C. I., Tovborg, M., Anthonsen, A., et al. (2011). Insights into the oxidative degradation of cellulose by a copper metalloenzyme that exploits biomass components. *Proc. Natl. Acad. Sci. USA*, 108 (37): 15079-84.

Quintero-Villegas, M. I., Aam, B. B., Rupnow, J., Sørlie, M., Eijsink, V. G. & Hutkins, R. W. (2013). Adherence inhibition of enteropathogenic *Escherichia coli* by chitooligosaccharides with specific degrees of acetylation and polymerization. *J. Agric. Food Chem.*, 61 (11): 2748-54.

Ratanavaraporn, J., Kanokpanont, S., Tabata, Y. & Damrongsakkul, S. (2009). Growth and osteogenic differentiation of adipose-derived and bone marrow-derived stem cells on chitosan and chitooligosaccharide films. *Carbohydr. Polym.*, 78 (4): 873-878.

Rhoades, J., Gibson, G., Formentin, K., Beer, M. & Rastall, R. (2006). Inhibition of the adhesion of enteropathogenic *Escherichia coli* strains to HT-29 cells in culture by chito-oligosaccharides. *Carbohydr. Polym.*, 64 (1): 57-59.

Rinaudo, M. (2006). Chitin and chitosan: Properties and applications. *Prog. Polym. Sci.*, 31 (7): 603-632.

Rouvinen, J., Bergfors, T., Teeri, T., Knowles, J. K. & Jones, T. A. (1990). Three-dimensional structure of cellobiohydrolase II from *Trichoderma reesei*. *Science*, 249 (4967): 380-6.

Rye, C. S. & Withers, S. G. (2000). Glycosidase mechanisms. *Curr. Opin. Chem. Biol.*, 4 (5): 573-80.

Saito, Y., Okano, T., Gaill, F., Chanzy, H. & Putaux, J. L. (2000). Structural data on the intra-crystalline swelling of β-chitin. *Int. J. Biol. Macromol.*, 28 (1): 81-8.

Sakon, J., Irwin, D., Wilson, D. B. & Karplus, P. A. (1997). Structure and mechanism of endo/exocellulase E4 from *Thermomonospora fusca*. *Nat. Struct. Biol.*, 4 (10): 810-8.

Sakuda, S., Isogai, A., Matsumoto, S., Suzuki, A. & Koseki, K. (1986). The structure of allosamidin, a novel insect chitinase inhibitor, produced by *Streptomyces Sp*. *Tetrahedron Lett.*, 27 (22): 2475-2478.

Sannan, T., Kurita, K. & Iwakura, Y. (1976). Studies on chitin, 2. Effect of deacetylation on solubility. *Macromol. Chem.*, 177 (12): 3589-3600.

Sawada, D., Nishiyama, Y., Langan, P., Forsyth, V. T., Kimura, S. & Wada, M. (2012). Water in crystalline fibers of dihydrate β-chitin results in unexpected absence of intramolecular hydrogen bonding. *PLoS One*, 7 (6): e39376.

Shang, B. Z., Chang, R. & Chu, J. W. (2013). Systems-level modeling with molecular resolution elucidates the rate-limiting mechanisms of cellulose decomposition by cellobiohydrolases. *J. Biol. Chem.*, 288 (40): 29081-9.

Sikorski, P., Sørbotten, A., Horn, S. J., Eijsink, V. G. & Vårum, K. M. (2006). *Serratia marcescens* chitinases with tunnel-shaped substrate-binding grooves show endo activity and different degrees of processivity during enzymatic hydrolysis of chitosan. *Biochemistry*, 45 (31): 9566-74.

Sikorski, P., Hori, R. & Wada, M. (2009). Revisit of α-chitin crystal structure using high resolution X-ray diffraction data. *Biomacromolecules*, 10 (5): 1100-5.

Sinnott, M. L. (1990). Catalytic mechanisms of enzymatic glycosyl transfer. *Chemical Reviews*, 90 (7): 1171-1202.

Stoddart, J. F. (1971). *Stereochemistry of Carbohydrates*: Wiley-Interscience.

Suzuki, K., Suzuki, M., Taiyoji, M., Nikaidou, N. & Watanabe, T. (1998). Chitin binding protein (CBP21) in the culture supernatant of *Serratia marcescens* 2170. *Biosci. Biotechnol. Biochem.*, 62 (1): 128-35.

Suzuki, K., Taiyoji, M., Sugawara, N., Nikaidou, N., Henrissat, B. & Watanabe, T. (1999). The third chitinase gene (chiC) of *Serratia marcescens* 2170 and the relationship of its product to other bacterial chitinases. *Biochem. J.*, 343 Pt 3: 587-96.

Suzuki, K., Sugawara, N., Suzuki, M., Uchiyama, T., Katouno, F., Nikaidou, N. & Watanabe, T. (2002). Chitinases A, B, and C1 of *Serratia marcescens* 2170 produced by recombinant *Escherichia coli*: Enzymatic properties and synergism on chitin degradation. *Biosci. Biotechnol. Biochem.*, 66 (5): 1075-83.

Synstad, B., Gåseidnes, S., Van Aalten, D. M., Vriend, G., Nielsen, J. E. & Eijsink, V. G. (2004). Mutational and computational analysis of the role of conserved residues in the active site of a family 18 chitinase. *Eur. J. Biochem.*, 271 (2): 253-62.

Synstad, B., Vaaje-Kolstad, G., Cederkvist, F. H., Saua, S. F., Horn, S. J., Eijsink, V. G. & Sørlie, M. (2008). Expression and characterization of endochitinase C from *Serratia marcescens* BJL200 and its purification by a one-step general chitinase purification method. *Biosci. Biotechnol. Biochem.*, 72 (3): 715-23.

Sørbotten, A., Horn, S. J., Eijsink, V. G. & Vårum, K. M. (2005). Degradation of chitosans with chitinase B from *Serratia marcescens*. Production of chito-oligosaccharides and insight into enzyme processivity. *FEBS J.*, 272 (2): 538-49.

Taylor, C. B., Payne, C. M., Himmel, M. E., Crowley, M. F., McCabe, C. & Beckham, G. T. (2013). Binding site dynamics and aromatic-carbohydrate interactions in

processive and non-processive family 7 glycoside hydrolases. *J. Phys. Chem. B*, 117 (17): 4924-33.

Terwisscha van Scheltinga, A. C., Kalk, K. H., Beintema, J. J. & Dijkstra, B. W. (1994). Crystal structures of hevamine, a plant defence protein with chitinase and lysozyme activity, and its complex with an inhibitor. *Structure*, 2 (12): 1181-9.

Terwisscha van Scheltinga, A. C., Armand, S., Kalk, K. H., Isogai, A., Henrissat, B. & Dijkstra, B. W. (1995). Stereochemistry of chitin hydrolysis by a plant chitinase/lysozyme and X-ray structure of a complex with allosamidin: evidence for substrate assisted catalysis. *Biochemistry*, 34 (48): 15619-23.

Terwisscha van Scheltinga, A. C., Hennig, M. & Dijkstra, B. W. (1996). The 1.8 Å resolution structure of hevamine, a plant chitinase/lysozyme, and analysis of the conserved sequence and structure motifs of glycosyl hydrolase family 18. *J. Mol. Biol.*, 262 (2): 243-57.

Teugjas, H. & Väljamäe, P. (2013). Product inhibition of cellulases studied with 14C-labeled cellulose substrates. *Biotechnol. Biofuels*, 6 (1): 104.

Tews, I., Perrakis, A., Oppenheim, A., Dauter, Z., Wilson, K. S. & Vorgias, C. E. (1996). Bacterial chitobiase structure provides insight into catalytic mechanism and the basis of Tay-Sachs disease. *Nat. Struct. Biol.*, 3 (7): 638-48.

Tews, I., Terwisscha van Scheltinga, A. C., Perrakis, A., Wilson, K. S. & Dijkstra, B. W. (1997). Substrate-assisted catalysis unifies two families of chitinolytic enzymes. *J. Am. Chem. Soc.*, 119 (34): 7954-7959.

Tharanathan, R. N. & Kittur, F. S. (2003). Chitin-the undisputed biomolecule of great potential. *Crit. Rev. Food Sci. Nutr.*, 43 (1): 61-87.

Turnbull, W. B. & Daranas, A. H. (2003). On the value of c: can low affinity systems be studied by isothermal titration calorimetry? *J. Am. Chem. Soc.*, 125 (48): 14859-66.

Uchiyama, T., Katouno, F., Nikaidou, N., Nonaka, T., Sugiyama, J. & Watanabe, T. (2001). Roles of the exposed aromatic residues in crystalline chitin hydrolysis by chitinase A from *Serratia marcescens* 2170. *J. Biol. Chem.*, 276 (44): 41343-9.

Vaaje-Kolstad, G., Houston, D. R., Rao, F. V., Peter, M. G., Synstad, B., van Aalten, D. M. & Eijsink, V. G. (2004). Structure of the D142N mutant of the family 18 chitinase ChiB from *Serratia marcescens* and its complex with allosamidin. *Biochim. Biophys. Acta*, 1696 (1): 103-11.

Vaaje-Kolstad, G., Horn, S. J., van Aalten, D. M., Synstad, B. & Eijsink, V. G. (2005a). The non-catalytic chitin-binding protein CBP21 from *Serratia marcescens* is essential for chitin degradation. *J. Biol. Chem.*, 280 (31): 28492-7.

Vaaje-Kolstad, G., Houston, D. R., Riemen, A. H., Eijsink, V. G. & van Aalten, D. M. (2005b). Crystal structure and binding properties of the *Serratia marcescens* chitin-binding protein CBP21. *J. Biol. Chem.*, 280 (12): 11313-9.

Vaaje-Kolstad, G., Westereng, B., Horn, S. J., Liu, Z., Zhai, H., Sørlie, M. & Eijsink, V. G. (2010). An oxidative enzyme boosting the enzymatic conversion of recalcitrant polysaccharides. *Science*, 330 (6001): 219-22.

Vaaje-Kolstad, G., Bøhle, L. A., Gåseidnes, S., Dalhus, B., Bjørås, M., Mathiesen, G. & Eijsink, V. G. (2012). Characterization of the chitinolytic machinery of *Enterococcus faecalis* V583 and high-resolution structure of its oxidative CBM33 enzyme. *J. Mol. Biol.*, 416 (2): 239-54.

Vaaje-Kolstad, G., Horn, S. J., Sørlie, M. & Eijsink, V. G. (2013). The chitinolytic machinery of *Serratia marcescens*--a model system for enzymatic degradation of recalcitrant polysaccharides. *FEBS J.*, 280 (13): 3028-49.

van Aalten, D. M., Synstad, B., Brurberg, M. B., Hough, E., Riise, B. W., Eijsink, V. G. & Wierenga, R. K. (2000). Structure of a two-domain chitotriosidase from *Serratia marcescens* at 1.9-Å resolution. *Proc. Natl. Acad. Sci. USA*, 97 (11): 5842-7.

van Aalten, D. M., Komander, D., Synstad, B., Gåseidnes, S., Peter, M. G. & Eijsink, V. G. (2001). Structural insights into the catalytic mechanism of a family 18 exo-chitinase. *Proc. Natl. Acad. Sci. USA*, 98 (16): 8979-84.

Vanholme, R., Demedts, B., Morreel, K., Ralph, J. & Boerjan, W. (2010). Lignin biosynthesis and structure. *Plant Physiol.*, 153 (3): 895-905.

Varrot, A., Frandsen, T. P., von Ossowski, I., Boyer, V., Cottaz, S., Driguez, H., Schulein, M. & Davies, G. J. (2003). Structural basis for ligand binding and processivity in cellobiohydrolase Cel6A from *Humicola insolens*. *Structure*, 11 (7): 855-64.

Velleste, R., Teugjas, H. & Väljamäe, P. (2010). Reducing end-specific fluorescence labeled celluloses for cellulase mode of action. *Cellulose*, 17 (1): 125-138.

von Ossowski, I., Ståhlberg, J., Koivula, A., Piens, K., Becker, D., Boer, H., Harle, R., Harris, M., Divne, C., Mahdi, S., et al. (2003). Engineering the exo-loop of *Trichoderma reesei* cellobiohydrolase, Ce17A. A comparison with *Phanerochaete chrysosporium* Cel7D. *J. Mol. Biol.*, 333 (4): 817-829.

Vuong, T. V. & Wilson, D. B. (2010). Glycoside hydrolases: catalytic base/nucleophile diversity. *Biotechnol. Bioeng.*, 107 (2): 195-205.

Vyas, N. K. (1991). Atomic features of protein-carbohydrate interactions. *Curr. Opin. Struct. Biol.*, 1 (5): 732-740.

Vårum, K. M., Anthonsen, M. W., Grasdalen, H. & Smidsrød, O. (1991a). 13C-n.m.r. studies of the acetylation sequences in partially N-deacetylated chitins (chitosans). *Carbohydr. Res.*, 217: 19-27.

Vårum, K. M., Anthonsen, M. W., Grasdalen, H. & Smidsrød, O. (1991b). Determination of the degree of N-acetylation and the distribution of N-acetyl groups in partially N-deacetylated chitins (chitosans) by high-field n.m.r. spectroscopy. *Carbohydr. Res.*, 211 (1): 17-23.

Watson, B. J., Zhang, H., Longmire, A. G., Moon, Y. H. & Hutcheson, S. W. (2009). Processive endoglucanases mediate degradation of cellulose by *Saccharophagus degradans*. *J. Bacteriol.*, 191 (18): 5697-705.

Westereng, B., Ishida, T., Vaaje-Kolstad, G., Wu, M., Eijsink, V. G., Igarashi, K., Samejima, M., Ståhlberg, J., Horn, S. J. & Sandgren, M. (2011). The putative endoglucanase PcGH61D from *Phanerochaete chrysosporium* is a metal-dependent oxidative enzyme that cleaves cellulose. *PLoS One*, 6 (11): e27807.

Wilson, D. B. (2009). Cellulases and biofuels. *Curr. Opin. Biotechnol.*, 20 (3): 295-9.

Wilson, D. B. & Kostylev, M. (2012). Cellulase processivity. *Methods Mol. Biol.*, 908: 93-9.

Wiseman, T., Williston, S., Brandts, J. F. & Lin, L. N. (1989). Rapid measurement of binding constants and heats of binding using a new titration calorimeter. *Anal. Biochem.*, 179 (1): 131-7.

Wolfenden, R., Lu, X. D. & Young, G. (1998). Spontaneous hydrolysis of glycosides. *J. Am. Chem. Soc.*, 120 (27): 6814-6815.

Wu, H., Aam, B. B., Wang, W., Norberg, A. L., Sørlie, M., Eijsink, V. G. & Du, Y. (2012). Inhibition of angiogenesis by chitooligosaccharides with specific degrees of acetylation and polymerization. *Carbohydr. Polym.*, 89 (2): 511-8.

Zakariassen, H., Aam, B. B., Horn, S. J., Vårum, K. M., Sørlie, M. & Eijsink, V. G. (2009). Aromatic residues in the catalytic center of chitinase A from *Serratia marcescens* affect processivity, enzyme activity, and biomass converting efficiency. *J. Biol. Chem.*, 284 (16): 10610-7.

Zakariassen, H., Eijsink, V. G. H. & Sørlie, M. (2010). Signatures of activation parameters reveal substrate-dependent rate determining steps in polysaccharide turnover by a family 18 chitinase. *Carbohydr. Polym.*, 81 (1): 14-20.

Zees, A. C., Pyrpassopoulos, S. & Vorgias, C. E. (2009). Insights into the role of the (α + β) insertion in the TIM-barrel catalytic domain, regarding the stability and the enzymatic activity of chitinase A from *Serratia marcescens*. *Biochim. Biophys. Acta*, 1794 (1): 23-31.

Zhou, W., Irwin, D. C., Escovar-Kousen, J. & Wilson, D. B. (2004). Kinetic studies of *Thermobifida fusca* Cel9A active site mutant enzymes. *Biochemistry*, 43 (30): 9655-63.

Zhu, Z., Zheng, T., Homer, R. J., Kim, Y. K., Chen, N. Y., Cohn, L., Hamid, Q. & Elias, J. A. (2004). Acidic mammalian chitinase in asthmatic Th2 inflammation and IL-13 pathway activation. *Science*, 304 (5677): 1678-82.

Paper I

Carbohydrate Research 407 (2015) 166–169

Contents lists available at ScienceDirect

Carbohydrate Research

journal homepage: www.elsevier.com/locate/carres

Note

Activation of enzymatic chitin degradation by a lytic polysaccharide monooxygenase

Anne Grethe Hamre [†], Kristine B. Eide [†], Hanne H. Wold, Morten Sørlie [*]

Department of Chemistry, Biotechnology and Food Science, Norwegian University of Life Sciences, PO Box 5003, N-1432 Ås, Norway

ARTICLE INFO

Article history:
Received 19 December 2014
Received in revised form
13 February 2015
Accepted 20 February 2015
Available online 2 March 2015

Keywords:
LPMO
Glycoside hydrolases
Kinetics
Rate enhancement
AA10
CBP21

ABSTRACT

For decades, the enzymatic conversion of recalcitrant polysaccharides such as cellulose and chitin was thought to solely rely on the synergistic action of hydrolytic enzymes, but recent work has shown that lytic polysaccharide monooxygenases (LPMOs) are important contributors to this process. Here, we have examined the initial rate enhancement an LPMO (CBP21) has on the hydrolytic enzymes (ChiA, ChiB, and ChiC) of the chitinolytic machinery of *Serratia marcescens* through determinations of apparent k_{cat} (k_{cat}^{app}) values on a β-chitin substrate. k_{cat}^{app} values were determined to be 1.7±0.1 s^{-1} and 1.7±0.1 s^{-1} for the *exo*-active ChiA and ChiB, respectively and 1.2±0.1 s^{-1} for the *endo*-active ChiC. The addition of CBP21 boosted the k_{cat}^{app} values of ChiA and ChiB giving values of 11.1±1.5 s^{-1} and 13.9±1.4 s^{-1}, while there was no effect on ChiC (0.9±0.1 s^{-1}).

Cellulose and chitin are the two most abundant biopolymers in nature having an annual production around hundred billion and one trillion tons making the enzymatic degradation of them very important, both biologically and economically.[1,2] They are insoluble polymers composed of β-(1,4)-linked units of D-glucopyranose and N-acetyl-D-glucosamine (GlcNAc) respectively.

Depolymerization of chitin and cellulose is efficiently achieved by synergistic enzyme cocktails composed of glycoside hydrolases (GHs) and lytic polysaccharide monooxygenases (LPMOs).[3–7] The glycoside hydrolases comprising these cocktails can have different modes of action including *endo*- and *exo*-activity as well as varying degrees of processivity.[8] Another feature is that they can have different preferences for which chain end they choose to attack (reducing or non-reducing end).

LPMOs have lately been reorganized into the Auxiliary Activity Family (AA) in the CAZy database.[9] They are a recently discovered group of oxidative copper-enzymes capable of cleaving chitin and cellulose chains using an unprecedented oxidative mechanism.[4,10,11] Their catalytic activity is dependent on the presence of molecular oxygen and an external electron donor, and the reaction leads to the generation of new chain ends.[4] It has been shown that LPMOs can enhance both the rate and extent of polysaccharide degradation.[4,12,13]

In this work, we have looked at the initial rate enhancement an LPMO has on GH catalyzed hydrolysis of a recalcitrant polysaccharide using the well-characterized chitinolytic machinery of *Serratia marcescens.* This machinery consists of one processive chitinase working from the reducing end (chitinase A (ChiA)), one processive chitinase working from the non-reducing end (chitinase B (ChiB)), a nonprocessive *endo*-acting chitinase (chitinase C (ChiC)), and an LPMO (CBP21).[5,14–16] CBP21 by itself has a relatively low activity (~1 min^{-1}), which is ~100 fold slower compared to the hydrolytic activity of the individual chitinases (albeit determined under non-saturating substrate conditions).[4,17] The product of CBP21 catalysis are new chain ends on the polymer as well as soluble oxidized chitooligosaccharides in small amounts.[4] When CBP21 and an individual chitinase (i.e., ChiA) are co-incubated with chitin, the only detectable product is $(GlcNAc)_2$ (see below).

To assess the rate enhancing effect, apparent catalytic rate constants for two forms of β-chitin degradation by ChiA, ChiB, and ChiC, alone or together with CBP21 were determined. Firstly, all GHs were incubated with different concentrations of β-chitin of 3 μm size (10, 20, and 30 mg/ml), and initial rates were determined by monitoring the concentration of product formation with respect to time (0, 4, 8, 12, and 16 min) from three independent measurements using HPLC (Fig. 1 and Fig. 2). Fig. 1 shows that initial rates

* Corresponding author. Tel.: +47 64965902; fax: +47 64965901.
E-mail address: morten.sorlie@nmbu.no (M. Sørlie).
† A. G. Hamre and K. B. Eide contributed equally to this work.

http://dx.doi.org/10.1016/j.carres.2015.02.010
0008-6215/

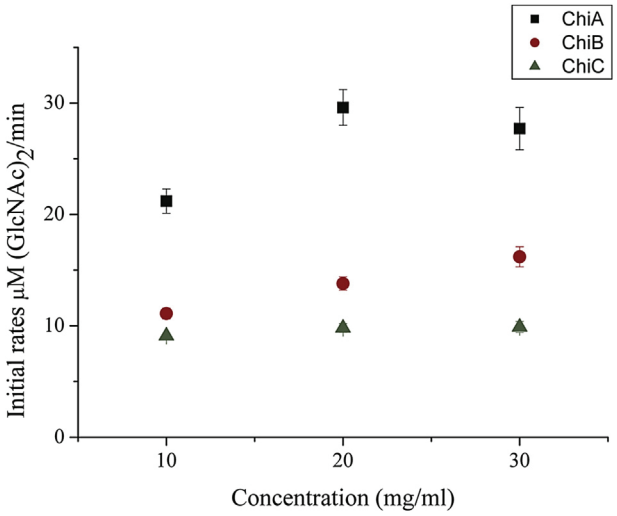

Fig. 1. Rate saturation plot from the degradation of 10, 20, and 30 mg/ml 3 µm β-chitin in 20 mM in Tris–HCl pH 8.0 by ChiA (black squares), ChiB (red circles), and ChiC (green triangles). Initial rates (µM $(GlcNAc)_2$/min) is plotted versus the concentration of β-chitin (mg/ml). (For interpretation of the references to colour in this figure legend, the reader is referred to the web version of this article.)

were constant from 20 mg/ml and higher for all three chitinases, hence being a measure of apparent V_{max}. The reaction conditions were thereafter changed; first the pH was changed to 6.1 before the substrate was changed to that of 180 µm size. Both conditions showed also substrate saturation at 20 mg/ml.

When the 3 µm β-chitin was hydrolyzed by ChiA and ChiB at pH 8.0, $(GlcNAc)_2$ was the only product while minor amounts of $(GlcNAc)_3$ and $(GlcNAc)_4$ were produced as well by ChiC. From initial rates, apparent rate constants (k_{cat}^{app}) were determined to be 1.7±0.1 s^{-1}, 1.7±0.1 s^{-1}, and 1.2±0.1 s^{-1} (Table 1, Fig. 2) for ChiA, ChiB, and ChiC respectively. By adding the LPMO CBP21 a 6- and 9-fold increase in k_{cat}^{app} was seen for the two *exo*-active chitinases ChiA and ChiB, respectively; equaling k_{cat}^{app} values of 11.1±1.5 s^{-1} and 13.9±1.4 s^{-1} (Table 1, Fig. 2). Interestingly, the *endo*-active chitinase ChiC showed that addition of CBP21 has no or little effect on k_{cat}^{app} having a value of 0.9±0.1 s^{-1} (Table 1, Fig. 2).

The effect was also tested on another β-chitin variant (180 µm microparticulate) at pH 6.1 (Table 2). For ChiA, the kinetic values increased from 2.7±0.4 s^{-1} to 13.7±3.5 s^{-1} when CBP21 was added. Finally, pH was varied to 6.1 for the 3 µm β-chitin substrate (Table 2). Again, a significant increase in k_{cat}^{app} was observed for ChiA from 2.2±0.3 s^{-1} to 9.2±2.7 s^{-1} in the presence of CBP21. Over the pH-range investigated in this study and by looking at two different substrates there are no significant effects on k_{cat}^{app}.

It has been postulated that oxidative cleavage of glycosidic bonds by a lytic polysaccharide monooxygenase creates new chain ends generating new points of attack on the recalcitrant polysaccharide.[4] Our results clearly show that the presence of an LPMO greatly enhances the initial rate of chitin degradation for the two *exo*-acting chitinases ChiA and ChiB being in line with this postulation. Since ChiA and ChiB have different directionalities and both experience a rate enhancement, this suggests that the presence of CBP21 generates new ends over the whole substrate. Interestingly, the presence of CBP21 did not affect the initial rate for the *endo*-acting ChiC on the substrate under the conditions used in our study. This contrasts the findings in the initial study by Vaaje-Kolstad et al. from 2010 where such a rate enhancement was observed for ChiC.[4] A major difference is that we operate with a~120 times higher substrate to enzyme ratio (20 mg/ml and 170 nM vs 0.45 mg/ml chitin and 500 nM respectively) to have substrate saturating

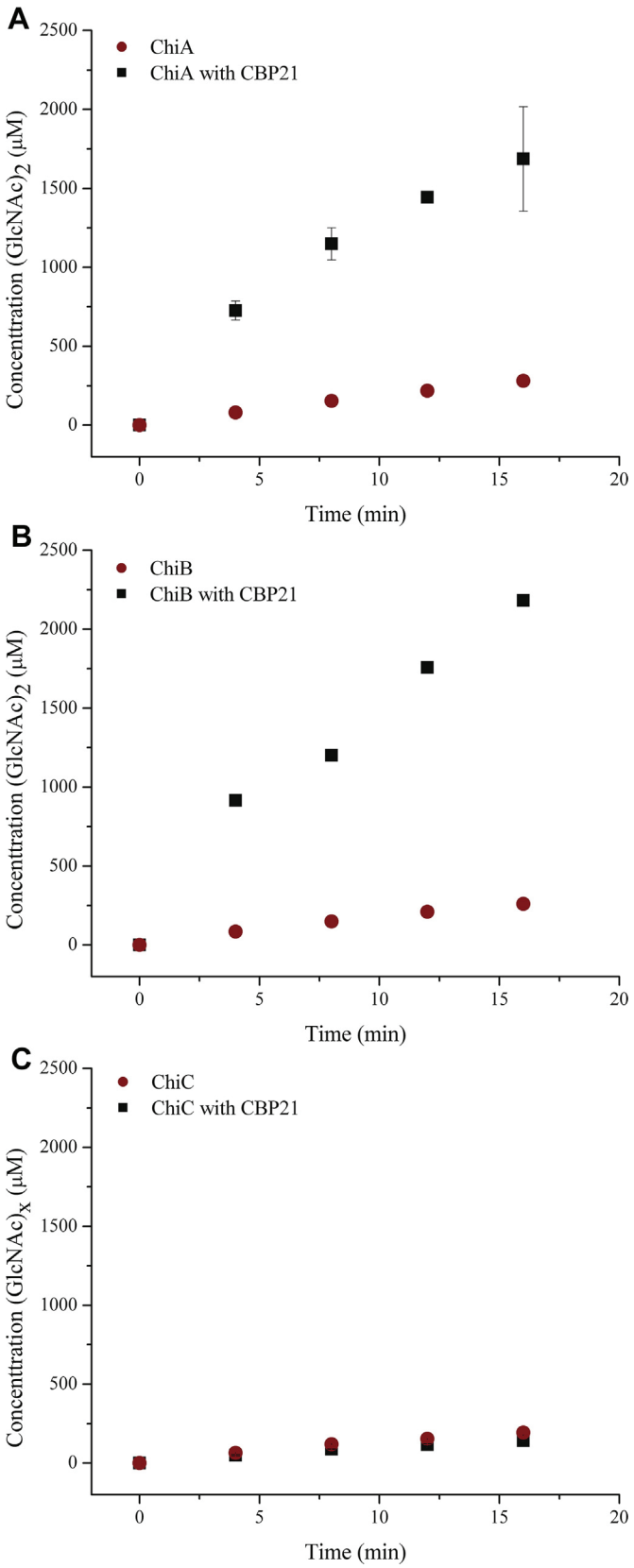

Fig. 2. Initial rates of $(GlcNAc)_2$ or $(GlcNAc)_x$ formation after the degradation of 20 mg/ml 3 µm β-chitin in 20 mM in Tris–HCl pH 8.0 by 170 nM ChiA (left), 156 nM ChiB (middle), and 170 nM ChiC (right) alone (red circles) and with 1 µM CBP21 present (black squares). (For interpretation of the references to colour in this figure legend, the reader is referred to the web version of this article.)

Table 1
Apparent rate constants for enzymatic chitin degradation of 3 μm β-chitin at t=37 °C and pH 8.0. R^2-values are given in parenthesis

ChiA	1.7±0.1 s^{-1} (0.99)	ChiB	1.7±0.1 s^{-1} (0.98)	ChiC	1.2±0.1 s^{-1} (0.99)
ChiA/CBP21	11.1±1.5 s^{-1} (0.97)	ChiB/CBP21	13.9±1.4 s^{-1} (0.99)	ChiC/CBP21	0.9±0.1 s^{-1} (0.99)

conditions. Under our conditions, there may be enough points for attack by the *endo*-acting ChiC, and the help from CBP21 is unnecessary initially. Interestingly, Nakagawa and co-workers observed that CBP21 hardly influenced the activity of ChiA on α-chitin.[18] This finding was rationalized by possible different face preferences on the chitinous substrate for the two different enzymes.

Previously, it has been shown that none of the chitinases of *S. marcescens* are capable of completely degrading the substrates used in our study by themselves.[12,19] This is likely due to obstacles on the substrate trapping the enzymes forming so-called traffic jams.[20,21] CBP21 has a rescuing effect on the three chitinases, including ChiC, meaning that the presence of an LPMO also helps removing obstacles on the substrate.[12]

In conclusion, we show that initial rates for the *exo*-acting GHs ChiA and ChiB, as described by k_{cat}^{app}, increases between six to nine-fold when the LPMO CBP21 is in the presence when working on β-chitin. Interestingly, k_{cat}^{app} for the *endo*-active ChiC was not affected initially by CBP21. The results show that the LPMO CBP21 creates new ends on the polysaccharide substrate in addition to having a rescuing effect on GHs that tend to get stuck on the substrate during the degradation process.

1. Experimental

1.1. Chemicals

N-acetylated chito-oligosaccharides were purchased from Megazyme (Wicklow, Ireland), while two different types of β-chitin, 3 μm and 180 μm, were purchased from Seikagaku and France chitine (Japan and France) respectively. Purified bovine serum albumin (BSA) was purchased from New England Biolabs (Ipswich, MA, USA). All other chemicals and reagents were of analytical grade.

1.2. Protein expression and purification

The genes encoding chitinase A, chitinase B, chitinase C, and CBP21 were all overexpressed in *Escherichia coli* as described elsewhere.[22–25] Further, the periplasmic extracts were purified on a column packed with chitin beads (New England Biolabs) (1.5 cm in diameter, 10 ml stationary phase in total). The beads were equilibrated in 50 mM Tris–HCl, pH 8.0. The flow rate was set to 2.5 ml/min. Bound enzymes were eluted with 20 mM acetic acid. Purified proteins were further concentrated by use of Amicon Ultra- Centrifugal filters (Millipore) and then stored in 100 mM Tris–HCl, pH 8.0 at 4 °C. Enzyme purity was verified by SDS-PAGE and estimated to be above 95% in all cases. Protein concentrations were determined by use of the Bradford Protein Assay from Bio-Rad.

Table 2
Apparent rate constants for enzymatic chitin degradation of two different β-chitin variants (3 and 180 μm) using two different pH-values (8.0 and 6.1) at t=37 °C

	ChiA	ChiA/CBP21
3 μm β-chitin, pH 8.0	1.7±0.1 s^{-1}	11.1±1.5 s^{-1}
3 μm β-chitin, pH 6.1	2.2±0.3 s^{-1}	9.2±2.7 s^{-1}
180 μm β-chitin, pH 6.1	2.7±0.4 s^{-1}	13.7±3.5 s^{-1}

1.3. Degradation of chitin without CBP21

Degradation of the two different types of β-chitin (20.0 mg/ml), 3 μm and 180 μm respectively, was carried out in 20 mM Tris/HCl, pH 8, containing 0.1 mg/ml BSA. The reaction tubes were incubated at 37 °C in an Eppendorf thermo mixer at 800 rpm to avoid settling of chitin particles. ChiA, ChiB, and ChiC were then added to the following concentrations; 170 nM, 156 nM and 170 nM. Samples of 75 μl were withdrawn at regular time points (0, 4, 8, 12, and 16 min), and the chitinases were inactivated by adding 75 μl 20 mM H_2SO_4. Prior to HPLC analysis all samples were filtrated through a 0.45 μm Duapore membrane (Millipore) to remove denatured protein and chitin particles. Samples were stored at −20 °C. All reactions used for quantification were run in triplicates.

Because the substrate is in large excess (20 mg/ml chitin correspond to a dimer concentration in the order of 50 mM), substrate saturating conditions were assumed. Use of reaction mixtures (T=37 °C) with an even higher chitin concentration (both 30 mg/ml and 50 mg/ml) gave similar initial rates, confirming that substrate concentrations indeed were saturating.

1.4. Degradation of chitin in the presence of CBP21

Degradation of 3 μm β-chitin (20.0 mg/ml) was carried out as described in section 2.3 with the exception of buffer content. The 20 mM Tris/HCl buffer at pH 8.0 contained 1 mM ascorbic acid, 5 mM magnesium chloride and 1 μM copper chloride in addition to 0.1 mg/ml BSA. CBP21 was added to a concentration of 1 μM 24 h before the addition of the respective chitinases. The reaction mixtures were incubated at 37 °C and 800 rpm at all times.

1.5. High performance liquid chromatography (HPLC)

Concentrations of chitooligosaccharides were determined using HPLC with a Rezex Fast fruit H^+ column (100 mm×7.8 mm) (Phenomonex). Samples of 8 μl were injected on the column, and the mono/oligosaccharides were eluted isocratically at 85 °C. 5 mM H_2SO_4 was used as mobile phase and the flow rate was set to 1 ml/min. Eluted oligosaccharides were monitored by recording absorption at 210 nm. The amount of chitooligosaccharides was quantified by integrating peak areas. Peak areas were compared with peak areas obtained with standard samples with known concentration of oligosaccharides.

Acknowledgments

This work was supported by Grant 209335/F20 from the Norwegian Research Council.

References

1. Tharanathan RN, Kittur FS. *Crit Rev Food Sci Nutr* 2003;**43**:61–87.
2. Kim J, Yun S, Ounaies Z. *Macromolecules* 2006;**39**:4202–6.
3. Horn SJ, Vaaje-Kolstad G, Westereng B, Eijsink VG. *Biotechnol Biofuels* 2012;**5**:45.
4. Vaaje-Kolstad G, Westereng B, Horn SJ, Liu Z, Zhai H, Sørlie M, et al. *Science* 2010;**330**:219–22.
5. Vaaje-Kolstad G, Horn SJ, Sørlie M, Eijsink VG. *FEBS J* 2013;**280**:3028–49.
6. Reese ET, Siu RG, Levinson HS. *J Bacteriol* 1950;**59**:485–97.
7. Merino ST, Cherry J. *Adv Biochem Eng Biotechnol* 2007;**108**:95–120.
8. Davies G, Henrissat B. *Structure* 1995;**3**:853–9.
9. Levasseur A, Drula E, Lombard V, Coutinho PM, Henrissat B. *Biotechnol Biofuels* 2013;**6**:41.

10. Aachmann FL, Sørlie M, Skjåk-Bræk G, Eijsink VG, Vaaje-Kolstad G. *Proc Natl Acad Sci U.S.A.* 2012;**109**:18779–84.
11. Quinlan RJ, Sweeney MD, Lo Leggio L, Otten H, Poulsen JC, Johansen KS, et al. *Proc Natl Acad Sci U.S.A.* 2011;**108**:15079–84.
12. Vaaje-Kolstad G, Horn SJ, van Aalten DM, Synstad B, Eijsink VG. *J Biol Chem* 2005;**280**:28492–7.
13. Forsberg Z, Vaaje-Kolstad G, Westereng B, Bunæs AC, Stenstrøm Y, MacKenzie A, et al. *Protein Sci* 2011;**20**:1479–83.
14. Fuchs RL, McPherson SA, Drahos DJ. *Appl Environ Microbiol* 1986;**51**:504–9.
15. Monreal J, Reese ET. *Can J Microbiol* 1969;**15**:689–96.
16. Igarashi K, Uchihashi T, Uchiyama T, Sugimoto H, Wada M, Suzuki K, et al. *Nat Commun* 2014;**5**:3975.
17. Horn SJ, Sørlie M, Vaaje-Kolstad G, Norberg AL, Synstad B, Vårum KM, et al. *Biocatal Biotransform* 2006;**24**:39–53.
18. Nakagawa YS, Eijsink VG, Totani K, Vaaje-Kolstad G. *J Agricult Food Chem* 2013;**61**:11061–6.
19. Hamre AG, Lorentzen SB, Väljamäe P, Sørlie M. *FEBS Lett* 2014;**588**:4620–4.
20. Igarashi K, Uchihashi T, Koivula A, Wada M, Kimura S, Okamoto T, et al. *Science* 2011;**333**:1279–82.
21. Kurasin M, Väljamäe P. *J Biol Chem* 2011;**286**:169–77.
22. Brurberg MB, Eijsink VG, Haandrikman AJ, Venema G, Nes IF. *Microbiology* 1995;**141**(Pt 1):123–31.
23. Brurberg MB, Eijsink VG, Nes IF. *FEMS Microbiol Lett* 1994;**124**:399–404.
24. Vaaje-Kolstad G, Houston DR, Riemen AH, Eijsink VG, van Aalten DM. *J Biol Chem* 2005;**280**:11313–9.
25. Synstad B, Vaaje-Kolstad G, Cederkvist FH, Saua SF, Horn SJ, Eijsink VG, et al. *Biosci Biotechnol Biochem* 2008;**72**:715–23.

Paper II

FEBS Letters 588 (2014) 4620–4624

journal homepage: www.FEBSLetters.org

Enzyme processivity changes with the extent of recalcitrant polysaccharide degradation

Anne Grethe Hamre [a], Silje Benedicte Lorentzen [a], Priit Väljamäe [b], Morten Sørlie [a,*]

[a] Department of Chemistry, Biotechnology and Food Science, Norwegian University of Life Sciences, PO 5003, N-1432 Ås, Norway
[b] Institute of Molecular and Cell Biology, University of Tartu, Tartu, Estonia

ARTICLE INFO

Article history:
Received 25 August 2014
Revised 16 October 2014
Accepted 16 October 2014
Available online 5 November 2014

Edited by Peter Brzezinski

Keywords:
Processivity
Recalcitrant polysaccharides

ABSTRACT

Glycoside hydrolases depolymerize polysaccharides. They can subtract single carbohydrate chains from polymer crystals and cleave glycosidic bonds without dissociating from the substrate after each catalytic event. This processivity is thought to conserve energy during polysaccharide degradation. Herein, we compare the processivity of components of the chitinolytic machinery of *Serratia marcescens*. The two processive chitinases ChiA and ChiB, the ChiB-W97A mutant, and the endochitinase ChiC were analyzed for the extent of degradation of three different chitin substrates. Moreover, enzyme processivity was assessed on the basis of the [(GlcNAc)2]/[GlcNAc] product ratio. The results show that the apparent processivity (Papp) greatly diminishes with the extent of degradation and confirm the hypothesis that Papp is limited by the length of obstacle free path on the substrate.

1. Introduction

To understand the mechanisms behind enzymatic hydrolysis of recalcitrant polysaccharides such as cellulose (a 1,4-β-linked polymer of D-glucose) and chitin (a 1,4-β-linked polymer of *N*-acetyl-D-glucosamine (GlcNAc) (Fig. 1) is of great biological and economic importance. Enzymes acting on cellulose or chitin face the challenges of associating with the insoluble substrate, disrupting the crystal packing, and guiding a single polymer chain into the catalytic center. Many polymer active enzymes act in a processive manner meaning that they bind individual polymer chains in long tunnels or deep clefts and hydrolyze a series of glycosidic linkages along the same chain before dissociation [1–5]. The general idea is that catalytic efficiency is improved by keeping the enzyme closely associated to the substrate in between subsequent hydrolytic reactions. In the case of crystalline substrates, calculations show that the enzymes face a free energy penalty of 5.6 kcal/mol pr. chitobiose unit and 5.4 kcal/mol pr. cellobiose unit in decrystallization energies signifying the importance for processive enzymes being capable of keeping once-detached single chains from re-associating with the insoluble material [3,5–8].

Intrinsic processivity of polymer active enzymes is governed by the rate constants k_{off} and k_{cat} meaning that it is the enzyme dissociation from the polymer chain and the catalytic constant that is important. This is summarized in the formula $P^{Intr} = (k_{cat} + k_{off})/k_{off}$ [9,10]. P^{Intr} values estimated for cellobiohydrolases are in the range of 1000 whereas the measured values of processivity, also referred to as apparent processivity (P_{app}), are more than an order of magnitude lower [9,11]. These findings have led to the hypothesis that P_{app} (number of cleavages per one productive binding event) is limited by the length of obstacle free path on the substrate [9,11–13]. Because processive enzymes have intrinsically low k_{off} values the encounter of an obstacle will cause an enzyme to halt. This limits the rate of enzyme recruitment [12] and causes so called traffic jams [14,15] on the polymer surface thus slowing the overall rate of polymer degradation. To test the possible correlation between the rate of polysaccharide degradation and P_{app}, we studied the changes of P_{app} upon a large range of the degree of chitin conversion. The well-characterized chitinolytic machinery of *Serratia marcescens* that contains two processive chitinases (ChiA and ChiB) and an endochitinase (ChiC) [16] was used. Chitin is an insoluble and heterogenous substrate, and therefore it is challenging to determine the processivity quantitatively [17]. The simplest way to measure P_{app} is to follow the profile of soluble products from hydrolysis. It has been proposed that the first cleavage from a polymer chain end will result in the release of an odd numbered oligosaccharide (e.g. mono- or trisaccharide) whereas all subsequent processive cleavages result in the release of disaccharides (Fig. 2). Assuming that the first product is a trisaccharide that is subsequently hydrolyzed to a mono- and a disaccharide the P_{app} is given by P_{app} = [disaccharide]/[monosaccharide]. This approach has several pitfalls, like the assumption of the exclusive formation of

* Corresponding author. Fax: +47 64965901.
E-mail address: morten.sorlie@nmbu.no (M. Sørlie).

http://dx.doi.org/10.1016/j.febslet.2014.10.034

odd numbered oligosaccharides from the first cleavage which may not hold as different enzymes may have different preferences for the orientation of the chain end relative to the polymer surface or different probability of endo-mode initiation. Despite these possible pitfalls, a recent high speed atomic force microscopy (HS AFM) study has revealed a good consistency between P_{app} values of cellobiohydrolases measured using product profiles and HS AFM results [18]. However, one may speculate that the fraction of enzymes performing very short runs on the polymer is underestimated in single molecule tracking studies leading to an overestimate of the degree of processivity. Here we quantified the soluble hydrolytic products $(GlcNAc)_2$ and GlcNAc in hydrolysis of chitin by *S. marcescens* chitinases and used their ratio as a measure of P_{app}. Although the absolute values of P_{app} should be treated with caution our results demonstrated the drastic reduction of P_{app} with the degree of chitin conversion.

2. Materials and methods

2.1. Chemicals

Chitooligosaccharides were obtained from Megazyme (Wicklow, Ireland). Squid pen β-chitin was purchased from France Chitin (180 μm microparticulate, Marseille, France) and α-chitin was purchased from Yaizu Suisankagaku Industry (Tokyo, Japan) and was sheared using a converge mill to a crystallinity of 74% as described by Nakagawa et al. [19]. All other chemicals were of analytical grade.

2.2. Protein expression and purification

The ChiA and ChiB [20], the ChiC [21], and ChiB-W97A [8] genes were expressed in *Escherichia coli* as described previously. The periplasmic extracts were loaded on a column packed with chitin beads (New England Biolabs) equilibrated in 50 mM Tris–HCl pH 8.0. After washing the column with the same buffer, the enzymes were eluted with 20 mM acetic acid. The buffer was then changed to 100 mM Tris–HCl pH 8.0 using Amicon Ultra-Centrifugal filters (Millipore). Enzyme purity was verified by SDS–PAGE and estimated to be >95%. Protein concentrations were determined by using the Bradford Protein Assay from Bio-Rad.

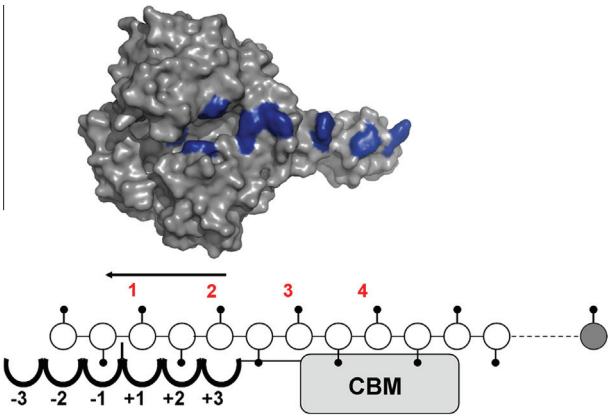

Fig. 2. Crystal structure of ChiB (top) and a schematic picture of ChiB in complex with a single chitin chain. Highlighted in blue are surface exposed aromatic amino acids that stacks with sugar moieties (being individual subsites). The glycosidic bond between the sugar residues in subsite −1 and +1 is enzymatically cleaved. A correctly positioned N-acetyl group (shown as sticks) in the −1 subsite is essential for the substrate-assisted catalysis. Due to that the smallest structural unit of chitin is a disaccharide, the product of repeated processive enzymatic actions will be dimers, $(GlcNAc)_2$. Monomers, GlcNAc, originate from initial productive binding when the sugar in the non-reducing end occupies a subsite with an odd number. For these reasons, a high ratio of $[(GlcNAc)_2]/[GlcNAc]$ indicates a high degree of apparent processivity.

2.3. Degradation of chitin

Hydrolysis of chitin (2.0 mg/ml) was carried out in 50 mM sodium acetate buffer at pH 6.1. The chitin samples were sonicated for 20 min in a sonication bath (Transsonic, Elma) to increase the surface of the substrate and thereby increase the availability of

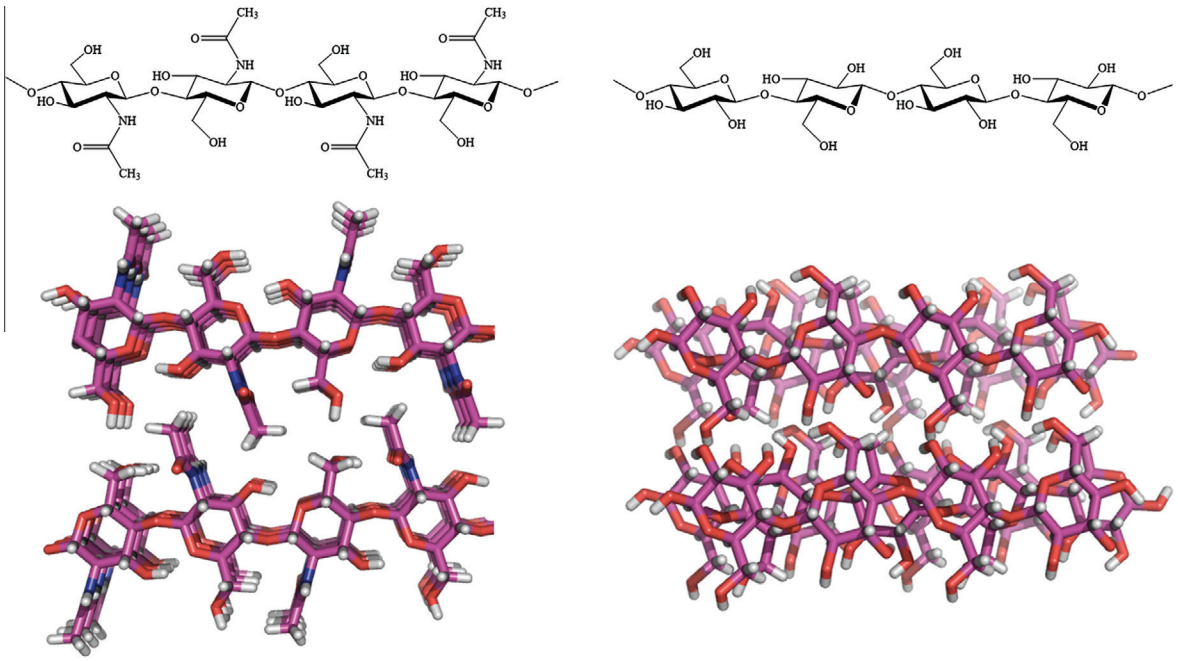

Fig. 1. Left: Chemical structure of chitin and how it stacks in an α-chitin polymer crystal structure. Right: Chemical structure of cellulose and how it stacks in a cellulose II polymer crystal structure [30]. Both chitin and cellulose have the sugar units rotated 180° relative to their neighboring residues, so that the smallest structural unit is a disaccharide.

chitin ends for the enzymes [22]. The reaction tubes were then incubated at 37 °C in an Eppendorf thermo mixer at 800 rpm to avoid settling of the chitin particles. The enzyme concentrations were in total 2.5 μM in all experiments. Aliquots of 75 μl were withdrawn at regular time intervals, and the enzymes were inactivated by adding 75 μl 20 mM H_2SO_4. Prior to further HPLC analysis all samples were filtrated through a 0.45 μm Duapore membrane (Millipore) to remove denatured protein and chitin particles. All reactions were run in duplicate, and all samples were stored at −20 °C until HPLC analysis. The degree of degradation is defined by the percentage of number of moles solubilized GlcNAc-units with respect to number of moles GlcNAc-units in solid form (chitin) used in the experiments.

2.4. High performance liquid chromatography (HPLC)

Concentrations of chitooligosaccharides were determined using HPLC with a Rezex Fast fruit H^+ column (100 mm length and 7.8 mm inner diameter) (Phenomenex). An 8 μl sample was injected on the column, and the mono/oligosaccharides were eluted isocratically at 1 ml/min with 5 mM H_2SO_4 at 85 °C. The chitooligosaccharides were monitored by measuring absorbance at 210 nm, and the amounts were quantified by measuring peak areas. Peak areas were compared with peak areas obtained with standard samples with known concentrations of mono- and disaccharides.

3. Results and discussion

Progress curves of degradation of a β-chitin (180 μm) by the processive *S. marcescens* chitinases ChiA and ChiB along with the endochitinase ChiC and a ChiB variant (ChiB-W97A) with reduced processivity are shown in Fig. 3. As is characteristic to the enzymatic degradation of recalcitrant polysaccharides we can see drastic decreases in hydrolysis rates already at moderate degrees of conversion. $(GlcNAc)_2$ and GlcNAc were the only soluble products detected and progress curves of formation are shown in Fig. 4. It is important to note that none of the enzymes are capable of cleaving $(GlcNAc)_2$ into two GlcNAc-units. At the initial stage of hydrolysis, the $[(GlcNAc)_2]/[GlcNAc]$ ratio was constant with average values of 30.1 ± 1.5, 24.3 ± 2.0, 14.3 ± 1.4 and 11.0 ± 1.8 for ChiA, ChiB, ChiC and ChiB-W97A respectively (Fig. 5). In a recent HS AFM study, the velocity of movement and the duration of processive runs of ChiA and ChiB on β-chitin were measured [23]. The authors estimated the half-life of processivity to be 21 and 13 cleavages for ChiA and ChiB respectively. These values can be converted to processivity values by dividing with ln2 [18]. Thus the HS AFM single molecule tracking resulted in processivity values of 30.3 and 18.8 for ChiA and ChiB, respectively, which are in good agreement with ChiA being more processive than ChiB as seen in our study. This also indicates that the $[(GlcNAc)_2]/[GlcNAc]$ ratio can be used as a simple measure of the processivity of these enzymes.

Comparison of the extent of chitin degradation and the initial processivity values suggests that enzymes with a higher initial degree of processivity are more efficient degraders of β-chitin. Interestingly at higher degree of chitin degradation, analysis of $[(GlcNAc)_2]/[GlcNAc]$ ratios reveals differences between the processive enzymes ChiA and ChiB and the less processive endo acting ChiC and ChiB-W97A (Fig. 4). In the case of ChiA and ChiB the $[(GlcNAc)_2]/[GlcNAc]$ ratio continuously decreased with the degree of chitin conversion whereas the effect of the extent of degradation to the processivity of ChiC and ChiB-W97A was less prominent. This suggests that endo enzymes rely less on processivity and that their rate is rather controlled by the presence of easily accessible regions on the chitin.

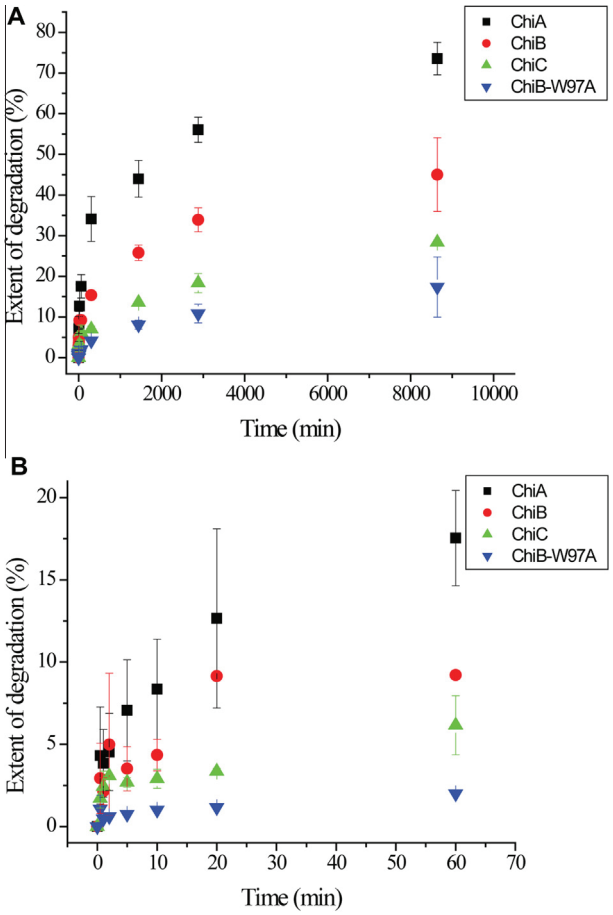

Fig. 3. (A) The extent of degradation of β-chitin (180 μm) with respect to time for two processive chitinases, an endochitinase, and a mutant with reduced degree of processivity from *Serratia marcescens*. The two processive chitinases (ChiA and ChiB) are more efficient degraders of chitin than the endochitinase and the mutant (ChiC and ChiB-W97A). (B) The degradation at initial time points. Hydrolysis was undertaken with 2.5 μM enzyme in 50 mM, pH 6.1 sodium acetate buffer at t = 37 °C with 2.0 mg/ml chitin.

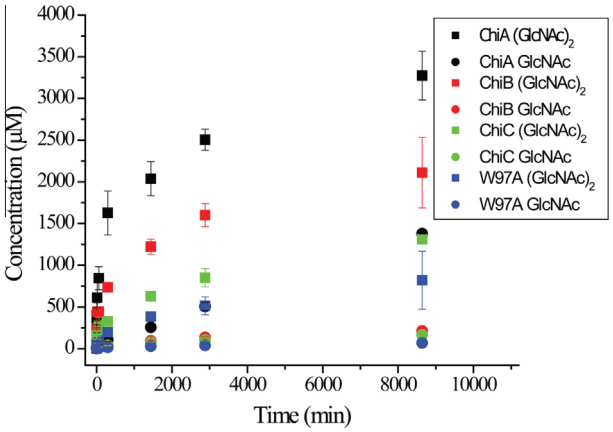

Fig. 4. Progress curves for the formation of $(GlcNAc)_2$ (squares) and GlcNAc (circles) after hydrolysis of β-chitin by ChiA (black), ChiB (red), ChiC (green) and ChiB W97A (blue). $(GlcNAc)_2$ and GlcNAc were the only products detected.

Since the $[(GlcNAc)_2]/[GlcNAc]$ ratio was time dependent, the processivity was also calculated based on the rates of $(GlcNAc)_2$ and GlcNAc formation ($P_{app} = v[(GlcNAc)_2]/v[GlcNAc]$). Rate based P_{app} values showed similar trends as the concentration based P_{app}

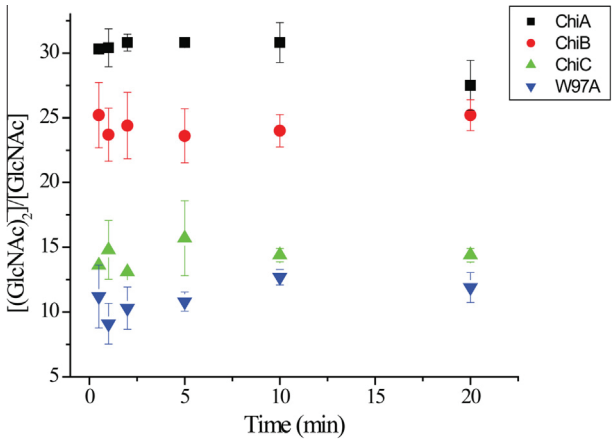

Fig. 5. Comparison of initial [$(GlcNAc)_2$]/[GlcNAc] ratios for the four different chitinases.

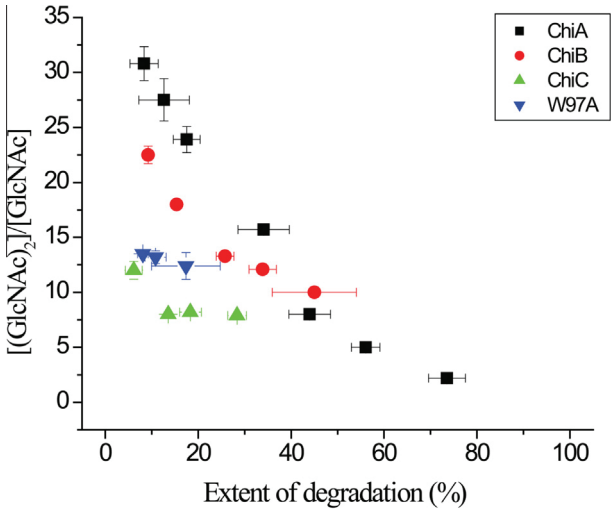

Fig. 6. Comparison of the [$(GlcNAc)_2$]/[GlcNAc] ratio against extent of degradation for the four different chitinases investigated.

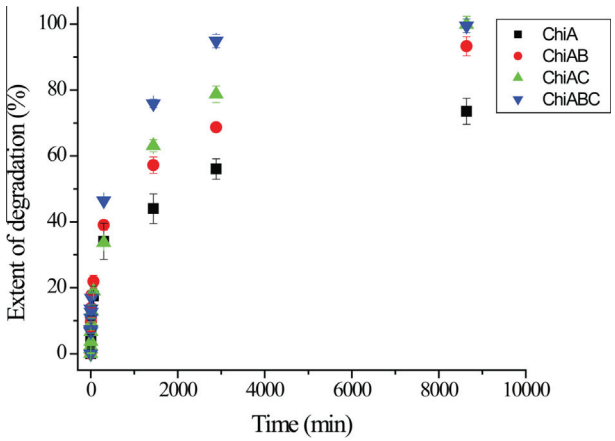

Fig. 7. The extent of degradation of chitin with respect to time for ChiA alone, together with ChiB, together with ChiC, and together with both ChiB and ChiC, respectively.

values, but the drop of P_{app} values with conversion was more pronounced (data not shown). The difference was most evident for ChiA where the rates of $(GlcNAc)_2$ and GlcNAc formation were nearly equal at conversions above 50%. Previously, studies of changes in product profiles (cellobiose/glucose ratio) in cellulose hydrolysis have revealed little or no changes in processivity with respect to conversion [18,24,25]. However, the degree of conversion remained below 10% in these studies. At these low degrees of conversion, we did not see significant changes in P_{app} either (Fig. 3). In a study by Fox et al. it was found that P_{app} of an individual cellobiohydrolase (*Tl*Cel7A) increased with substrate degradation up to 60% conversion [13]. The reasons behind the different behavior of *Tl*Cel7A and the different *S. marcescens* chitinases to this respect remain to be studied. Moreover, the P_{app} of *Tl*Cel7A decreased with increasing concentration of an endoglucanase (*Tem*GH5). The effect on P_{app} by addition of ChiB and ChiC, by themselves and together, with ChiA was also investigated in our study. At the initial stage of hydrolysis, the [$(GlcNAc)_2$]/[GlcNAc] ratio was observed to be 27.1 ± 1.3 for ChiA and ChiB, 26.3 ± 2.0 for ChiA and ChiC, and 22.1 ± 2.0 for ChiA, ChiB, and ChiC combined. For ChiA in the presence of either ChiB or ChiC, these values are intermediate between those observed for ChiA and ChiB alone (30.1 ± 1.5 and 24.3 ± 2.0, respectively). When all three chitinases are present, the observed P_{app} value is close to that observed for ChiB alone. Even though initial P_{app} was smaller for ChiA in combination with other chitinases, both the rate of hydrolysis (after the first initial 60 min) as well as the extent of degradation was larger (Fig. 7).

Finally, the effect of the origin of the substrate on P_{app} was assessed by allowing ChiA to incubate with a sheared α-chitin. Here, at the initial stage of hydrolysis, the [$(GlcNAc)_2$]/[GlcNAc] ratio was observed to be 14.2 ± 0.5, significantly smaller than what was observed for the β-chitin (30.1 ± 1.5) used in this study. The anti-parallel orientation of the polymer chains of α-chitin allows a high number of hydrogen bonds to be formed resulting in a tight packing of the polymeric strands and high stability of the crystalline structure [26,27]. Moreover, this tight packing exclude the presence of water. The parallel orientation of the polymer strands in β-chitin allows for up to two water molecules pr. *N*-acetylglucosamine residue making this form less recalcitrant [28,29], and hence likely easier to be degraded in a processive manner. With this in mind, the decreased [$(GlcNAc)_2$]/[GlcNAc] ratio with respect to extent of degradation as shown in Fig. 6 may also in part be connected with the hydration of the β-chitin in that the content of water molecules is decreased inside of the substrate making this part of the crystal more recalcitrant. The addition of ChiB to ChiA in α-chitin degradation only slightly altered the initial P_{app} (15.5 ± 1.0).

Together our data suggest that the substrate becomes more recalcitrant with conversion shown with a decrease in processivity of processive enzymes. Also, we see a difference between substrates. It is therefore essential to report both the nature of the substrate that is used as well as having control of the extent of substrate degradation when reporting the degree of processivity. As previously proposed for cellulose hydrolysis the degradation of chitin by processive chitinases is limited by the length of obstacle free paths on the substrate [9,11–13]. Initially ChiA has a higher degree of processivity than ChiB while at the end points the [$(GlcNAc)_2$]/[GlcNAc] ratio is higher for ChiB than ChiA. Also, the end points for ChiA and ChiB differs with approximately 30%. These are several factors making us strongly suggesting that the initial degradation is the best measure of processivity and that having control of the extent of substrate degradation is important. Although the role of other factors, like product inhibition, cannot be excluded our data suggest that the length of obstacle free path during hydrolysis is an important contributor in controlling the rate of chitin degradation.

Acknowledgements

The research leading to these results has received funding from the Norwegian Financial Mechanism (Grant EMP171) and Grant 209335/F20 from the Norwegian Research Council.

References

[1] Zakariassen, H., Eijsink, V.G.H. and Sørlie, M. (2010) Signatures of activation parameters reveal substrate-dependent rate determining steps in polysaccharide turnover by a family 18 chitinase. Carbohydr. Polym. 81, 14–20.
[2] Davies, G. and Henrissat, B. (1995) Structures and mechanisms of glycosyl hydrolases. Structure 3, 853–859.
[3] Teeri, T.T. (1997) Crystalline cellulose degradation: new insight into the function of cellobiohydrolases. Trends Biotechnol. 15, 160–167.
[4] Varrot, A., Frandsen, T.P., von Ossowski, I., Boyer, V., Cottaz, S., Driguez, H., Schulein, M. and Davies, G.J. (2003) Structural basis for ligand binding and processivity in cellobiohydrolase Cel6A from *Humicola insolens*. Structure 11, 855–864.
[5] von Ossowski, I., Stahlberg, J., Koivula, A., Piens, K., Becker, D., Boer, H., Harle, R., Harris, M., Divne, C., Mahdi, S., Zhao, Y., Driguez, H., Claeyssens, M., Sinnott, M.L. and Teeri, T.T. (2003) Engineering the exo-loop of *Trichoderma reesei* cellobiohydrolase, Cel7A. A comparison with *Phanerochaete chrysosporium* Cel7D. J. Mol. Biol. 333, 817–829.
[6] Beckham, G.T. and Crowley, M.F. (2011) Examination of the α-chitin structure and decrystallization thermodynamics at the nanoscale. J. Phys. Chem. B 115, 4516–4522.
[7] Beckham, G.T., Matthews, J.F., Peters, B., Bomble, Y.J., Himmel, M.E. and Crowley, M.F. (2011) Molecular-level origins of biomass recalcitrance: decrystallization free energies for four common cellulose polymorphs. J. Phys. Chem. B 115, 4118–4127.
[8] Horn, S.J., Sikorski, P., Cederkvist, J.B., Vaaje-Kolstad, G., Sørlie, M., Synstad, B., Vriend, G., Vårum, K.M. and Eijsink, V.G.H. (2006) Costs and benefits of processivity in enzymatic degradation of recalcitrant polysaccharides. Proc. Natl. Acad. Sci. U.S.A. 103, 18089–18094.
[9] Kurašin, M. and Väljamäe, P. (2011) Processivity of cellobiohydrolases is limited by the substrate. J. Biol. Chem. 286, 169–177.
[10] Payne, C.M., Jiang, W., Shirts, M.R., Himmel, M.E., Crowley, M.F. and Beckham, G.T. (2013) Glycoside hydrolase processivity is directly related to oligosaccharide binding free energy. J. Am. Chem. Soc. 135, 18831–18839.
[11] Cruys-Bagger, N., Tatsumi, H., Ren, G.R., Borch, K. and Westh, P. (2013) Transient kinetics and rate-limiting steps for the processive cellobiohydrolase Cel7A: effects of substrate structure and carbohydrate binding domain. Biochemistry 52, 8938–8948.
[12] Jalak, J. and Valjamae, P. (2010) Mechanism of initial rapid rate retardation in cellobiohydrolase catalyzed cellulose hydrolysis. Biotechnol. Bioeng. 106, 871–883.
[13] Fox, J.M., Levine, S.E., Clark, D.S. and Blanch, H.W. (2012) Initial- and processive-cut products reveal cellobiohydrolase rate limitations and the role of companion enzymes. Biochemistry 51, 442–452.
[14] Igarashi, K., Uchihashi, T., Koivula, A., Wada, M., Kimura, S., Okamoto, T., Penttilä, M., Ando, T. and Samejima, M. (2011) Traffic jams reduce hydrolytic efficiency of cellulase on cellulose surface. Science 333, 1279–1282.
[15] Shang, B.Z., Chang, R. and Chu, J.-W. (2013) Systems-level modeling with molecular resolution elucidates the rate-limiting mechanisms of cellulose decomposition by cellobiohydrolases. J. Biol. Chem. 288, 29081–29089.
[16] Vaaje-Kolstad, G., Horn, S.J., Sørlie, M. and Eijsink, V.G.H. (2013) The chitinolytic machinery of *Serratia marcescens* – a model system for enzymatic degradation of recalcitrant polysaccharides. FEBS J. 280, 3028–3049.
[17] Horn, S.J., Sørlie, M., Vårum, K.M., Väljamäe, P. and Eijsink, V.G.H. (2012) Measuring processivity. Methods Enzymol., 69–95 (Academic Press).
[18] Nakamura, A., Watanabe, H., Ishida, T., Uchihashi, T., Wada, M., Ando, T., Igarashi, K. and Samejima, M. (2014) Trade-off between processivity and hydrolytic velocity of cellobiohydrolases at the surface of crystalline cellulose. J. Am. Chem. Soc. 136, 4584–4592.
[19] Nakagawa, Y.S., Eijsink, V.G.H., Totani, K. and Vaaje-Kolstad, G. (2013) Conversion of α-chitin substrates with varying particle size and crystallinity reveals substrate preferences of the chitinases and lytic polysaccharide monooxygenase of *Serratia marcescens*. J. Agric. Food Chem. 61, 11061–11066.
[20] Brurberg, M.B., Nes, I.F. and Eijsink, V.G.H. (1996) Comparative studies of chitinases A and B from *Serratia marcescens*. Microbiology 142, 1581–1589.
[21] Synstad, B., Vaaje-Kolstad, G., Cederkvist, F.H., Saua, S.F., Horn, S.J., Eijsink, V.G.H. and Sørlie, M. (2008) Expression and characterization of endochitinase C from *Serratia marcescens* BJL200 and its purification by a one-step general chitinase purification method. Biosci. Biotechnol. Biochem. 72, 715–723.
[22] Fan, Y.M., Saito, T. and Isogai, A. (2008) Preparation of chitin nanofibers from squid pen beta-chitin by simple mechanical treatment under acid conditions. Biomacromolecules 9, 1919–1923.
[23] Igarashi, K., Uchihashi, T., Uchiyama, T., Sugimoto, H., Wada, M., Suzuki, K., Sakuda, S., Ando, T., Watanabe, T. and Samejima, M. (2014) Two-way traffic of glycoside hydrolase family 18 processive chitinases on crystalline chitin. Nat. Commun. 5, 3975.
[24] Eriksson, T., Karlsson, J. and Tjerneld, F. (2002) A model explaining declining rate in hydrolysis of lignocellulose substrates with cellobiohydrolase I (cel7A) and endoglucanase I (cel7B) of *Trichoderma reesei*. Appl. Biochem. Biotechnol. 101, 41–60.
[25] Medve, J., Karlsson, J., Lee, D. and Tjerneld, F. (1998) Hydrolysis of microcrystalline cellulose by cellobiohydrolase I and endoglucanase II from *Trichoderma reesei*: adsorption, sugar production pattern, and synergism of the enzymes. Biotechnol. Bioeng. 59, 621–634.
[26] Minke, R. and Blackwell, J. (1978) The structure of alpha-chitin. J. Mol. Biol. 120, 167–181.
[27] Sikorski, P., Hori, R. and Wada, M. (2009) Revisit of α-chitin crystal structure using high resolution X-ray diffraction data. Biomacromolecules 10, 1100–1105.
[28] Kobayashi, K., Kimura, S., Togawa, E. and Wada, M. (2010) Crystal transition between hydrate and anhydrous β-chitin monitored by synchrotron X-ray fiber diffraction. Carbohydr. Polym. 79, 882–889.
[29] Sawada, D., Nishiyama, Y., Langan, P., Forsyth, V.T., Kimura, S. and Wada, M. (2012) Water in crystalline fibers of dihydrate beta-chitin results in unexpected absence of intramolecular hydrogen bonding. PLoS One 7, 8.
[30] Petrov, M., Lymperakis, L., Friák, M. and Neugebauer, J. (2013) Ab initio based conformational study of the crystalline α-chitin. Biopolymers 99, 22–34.

Paper III

Thermodynamic relationships with processivity in *Serratia marcescens* family 18 chitinases

Anne Grethe Hamre,[1†] Suvamay Jana,[2†] Matilde Mengkrog Holen,[1] Geir Mathiesen,[1] Priit Väljamäe,[3] Christina M. Payne,[2] and Morten Sørlie[1*]*

[1] Department of Chemistry, Biotechnology and Food Science, Norwegian University of Life Sciences, PO 5003, N-1432 Ås, Norway.

[2] Department of Chemical and Materials, University of Kentucky, Lexington, Kentucky 40506, United States.

[3] Institute of Molecular and Cell Biology, University of Tartu, Tartu, Estonia.

[†] These authors contributed equally to this work.

[*] To whom correspondence should be addressed. E-mail: morten.sorlie@nmbu.no, Tel.: +47-67232562 and Fax: +47-64965901 or christy.payne@uky.edu, Tel.: + 859-257-2902 and Fax: + 859-323-1929

ABSTRACT

The enzymatic degradation of recalcitrant polysaccharides is accomplished by synergistic enzyme cocktails of glycoside hydrolases (GHs) and accessory enzymes. Many GHs are processive which means that they remain attached to the substrate in between subsequent hydrolytic reactions. Chitinases are GHs that catalyze the hydrolysis of chitin (β-1,4-linked *N*-acetylglucosamine). Previously, a relationship between active site topology and processivity has been suggested while recent computational efforts have suggested a link between the degree of processivity and ligand binding free energy. We have investigated these relationships by employing computational (molecular dynamics (MD)) and experimental (isothermal titration calorimetry (ITC)) approaches to gain insight into the thermodynamics of substrate binding to *Serratia marcescens* chitinases ChiA, ChiB, and ChiC. We show that increased processive ability indeed corresponds to more favorable binding free energy and that this likely is a general feature of GHs. Moreover, ligand binding in ChiB is entropically driven, in ChiC it is enthalpically driven, and the enthalpic and entropic contributions to ligand binding in ChiA are equal. Furthermore, water is shown to be especially important in ChiA-binding. This work provides new insight into oligosaccharide binding, getting us one step closer to understand how GHs efficiently degrade recalcitrant polysaccharides.

1. Introduction

Polymeric carbohydrate constructs, polysaccharides, are the fundamental building blocks for many of nature's most important structures and functions. The enzymatic hydrolysis of glycosidic linkages, the covalent bonds joining carbohydrates, is generally acid-catalyzed by glycoside hydrolases (GHs) using one of two different mechanisms: either one that results in retention or one that results in inversion of the anomeric configuration.[1] To efficiently degrade the complex and frequently recalcitrant polysaccharide architecture[2], microorganisms employ synergistic enzyme-cocktails of GHs and other accessory enzymes, each of which has a specific function in the degradation. [3,4,5,6] GHs are known to cleave the polymer chains randomly in what is termed endo-initiated hydrolysis, or they may have a preference for hydrolyzing chain ends from either the reducing or non-reducing end of the substrate by what is called exo-initiated hydrolysis. Many GHs capable of the latter also exhibit the ability to conduct endo-initiated hydrolysis.[7] Furthermore, processive and non-processive GHs work together to optimize polysaccharide degradation. Processive enzymes bind individual polymer chains in long tunnels or deep clefts and repeatedly hydrolyze series of glycosidic linkages along the same chain before dissociation[1], while non-processive enzymes generate new, free chain ends through rapid association, hydrolysis, and dissociation events.

Chitin, a β-1,4-linked insoluble, linear polymer of *N*-acetylglucosamine (GlcNAc) is the second most abundant polysaccharide in nature.[8] Chitin owes this abundance to its prevalence as a structural component among many species including the cell wall of most fungi[9], the microfilarial sheath of parasitic nematodes[10,11], the exoskeleton of all types of arthropods[12], and the lining of many insects guts.[13] The GlcNAc units that chitin consists of are rotated 180° relative to each other such that the characteristic *N*-acetyl groups of each pyranose are on opposite sides.[14] The structural unit of chitin is thus a dimer of GlcNAc.

Chitin is formed when the long GlcNAc chains orient themselves into well-packed layers mediated by hydrogen bond networks.[14,15,16,17]

Chitinases are GHs that catalyze the conversion of chitin into chitobiose units. Based on their characteristic TIM barrel fold and amino acid sequence, they are classified as family 18 GHs (GH18) (www.cazy.org).[18] Family 18 chitinases conduct hydrolysis through a unique, substrate-assisted mechanism in which the *N*-acetyl group of the sugar in subsite −1 acts as the nucleophile. All GH18 chitinases degrade chitin with retention of the stereochemistry at the anomeric carbon.[18,19,20,21,22] The similarity in catalytic mechanism is a result of shared sequence motifs that form the catalytic $(\beta/\alpha)_8$-barrel active site: a characteristic DXXDXDXE motif ending with the catalytic acid and an SXGG motif.[23,24] In addition to the catalytic residues in negative subsites, all available structures possess a family-specific hydrophobic platform consisting of one or two highly conserved aromatic acid residues close to subsite −1.[25]

The chitinolytic machinery of the Gram-negative soil bacteria *Serratia marcescens* has often been used as a model system to understand enzymatic degradation of recalcitrant polysaccharides.[5] The *S. marcescens* suite of enzymes consists of three multi-modular chitinases, Chitinase A, B, and C, among a host of other enzymes. Chitinase A (ChiA) is a reducing end-specific processive chitinase, moving towards the non-reducing end as the substrate is hydrolyzed, while Chitinase B (ChiB) is a non-reducing end-specific processive chitinase acting towards the reducing end. [5,26,27,28,29,30] It has previously been suggested that a relationship between the topology of the GH active site and its mode of action exists.[1] Along these lines, ChiA exhibits a relatively open active site cleft, a typical feature of endo-acting enzymes.[1, 28] However, ChiB has a partially closed active site cleft, lending a more tunnel-like active site topology that is frequently observed in exo-acting enzymes.[1, 29] Chitinase C (ChiC) is a non-processive, endo-acting enzyme with a shallow substrate

binding cleft.[31,32] The open cleft is thought to enable the random association/dissociation processes. The full length ChiC, also referred to as ChiC1, tends to be cleaved by endogenous proteases to yield ChiC2, comprising the catalytic domain only.[23,33,34]

Overall, the three chitinases exhibit distinct differences with regard to topology and processive ability. To this extent, a recent computational study suggests that a positive correlation exists between the degree of processivity and free energy changes.[35] Based on this study, we further hypothesize that the innate differences between the chitinases will manifest in their thermodynamic signatures upon substrate binding. To investigate this hypothesis, we employ computational and experimental approaches toward determining changes in free energy, enthalpy, and entropy upon substrate binding and the molecular-level contributions to these changes. Free energy changes of binding hexa-*N*-acetylglucosamine, $(GlcNAc)_6$, to ChiA, ChiB, and ChiC were determined using free energy perturbation with Hamiltonian replica exchange molecular dynamics (FEP/λ-REMD). The experimental complement to this calculation, isothermal titration calorimetry (ITC), was used as a means of comparison and to identify the enthalpic and entropic contributions to free energies of binding. Molecular dynamics (MD) simulations provide additional insight into how the chitinase active sites contribute to ligand binding. The free energy changes are compared with existing apparent processivity measurements[36] to reveal how thermodynamic signatures are related to enzymatic functionality.

2. Materials and methods

2.1 Chemicals.

Hexa-*N*-acetylglucosamine was obtained from Megazyme (Wicklow, Ireland). All other chemicals were of analytical grade.

2.2 Enzymes.

Site directed mutagenesis

In order to measure the free energies of the binding between $(GlcNAc)_6$ and ChiA, ChiB, and ChiC with ITC catalytically inactivated enzymes (mutation of the catalytic acid (Glu to Gln)) must be used. ChiA-E315Q and ChiB-E144Q are previously constructed.[37,38] ChiC-E141Q was prepared using the QuikChange™ site directed mutagenesis kit from Stratagene (La Jolla, CA, USA), as described by the manufacturer. The primers used for the mutagenesis are listed in Table 1 and were purchased from Life Technologies (Carlsbad, CA, USA). To confirm that the *chic* gene contained the desired mutations and to check for the occurrence of non-desirable mutations, the mutated gene was sequenced using GATC Biotech's (Constance, Germany) LIGHTrun sequencing service before it was transformed into *Escherichia coli* BL21Star (DE3) cells (Life Technologies).

Table 1. Primers used for site-directed mutagenesis and PCR amplification

Enzyme	Primer	Sequence
		Site-directed mutagenesis[a]
ChiC-E141Q	Forward	5'CTGGATATCGATCTG**CAG**CAGGCGGCGATCGGC 3'
	Reverse	5'GCCGATCGCCGCCTG**CTG**CAGATCGATATCCAG 3'
		PCR-amplification[b]
ChiA-E315Q	Forward	5'TCGAAGGTCGT*CATATG*GCCGCGCCGGGC 3'
	Revers	5'CAGCCGGATC*CTCGAG*TTATTGAACGCCGGCGC 3'
ChiC-E141Q	Forward	5'TCGAAGGT*CATATG*AGCACAAATAACACTATTAATGC 3'
	Reverse	5' GCAGCCGGATC*CTCGAG*TTAGGCGATGAGCTGCCA 3'

[a] Mutated nucleotides in bold, [b] Restriction sites in italics

Construction of His_{10}-ChiA-E315Q and His_{10}-ChiC-E141Q

His_{10}-ChiB-E144Q is previously constructed.[38] To subclone ChiA-E315Q[37] and ChiC-E141Q into the vector pET16b (Novagen, Madison, WI, USA), the chitinase fragments were amplified by PCR using primers listed in Table 1 (Life Technologies). PCR reactions were conducted with Q5® High-Fidelity 2X Master Mix (New England Biolabs, Ipswich, MA, USA). The amplification protocol consisted of an initial denaturation cycle of 30 s at 98 °C, followed by 30 cycles of 5 s at 98 °C, 30 s at 55 °C, and 30 s at 72 °C, and a final step of 2 min at 72 °C. Both PCR-fragments were cloned into a NdeI/XhoI digested pET16b by using the In-Fusion HD Cloning kit (Clontech Laboratories, Kyoto, Japan). The resulting pET16b constructs were sequenced using GATC Biotech's LIGHTrun sequencing service to confirm the correct insert before they were transformed into *E. coli* BL21Star (DE3) cells (Life Technologies).

Protein expression

For protein expression, *E.coli* BL21(DE3) cells containing the appropriate plasmid (His_{10}-ChiA-E315Q, His_{10}-ChiB-E144Q or His_{10}-ChiC-E141Q) were inoculated into 25 ml LB medium containing 115 µg/ml ampicillin and grown at 37 °C and 200 rpm for 16 h. Cell culture were then inoculated into 250 ml LB medium containing 115 µg/ml ampicillin to an OD_{600} of 0.1. This culture was cultivated until the OD_{600} reached 0.8-1.0. The temperature was decreased to 22°C, and gene expression was induced with 1 mM isopropyl-β-D-thiogalactopyranoside (IPTG) for 20 h. The cells were then harvested by centrifugation (8000 rpm, 20 min at 4 °C). Periplasmic fractions were prepared by osmotic shocking as described elsewhere.[38] A cytoplasmic protein extraction was also performed by resuspending the spheroplasts in lysis buffer (0.1 mg/ml lysozyme, 50 mM Tris-HCl, 50

mM NaCl, 4 mM $MgCl_2$, 1 mM EDTA, 0.1 mM PMSF pH 8.0) and incubating it at 37 °C for 30 min. Cell debris was removed by centrifugation (8000 rpm, 20 min at 4 °C). The resulting supernatant was used for enzyme purification. Both the periplasmic and cytoplasmic extracts were sterilized by filtration (0.2 μm) prior to protein purification.

Protein purification

Proteins were purified on a column packed with Ni-NTA Agarose matrix (Qiagen, Venlo, Netherlands) (1.5 cm in diameter, 5 ml stationary phase in total). The column was pre-equilibrated in a buffer containing 20 mM Tris-HCl, 20 mM imidazole, and 500 mM NaCl at pH 8.0 before the periplasmic and cytoplasmic extracts were applied. After washing with a buffer containing 20 mM Tris-HCl and 500 mM NaCl at pH 8.0, fractions containing the enzyme were eluted with a buffer containing 20 mM Tris-HCl, 250 mM imidazole, and 500 mM NaCl at pH 8.0. A flow rate of 2.5 ml/min was used at all times. Enzyme purity was verified by SDS-PAGE and fractions containing purified enzyme were concentrated and transferred (Macrosep Advance Centrifugal Device, 10 kDa cutoff, Pall corporation, Port Washington, USA) to 20 mM potassium phosphate buffer pH 6.0. Protein concentrations were determined by using the Bradford Protein Assay from Bio-Rad (Hercules, CA, USA).

2.3 Isothermal Titration Calorimetry Experiments

ITC experiments with His_{10}-ChiA-E315Q and His_{10}-ChiC-E141Q were performed with a VP-ITC system from Microcal, Inc. (Northampton, MA, USA).[39] Solutions were thoroughly degassed prior to experiments to avoid air bubbles in the calorimeter. All reactions took place in 20 mM potassium phosphate buffer pH 6.0. Standard ITC conditions were 500 μM of $(GlcNAc)_6$ in the syringe and 15 μM of enzyme in the reaction cell. Normally, 40-60 injections of 4-6 μl $(GlcNAc)_6$ were injected into the reaction cell at 180s

intervals at 20, 25, 30, or 37 °C with a stirring speed of 260 rpm. At least two independent titrations were performed for each binding reaction. The heat of ionization of the buffer is 1.22 kcal/mol.[40] The temperature dependency of His_{10}-ChiB-E144Q has previously been determined.[41]

2.4 Analysis of calorimetric data.

ITC data were collected automatically using the Microcal Origin v.7.0 software accompanying the VP-ITC system.[39] Prior to further analysis, data were corrected for heat dilution by subtracting the heat remaining after saturation of binding sites on the enzyme. Data were fitted using a non-linear least-squares algorithm using a single-site binding model employed by the Origin software that accompanies the VP-ITC system. All data from the binding reactions fit well with the single site binding model, yielding the stoichiometry (n), equilibrium binding association constant (K_a), and the reaction enthalpy change ($\Delta H_r°$) of the reaction. The equilibrium binding dissociation constant (K_d), reaction free energy change ($\Delta G_r°$) and the reaction entropy change ($\Delta S_r°$) were calculated from the relation described in Equation 1.

$$\Delta G_r° = -RT\ln K_a = R\mathrm{T}\ln K_d = \Delta H_r° - T\Delta S_r° \quad (1)$$

Errors are reported as standard deviations of at least two experiments at each temperature. A description of how the entropic term is parameterized has previously been described in detail.[42,43]

2.5 Simulation methodology

Construction of chitinase models

The inputs for MD simulations and free energy calculations were built from crystal structures of ChiA, ChiB, and ChiC obtained from Protein Data Bank entries 1EHN[44], 1OGG[45], and 4AXN[32], respectively. In all, 8 chitinase models were constructed including: ChiA, ChiB, and ChiC both with and without ligand states. For ChiA and ChiB, two different ligand-bound simulations were constructed with the hexameric ligand occupying either the −3 to +3 binding subsites or the −4 to +2 (ChiA) and −2 to +4 (ChiB) binding subsites. The consideration of these two cases is based on experimental evidences suggesting that a GlcNAc-moiety may occupy the third product subsite after the catalytic acid (i.e. +3 for ChiA and −3 for ChiB). In the case of ChiB, occupancy of the −3 to +3 subsites is estimated as 20%, while occupancy of the −2 to +4 sites is estimated as 80%.[46] In the case of ChiA, $(GlcNAc)_5$ has equal probability for productive binding from −3 to +2 as −2 to +3.[47] A cartoon illustrating the ligand bound states for all three chitinases and their positions relative to each other is given in Figure 1.

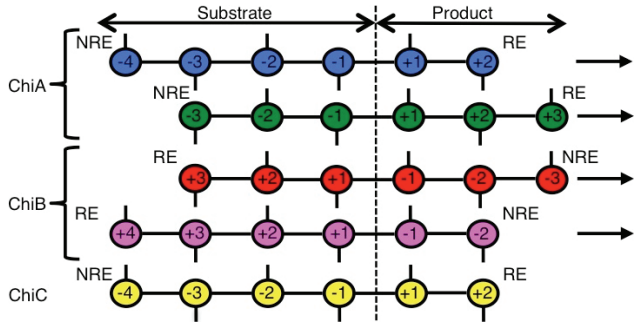

Figure 1. Schematic of $(GlcNAc)_6$ occupancy for each of the three chitinases considered in the simulations. The circles represent the pyranose sugar rings, and the black sticks attached to the circles correspond to the *N*-acetyl group. The black lines connecting each pyranose ring circle represent β-1,4 glycosidic linkages. The arrows indicate the direction the substrate slides through the active-site cleft (i.e., ChiA is reducing-end (RE) specific, and ChiB is non-reducing end (NRE) specific). ChiC is an endo-acting, non-processive enzyme, thus, no directionality arrow is shown.

Construction of the chitinase models required modification of the PDB structures so as to represent the wild-type, ligand bound systems in catalytically active conformations. For ChiA, the E315Q mutation in the 1EHN PDB was reversed, and the $(GlcNAc)_8$ bound ligand was shortened to $(GlcNAc)_6$ bound from subsite −4 to +2. For the −3 to +3 binding sites, the ligand bound structure was prepared by aligning the 1EHN PDB structure with 1E6N, which contains a bound chito-pentaose ligand. The sugar in the −4 binding subsite, from the 1EHN structure was removed, and the +3 sugar from 1E6N was added.[47] Similarly for ChiB, the 1OGG PDB D142N mutation was reverted to the wild-type Asp. The initial coordinates of the ChiB $(GlcNAc)_6$ ligand docked in the −3 to +3 subsites were obtained through structural alignment of PDB entries 1E6N and 1OGG in PyMOL.[22, 48] The second $(GlcNAc)_6$ bound structure of ChiB, docked in subsites −2 to +4, was constructed by removing a pyranose sugar ring from subsite −3 and manually adding a sugar ring at the +4 site. The manual addition of pyranose rings in ChiA and ChiB included additional stepwise

minimization gradually releasing restraints on the surrounding system to ensure the addition did not adversely affect dynamics of the remaining 5 pyranose rings. For ChiC, the $(GlcNAc)_6$ ligand was docked in the −4 to +2 subsites following the procedure described previously by Payne et al.[32] where a combination of ligands obtained from the structurally similar enzymes hevamine from *Hevea brasiliensis* and the NCTU2 chitinase from *Bacillus cereus* (1KQY[49] and 3N18[50]) were aligned. In ChiA and ChiB, complete proteins were considered; whereas for ChiC, only the catalytic domain (ChiC2) was simulated, as described above. The initial apo enzyme structures were constructed by removing the ligand from the active site of the above-described models. H++ was used to calculate the protonation states of all of our enzymes with and without ligand states at pH 6 and an internal and external dielectric constant of 10 and 80, respectively.[51,52,53] The protonation states are given in Table S1 of the Supporting Information. Disulfide bonds were specified according to the structural studies (Table S1).

Molecular dynamics simulations

The structures were explicitly solvated with water, minimized, heated, and density equilibrated in CHARMM.[54] The CHARMM36 all-atom force field with CMAP corrections was used to model the protein and carbohydrate interactions.[54,55,56] Water was modeled with the modified TIP3P force field.[57,58] After equilibration, 100 ns simulations in the NVT ensemble were performed using NAMD.[59] VMD was used for visualization of all trajectories.[60] Additional details regarding system construction, simulation parameters, and protocol have been provided in the Supporting Information.

Free energy perturbation with replica exchange molecular dynamics (FEP/λ-REMD)

FEP/λ-REMD is a computational protocol developed by Deng and Roux[61] and further modified by Jiang et al.[62,63], where free energy perturbation is coupled with replica exchange molecular dynamics to improve Boltzmann sampling of kinetically trapped conformations. Free energy calculations of this type involve two thermodynamic steps: (1) ligand decoupling from the protein-ligand complex and (2) ligand decoupling from the solvated ligand system. The difference in free energy values from these two steps results in the absolute ligand binding free energy ($\Delta G°_b$) of the enzyme-ligand complex (Figure 2).

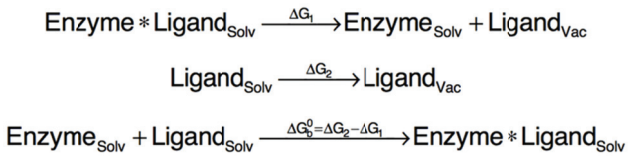

Figure 2. Thermodynamic cycle for determining $\Delta G°_b$ with FEP/λ-REMD. "Solv" refers to the solvated system and "Vac" refers to the vacuum.

To evaluate ΔG_1 in the first thermodynamic step, we used a potential energy function, U, which was expressed in terms of repulsive, dispersive, and electrostatic thermodynamic coupling parameters, λ_{rep}, λ_{dis}, λ_{elec}, respectively, and an additional restraint parameter, λ_{rstr}, as shown in Equation 2.

$$U = U_0 + \lambda_{rep}U_{rep} + \lambda_{dis}U_{dis} + \lambda_{elec}U_{elec} + \lambda_{rstr}U_{rstr} \quad (2)$$

The thermodynamic lambda parameters, λ_{rep}, λ_{dis}, and λ_{elec}, control shifted Weeks-Chandler-Anderson repulsive and dispersive components of the Lennard-Jones potential, U_{rep} and U_{dis}, and Columbic interactions, U_{elec}, respectively.[64] The restraint parameter, λ_{rstr}, controls translation and rotation in the ligand using a restraint potential, U_{rstr}. U_0 represents the potential energy of the system containing the non-interacting ligand. A standard Metropolis

Monte Carlo algorithm was used to describe the exchange probability between swaps of systems with different Hamiltonians. The ligand solvation energy, ΔG_2, in the second thermodynamic step was calculated in a similar fashion, though without the restraint term.

All of the free energy simulations were constructed from a 25-ns snapshot obtained from the MD simulations and run for a total of 3.5 ns (35 sequential FEP calculations of 0.1 ns each). Each free energy calculation used a set of 128 replicas (72 repulsive, 24 dispersive, and 32 for electrostatics) with an exchange frequency of 1/100 steps (0.1 ps). The free energies and statistical uncertainty of the repulsive, dispersive, and electrostatic contributions were determined by using the multistate Bennett acceptance ratio (MBAR) on the energies collected during simulation.[65] Convergence of the free energy values was assessed by monitoring the time evolution of all 35 FEP calculations (Figure S3). The first 1.5 ns of data were discarded as equilibration, and the last 2 ns of data were used to determine ligand binding free energy and corresponding standard deviation.

3. Results

3.1 Binding of $(GlcNAc)_6$ to ChiA, ChiB, and ChiC determined with FEP/λ-REMD

Ligand binding free energies of two processive chitinases, ChiA and ChiB, and a non-processive chitinase, ChiC, were determined to understand the contributions of active site architecture to binding free energy (Table 2). The binding free energies for ChiA and ChiB were determined with the ligand in two different locations; in the −3 to +3 subsites (ChiA and ChiB) and the −4 to +2 subsites (ChiA) or the −2 to +4 subsites (ChiB). The latter cases were examined to understand the effect product site binding has on binding free energy (i.e., binding a trimer in the product subsites as a result of acetyl positioning rather than the standard dimer product of a processive chitinase). The binding free energy values are provided alongside the corresponding repulsive, dispersive, electrostatic, and restraint

components. The solvation free energy of $(GlcNAc)_6$ is also reported. Errors associated with each contribution to the binding free energy (i.e., repulsive, dispersive, and electrostatic) represent 1 standard deviation over the last 2 ns of collected data, which is more conservative than that from MBAR. The error of the binding free energy was computed by taking the square root of the sum of the squared standard deviations of the chito-oligomer solvation free energy (ΔG_2) and the free energy needed to decouple the ligand from the enzyme-ligand complex (ΔG_1). The binding free energy as a function of time is given in the Supporting Information (Figure S3).

Table 2. Absolute ($\Delta G°_b$) ligand binding free energy calculated from FEP/λ-REMD at 300 K and pH 6.

	ΔG_b° [a]	ΔG_{rep} [a]	ΔG_{dis} [a]	ΔG_{elec} [a]	ΔG_{rstr} [a]
$(GlcNAc)_6$	-----	78.8 ± 1.1	−73.2 ± 0.7	−90.0 ± 0.8	-----
ChiA (-3 to +3)	−13.4 ± 2.2	117.3 ± 2.1	−126.4 ± 1.2	−88.2 ± 1.0	−0.5
ChiA (-4 to +2)	−16.7 ± 1.4	124.9 ± 2.2	−132.3 ± 0.4	−93.4 ± 1.5	−0.2
ChiB (-3 to +3)	−6.2 ± 1.5	119.6 ± 1.5	−124.1 ± 0.3	−85.9 ± 1.2	−0.2
ChiB (-2 to +4)	−15.2 ± 1.3	124.1 ± 1.3	−129.0 ± 0.3	−94.5 ± 1.1	−0.2
ChiC (-4 to +2)	−9.6 ± 1.6	109.4 ± 2.0	−113.4 ± 0.5	−89.5 ± 0.8	−0.5

[a] kcal/mol

3.2 Binding of $(GlcNAc)_6$ to ChiA and ChiC determined with ITC

The binding of hexa-*N*-acetylglucosamine to ChiA-E315Q and ChiC-E141Q at pH 6.0 (20 mM potassium phosphate buffer) at different temperatures (20-37 °C) was studied using ITC. Figure 3 illustrates a typical ITC thermogram and theoretical fit to the experimental data at t = 30 °C. For ChiA-E315Q, the binding to $(GlcNAc)_6$ has a K_d = 0.56

± 0.03 μM ($\Delta G_r°$ = −8.7 ± 0.1 kcal/mol, Table 3). The reaction is accompanied by an enthalpic change ($\Delta H_r°$) of −4.5 ± 0.2 kcal/mol and an entropic change ($\Delta S_r°$) of 13.9 ± 0.7 cal/K·mol ($-T\Delta S_r°$ = −4.2 ± 0.2 kcal/mol). The change in the heat of the reaction, as determined by Equation 3, was found to be −241 ± 12 cal /K·mol.

$$\Delta C_{p.r} = \left(\frac{\partial \Delta H_r^\circ}{\partial T} \right) \tag{3}$$

At t = 30 °C, ChiC-E141Q binds $(GlcNAc)_6$ with K_d = 0.10 ± 0.02 μM ($\Delta G_r°$ = −9.7 ± 0.1 kcal/mol, Table 3). The enthalpic change of the reaction is −7.8 ± 0.2 kcal/mol while the entropic change is 6.3 ± 0.7 cal/K·mol ($-T\Delta S_r°$ = −1.9 ± 0.2 kcal/mol). The change in the heat of the reaction was determined to be −158 ± 12 cal/K·mol. These values are reported in tabular form alongside previously determined values for ChiB for ease of comparison (Table 3).[38]

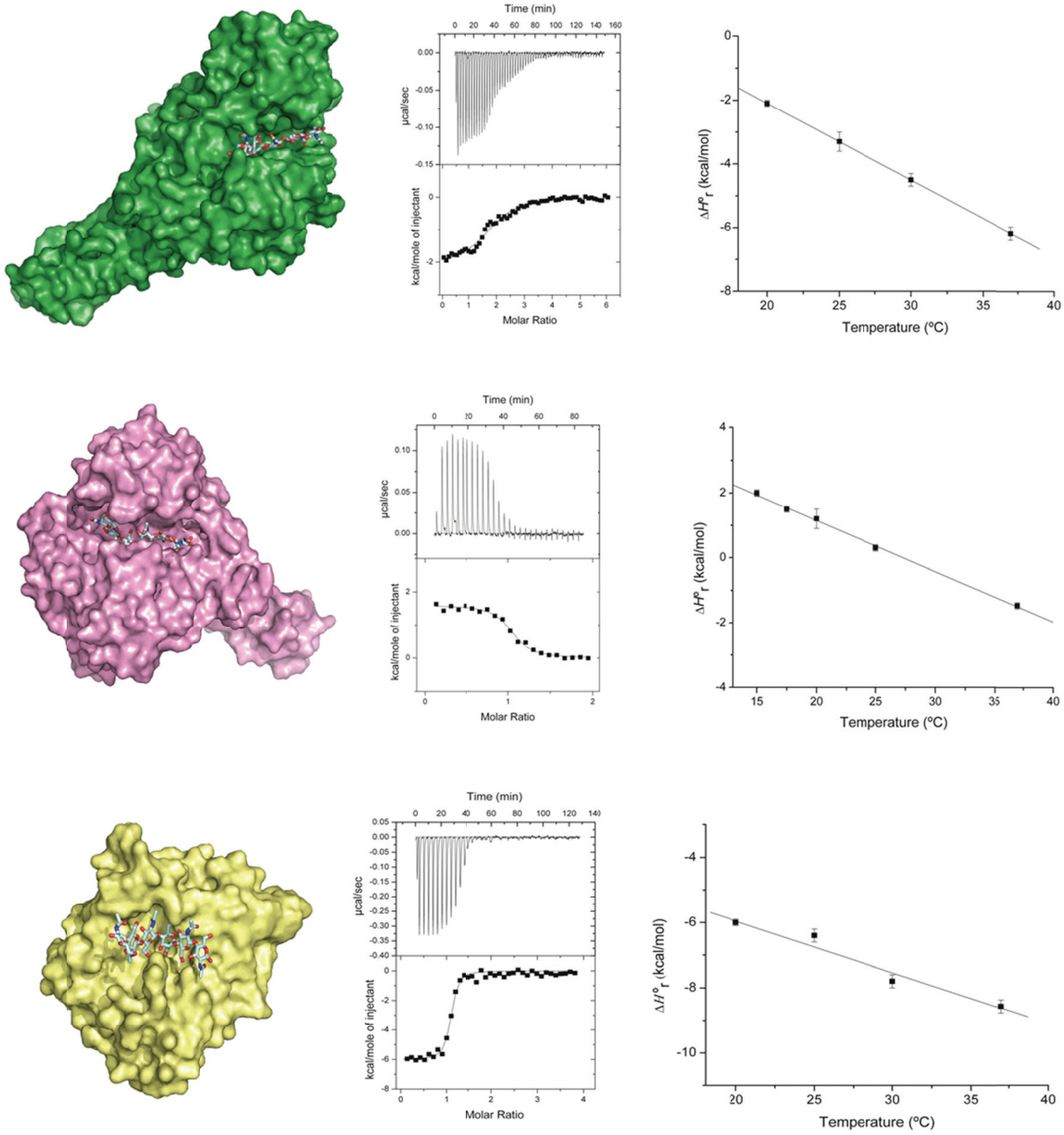

Figure 3. Left panel: Crystal structures of $(GlcNAc)_6$ bound to ChiA, ChiB, and ChiC respectively. Middle panel: Binding isotherms (top) with theoretical fits (bottom) for the binding of $(GlcNAc)_6$ to ChiA, ChiB, and ChiC at t = 20 °C in 20 mM potassium phosphate at pH 6.0. Right panel: Temperature dependence of $(GlcNAc)_6$ to ChiA, ChiB, and ChiC at t = 20 °C in 20 mM potassium phosphate at pH 6.0. The value of $\Delta C_{p,r}$ is −241 cal/K·mol, −158 cal/K·mol, and −158 cal/K·mol for ChiA, ChiB, and ChiC respectively.

Table 3. Thermodynamic parameters for $(GlcNAc)_6$ binding to ChiA, ChiB, and ChiC of *Serratia marcescens* at t = 30 °C, pH = 6.0

Enzyme	K_d[a]	ΔG_r°[b]	ΔH_r°[b]	$-T\Delta S_r^{\circ}$[b]	$-T\Delta S_{solv}^{\circ}$[b,d]	$-T\Delta S_{conf}^{\circ}$[b]	$-T\Delta S_{mix}^{\circ}$[b]	$\Delta C_{p,r}^{\circ}$[c, e]
ChiA	0.56 ± 0.03	−8.7 ± 0.1	−4.5 ± 0.2	−4.2 ± 0.2	−17.5 ± 1.0	10.9 ± 1.0	2.4	−241 ± 12
ChiB[fg]	0.20 ± 0.03	−9.3 ± 0.1	−0.1 ± 0.3	−9.2 ± 0.3	−11.5 ± 0.5	−0.1 ± 0.6	2.4	−158 ± 5
ChiC	0.10 ± 0.02	−9.7 ± 0.1	−7.8 ± 0.2	−1.9 ± 0.2	−11.5 ± 1.0	7.2 ± 1.0	2.4	−158 ± 12

[a] μM, [b] kcal/mol, [c] cal/K·mol, [d] $\Delta S_{solv}^{\circ} = \Delta C_p \ln(T_{303\,K}/T_{385\,K})$ derived using $\Delta S_r^{\circ} = \Delta S_{solv}^{\circ} + \Delta S_{mix}^{\circ} + \Delta S_{conf}^{\circ}$ where $\Delta S_{mix}^{\circ} = R\ln(1/55.5) = -8$ cal/K·mol ("cratic" term), [e] derived from the temperature dependence of ΔH_r°,

[f] derived from the interpolation of values above and below t = 30 °C, [g 41]

3.3 Parameterization of the entropic term

The entropic term, ΔS_r°, can be viewed as the sum of translational, solvational and conformational entropic changes, ΔS_{mix}, ΔS_{solv}, and ΔS_{conf}, respectively, as shown in Equation 4.[66]

$$\Delta S_r^{\circ} = \Delta S_{mix}^{\circ} + \Delta S_{solv}^{\circ} + \Delta S_{conf}^{\circ} \quad (4)$$

By recognizing that the entropy of solvation is close to zero for proteins near T = 385 K, $\Delta C_{p,r}^{\circ}$ can be related to the solvation entropy change (ΔS_{solv}°) of the binding reaction at t = 30 °C as described by Equation 5.[66,67,68]

$$\Delta S_{solv}^{\circ} = \Delta C_{p,r} \ln\left(\frac{303\,K}{385\,K}\right) \quad (5)$$

Using this relationship, a ΔS_{solv}° of 58 ± 3 cal/K·mol and 38 ± 3 cal/K·mol can be calculated for ChiA-E315Q and ChiC-E141Q, respectively. These numbers represent −17.5

± 1.0 kcal/mol and −11.5 ± 1.0 kcal/mol ($-T\Delta S_{solv}°$) of the total free energy change of −8.7 ± 0.1 kcal/mol and −9.7 ± 0.1 kcal/mol for the binding reaction between ChiA-E315Q and ChiC-E141Q and $(GlcNAc)_6$, respectively.

Furthermore, the translational entropic change ($\Delta S_{mix}°$) of the reaction can be calculated as a "cratic" term, a statistical correction that reflects mixing of solute and solvent molecules and the changes in translational/rotational degrees of freedom (Equation 6).[66]

$$\Delta S_{mix}° = R\ln (1/55.5) \quad (6)$$

Using this approach, a $\Delta S_{mix}°$ of −8 cal/K·mol can be calculated corresponding to a $-T\Delta S_{mix}°$ of 2.4 kcal/mol for both ChiA-E315Q and ChiC-141Q. The conformational entropy change can then be calculated by Equation 3, leading to a $\Delta S_{conf}°$ of −36 ± 3 cal/K·mol and −24 ± 3 cal/K·mol. These numbers correspond to a $-T\Delta S_{conf}°$ of 10.9 ± 1.0 kcal/mol and 7.2 ± 1.0 kcal/mol for ChiA-E315Q and ChiC-E141Q, respectively.

3.4 Active site dynamics from MD simulations

Molecular dynamics simulations were conducted to elucidate molecular contributions to the various components of the thermodynamic signatures of substrate binding. From the simulation trajectories, we determined several quantities that directly connect with enthalpic and entropic changes upon binding. Here, we primarily focus on the average number of water molecules displaced upon ligand binding (Figure 4), a quantity that directly relates to $\Delta S_r°$ through ΔS_{solv}. To determine the number of water molecules displaced upon ligand binding, we calculated the number of water molecules occupying the active sites of both the ligand-free and bound chitinases over the 100-ns MD trajectories.

The difference between the number of water molecules in an empty active site and the bound active site represents the number of water molecules displaced as a result of ligand binding. The number of water molecules occupying a given binding site was determined by considering the ligand-bound chitinases and selecting amino acid residues within 6 Å of the ligand. This set of amino acids was then used as a fixed frame of reference for counting the number of water molecules within the active site over time. For each frame of the eight simulation trajectories, we determined the number of water molecules within 6 Å of the previously defined amino acids, which was averaged as representative of the binding state. The average number of water molecules displaced upon ligand binding is higher for the processive chitinases, ChiA and ChiB, than for the non-processive ChiC. In general, ChiA and ChiB displace between 50 and 75 water molecules. The values for ChiA and ChiB, regardless of binding site occupancy (i.e., how many product binding sites are occupied), are within error of each other. ChiC displaces ~20 water molecules upon binding the $(GlcNAc)_6$ ligand, which reflects the more open active site topology that leaves the entire face of the $(GlcNAc)_6$ ligand solvent exposed.

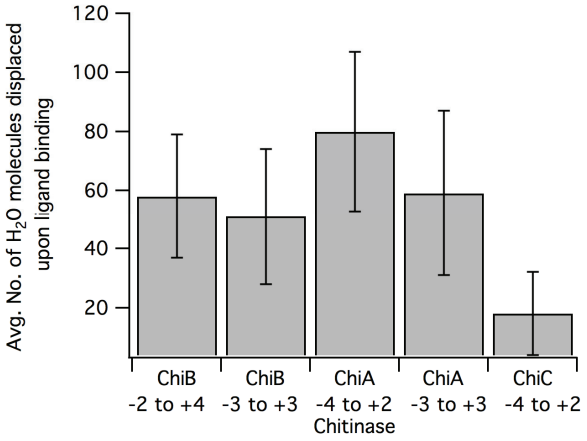

Figure 4. Average number of water molecules displaced upon binding $(GlcNAc)_6$ to ChiA, ChiB, and ChiC from MD simulations. Active site desolvation upon ligand binding corresponds to experimental estimates of the solvation entropy obtained from parameterization of ITC data. Active site desolvation refers to average number of water molecules displaced upon binding of ligand $GlcNAc_6$ to all three chitinases. Error bars represent one standard deviation.

Moreover, root mean square fluctuations (RMSF) of the protein backbone over the course of 100 ns MD simulations were also undertaken and the result show that ChiA appears to rigidify upon binding $(GlcNAc)_6$ and exhibits somewhat less fluctuation than apo ChiA (Figure 5A). Similarly, the flexibility of ChiB with the ligand bound in the −3 to +3 binding sites is virtually unchanged upon ligand binding (Figure 5B). The relationship of ChiC flexibility to conformational entropy contributions is not as obvious as for ChiA and ChiB (Figure 5C). Interestingly, a slight increase in protein flexibility is observed when ChiB binds $(GlcNAc)_6$ in the −2 to +4 sites. Most regions of ChiC are unaffected by ligand binding, but some regions slightly increase in flexibility. By observing higher RMSF of ligand over all binding sites in ChiC in comparison to processive ChiA and ChiB, we assume that lower affinity for the ligand results in higher unfavorable enthalpic contribution making overall enthalpy-entropy compensation unfavorable.

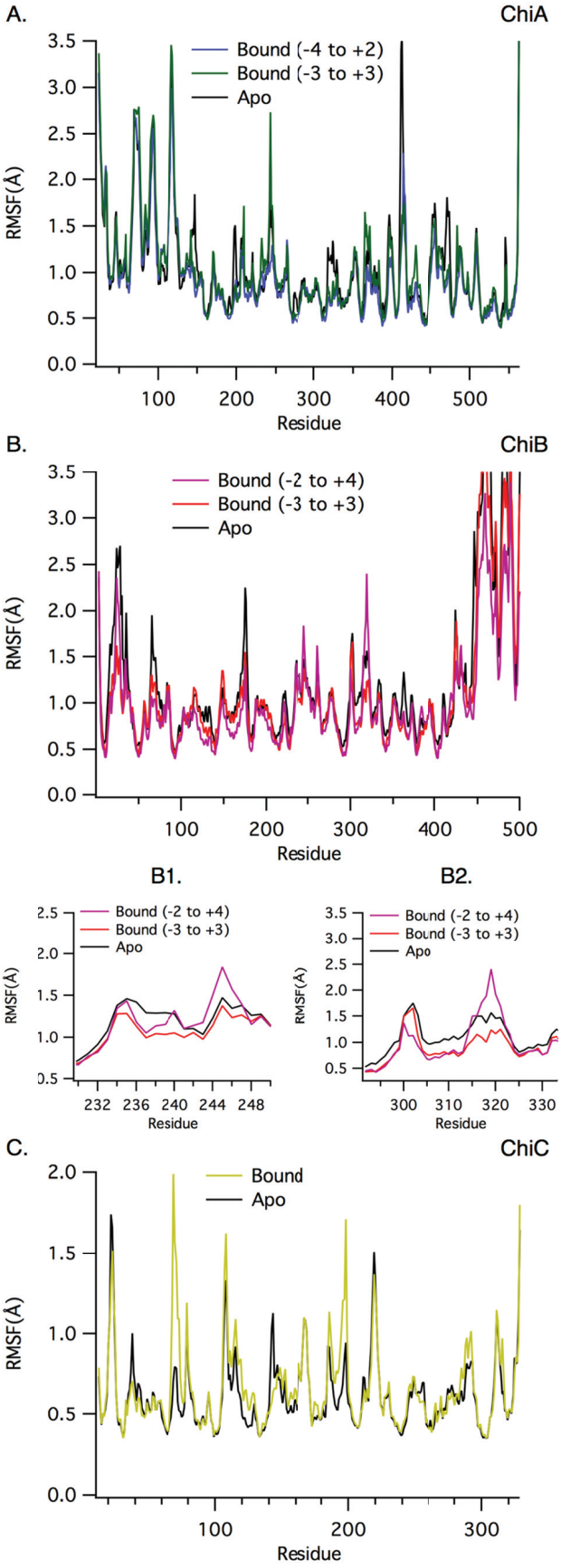

Figure 5. The RMSF of ChiA (A), ChiB (B) and ChiC (C) protein residue backbones over 100-ns MD simulations for apo and different ligand bound states are shown. Considering only the catalytic domains, the maximum RMSF values are 3.5, 3.3, and 1.9 Å for ChiA, ChiB, and ChiC, respectively. Accordingly, the *y*-axes have been truncated for clarity. Insets B.1 and B.2 focus on the RMSF of selected ChiB residues displaying interesting behavior while the ligand occupies different binding sites (B.1 for residues 239 to 240 and B.2 for residues 315 to 322).

Additional MD simulation results are described in the Supplemental Information. There, we address how fluctuation of the ligand (Figure S1), as measured by root mean square fluctuation, relates to binding free energy. Analysis of the number of hydrogen bonds formed between the ligand and the substrate provides additional insight into observed differences in binding free energy resulting from binding site occupancy (Figure S2).

4. Discussion

The relationship of processive ability with binding free energy.

The relationship between processive ability and ligand binding free energy in GHs was previously hypothesized on the basis of calculated binding free energies for processive family 7 GHs.[35] The study suggested that increasing degree of processive ability was correlated with increasing affinity of the GH7 cellulases for the cellononaose oligomers. Combining a probabilistic description of processive ability, intrinsic processivity (P^{Intr}), with thermodynamics of chemical equilibrium, a mathematical description of the relationship of processivity with free energy was suggested (Equation 7):

$$\frac{\Delta G_{\mathrm{b}}^{\circ}}{RT} = \ln\left(\frac{P^{\mathrm{Intr}} \cdot k_{\mathrm{on}}}{k_{\mathrm{cat}}}\right) \tag{7}$$

where R is the universal gas constant, T is the temperature, k_{on} is the association rate coefficient, and k_{cat} is the catalytic rate coefficient. Cellulase processivity measurements vary significantly depending on the method and substrates used, making comparisons across laboratories extremely difficult. Accordingly, the Payne *et al*. study was somewhat limited by the availability of only two processivity measurements of differently able GH7s. The assumptions underlying Equation 7, (1) that k_{cat} is much higher than k_{off} and (2) that the

enzyme-substrate association process reaches equilibrium, are thought to be general for all GHs. Thus, the investigation of this relationship in a model GH system, *S. marcescens* chitinases, is expected to yield valuable insight toward both the validity of Equation 7 and its generality.

Intrinsic processivity describes the theoretical maximum processive potential of a given enzyme. The value is derived from a statistical estimation of the likelihood of the GH to dissociate from the substrate versus to take a processive, catalytic step forward on the substrate.[69] Experimental measurements of intrinsic processivity proves difficult for a host of reasons[70], and thus, relatively few determinations of GH intrinsic processivity have been reported. Apparent processivity, P^{app}, is the actual measured value of processive ability, which encompasses environmental factors such as substrate accessibility and environmental conditions. We recently observed that P^{app} declines over time as the extent of substrate degradation increases, underlying the importance of uniformity in experimental determinations of processivity.[36] However, we also determined that initial P^{app} determinations provide the best measure of processive ability for comparative purposes. These initial P^{app} values are expected to trend with P^{Intr} and thus provide the means by which to qualitatively compare chitinase processive ability with ligand binding free energy.

Previously reported P^{app} measurements suggest that ChiA is more processive than ChiB, and that ChiC is least processive.[36] Apparent processivity was determined from the initial ratio of dimeric to monomeric products, the $[(GlcNAc)_2]/[GlcNac]$ ratio, of β-chitin degradation. ChiA appears to be slightly more processive than ChiB, with measured initial P^{app} values of 30.1 ± 1.5 and 24.3 ± 2.0, respectively. ChiC exhibits a P^{app} of 14.3 ± 1.4.

The calculated free energies of binding $(GlcNAc)_6$ to the three *S. marcescens* chitinases, ChiA, ChiB, and ChiC, reveal that increased processive ability corresponds to more favorable binding free energy, as hypothesized in Equation 7. Here, we consider the most

relevant binding site occupancy, −4 to +2, for ChiA and ChiC and −2 to +4 for ChiB (Figure 1), which encompasses the ligand binding scenario encountered in determination of P^{app} (i.e, two product subsites and four substrate subsites are occupied, to generate a dimer). The calculated binding free energies were −16.7 ± 1.4 kcal/mol, −15.2 ± 1.3 kcal/mol, and –9.6 ± 1.6 kcal/mol for ChiA, ChiB, and ChiC, respectively. ChiA binds the $(GlcNAc)_6$ with the highest affinity, while ChiC has the lowest affinity. Accordingly, ChiA is reported to be the most processive of the three chitinases, while ChiC is the least processive.

Quantitative validation of Equation 7 is not currently feasible, given available experimental data. Although the estimates of k_{cat} values for ChiA are available, the k_{off} values have not been measured for chitinases so far.[71] Moreover, the relationship of processivity to ligand binding free energy describes a fully-engaged GH, ready to perform a catalytic event. As we will describe, ITC measurements of binding free energy may not always capture the ligand in such a conformation, wherein two product subsites are bound and the distorted Michaelis complex is completely formed.

Effects of binding site occupancy on binding free energy

Both ITC and free energy calculations suggest that binding $(GlcNAc)_6$ across the −3 to +3 binding sites of ChiA and ChiB, with three pyranose rings on either side of the catalytic cleavage site (+1/−1), is less favorable than when two product subsites and four substrate subsites are bound. From calculation, ChiA binds $(GlcNAc)_6$ in the −3 to +3 subsites with a free energy of −13.4 ± 2.2 kcal/mol, slightly less than across the −4 to +2 subsites. The difference between binding $(GlcNAc)_6$ in the −3 to +3 subsites and the −2 to +4 subsites is even more substantial in ChiB. ChiB binds $(GlcNAc)_6$ in the −3 to +3 subsites with a free energy of −6.2 ± 1.5 kcal/mol, less than half the free energy of binding to the −2 to +4 subsites.

The variation in ligand binding free energy as a function of binding site occupation suggests that there is significant variation in affinity for the ligand in the product and substrate binding sites. In ChiB, the significant reduction in binding affinity resulting simply from a 1-site shift into the product side indicates that substrate-side binding is much tighter than product site binding, which is consistent with experimental studies suggesting that ChiB is not product inhibited.[31] Thus, one would not expect the product binding sites to contribute an abnormally high degree of affinity. This contrasts the cellulose-active cellobiohydrolase, *Trichoderma reesei* Cel7A, which is known to be product inhibited, and the product binding sites have been shown to contribute significantly to the overall ligand binding free energy.[35, 72] The difference in free energy of binding $(GlcNAc)_6$ to ChiA in the −3 to +3 and −4 to +2 sites is more subtle than in ChiB, which is again related to the product inhibition.[71] Like *T. reesei* Cel7A, ChiA is somewhat inhibited by its dimeric product, meaning the +1 and +2 binding sites contribute more to binding the ligand than the equivalent sites (−1 and −2) in ChiB. Nevertheless, a clear difference in the binding free energies as a function of bound position exists for both ChiA and ChiB, which is important in interpreting experimental measurements of free energy. Finally, we note that a recent high-speed atomic force microscopy study connected binding affinity on the substrate-binding side of ChiA and ChiB active site tunnels with processive ability, suggesting more available substrate binding sites in an enzyme active site correlates with higher processive ability.[73]

Experimental measurements of the free energies of binding $(GlcNAc)_6$ to ChiA and ChiB are less favorable than calculated values. Experimental data for the ligand binding free energy and accompanying thermodynamic parameters in ChiA and ChiC were obtained by performing temperature dependency measurements by ITC (Table 3). These values have previously been reported for ChiB.[41] For simplicity in discussion, we refer to the his-tagged

catalytically inactive variants used in the ITC experiments, His_{10}-ChiA-E315Q, His_{10}-ChiB-E144Q, and His_{10}-ChiC-E141Q, as ChiA, ChiB, and ChiC, respectively. The ITC measurements of affinity for ChiA, ChiB, and ChiC for $(GlcNAc)_6$ indicate each of these enzymes bind the hexamer ligand with approximately equal binding strength (−8.7 ± 0.1 kcal/mol, −9.3 ± 0.1 kcal/mol, and −9.7 ± 0.1 kcal/mol for ChiA, ChiB, and ChiC, respectively). The calculated value for ChiC (−9.6 ± 1.6) is in near perfect agreement with the experimentally obtained value. However, computational assessments of ChiA and ChiB $(GlcNAc)_6$ affinity in the −4 to +2 and −2 to +4 sites are markedly more favorable than the ITC determinations.

Rather than suggesting inaccuracy in the calculations, we posit that ITC measurements capture a mean of the possible binding conformations. Calculations generally tend to overestimate binding favorability. However, the 5-6 kcal/mol difference observed here is suggestive of a more substantial physical issue rather than computational inaccuracy, particularly with the apparent accuracy of the ChiC calculation. Based on the above comparison of ChiA and ChiB binding the ligand with either a dimer or trimer in the product binding sites, we suggest that the ITC measurements of ChiA and ChiB describe the mean of at least two different hexameric ligand binding scenarios. It has previously been reported that ChiA equally favors productive binding of $(GlcNAc)_5$ in the −2 to +3 sites and the −3 to +2 sites suggesting that the +3 subsite may interact with $(GlcNAc)_6$ binding as well.[47] Similarly, Horn et al. estimate from product profiles that $(GlcNAc)_6$ may bind in the −3 to +3 binding sites of ChiB approximately 20% of the time.[46] Confirmation of this hypothesized variation in binding mode is difficult and likely not possible by ITC alone, as the enzymes must be catalytically inactivated to assess binding free energy. Moreover, it is possible that the catalytically active wild-type enzymes may not bind hexamer in the same

fashion as inactivated enzymes, so product profiles may not accurately represent binding site occupation.

Related to the catalytically inactivated variants used in ITC, we anticipate that the formation of the distorted intermediate ligand conformation, part of the GH reaction coordinate, also may contribute to the observed differences between ITC and calculated free energies. Enzymatic reactions go through at least two distinct steps. First, the substrate reversibly binds to the enzyme forming an enzyme-substrate complex, called the Michaelis complex. Thereafter, the enzyme catalyzes the chemical step and releases the product. In GHs, the formation of the Michaelis complex generally reflects a significant distortion of the −1 binding site pyranose ring (e.g., boat, skew, envelope, etc.) away from the energetically favorable $^{4}C_{1}$ conformation.[1, 74] Certainly, this is true for GH18 chitinases along their hydrolytic reaction coordinate[21-22], which adopt a $^{1,4}B$ boat conformation just prior to hydrolysis. Biarnes et al. computed the free energy landscape of all accessible β-glucopyranose conformers, including approximate energetic barriers to transformation between ring states as represented by the Stoddart's diagram. Based on this free energy landscape, the energetic barrier associated with traversing from the $^{4}C_{1}$ conformation, through the $^{4}H_{5}$ and $^{1}S_{5}$ conformations, to the $^{1,4}B$ distorted conformation, as required of GH18 ChiA and ChiB, is approximately 8 kcal/mol.[75] Alternative conformational routes for ChiA and ChiB pass through areas with even higher energetic barriers, mainly in the area 10-15 kcal/mol. It is therefore possible to imagine that even small deviations from a complete formation of the Michaelis-complex will have great impact on the binding free energy values. While we can ensure that the complete, distorted Michaelis complex was formed when performing FEP/λ-REMD calculations, we are unable to directly ascertain whether this is the case when determining free energies from ITC.

Thermodynamic signatures of ligand binding.

Water plays a critical role in protein function; it aids in formation of correct protein folds, for flexibility in carrying out biological functions, and is responsible for mediating protein-protein, protein-ligand, and protein-DNA interactions. Binding between biomolecules is usually accompanied by the displacement of bound water molecules from the binding sites and formation of direct interactions between the binding molecules, even though it has been observed that the water molecules sometimes are not completely removed from the binding interface.[76] The balance between the direct interactions gained and the solvation interactions lost determines whether such interactions are favorable, neutral, or unfavorable to binding affinity. This means that favorability is dependent on whether the strong interactions between protein and ligand can compensate for the loss of beneficial interactions between water molecules and the protein-ligand complex.[76-77] It has been observed that even if the entropy increases when a water molecule is released to solution, the enthalpy can favor the bound water molecule because this will stabilize binding between protein and ligand.[77] Relative to *S. marcescens* chitinases, we previously observed that the average number of water molecules in the +1/−1 binding sites of non-processive chitinases tended to be higher than in processive chitinases.[32] There also appeared to be a relationship between which side of the +1/−1 cleavage location water molecules congregated and end-specificity. Accordingly, we anticipated the solvational entropy change upon ligand binding would yield additional insight into the role of water molecules in chito-oligomeric binding, beyond examination of only the ligand-bound state.

The solvational entropic change, determined from change in heat capacity ($\Delta C_{p,r}°$) measured by ITC, and MD simulations indicate that water molecules play a significant role in ChiA substrate binding, but less so in ChiB and ChiC. The change in heat capacity when $(GlcNAc)_6$ binds with ChiA was nearly 100 cal/K·mol larger (−241 cal/K mol) than for

either ChiB and ChiC (both −158 cal/K mol). $\Delta C_{p,r}°$ is directly proportional to $\Delta S_{solv}°$ (Equation 3); hence, the term $-T\Delta S_{solv}°$ was markedly more negative and energetically beneficial for ChiA than ChiB or ChiC. The favorability of $-T\Delta S_{solv}°$ physically corresponds to a greater degree of desolvation upon $(GlcNAc)_6$ binding (Table 3). Similarly, the average number of water molecules displaced upon binding $(GlcNAc)_6$ to the chitinases, determined from MD simulations, indicates more water molecules tend to be displaced in binding to ChiA, followed by ChiB and ChiC (Figure 4). Though, the number of water molecules displaced by ChiC is substantially lower than either ChiA or ChiB, reflective of the more open, shallow binding cleft. The position of the ligand within the active site appears to minimally affects number of water molecules displaced, which means that the ITC determinations of thermodynamic signatures are representative of the driving forces behind binding, even if the measurements do represent a mean rather than a single occupancy.

The best known family 18 inhibitor is the pseudotrisaccharide allosamidin, produced by *Streptomyces* sp.[78] It binds from subsite −3 to −1 for all chitinases, where the allosamizoline group of allosamidin resembles the oxazolinium ion intermediate structure formed in the retaining substrate assisted catalysis.[20] Binding of ChiA, ChiB, and ChiC to allosamidin has previously been reported (Table 4). We revisit the findings here, as when combined with the current study, allosamidin binding provides a unique perspective into contributions of the various binding subsites.[42, 79] In the case of ChiA, ChiB, and ChiC binding to allosamidin, $\Delta C_{p,r}°$ is twice as large for ChiC (−120 ± 15 cal/K·mol) as for ChiA and ChiB (−61 ± 13 cal/K·mol and −63 ± 4 cal/K·mol, respectively).[79]

Table 4. Thermodynamic parameters for allosamidin binding to ChiA, ChiB, and ChiC of *Serratia marcescens* at t = 30 °C, pH = 6.0

Enzyme	K_d[a]	ΔG_r°[b]	ΔH_r°[b]	$-T\Delta S_r^{\circ}$[b]	$-T\Delta S_{solv}^{\circ}$[b,d]	$-T\Delta S_{conf}^{\circ}$[b]	$-T\Delta S_{mix}^{\circ}$[b]	$\Delta C_{p,r}^{\circ}$[c,e]
ChiA[f]	0.17 ± 0.06	−9.4 ± 0.2	−6.2 ± 0.2	−3.2 ± 0.3	−4.5 ± 1.3	−1.1 ± 1.3	2.4	−61 ± 13
ChiB[g]	0.16 ± 0.04	−9.4 ± 0.1	3.8 ± 0.2	−13.2 ± 0.2	−4.5 ± 0.5	−11.1 ± 0.6	2.4	−63 ± 4
ChiC[f]	2.0 ± 0.2	−7.9 ± 0.1	−0.6 ± 0.1	−7.3 ± 0.1	−8.7 ± 1.3	−1.0 ± 1.3	2.4	−120 ± 15

[a] μM, [b] kcal/mol, [c] cal/K·mol, [d] $\Delta S_{solv}^{o} = \Delta C_p \ln(T_{303\,K}/T_{385\,K})$ derived using $\Delta S_r^{\circ} = \Delta S_{solv}^{o} + \Delta S_{mix}^{o} + \Delta S_{conf}^{o}$ where $\Delta S\text{mix}^{o} = R\ln(1/55.5) = -8$ cal/K mol ("cratic" term), [e] derived from the temperature dependence of $\Delta H\text{r}^{\circ}$,

[f] [79], [g] [80].

By comparing the thermodynamic signatures of $(GlcNAc)_6$ binding, allosamidin binding and the difference between the two, one gains insight into contributions over the whole active site. The difference between $(GlcNAc)_6$ and allosamidin solvational entropy change, $(-T\Delta S_{solv}^{\circ}{}_{(GlcNAc)6}) - (-T\Delta S_{solv}^{\circ}{}_{allosamidin})$, yields an estimate of the remaining contributions from the +1, +2, and +3 binding subsites, $-T\Delta S_{solv}^{\circ}{}_{subsite\ +1,+2,+3}$ (Figure 6). Such a difference implies that ChiC is most desolvated in negative subsites (substrate), ChiA in positive subsites (product), and equally across ChiB (Figure 6). ChiA studies have shown that it has a powerful affinity in subsite +3 (unpublished results; [46-47]). The enzyme active site is more solvent accessible in subsite +3 than, for example, in subsite −3. Along with the thermodynamical data presented here, we offer this as explanation of why ChiA is more desolvated in positive subsites, bearing in mind this is a simplification for the purposes of discussion. Beneficial changes in the solvation entropy may also be caused by release of entropically constrained water molecules and is not necessarily a measure of the number of released water molecules on the surface of the protein.

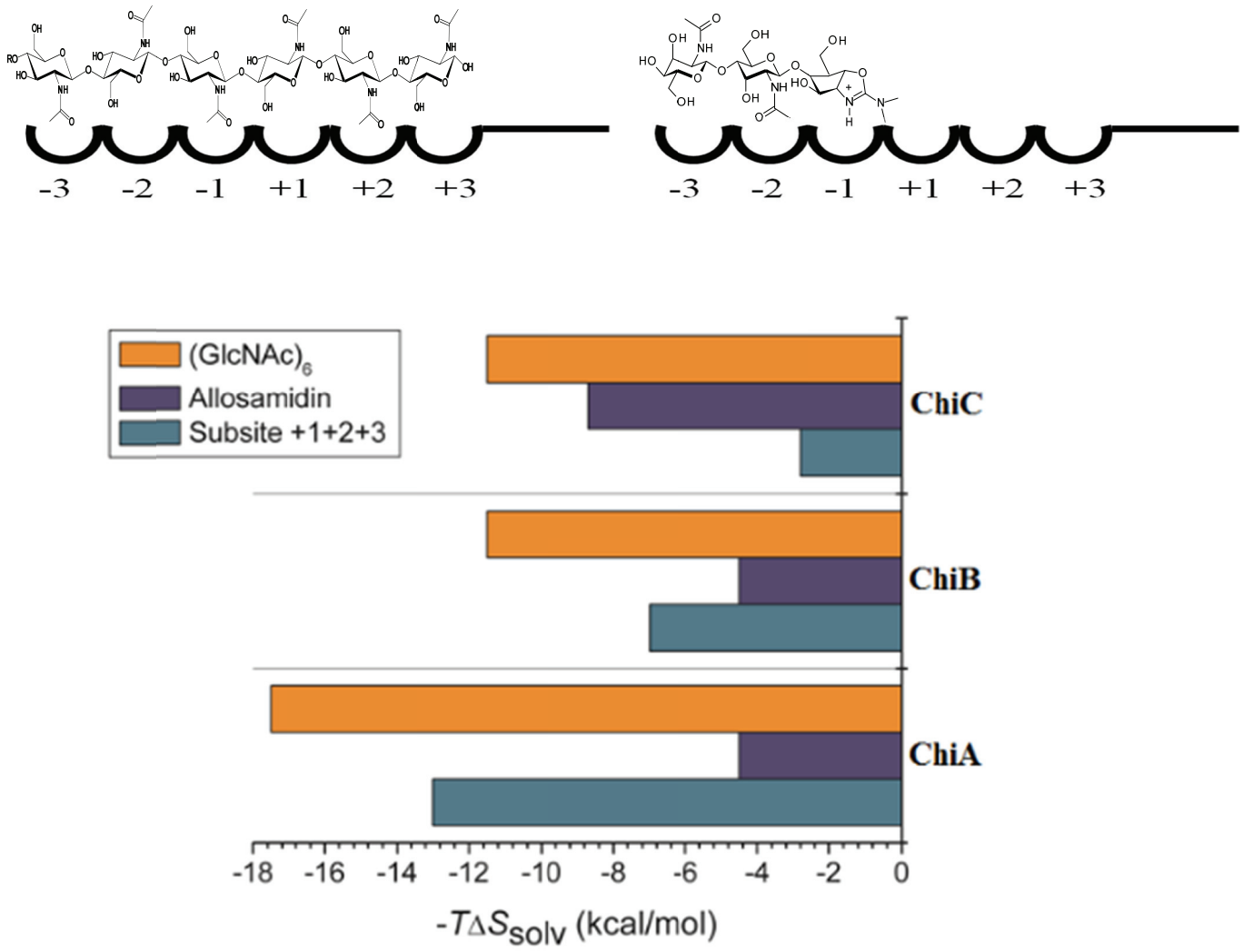

Figure 6. Upper panel: Chemical structures of $(GlcNAc)_6$ (left) and allosamidin (right) aligned in their respective subsites. Lower panel: Schematic representation of $-T\Delta S_{solv}°_{(GlcNAc)6}$ (cyan), $-T\Delta S_{solv}°_{allosamidin}$ (blue), and $-T\Delta S_{solv}°_{subsite\ +1,+2,+3}$ (orange) for ChiA, ChiB, and ChiC.

Parameterization of the entropic term from the ITC experiments also yielded estimates for the conformational entropy change ($-T\Delta S_{conf}°$) upon $(GlcNAc)_6$ binding. Interestingly, these values are unfavorable for ChiA (10.9 kcal/mol) and "neutral" for ChiB (−0.1 kcal/mol) in line with the observations from the RMSF MD simulations of the protein backbone (Figure 5A and 5B). For ChiC, the value is also unfavorable (7.2 kcal/mol) and

the relationship of ChiC flexibility to conformational entropy contributions is not as obvious as for ChiA and ChiB (Figure 5C).

The slight increase in protein flexibility when ChiB binds $(GlcNAc)_6$ in the −2 to +4 sites offers an intriguing explanation for the apparent enhancement in binding over the −3 to +3 binding sites (Figure 5B). The enhanced flexibility would have the effect of increasing the favorability of conformational entropy change. Along with this, we observe enhanced hydrogen bonding as a result of the ligand to the −2 to +4 binding sites (Figure S2B), which would also serve to improve the favorability of the enthalpic term. Together, these variations in molecular behavior would improve the overall affinity of ChiB for $(GlcNAc)_6$ in the −2 to +4 binding site.

Finally, in the case of each chitinase, $-T\Delta S_{conf}^{\circ}$ is less favorable for allosamidin binding than $(GlcNAc)_6$, where the increase in $-T\Delta S_{conf}^{\circ}$ is roughly equal for all chitinases (9 ± 1 kcal/mol). This behavior arises from the general flexibility of longer ligands, such as $(GlcNAc)_6$, over shorter ones, such as allosamidin. Additionally, larger portions of the proteins will bind $(GlcNAc)_6$ compared to allosamidin, resulting in a loss of flexibility in these parts of the proteins.

4. Conclusion

Comparison of apparent processivity measurements for ChiA, ChiB, and ChiC with calculated ligand binding free energies suggests the hypothesized relationship between the two (Equation 7) is general to GHs. Despite the current inability to quantitatively verify the relationship, this is an important finding, as it appears to generally describe an entire class of carbohydrate active enzymes. Of course, developing enzymes that bind too tightly will eventually result in inhibition, along the lines of the Sabatier principle; thus, quantitative investigations are critical to establishing the limitations of processive GH function and the

hypothesized relationship in modeling real behavior. Comparison of the free energies of binding $(GlcNAc)_6$ to ChiA, ChiB, and ChiC from simulation and ITC reveal potential limitations in comparing thermodynamic properties where the conformational state is unknown. We suspect that the very large energetic penalty associated with formation of the distorted Michaelis complex significantly contributes to differences between simulation and experiment. We also anticipate that the enzymes bind the hexameric ligand in several possible manners, which yields an average evolution of heat when using the ITC methodology. Despite the differences in free energies, both MD simulations and ITC suggest water plays a significant role in $(GlcNAc)_6$ binding to ChiA. Estimates of desolvation, through comparison with allosamidin binding, suggest ChiA product sites experience significant desolvation upon ligand binding; whereas, ChiC substrate sites are desolvated. ChiB appears to be equally desolvated across the length of the active site. The change in conformational entropy upon $(GlcNAc)_6$ binding in ChiA, ChiB, and ChiC is generally unfavorable or neutral at best, arising from the protein's need to stabilize a large flexible ligand. In general, ligand binding in ChiB is entropically driven, ChiC is enthalpically driven, and the enthalpic and entropic contributions to ligand binding in ChiA are equal. Overall, this study provides new insights into GH oligosaccharide binding that serve as the foundation for future GH protein engineering efforts through more "rational design" approaches.

Acknowledgements

This work was supported by grants from the Norwegian Research Council 209335/F20 (MS) and the Oak Ridge Associated Universities Ralph E. Powe Junior Faculty Award (FY2014_419) (CMP). The computational work primarily used the Extreme Science and Engineering Discovery Environment (XSEDE), which is supported by National Science

Foundation grant number ACI-1053575.[81] We thank the University of Kentucky Center for Computational Sciences for providing additional computational support.

Associated content

Supporting information

Additional information about computational methods and simulation results are provided. Complete simulation details for all eight MD simulations are found in table S1. Figure S1 shows how fluctuation of the ligand relates to binding free energy as measured by RMSF. Analysis of the number of hydrogen bonds formed between the ligand and the substrate is provided in Figure S3. The binding free energy as a function of time is given in Figure S4. This material is available free of charge via the Internet at http://pubs.acs.org.

Author information

Corresponding author

* To whom correspondence should be addressed. E-mail: morten.sorlie@nmbu.no, Tel.: +47-67232562 and Fax: +47-64965901 or christy.payne@uky.edu, Tel.: + 859-257-2902 and Fax: + 859-323-1929

Reference List

1. Davies, G.; Henrissat, B., Structures and mechanisms of glycosyl hydrolases. *Structure* **1995,** *3* (9), 853-9.
2. Himmel, M. E.; Ding, S. Y.; Johnson, D. K.; Adney, W. S.; Nimlos, M. R.; Brady, J. W.; Foust, T. D., Biomass recalcitrance: engineering plants and enzymes for biofuels production. *Science* **2007,** *315* (5813), 804-7.
3. Payne, C. M.; Knott, B. C.; Mayes, H. B.; Hansson, H.; Himmel, M. E.; Sandgren, M.; Ståhlberg, J.; Beckham, G. T., Fungal cellulases. *Chem. Rev.* **2015,** *115* (3), 1308-448.
4. Reese, E. T.; Siu, R. G.; Levinson, H. S., The biological degradation of soluble cellulose derivatives and its relationship to the mechanism of cellulose hydrolysis. *J. Bacteriol.* **1950,** *59* (4), 485-97.
5. Vaaje-Kolstad, G.; Horn, S. J.; Sørlie, M.; Eijsink, V. G., The chitinolytic machinery of *Serratia marcescens*--a model system for enzymatic degradation of recalcitrant polysaccharides. *FEBS J.* **2013,** *280* (13), 3028-49.
6. Wilson, D. B., Studies of *Thermobifida fusca* plant cell wall degrading enzymes. *Chem. Rec.* **2004,** *4* (2), 72-82.
7. Ståhlberg, J.; Johansson, G.; Pettersson, G., *Trichoderma reesei* has no true exo-cellulase: all intact and truncated cellulases produce new reducing end groups on cellulose. *Biochim. Biophys. Acta* **1993,** *1157* (1), 107-13.
8. Tharanathan, R. N.; Kittur, F. S., Chitin-the undisputed biomolecule of great potential. *Crit. Rev. Food Sci. Nutr.* **2003,** *43* (1), 61-87.
9. Debono, M.; Gordee, R. S., Antibiotics that inhibit fungal cell wall development. *Annu. Rev. Microbiol.* **1994,** *48*, 471-97.
10. Araujo, A. C.; Souto-Padron, T.; de Souza, W., Cytochemical localization of carbohydrate residues in microfilariae of Wuchereria bancrofti and Brugia malayi. *J. Histochem. Cytochem.* **1993,** *41* (4), 571-8.
11. Fuhrman, J. A.; Piessens, W. F., Chitin synthesis and sheath morphogenesis in Brugia malayi microfilariae. *Mol. Biochem. Parasitol.* **1985,** *17* (1), 93-104.
12. Neville, A. C.; Parry, D. A.; Woodhead-Galloway, J., The chitin crystallite in arthropod cuticle. *J. Cell. Sci.* **1976,** *21* (1), 73-82.
13. Shahabuddin, M.; Kaslow, D. C., Plasmodium: parasite chitinase and its role in malaria transmission. *Exp. Parasitol.* **1994,** *79* (1), 85-8.
14. Gardner, K. H.; Blackwell, J., Refinement of the structure of β-chitin. *Biopolymers* **1975,** *14* (8), 1581-95.
15. Minke, R.; Blackwell, J., The structure of α-chitin. *J. Mol. Biol.* **1978,** *120* (2), 167-81.
16. Sawada, D.; Nishiyama, Y.; Langan, P.; Forsyth, V. T.; Kimura, S.; Wada, M., Direct determination of the hydrogen bonding arrangement in anhydrous beta-chitin by neutron fiber diffraction. *Biomacromolecules* **2012,** *13* (1), 288-91.
17. Sikorski, P.; Hori, R.; Wada, M., Revisit of α-chitin crystal structure using high resolution X-ray diffraction data. *Biomacromolecules* **2009,** *10* (5), 1100-5.
18. Lombard, V.; Golaconda Ramulu, H.; Drula, E.; Coutinho, P. M.; Henrissat, B., The carbohydrate-active enzymes database (CAZy) in 2013. *Nucleic Acids Res.* **2014,** *42* (Database issue), D490-5.
19. Armand, S.; Tomita, H.; Heyraud, A.; Gey, C.; Watanabe, T.; Henrissat, B., Stereochemical course of the hydrolysis reaction catalyzed by chitinases A1 and D from Bacillus circulans WL-12. *FEBS Lett.* **1994,** *343* (2), 177-80.
20. Terwisscha van Scheltinga, A. C.; Armand, S.; Kalk, K. H.; Isogai, A.; Henrissat, B.; Dijkstra, B. W., Stereochemistry of chitin hydrolysis by a plant chitinase/lysozyme and X-

ray structure of a complex with allosamidin: evidence for substrate assisted catalysis. *Biochemistry* **1995,** *34* (48), 15619-23.
21. Tews, I.; Terwisscha van Scheltinga, A. C.; Perrakis, A.; Wilson, K. S.; Dijkstra, B. W., Substrate-assisted catalysis unifies two families of chitinolytic enzymes. *J. Am. Chem. Soc.* **1997,** *119* (34), 7954-7959.
22. van Aalten, D. M.; Komander, D.; Synstad, B.; Gåseidnes, S.; Peter, M. G.; Eijsink, V. G., Structural insights into the catalytic mechanism of a family 18 exo-chitinase. *Proc. Natl. Acad. Sci. USA* **2001,** *98* (16), 8979-84.
23. Suzuki, K.; Taiyoji, M.; Sugawara, N.; Nikaidou, N.; Henrissat, B.; Watanabe, T., The third chitinase gene (chiC) of *Serratia marcescens* 2170 and the relationship of its product to other bacterial chitinases. *Biochem. J.* **1999,** *343 Pt 3*, 587-96.
24. Terwisscha van Scheltinga, A. C.; Hennig, M.; Dijkstra, B. W., The 1.8 Å resolution structure of hevamine, a plant chitinase/lysozyme, and analysis of the conserved sequence and structure motifs of glycosyl hydrolase family 18. *J. Mol. Biol.* **1996,** *262* (2), 243-57.
25. Nerinckx, W.; Desmet, T.; Claeyssens, M., A hydrophobic platform as a mechanistically relevant transition state stabilising factor appears to be present in the active centre of all glycoside hydrolases. *FEBS Lett.* **2003,** *538* (1-3), 1-7.
26. Horn, S. J.; Sikorski, P.; Cederkvist, J. B.; Vaaje-Kolstad, G.; Sørlie, M.; Synstad, B.; Vriend, G.; Vårum, K. M.; Eijsink, V. G., Costs and benefits of processivity in enzymatic degradation of recalcitrant polysaccharides. *Proc. Natl. Acad. Sci. USA* **2006,** *103* (48), 18089-94.
27. Hult, E. L.; Katouno, F.; Uchiyama, T.; Watanabe, T.; Sugiyama, J., Molecular directionality in crystalline β-chitin: hydrolysis by chitinases A and B from *Serratia marcescens* 2170. *Biochem. J.* **2005,** *388* (Pt 3), 851-6.
28. Perrakis, A.; Tews, I.; Dauter, Z.; Oppenheim, A. B.; Chet, I.; Wilson, K. S.; Vorgias, C. E., Crystal structure of a bacterial chitinase at 2.3 Å resolution. *Structure* **1994,** *2* (12), 1169-80.
29. van Aalten, D. M.; Synstad, B.; Brurberg, M. B.; Hough, E.; Riise, B. W.; Eijsink, V. G.; Wierenga, R. K., Structure of a two-domain chitotriosidase from *Serratia marcescens* at 1.9-Å resolution. *Proc. Natl. Acad. Sci. USA* **2000,** *97* (11), 5842-7.
30. Zakariassen, H.; Aam, B. B.; Horn, S. J.; Vårum, K. M.; Sørlie, M.; Eijsink, V. G., Aromatic residues in the catalytic center of chitinase A from *Serratia marcescens* affect processivity, enzyme activity, and biomass converting efficiency. *J. Biol. Chem.* **2009,** *284* (16), 10610-7.
31. Horn, S. J.; Sørbotten, A.; Synstad, B.; Sikorski, P.; Sørlie, M.; Vårum, K. M.; Eijsink, V. G., Endo/exo mechanism and processivity of family 18 chitinases produced by *Serratia marcescens*. *FEBS J.* **2006,** *273* (3), 491-503.
32. Payne, C. M.; Baban, J.; Horn, S. J.; Backe, P. H.; Arvai, A. S.; Dalhus, B.; Bjørås, M.; Eijsink, V. G.; Sørlie, M.; Beckham, G. T.; Vaaje-Kolstad, G., Hallmarks of processivity in glycoside hydrolases from crystallographic and computational studies of the *Serratia marcescens* chitinases. *J. Biol. Chem.* **2012,** *287* (43), 36322-30.
33. Gal, S. W.; Choi, J. Y.; Kim, C. Y.; Cheong, Y. H.; Choi, Y. J.; Lee, S. Y.; Bahk, J. D.; Cho, M. J., Cloning of the 52-kDa chitinase gene from *Serratia marcescens* KCTC2172 and its proteolytic cleavage into an active 35-kDa enzyme. *FEMS Microbiol. Lett.* **1998,** *160* (1), 151-8.
34. Synstad, B.; Vaaje-Kolstad, G.; Cederkvist, F. H.; Saua, S. F.; Horn, S. J.; Eijsink, V. G.; Sørlie, M., Expression and characterization of endochitinase C from *Serratia marcescens* BJL200 and its purification by a one-step general chitinase purification method. *Biosci. Biotechnol. Biochem.* **2008,** *72* (3), 715-23.

35. Payne, C. M.; Jiang, W.; Shirts, M. R.; Himmel, M. E.; Crowley, M. F.; Beckham, G. T., Glycoside hydrolase processivity is directly related to oligosaccharide binding free energy. *J. Am. Chem. Soc.* **2013,** *135* (50), 18831-9.
36. Hamre, A. G.; Lorentzen, S. B.; Väljamäe, P.; Sørlie, M., Enzyme processivity changes with the extent of recalcitrant polysaccharide degradation. *FEBS Lett.* **2014,** *588* (24), 4620-4.
37. Dybvik, A. I.; Norberg, A. L.; Schute, V.; Soltwisch, J.; Peter-Katalinic, J.; Vårum, K. M.; Eijsink, V. G.; Dreisewerd, K.; Mormann, M.; Sørlie, M., Analysis of noncovalent chitinase-chito-oligosaccharide complexes by infrared-matrix assisted laser desorption ionization and nanoelectrospray ionization mass spectrometry. *Anal. Chem.* **2011,** *83* (11), 4030-6.
38. Norberg, A. L.; Karlsen, V.; Hoell, I. A.; Bakke, I.; Eijsink, V. G.; Sørlie, M., Determination of substrate binding energies in individual subsites of a family 18 chitinase. *FEBS Lett.* **2010,** *584* (22), 4581-5.
39. Wiseman, T.; Williston, S.; Brandts, J. F.; Lin, L. N., Rapid measurement of binding constants and heats of binding using a new titration calorimeter. *Anal. Biochem.* **1989,** *179* (1), 131-7.
40. Fukada, H.; Takahashi, K., Enthalpy and heat capacity changes for the proton dissociation of various buffer components in 0.1 M potassium chloride. *Proteins* **1998,** *33* (2), 159-66.
41. Norberg, A. L.; Eijsink, V. G. H.; Sørlie, M., Dissecting factors that contribute to ligand-binding energetics for family 18 chitinases. *Thermochim. Acta* **2010,** *511* (1-2), 189-193.
42. Cederkvist, F. H.; Saua, S. F.; Karlsen, V.; Sakuda, S.; Eijsink, V. G.; Sørlie, M., Thermodynamic analysis of allosamidin binding to a family 18 chitinase. *Biochemistry* **2007,** *46* (43), 12347-54.
43. Zakariassen, H.; Sørlie, M., Heat capacity changes in heme protein-ligand interactions. *Thermochim. Acta* **2007,** *464* (1-2), 24-28.
44. Papanikolau, Y.; Prag, G.; Tavlas, G.; Vorgias, C. E.; Oppenheim, A. B.; Petratos, K., High resolution structural analyses of mutant chitinase A complexes with substrates provide new insight into the mechanism of catalysis. *Biochemistry* **2001,** *40* (38), 11338-43.
45. Vaaje-Kolstad, G.; Houston, D. R.; Rao, F. V.; Peter, M. G.; Synstad, B.; van Aalten, D. M.; Eijsink, V. G., Structure of the D142N mutant of the family 18 chitinase ChiB from *Serratia marcescens* and its complex with allosamidin. *Biochim. Biophys. Acta* **2004,** *1696* (1), 103-11.
46. Horn, S. J.; Sørlie, M.; Vaaje-Kolstad, G.; Norberg, A. L.; Synstad, B.; Vårum, K. M.; Eijsink, V. G. H., Comparative studies of chitinases A, B and C from *Serratia marcescens*. *Biocatal. Biotransform.* **2006,** *24* (1-2), 39-53.
47. Norberg, A. L.; Dybvik, A. I.; Zakariassen, H.; Mormann, M.; Peter-Katalinic, J.; Eijsink, V. G.; Sørlie, M., Substrate positioning in chitinase A, a processive chito-biohydrolase from *Serratia marcescens*. *FEBS Lett.* **2011,** *585* (14), 2339-44.
48. Schrödinger, L. *The PyMOL Molecular Graphics System*, 1.5.0.4.
49. Bokma, E.; Rozeboom, H. J.; Sibbald, M.; Dijkstra, B. W.; Beintema, J. J., Expression and characterization of active site mutants of hevamine, a chitinase from the rubber tree *Hevea brasiliensis*. *Eur. J. Biochem.* **2002,** *269* (3), 893-901.
50. Hsieh, Y. C.; Wu, Y. J.; Chiang, T. Y.; Kuo, C. Y.; Shrestha, K. L.; Chao, C. F.; Huang, Y. C.; Chuankhayan, P.; Wu, W. G.; Li, Y. K.; Chen, C. J., Crystal structures of *Bacillus cereus* NCTU2 chitinase complexes with chitooligomers reveal novel substrate binding for catalysis: a chitinase without chitin binding and insertion domains. *J. Biol. Chem.* **2010,** *285* (41), 31603-15.

51. Anandakrishnan, R.; Aguilar, B.; Onufriev, A. V., H++ 3.0: automating pK prediction and the preparation of biomolecular structures for atomistic molecular modeling and simulations. *Nucleic Acids Res.* **2012,** *40* (Web Server issue), W537-41.
52. Gordon, J. C.; Myers, J. B.; Folta, T.; Shoja, V.; Heath, L. S.; Onufriev, A., H++: a server for estimating pKas and adding missing hydrogens to macromolecules. *Nucleic Acids Res.* **2005,** *33* (Web Server issue), W368-71.
53. Myers, J.; Grothaus, G.; Narayanan, S.; Onufriev, A., A simple clustering algorithm can be accurate enough for use in calculations of pKs in macromolecules. *Proteins* **2006,** *63* (4), 928-38.
54. Brooks, B. R.; Brooks, C. L., 3rd; Mackerell, A. D., Jr.; Nilsson, L.; Petrella, R. J.; Roux, B.; Won, Y.; Archontis, G.; Bartels, C.; Boresch, S.; Caflisch, A.; Caves, L.; Cui, Q.; Dinner, A. R.; Feig, M.; Fischer, S.; Gao, J.; Hodoscek, M.; Im, W.; Kuczera, K.; Lazaridis, T.; Ma, J.; Ovchinnikov, V.; Paci, E.; Pastor, R. W.; Post, C. B.; Pu, J. Z.; Schaefer, M.; Tidor, B.; Venable, R. M.; Woodcock, H. L.; Wu, X.; Yang, W.; York, D. M.; Karplus, M., CHARMM: the biomolecular simulation program. *J. Comput. Chem.* **2009,** *30* (10), 1545-614.
55. Mackerell, A. D.; Feig, M.; Brooks, C. L., Extending the treatment of backbone energetics in protein force fields: Limitations of gas-phase quantum mechanics in reproducing protein conformational distributions in molecular dynamics simulations. *J. Comput. Chem.* **2004,** *25* (11), 1400-1415.
56. MacKerell, A. D.; Bashford, D.; Bellott, M.; Dunbrack, R. L.; Evanseck, J. D.; Field, M. J.; Fischer, S.; Gao, J.; Guo, H.; Ha, S.; Joseph-McCarthy, D.; Kuchnir, L.; Kuczera, K.; Lau, F. T.; Mattos, C.; Michnick, S.; Ngo, T.; Nguyen, D. T.; Prodhom, B.; Reiher, W. E.; Roux, B.; Schlenkrich, M.; Smith, J. C.; Stote, R.; Straub, J.; Watanabe, M.; Wiorkiewicz-Kuczera, J.; Yin, D.; Karplus, M., All-atom empirical potential for molecular modeling and dynamics studies of proteins. *The journal of physical chemistry. B* **1998,** *102* (18), 3586-616.
57. Jørgensen, W. L.; Chandrasekhar, J.; Madura, J. D.; Impey, R. W.; Klein, M. L., Comparison of simple potential functions for simulating liquid water. *J Chem Phys* **1983,** *79* (2), 926-935.
58. Durell, S. R.; Brooks, B. R.; Bennaim, A., Solvent-induced forces between 2 hydrophilic groups. *J. Phys. Chem.* **1994,** *98* (8), 2198-2202.
59. Phillips, J. C.; Braun, R.; Wang, W.; Gumbart, J.; Tajkhorshid, E.; Villa, E.; Chipot, C.; Skeel, R. D.; Kalé, L.; Schulten, K., Scalable molecular dynamics with NAMD. *J. Comput. Chem.* **2005,** *26* (16), 1781-1802.
60. Humphrey, W.; Dalke, A.; Schulten, K., VMD: visual molecular dynamics. *J. Mol. Graph.* **1996,** *14* (1), 33-8, 27-8.
61. Deng, Y. Q.; Roux, B., Calculation of standard binding free energies: Aromatic molecules in the T4 lysozyme L99A mutant. *J. Chem. Theory Comput.* **2006,** *2* (5), 1255-1273.
62. Jiang, W.; Hodoscek, M.; Roux, B., Computation of absolute hydration and binding free nergy with Free Energy Perturbation Distributed Replica-Exchange Molecular Dynamics (FEP/REMD). *J. Chem. Theory Comput.* **2009,** *5* (10), 2583-2588.
63. Jiang, W.; Roux, B., Free Energy Perturbation Hamiltonian Replica-Exchange Molecular Dynamics (FEP/H-REMD) for absolute ligand binding free energy calculations. *J. Chem. Theory Comput.* **2010,** *6* (9), 2559-2565.
64. Deng, Y. Q.; Roux, B., Hydration of amino acid side chains: Nonpolar and electrostatic contributions calculated from staged molecular dynamics free energy simulations with explicit water molecules. *The journal of physical chemistry. B* **2004,** *108* (42), 16567-16576.

65. Shirts, M. R.; Chodera, J. D., Statistically optimal analysis of samples from multiple equilibrium states. *The Journal of chemical physics* **2008,** *129* (12), 124105.
66. Baker, B. M.; Murphy, K. P., Dissecting the energetics of a protein-protein interaction: the binding of ovomucoid third domain to elastase. *J. Mol. Biol.* **1997,** *268* (2), 557-69.
67. Baldwin, R. L., Temperature dependence of the hydrophobic interaction in protein folding. *Proc. Natl. Acad. Sci. USA* **1986,** *83* (21), 8069-72.
68. Murphy, K. P.; Privalov, P. L.; Gill, S. J., Common features of protein unfolding and dissolution of hydrophobic compounds. *Science* **1990,** *247* (4942), 559-61.
69. Kurasin, M.; Väljamäe, P., Processivity of cellobiohydrolases is limited by the substrate. *J. Biol. Chem.* **2011,** *286* (1), 169-77.
70. Horn, S. J.; Sørlie, M.; Vårum, K. M.; Väljamäe, P.; Eijsink, V. G., Measuring processivity. *Methods Enzymol.* **2012,** *510*, 69-95.
71. Kuusk, S.; Sørlie, M.; Väljamäe, P., The predominant molecular state of bound enzyme determines the strength and type of product inhibition in the hydrolysis of recalcitrant polysaccharides by processive enzymes. *J. Biol. Chem.* **2015**.
72. Colussi, F.; Sørensen, T. H.; Alasepp, K.; Kari, J.; Cruys-Bagger, N.; Windahl, M. S.; Olsen, J. P.; Borch, K.; Westh, P., Probing substrate interactions in the active tunnel of a catalytically deficient cellobiohydrolase (cel7). *J. Biol. Chem.* **2015,** *290* (4), 2444-54.
73. Igarashi, K.; Uchihashi, T.; Uchiyama, T.; Sugimoto, H.; Wada, M.; Suzuki, K.; Sakuda, S.; Ando, T.; Watanabe, T.; Samejima, M., Two-way traffic of glycoside hydrolase family 18 processive chitinases on crystalline chitin. *Nat. Commun.* **2014,** *5*, 3975.
74. Knott, B. C.; Haddad Momeni, M.; Crowley, M. F.; Mackenzie, L. F.; Gotz, A. W.; Sandgren, M.; Withers, S. G.; Ståhlberg, J.; Beckham, G. T., The mechanism of cellulose hydrolysis by a two-step, retaining cellobiohydrolase elucidated by structural and transition path sampling studies. *J. Am. Chem. Soc.* **2014,** *136* (1), 321-9.
75. Biarnes, X.; Ardevol, A.; Planas, A.; Rovira, C.; Laio, A.; Parrinello, M., The conformational free energy landscape of beta-D-glucopyranose. Implications for substrate preactivation in beta-glucoside hydrolases. *J. Am. Chem. Soc.* **2007,** *129* (35), 10686-93.
76. Ladbury, J. E., Just add water! The effect of water on the specificity of protein-ligand binding sites and its potential application to drug design. *Chem. Biol.* **1996,** *3* (12), 973-80.
77. Li, Z.; Lazaridis, T., The effect of water displacement on binding thermodynamics: concanavalin A. *The journal of physical chemistry. B* **2005,** *109* (1), 662-70.
78. Sakuda, S.; Isogai, A.; Matsumoto, S.; Suzuki, A., Search for microbial insect growth regulators. II. Allosamidin, a novel insect chitinase inhibitor. *J. Antibiot. (Tokyo)* **1987,** *40* (3), 296-300.
79. Baban, J.; Fjeld, S.; Sakuda, S.; Eijsink, V. G. H.; Sørlie, M., The roles of three *Serratia marcescens* chitinases in chitin conversion are reflected in different thermodynamic signatures of allosamidin binding. *The journal of physical chemistry. B* **2010,** *114* (18), 6144-6149.
80. Cederkvist, F. H.; Parmer, M. P.; Vårum, K. M.; Eijsink, V. G. H.; Sørlie, M., Inhibition of a family 18 chitinase by chitooligosaccharides. *Carbohyd. Polym.* **2008,** *74* (1), 41-49.
81. Towns, J.; Cockerill, T.; Dahan, M.; Foster, I.; Gaither, K.; Grimshaw, A.; Hazlewood, V.; Lathrop, S.; Lifka, D.; Peterson, G. D.; Roskies, R.; Scott, J. R.; Wilkins-Diehr, N., XSEDE: Accelerating scientific discovery. *Comput. Sci. Eng.* **2014,** *16* (5), 62-74.

TOC

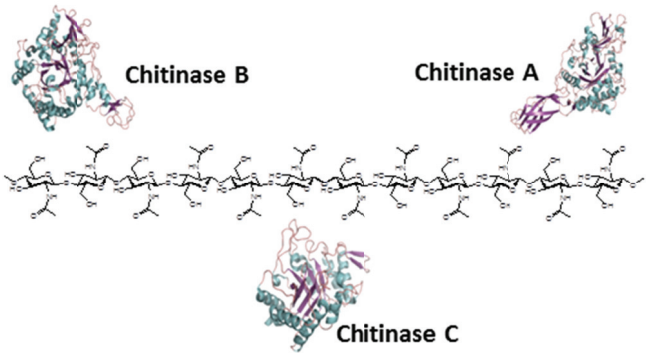

Supporting Information

Thermodynamic relationships with processivity in *Serratia marcescens* family 18 chitinases

Anne Grethe Hamre,[1†] *Suvamay Jana,*[2†] *Matilde Mengkrog Holen,*[1] *Geir Mathiesen,*[1] *Priit Väljamäe,*[3] *Christina M. Payne,*[2*] *and Morten Sørlie*[1*]

[1] Department of Chemistry, Biotechnology and Food Science, Norwegian University of Life Sciences, PO 5003, N-1432 Ås, Norway.

[2] Department of Chemical and Materials, University of Kentucky, Lexington, Kentucky 40506, United States.

[3] Institute of Molecular and Cell Biology, University of Tartu, Tartu, Estonia.

[†] These authors contributed equally to this work.

[*] To whom correspondence should be addressed. E-mail: morten.sorlie@nmbu.no, Tel.: +47-67232562 and Fax: +47-64965901 or christy.payne@uky.edu, Tel.: + 859-257-2902 and Fax: + 859-323-1929

Computational Methods

System preparation and MD simulations

After building initial systems from crystal structures as described in the manuscript, vacuum minimization was performed in CHARMM[1] to overcome initial bad contacts between overlapping atoms. In the cases of ChiA, ChiB, and ChiC where the ligand occupies the −4 to +2, −3 to +3, and −4 to +2 binding sites, respectively, 100 steps of steepest descent minimization (SD) were performed on the entire protein ligand complex followed by 100 steps of adopted basis Newton Raphson minimization (ABNR). In case of ChiA and ChiB where the ligand binds from the −3 to +3 site and −2 to +4 site, a two-step vacuum minimization protocol was followed. For ChiA, the entire protein and ligand bound from the −3 to +2 site was fixed, and the +3 site sugar was allowed to move freely for 100 SD steps followed by 100 ABNR steps. The harmonic restraints were then removed from the system, and the entire protein-ligand complex was minimized for 100 SD and 100 ABNR steps. Similarly, for ChiB, the entire protein and the ligand bound from the −2 to +3 site was fixed allowing the +4 site sugar to move freely for 100 SD steps followed by 100 ABNR steps. All restraints were removed and the entire ChiB protein-ligand complex was minimized for 100 SD and 100 ABNR steps. After initial minimization, all simulation sets were solvated with water molecules, and sodium ions were added for charge neutrality. Complete setup details are provided in Table S1.

For all MD simulations following solvation, the water molecules were minimized for 10 000 steps of SD keeping the protein and ligand (if present) rigid. The protein and water were then minimized for 10 000 SD steps, and finally, the entire system was minimized for 10 000 steps using SD. The system was then heated from 100 K to 300 K in steps of 4 ps with 50 K increments, and the density was equilibrated in the NPT ensemble with the Nosè-Hoover thermostat and barostat for 100 ps.[2,3] Following density equilibrations in

CHARMM, MD simulations were conducted in NAMD for 100 ns in the NVT ensemble at 300K with a 2 fs time step.[4] Long-range electrostatic interactions were described using the Particle Mesh Ewald method with a sixth order b-spline, a Gaussian distribution width of 0.312 Å, and a 1 Å grid spacing.[5] The non-bonded cutoff distance was 10 Å with a switching distance of 9 Å and a non-bonded pair list distance of 12 Å. The SHAKE algorithm was also used to fix all hydrogen distances for computational efficiency. [6]

Free energy Simulations

For both solvation and binding site free energy calculations, 128 FEP windows ran concurrently with an acceptance ratio of > 70% along the alchemical path. The simulations were performed in the NVT ensemble at 300 K with a 1 fs timestep. The force field parameters for FEP/λ-REMD were, for concistency, as described in the manuscript for the MD simulations. To determine enzyme-ligand free energy (ΔG_1), a positional restraint (spring constant 10 kcal/mol/Å^2) was used to maintain a fixed distance between the initial center of mass of the ligand and the protein.

Table S1. Simulation details for all eight MD simulations considered in this study.

	ChiA			ChiB			ChiC	
	Apo	Bound	Bound	Apo	Bound	Bound	Apo	Bound
Crystal Structures used to build systems	1EHN[7]	1EHN[7] (-4 to +2)	1EHN[7] & 1E6N[8] (-3 to +3)	1OGG[9]	1OGG[9] & 1E6N[8] (-3 to +3)	1OGG[9] & 1E6N[8] (-2 to +4)	4AXN[10]	4AXN[10], 1KQY[11] & 3N18[12] (-4 to +2)
Periodic Boundary Conditions [Å]^3	120x120x120			120x120x120			80x80x80	
Atoms	174569	174725	174728	174583	174583	174547	51869	51926
Sodium Ions	2			3			2	
Protonated Residues	Asp313; Glu315; Glu540			Asp142; Glu144			Asp139; Glu141	
Disulfide Bonds	Cys115- Cys120; Cys195- Cys218			Cys328- Cys331			----	

MD simulation results

Root mean square fluctuation (RMSF) of the ligand

From the 100 ns trajectories, the RMSF of the ligand on a per binding site basis was calculated (Figure S1). The pyranose residues in the product side of non-processive ChiC (+1 and +2 ligand binding site) fluctuate significantly more than those of processive chitinases ChiA and ChiB, in line with previous observations illustrating that the product side residues of ChiC have comparatively lower affinity towards substrate than processive chitinases allowing ease of product expulsion.[10]

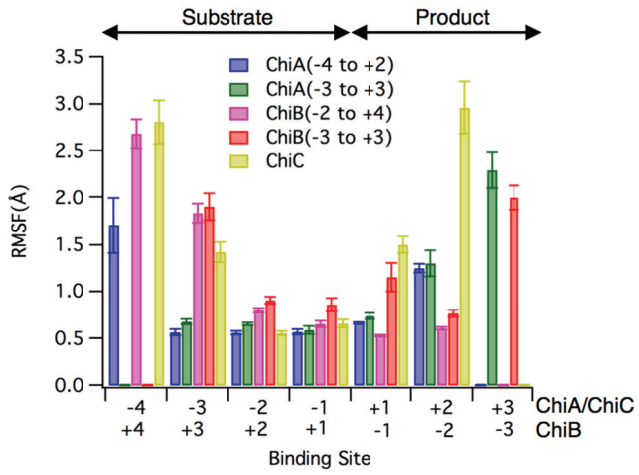

Figure S1. Root mean square fluctuation RMSF) of the $(GlcNAc)_6$ oligomer by binding site. Error bars for the RMSF values were obtained through 2.5 ns block averaging.

Hydrogen bond analysis

Along with the RMSF of the ChiB protein backbone, we also performed hydrogen bond analysis to provide additional insights into the significant change in free energy associated with binding site occupation (i.e., when the ligand occupies either binding sites −3 to +3 or −2 to +4). Here, we anticipate the difference in protein backbone fluctuation as the ligand occupies different binding sites in ChiB (Figure 5B) results from addition of pyranose rings at the +4 and −3 sites, which can be illustrated in terms of hydrogen bond analysis (Figure S2).

From the MD simulation trajectories, we determined the number of hydrogen bonds formed between Asp316 to Pro317 of the ChiB product side and the last product side pyranose ring of the two different ligand binding site locations (Figure S2A and S2C). We also examined hydrogen bonds between the tunnel entrance residues of ChiB (Phe239 and Tyr240) and the +3 site pyranose in the −3 to +3 ligand-bound case and the +4 site pyranose in the −2 site to +4 ligand-bound case (Figure S2B and S2D). The protein residues were selected based on observed differences in fluctuation within the ChiB backbone as shown in Figure 5B. Here,

we define a hydrogen bond as within 3.4 Å of the donor or acceptor and 60° from linear.

Figure S2C illustrates that in the presence of 3 product subsites, ChiB residues Asp316 and Pro317 maintain hydrogen bonds with the ligand most of the 100-ns MD simulations. However, no hydrogen bonding was observed when only 2 product subsites were available. Further, while the ligand is bound in the −3 to +3 binding sites, Asp316 and Pro317 does not appear to hydrogen bond with the −2 pyranose ring, which suggests the availability of third pyranose ring on the product side is responsible for enhanced hydrogen bonding with Asp316 and Pro317. This ultimately results in rigidification of ChiB residues from 315 to 322. We anticipate binding a pyranose ring in the −3 product site enhances favorable enthalpic contribution but unfavorable entropic contribution.

Figure S2D illustrates that throughout most of the 100-ns simulations, Phe239 and Tyr240 form hydrogen bonds with a pyranose in the +4 binding site. Very sparse hydrogen bonding between Phe239 and Tyr240 was observed in the −3 to +3 binding occupancy. Here, we suspect that favorable enthalpic contributions dominate in the presence of a +4 site pyranose sugar.

We also note that the binding of a +4 substrate pyranose facilitates interaction with the tunnel entrance residues, Phe239 and Tyr240, strengthening the observations that substrate-binding sites contribute more in binding than product sites. This is in line with a previous experimental study indicating that Tyr240 is critical to binding and hydrolysis.[13]

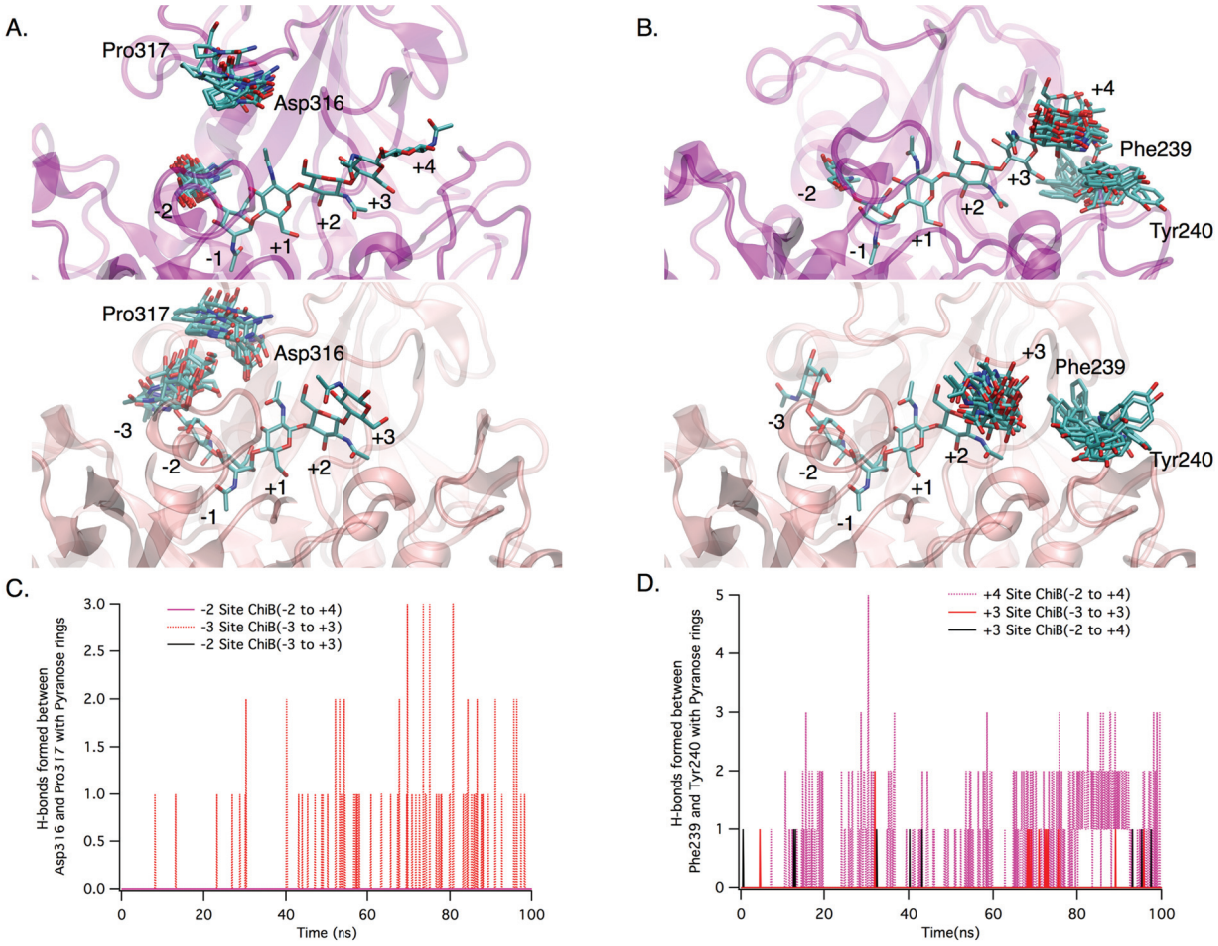

Figure S2. Time-resolved hydrogen bonding of key ChiB active site regions and the bound $(GlcNAc)_6$ ligand. (A) Illustration of hydrogen bonds formed between ChiB product-side residues Asp316 and Pro317 and the last product side pyranose ring while the $(GlcNAc)_6$ ligand occupies −2 to +4 binding sites and −3 to +3 binding sites. (B) Illustration of the hydrogen bonds formed between ChiB substrate-side entrance residues Phe239 and Tyr240 to the first tunnel entrance pyranose ring while ligand binds from −2 to +4 sites and −3 to +3 sites, respectively. (C) Hydrogen bonds formed between selected product-side pyranose rings and residues Asp316 and Pro317. (D) Hydrogen bonds formed between selected substrate-side pyranose rings and residues Phe239 and Tyr240.

Free energy results

As described in the manuscript, the absolute binding free energies were obtained from 35 sequential 0.1 ns calculations, wherein the sequential calculation was restarted from the previous calculation's final configuration. Figure S3 illustrates the time progression of the calculated Gibbs free energy of each of these 0.1 ns blocks. The final 2 ns of each free energy calculation were used to determine the average absolute binding free energy.

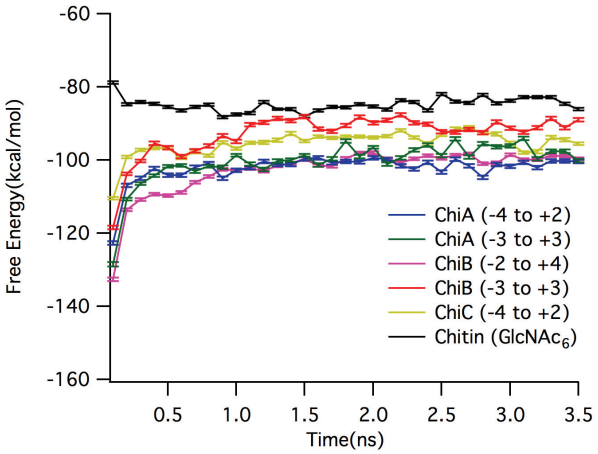

Figure S3. Gibbs free energy calculated from 35 sequential 0.1 ns FEP/ λ-REMD calculations. The statistical certainty of each 0.1 ns calculation was estimated using MBAR.[14]

References

1. Brooks, B. R.; Brooks, C. L., 3rd; Mackerell, A. D., Jr.; Nilsson, L.; Petrella, R. J.; Roux, B.; Won, Y.; Archontis, G.; Bartels, C.; Boresch, S.; Caflisch, A.; Caves, L.; Cui, Q.; Dinner, A. R.; Feig, M.; Fischer, S.; Gao, J.; Hodoscek, M.; Im, W.; Kuczera, K.; Lazaridis, T.; Ma, J.; Ovchinnikov, V.; Paci, E.; Pastor, R. W.; Post, C. B.; Pu, J. Z.; Schaefer, M.; Tidor, B.; Venable, R. M.; Woodcock, H. L.; Wu, X.; Yang, W.; York, D. M.; Karplus, M., CHARMM: the biomolecular simulation program. *J. Comput. Chem.* **2009,** *30* (10), 1545-614.
2. Hoover, W. G., Canonical dynamics: Equilibrium phase-space distributions. *Phys. Rev. A* **1985,** *31* (3), 1695-1697.
3. Nose, S.; Klein, M. L., Constant pressure molecular-dynamics for molecular-systems. *Mol. Phys.* **1983,** *50* (5), 1055-1076.
4. Phillips, J. C.; Braun, R.; Wang, W.; Gumbart, J.; Tajkhorshid, E.; Villa, E.; Chipot, C.; Skeel, R. D.; Kalé, L.; Schulten, K., Scalable molecular dynamics with NAMD. *J. Comput. Chem.* **2005,** *26* (16), 1781-1802.
5. Essmann, U.; Perera, L.; Berkowitz, M. L.; Darden, T.; Lee, H.; Pedersen, L. G., A smooth particle mesh ewald method. *The Journal of chemical physics* **1995,** *103* (19), 8577-8593.
6. Ryckaert, J. P.; Ciccotti, G.; Berendsen, H. J. C., Numerical-integration of cartesian equations of motion of a system with constraints - molecular-dynamics of N-alkanes. *J. Comput. Phys.* **1977,** *23* (3), 327-341.
7. Papanikolau, Y.; Prag, G.; Tavlas, G.; Vorgias, C. E.; Oppenheim, A. B.; Petratos, K., High resolution structural analyses of mutant chitinase A complexes with substrates provide new insight into the mechanism of catalysis. *Biochemistry* **2001,** *40* (38), 11338-43.
8. van Aalten, D. M.; Komander, D.; Synstad, B.; Gåseidnes, S.; Peter, M. G.; Eijsink, V. G., Structural insights into the catalytic mechanism of a family 18 exo-chitinase. *Proc. Natl. Acad. Sci. USA* **2001,** *98* (16), 8979-84.
9. Vaaje-Kolstad, G.; Houston, D. R.; Rao, F. V.; Peter, M. G.; Synstad, B.; van Aalten, D. M.; Eijsink, V. G., Structure of the D142N mutant of the family 18 chitinase ChiB from *Serratia marcescens* and its complex with allosamidin. *Biochim. Biophys. Acta* **2004,** *1696* (1), 103-11.
10. Payne, C. M.; Baban, J.; Horn, S. J.; Backe, P. H.; Arvai, A. S.; Dalhus, B.; Bjørås, M.; Eijsink, V. G.; Sørlie, M.; Beckham, G. T.; Vaaje-Kolstad, G., Hallmarks of processivity in glycoside hydrolases from crystallographic and computational studies of the *Serratia marcescens* chitinases. *J. Biol. Chem.* **2012,** *287* (43), 36322-30.
11. Bokma, E.; Rozeboom, H. J.; Sibbald, M.; Dijkstra, B. W.; Beintema, J. J., Expression and characterization of active site mutants of hevamine, a chitinase from the rubber tree *Hevea brasiliensis*. *Eur. J. Biochem.* **2002,** *269* (3), 893-901.
12. Hsieh, Y. C.; Wu, Y. J.; Chiang, T. Y.; Kuo, C. Y.; Shrestha, K. L.; Chao, C. F.; Huang, Y. C.; Chuankhayan, P.; Wu, W. G.; Li, Y. K.; Chen, C. J., Crystal structures of *Bacillus cereus* NCTU2 chitinase complexes with chitooligomers reveal novel substrate binding for catalysis: a chitinase without chitin binding and insertion domains. *J. Biol. Chem.* **2010,** *285* (41), 31603-15.
13. Katouno, F.; Taguchi, M.; Sakurai, K.; Uchiyama, T.; Nikaidou, N.; Nonaka, T.; Sugiyama, J.; Watanabe, T., Importance of exposed aromatic residues in chitinase B from *Serratia marcescens* 2170 for crystalline chitin hydrolysis. *J. Biochem.* **2004,** *136* (2), 163-8.
14. Shirts, M. R.; Chodera, J. D., Statistically optimal analysis of samples from multiple equilibrium states. *The Journal of chemical physics* **2008,** *129* (12), 124105.

Paper IV

Processivity, substrate positioning and binding; the role of polar residues in a family 18 glycoside hydrolase

Anne Grethe Hamre[†1], Suvamay Jana[*1], Nicole K. Reppert[†], Christina M. Payne[*2], and Morten Sørlie[†2]

[†]Department of Chemistry, Biotechnology and Food Science, Norwegian University of Life Sciences, PO 5003, N-1432 Ås, Norway.

[*] Department of Chemical and Materials Engineering, University of Kentucky, Lexington, Kentucky 40506, United States

#Running title: Strong binding polar residues are important for processivity

[1]A. G. Hamre and S. Jana contributed equally to this work.

[2]To whom correspondence should be addressed: E-mail address: morten.sorlie@nmbu.no and christy.payne@uky.edu. Tel.: +47-67232562 and Fax: +47-64965901 (MS); Tel.: + 859-257-2902 and Fax: + 859-323-1929 (CMP).

Keywords: Chitin, cellulose, glycoside hydrolase, chitinase, cellulase, processivity, binding free energy, molecular dynamics

Background: The role of polar residues in the hydrolysis of recalcitrant polysaccharides is virtually unknown.

Results: Polar residues play important roles in processivity and positioning of the substrate.

Conclusion: Beyond the canonical carbohydrate-aromatic stacking interactions, strong binding polar residues can play a key role in processivity

Significance: Compliments the understanding of how glycoside hydrolases are able to depolymerize recalcitrant polysaccharides.

ABSTRACT

The enzymatic degradation of recalcitrant polysaccharides such as cellulose (β-1,4-linked glucose) and chitin (β-1,4-linked *N*-acetylglucosamine) by glycoside hydrolases (GHs) is of significant biological and economical importance. In nature, depolymerization is primarily accomplished by processive GHs, which remain attached to the substrate in between subsequent hydrolytic reactions. Recent computational efforts have suggested that the processive ability of a GH is directly linked to ligand binding free energy. The contribution of individual aromatic residues in the active site of these enzymes has been extensively studied, illustrating their importance in both processivity and positioning of the substrate in the active site. In the present study, we offer the first experimental evidence confirming correlation of binding free energy and degree of processivity and that polar residues are essential for maintaining processive ability. Exchanging Thr^{276} with Ala in substrate binding subsite –2 results in a reduction of both enthalpy (2.6 and 3.8 kcal/mol) and free energy (0.5 kcal/mol and 2.2 kcal/mol) for the binding to the substrate $(GlcNAc)_6$ and the inhibitor allosamidin, respectively, compared to that of the wild type. Moreover, initial apparent processivity as measured by $[(GlcNAc)_2]/[GlcNAc]$ ratios (17.1 ± 0.4 vs. 30.1 ± 1.5) and chitin degradation efficiency (20 % vs. 75 %) are greatly reduced for ChiA-T276A vs. the wild type. Mutation of Arg^{172} to Ala, which interacts with sugar moieties in substrate binding subsites –4, –3, and –2, reduces the recognition and positioning of the substrate into the active site.

Chitin and cellulose are insoluble, linear homopolymers consisting of β-1,4 linked *N*-acetyl-glucosamine (GlcNAc; **A**-unit) and β-1,4 linked glucose units, respectively. The individual sugar moieties are rotated 180° relative to each other, yielding a disaccharide structural unit (1). Depolymerization of chitin and cellulose to soluble, dimeric units is typically accomplished through the action of glycoside hydrolases (GHs)[3] known as cellulases and chitinases, respectively. Chitin and cellulose polysaccharides are the two most abundant biopolymers in nature with an annual production amounting to 100 billion and one trillion tons, respectively (2,3). With such massive availability, these polysaccharides represent a nearly unlimited source of raw material for the production of fuels and specialty chemicals through enzymatic approaches. However, efficient enzymatic degradation of these materials is critical to the economic viability of any commercial conversion process. Accordingly, engineering enzymes for new and more efficient conversion requires development of fundamental knowledge of both catalytic mechanisms and the means by which the enzyme interacts with the polysaccharide substrate.

Glycoside hydrolases catalyze the hydrolysis of *O*-glycosidic bonds between two or more carbohydrates or between a carbohydrate and a non-carbohydrate moiety (www.cazy.org (4)). In general, hydrolysis occurs via acid catalysis that requires two critical residues: one proton donor and a nucleophile/base (5). Each enzyme has a customized mode of action, either by random cleavage of polymer chains (endo-acting enzymes) or by preferential cleavage of the reducing or non-reducing ends of chains (exo-acting enzymes). Both endo- and exo-mechanisms can be combined with processive action, meaning that the enzymes bind individual polymer chains in long tunnels or deep clefts and hydrolyze a series of glycosidic linkages along the same chain before dissociation (6). This range of potential functions have historically made characterization of these enzymes, particularly cellulases, quite difficult.

In nature, processive GHs are the primary enzymes responsible for polysaccharide depolymerization. It is thought that processivity enhances catalytic efficiency by keeping the enzyme closely associated to the substrate in between subsequent hydrolytic reactions and keeping once-detached single chains from re-associating with the insoluble material (7,8). Hydrolysis of recalcitrant polysaccharides by exo-processive enzymes can be divided into at least 4 putative steps: (i) binding to the polymer surface; (ii) recognition and capture of the chain end; (iii) formation of the productive complex and processive hydrolysis of the polymer chain, and; (iv) dissociation (9). For processes ii) and iii), it is vital that individual binding subsites recognize and orient their specific substrates through formation of intermolecular bonds. In protein-carbohydrate complexes, the dominant interactions are hydrogen bonding and carbohydrate-aromatic stacking interactions, which also happen to be the primary determinants of ligand binding free energy. Accordingly, it has been hypothesized that ligand binding free energy may be directly correlated with processive ability. Using free energy calculations, Payne et al. qualitatively illustrated this relationship for Family 7 GHs (10); though, this study was inherently limited given the dearth of experimental measurements of processivity and binding free energy. Experiments quantifying the relationship of binding free energy with processivity do not yet exist.

Stacking or hydrophobic interactions can be formed between aromatic residues, in particular tryptophans, at the binding site of the enzyme and one or both sides of the sugar ring (11,12). Such interactions have been explored in many studies showing that many processive GHs have a path of conserved solvent exposed aromatic residues leading into the active site cleft (13,14). The hydrophobic interactions create a flexible sheath allowing the polymeric substrate to slide through the active site as well as playing a central role in the binding and guidance of the insoluble substrate into the active site cleft (14-16). Mutagenesis of these aromats nearly abolishes processivity (17-19). Hydrogen bonding can occur between polar residues and sugar-hydroxyl groups that have the potential to be involved in as many as three hydrogen bonds; one as a donor and two as an acceptor (12). A computational study of a processive *Trichoderma reesei* cellulase implicates polar residues in product inhibition, having the effect of reduced overall turnover (20). In a maltooligosaccharide – maltoporin model, it has been shown that the combination of hydrogen bonding and hydrophobic interactions makes a smoother energy profile with regard to processivity than the two interactions alone (21). The latter study highlights the importance of both polar-mediated hydrogen bonding and aromatic-mediated hydrophobic stacking. Nevertheless, the role of polar residues in GH activity, processivity, and substrate binding is virtually unknown.

The chitinolytic machinery of the gram-negative soil bacteria *Serratia marcescens* offers several advantages toward the study of processive GH action, and thus, is often used as model system for enzymatic degradation of recalcitrant polysaccharides (22-25). The suite of *S. marcescens* chitinases includes two processive enzymes, one of which is chitinase A (ChiA), a Family 18 GH that preferentially acts from the reducing end of the sugar chain. The active site of ChiA has a deep, cleft-like architecture, where the catalytic domain contains 4 substrate (−4 to −1) and 3 product (+1 to +3) subsites. The carbohydrate binding module, fused with the catalytic domain, exhibits additional substrate binding sites extending toward the catalytic domain (19,26-28). In the catalytic domain of ChiA, the roles of three aromatic residues (Trp^{167}, Trp^{275}, and Phe^{396}) in substrate binding, processivity, and activity have been characterized. Of the three, Trp^{167}, situated in the −3 substrate binding subsite, was shown to be most important to processivity, efficiency of chitin degradation, and for the recognition and positioning of the substrate before hydrolysis (19,29). A comparable study of the ChiA polar residues will provide a complete description of the protein-carbohydrate interactions governing processive ability, and further, can shed light on the relationship of binding free energy with processive ability.

In the present study, we investigate the role of two polar residues, Arg^{172} and Thr^{276}, in catalysis of glycosidic linkages, substrate binding, and processivity. These two polar residues have been selected on the basis of their position in the active site, avoiding residues that will clearly abolish activity (as part of the reaction mechanism). Arg^{172} and Thr^{276} are

likely to participate in hydrogen bonding with the substrate, and as such, play key roles. We apply experimental and computational approaches to uncover the roles of these specific residues. Further, our investigation yields the experimental evidence toward validation of the relationship of binding free energy with processivity. Site directed mutagenesis has been used to obtain R172A and T276A variants. We have characterized the effects of these mutations with respect to wild-type using standard enzymological methods to determine apparent processivity (HPLC), the equilibrium binding association constant (K_a) and $\Delta H°_r$ (isotherm titration calorimetry (ITC)), and the preference of acetylated and deacetylated units in the different subsites (MS). To understand the molecular-scale effects these residues have on substrate binding, molecular dynamics simulations of the wild-type and variants have been developed.

EXPERIMENTAL PROCEDURES

Chemicals.

Chito-oligosaccharides (CHOS) were obtained from Megazyme (Wicklow, Ireland). Squid pen *β*-chitin was purchased from France Chitin (180µm microparticulate, Marseille, France). Allosamidin was isolated from *Streptomyces sp.,* and the purity was controlled by ^{1}H NMR as described elsewhere (30). Previously, the structure of allosamidin has been verified by both NMR and crystallography (31). All other chemicals were of analytical grade.

Enzymes.

Site directed mutagenesis

Mutagenesis of ChiA-R172A, ChiA-T276A, ChiA-E315Q-R172A, and ChiA-E315Q-T276A was performed using the QuikChange™ site directed mutagenesis kit from Stratagene (La Jolla, CA, USA), as described by the manufacturer. To concentrate the DNA, the Pellet Paint® Co-Precipitant kit from Novagen (Madison, WI, USA) was used as described in the product manual. The primers and templates used for the mutagenesis are listed in Table 1 and were purchased from Life Technologies (Carlsbad, CA, USA). To confirm that the genes contained the desired mutations and to check for the occurrence of nondesirable mutations, the mutated genes were sequenced using GATC Biotechs (Conctance, Germany) LIGHTrun Sequencing service before they were transformed into *Escherichia coli* BL21Star (DE3) cells (Life Technologies, Carlsbad, CA, USA).

Construction of His_{10}-ChiA-E315Q-R172A and His_{10}-ChiA-E315Q-T276A

In order to subclone the inactive mutants ChiA-E315Q-R172A and ChiA-E315Q-T276A from pMay2-10 to pET16b (Novagen, Madison, WI, USA), the chitinase fragments were amplified by PCR to introduce NdeI and XhoI restriction sites. PCR reactions were conducted with Q5® High-Fidelity 2X Master Mix (New England Biolabs, Ipswich, MA). The amplification protocol consisted of an initial denaturation cycle of 30 s at 98 °C, followed by 30 cycles of 5 s at 98 °C, 30 s at 55 °C, 30 s at 72 °C, and a final step of 2 min at 72 °C. The following primers, purchased from Life Technologies (Carlsbad, CA, USA), were used in the PCR reaction:
5'TCGAAGGTCGTCATATGGCCGCGCCGGGC'3 (forward) and
5'CAGCCGGATCCTCGAGTTATTGAACGCCGGCGC'3 (reverse). The amplified insert was subcloned via NdeI and XhoI (New England Biolabs, Ipswich, MA, USA) restriction sites into pET16b by using the In-Fusion HD Cloning kit (Clontech Laboratories, Kyoto, Japan). The resulting pET16b constructs were sequenced using GATC Biotechs (Conctance, Germany) LIGHTrun sequencing service to confirm the correct insert before they were transformed into *E. coli* Rosetta 2(DE3) cells (Life Technologies, Carlsbad, CA, USA).

Protein expression and purification of single mutants

ChiA-R172A and ChiA-T276A genes were expressed in *E. coli* as described previously (32,33). For protein purification, the periplasmic extracts were loaded on a column packed with chitin beads (New England Biolabs) (1.5 cm in diameter, 10 ml stationary phase in total) and equilibrated in 50 mM Tris-HCl pH 8.0. After washing the column with the same buffer, the enzymes were eluted with 20 mM acetic acid. The buffer was then changed to 100 mM Tris-HCl (pH 8.0) using Macrosep Advance Centrifugal Device (30 kDa cutoff, Pall corporation, Port Washington, USA). Enzyme purity was verified by SDS-PAGE, and protein concentrations were determined by using the Bradford Protein Assay from Bio-Rad (Hercules, CA, USA).

Protein expression and purification of double, inactive mutants

For protein expression, *E. coli* Rosetta 2(DE3) cells containing the appropriate plasmid (ChiA-E315Q-R172A, ChiA-E315Q-T276A) were inoculated into 25 mL Terrific Broth (TB) medium containing 115 µg/mL ampicillin and 50 µg/mL chloramphenicol and grown at 37 °C and 200 rpm for 16 h. Cell culture were then inoculated into 250 mL TB medium containing 115 µg/mL ampicillin and 50 µg/mL chloramphenicol to an OD_{600} of 0.1. This culture was cultivated until the OD_{600} reached 0.8-1.0. The temperature was decreased to 22°C, and gene expression was induced with 1 mM isopropyl-β-D-thiogalactopyranoside for 20 h. The cells were harvested by centrifugation (8000 rpm, 20 min at 4 °C). Periplasmic fractions were prepared by osmotic shocking as described elsewhere (34). A cytoplasmic protein extraction was also performed by resuspending the spheroplasts in lysis buffer (0.1 mg/mL lysozyme, 50 mM Tris-HCl, 50 mM NaCl, 4 mM $MgCl_2$, 1 mM EDTA, 0.1 mM PMSF; pH 8.0) before incubating it at 37 °C for 30 min. Cell debris was removed by centrifugation (8000 rpm, 20 min at 4 °C). The resulting supernatant was used for further enzyme purification. Both the periplasmic and cytoplasmic extracts were sterilized by filtration (0.2 µm) prior to protein purification.

Proteins were purified on a column packed with Ni-NTA Agarose matrix (Qiagen, Venlo, Netherlands) (1.5 cm in diameter, 5 ml stationary phase in total). The column was pre-equilibrated in buffer A (20 mM Tris-HCl, 20 mM imidazole, 500 mM NaCl, pH 8.0) before the periplasmic and cytoplasmic extracts were applied. After washing with buffer B (20 mM Tris-HCl, 500 mM NaCl, pH 8.0), fractions containing the enzyme were eluted with buffer C (20 mM Tris-HCl, 250 mM imidazole, 500 mM NaCl, pH 8.0). A flow rate of 2.5 mL/min was used at all times. Enzyme purity was verified by SDS-PAGE, and fractions containing purified enzyme were concentrated and transferred (Macrosep Advance Centrifugal Device, 30 kDa cutoff, Pall corporation, Port Washington, USA) to 20 mM potassium phosphate buffer pH 6.0. Enzyme purity was verified by SDS-PAGE while protein concentrations were determined by using the Bradford Protein Assay from Bio-Rad (Hercules, CA, USA).

Degradation of chitosan

Chitosan was dissolved in 80 mM sodium acetate buffer (pH 5.5) to a final concentration of 10 mg/mL as described previously (35). Chitosan with a fraction of *N*-acetylated units (F_A) = 0.65 was depolymerized by adding 2.5 µg enzyme per 1 mg chitosan. The reactions were run to completion (maximum degree of scission (α)) before enzyme activity was stopped by lowering the pH with 150 µL 1 M HCl and 2 minutes boiling (35).

2-aminoacridone derivatization and sequence determination of chito-oligosaccharides

In order to determine the sequence of chitosan oligomers, the oligosaccharides were derivatized by reductive amination of the reducing end with 2-aminoacridone (AMAC) as described previously (36,37).

Matrix assisted laser desorption/ionization mass spectrometry

Sequencing of the pentameric chitosan oligomers (Degree of polymerization (DP) = 5) was performed using MALDI-TOF/TOF-MS/MS as described earlier (36). MS spectra were acquired using an UltraflexTM TOF/TOF mass spectrometer (Bruker Daltonik GmbH, Bremen, Germany) with gridless ion optics under control of Flexcontrol. For sample preparation, 1 µl of the reaction products was mixed with 1 µl 10 % 2,5-dihydroxybenzoic acid (DHB) in 30 % ethanol and spotted onto a MALDI target plate. The MS experiments were conducted using an accelerating potential of 20 kV in the reflectron mode.

Degradation of chitin

Hydrolysis of chitin was carried out as described previously (38). The extent of degradation is defined as the percentage of number of moles of solubilized GlcNAc-units with respect to number of moles GlcNAc-units in solid form (chitin) used in the experiments.

High performance liquid chromatography (HPLC)

Concentrations of mono- and disaccharides were determined using HPLC with a Rezex Fast fruit H^+ column (100 mm length and 7.8 mm inner diameter) (Phenomenex). An 8 µl sample was injected on the column, and the mono- and

disaccharides were eluted isocratically at 1 mL/min with 5 mM H_2SO_4 at 85 °C. The mono- and disaccharides were monitored by measuring absorbance at 210 nm, and the amounts were quantified by measuring peak areas. Peak areas were compared with peak areas obtained with standard samples with known concentrations of mono- and disaccharides.

Isothermal Titration Calorimetry
ITC experiments were performed with a VP-ITC system from Microcal, Inc. (Northampton, MA) (39). Solutions were thoroughly degassed by vacuum pump prior to experiments to avoid air bubbles in the calorimeter. Standard ITC conditions were 250 µM of allosamidin or 500 µM of hexa-*N*-acetyl glucosamine $(GlcNAc)_6$ in the syringe and 15 µM of enzyme in the reaction cell in 20 mM potassium phosphate buffer of pH 6.0. The only exception was for ChiA-E315Q-T276A against $(GlcNAc)_6$. To ensure a *c*-value between 10 and 1000, which is a prerequisite for meaningful calculations of K_a (39) 1 mM $(GlcNAc)_6$ and 30 µM enzyme were used yielding a *c*-value of 25. Aliquots of 4-8 µl were injected into the reaction cell at 180s intervals at 30 °C with a stirring speed of 260 rpm. 45 injections were performed. At least two independent titrations were performed for each binding reaction.

Analysis of calorimetric data
ITC data were collected automatically using the Microcal Origin v.7.0 software accompanying the VP-ITC system (39). Prior to further analysis, data were corrected for heat dilution by subtracting the heat remaining after saturation of binding sites on the enzyme. Data were fitted using a non-linear least-squares algorithm using a single-site binding model employed by the Origin software that accompanies the VP-ITC system. All data from the binding reactions fitted well with the single site binding model yielding the stoichiometry (*n*), equilibrium binding association constant (K_a), and the reaction enthalpy change ($\Delta H_r°$) of the reaction. The equilibrium binding dissociation constant (K_d), reaction free energy change ($\Delta G_r°$) and the reaction entropy change ($\Delta S_r°$) were calculated from the relation described in Equation 1.

$$\Delta G_r° = -RT\ln K_a = RT\ln K_d = \Delta H_r° - T\Delta S_r° \quad (1)$$

Errors are reported as standard deviations of at least three experiments.

Molecular dynamics (MD)simulations
Classical MD simulations were constructed for the three ChiA systems: ChiA-WT, ChiA-R172A, and ChiA-T276A. The initial coordinates for all three MD simulation sets were from the protein data bank entry 1EHN (26). The E315Q mutation of the 1EHN structure was reversed in each case using the PyMOL mutagenesis tool. Similarly, the R172A and T276A variants were constructed from the wild-type coordinates. The $(GlcNAc)_6$ ligand was also obtained from 1EHN. The deposited structure exhibits a $(GlcNAc)_8$ ligand bound from the −6 to +2 binding subsites. In accordance with experimental protocol, we manually shortened this ligand by deleting the atoms in the −6 and −5 subsites, leaving a bound $(GlcNAc)_6$ in the −4 to +2 sites. The acetyl group of the +1 pyranose ring and the side chain of Asp^{313} were manually rotated around their range of dihedrals, such that the catalytic residues and the +1 sugar reflected the catalytically active conformation of a Family 18 chitinase (40). The protonation states for each simulation were determined using H++ at a pH of 6.0 and an internal and external dielectric constant of 10 and 80, respectively (41-43). Two disulfide bridges observed in the structure also covalently bonded, between Cys^{115} and Cys^{120} and Cys^{195} and Cys^{218}. Sodium ions were added to each system to ensure the total system charge equaled zero.

The constructed systems were then minimized in vacuum, solvated, and re-minimized. The vacuum minimizations were performed to remove any initial bad contacts between overlapping atoms as a result of the addition of hydrogens. The initial minimization protocol included 1000 iterations of steepest descent (SD) followed by 1000 iterations of adopted basis Newton Raphson (ABNR), each applied to the entire protein-ligand complex. The minimized systems were then solvated in explicit TIP3P water. The periodic boundary conditions were 120 Å x 120 Å x 120 Å. This box size was selected such that the protein had a minimum of 10 Å solvent buffer on each side. The total system size for each simulation is approximately 175,000 atoms. The solvated systems were then minimized again according

to a stepwise protocol: (1) the water molecules were minimized for 10,000 SD steps, keeping the protein and ligand rigid; (2) the protein and water were then minimized for 10,000 SD steps keeping the ligand fixed; and (3) the entire system was minimized for 10,000 steps using SD.

The completely constructed systems were then heated and equilibrated prior to collection of production MD simulation data. In all cases, the CHARMM36 all-atom force field with CMAP (44-46) corrections was used to model the protein and carbohydrate interactions, and water with modified TIP3P (47,48) force field. The systems were heated from 100 K to 300 K in 50 K increments over the span of 4 ps. The system density was equilibrated in the NPT ensemble for 100 ps. The Nosè-Hoover thermostat and barostat were used for pressure control (49,50). The systems were constructed, minimized, heated, and equilibrated using CHARMM c37b1 (44).

After equilibration, the simulations were moved into the NAMD simulation package for efficient integration (51). In the NVT ensemble, 250-ns simulations were performed of each of the three systems at 300 K. The periodic volumes were based on the final values from the NPT equilibrations in CHARMM. Each simulation used a 2-fs time step for the integration scheme. The Particle Mesh Ewald method was used to describe long-range electrostatics with a sixth order b-spline, a Gaussian distribution width of 0.312 Å, and a 1 Å grid spacing (52). A non-bonded cutoff distance of 10 Å, a switching distance of 9 Å, and a non-bonded pair list distance of 12 Å were used. All hydrogen atom distances were fixed using the SHAKE algorithm (53). VMD was used for visualization of all the trajectories and hydrogen bond analysis (54).

Results

Mutant design

ChiA is exo-processive acting from the reducing end of the substrate. According to accepted naming convention, ChiA substrate binding subsites are identified by negative numbers, with hydrolysis occurring between the −1 and +1 binding sites. Several important intermolecular interactions between the chito-oligosaccharide substrate and the enzyme occur in substrate binding subsites −2, −3, and −4 (Figure 1), as discussed by Norberg and co-workers (29). Arg^{172} is notable in that it interacts with the substrate in three subsites, −2, −3, and −4, rather than through a single proximal interaction. In the −4 subsite, Arg^{172} interacts with the acetyl group carbonyl oxygen. Though, the −2 subsite GlcNAc is too distant to regularly form hydrogen bonds with Arg^{172}, the influence on the charged protein side chain is likely electrostatically interacting with the C3 secondary alcohol or the acetyl group. In subsite −3, Arg^{172} participates in a bifurcated hydrogen bond to the GlcNAc primary alcohol, in conjunction with Glu^{473}.

Similarly, Thr^{276} interacts with both the −2 and −3 GlcNAc moieties. In the −3 subsite, the threonine OH group forms a hydrogen bond with the substrate carbonyl oxygen. Thr^{276}, together with Trp^{275}, forms hydrogen bonds with the −2 GlcNAc primary alcohol through the protein backbone. Given the ability of Arg^{172} and Thr^{276} to form strong electrostatic – dipole interactions and their proximity to multiple hydrogen bonding partners along the length of the active site cleft, we anticipate each residue plays a role in substrate binding, processivity, and possibly catalytic turnover. Mutating these residues to alanine effectively abolishes the electrostatic potential of the residue and negates the ability to hydrogen bond except through backbone-mediated interactions. This latter point is particularly important for examination of the effect of mutating Thr^{276} to alanine, where loss in binding or processive ability may then be attributed to interaction of Thr^{276} with the carbonyl oxygen in the −3 subsite.

Degradation of chitosan

Deacetylation of chitin yields the water-soluble, heterologous de-*N*-acetylated analog, chitosan, that consists of linear β-1,4-linked *N*-glucosamine (GlcN; **D**-unit) and GlcNAc units (55,56). It can be prepared with varying amount and pattern of *N*-acetylated units as well as varying length of the polymer chain (57,58). Characteristic of Family 18 GHs is that the chitinases degrade chitin with retention of the stereochemistry at the anomeric carbon (www.cazy.org (4)). They also employ a specialized substrate-assisted mechanism in

which the *N*-acetyl group of the sugar in subsite −1 acts as the nucleophile (40,59-61). As a result, Family 18 chitinases have an absolute preference for acetylated units in this subsite. For this reason, degradation of chitosan by chitinases has proven to be a useful tool in the determination of both processivity (19,35) as well as substrate positioning (29). In this study, chitosan with a degree of acetylation of 65 % was degraded by ChiA-R172A and ChiA-T276A to a maximum degree of scission. The pentameric products obtained were analyzed with respect to sequence of acetylated and deacetylated units by reducing end labeling and MALDI-TOF-TOF-MS/MS (37). Such sequences detail the preferences each individual subsite has for acetylated vs. deacetylated units, and hence show its importance in recognizing and positioning of the substrate before hydrolysis (29,36). The sequences (Table 2) show, in addition to the absolute preference for an **A** in subsite −1, a preference for an acetylated unit in subsites −3 and −4 for ChiA-T276A while ChiA-R172A has no strong preferences as seen by the many different sequences present. In comparison, ChiA-WT has a preference for an acetylated unit in subsites −1, −2, and −4 (29).

Degradation of chitin

Apparent processivity (P^{app}) is defined as the average number of consecutive catalytic cycles performed per initiated processive run (either through endo- or exo-mode of attachment) along the crystalline substrate. This value can be measured by a number of different methods, depending on the substrate (38,62,63). A common means of measuring P^{app} in chitinases is by determining the [$(GlcNAc)_2$/(GlcNAc)] ratio. Given the requirement for the *N*-acetyl group in hydrolysis, this approach yields consistent results in determining processive degradation of chitin polysaccharides. In the case of a processive enzyme, the first cleavage from a polymer chain end will result in the release of an odd-numbered oligosaccharide (e.g., mono- or trisaccharide), whereas all subsequent cleavages result in the production of disaccharides because of the 180 ° rotation of the GlcNAc-units. For non-processive enzymes, the same measurement will result in a random distribution of oligosaccharide lengths. In each case, the steady-state ratio of dimers to monomers represents the relative processive ability; neither processive nor non-processive chitinases are capable of hydrolyzing $(GlcNAc)_2$. Lower ratios are indicative of more initiated runs associated with the inability to maintain prolonged substrate association. The [$(GlcNAc)_2$/(GlcNAc)] ratio is valid if it is assumed that the first product is a trisaccharide that subsequently is hydrolyzed to a mono- and disaccharide (38,62).

P^{app} tends to decrease as the substrate is consumed, most likely because the substrate becomes enriched of more recalcitrant parts where there are less obstacle-free paths for processive enzymes (38,63,64). Without the addition of accessory enzymes and glucosidases, the enzymes eventually encounter obstacles or fail to release from the substrate causing traffic jams of unproductively bound enzymes. It is thus important to assess processivity during the early stages of the reaction (38). Here, initial degradation of β-chitin yielded [$(GlcNAc)_2$/(GlcNAc)] ratios of 25.9 ± 0.9 and 17.1 ± 0.4 for ChiA-R172A and ChiA-T276A, respectively. The value for wild-type, ChiA-WT, has previously been determined to be 30.1 ± 1.5 (Figure 2) (38).

Distinct differences between the three enzymes can also be seen with regard to the degradation efficiency. ChiA-WT has the ability to degrade 75 % of the β-chitin while 50 % is degraded by ChiA-R172A. Only 20 % β-chitin is degraded when ChiA-T276A is used (Figure 3).

Thermodynamics

To assess the contribution Arg^{172} and Thr^{276} have on the binding free energy between ChiA and substrate, ITC measurements were undertaken for the individual mutants and the soluble substrate $(GlcNAc)_6$ and the well-known inhibitor allosamidin. Both ligands are similar to the natural substrate and cover the important catalytic subsites −3 to −1 (Figure 1). When allosamidin is the ligand, catalytically active enzymes can be applied (less perturbation of the system), in contrast to when $(GlcNAc)_6$ is the ligand and catalytically inactivated enzymes (mutation of the catalytic acid (Glu to Gln)) must be used.

The binding of $(GlcNAc)_6$ to ChiA-WT was undertaken at pH 6.0 (20 mM potassium phosphate buffer) and 30 °C. To determine the $(GlcNAc)_6$ binding thermodynamics, an inactive variant of the enzyme was used. Thus, the free

energy values of $(GlcNAc)_6$ were determined with a single point mutation (E315Q) representing wild-type and double mutations for ChiA-R172A and ChiA-T276A. A typical thermogram and theoretical fit to the experimental data is given in Figure 4. ChiA binds $(GlcNAc)_6$ with a K_d of 0.56 ± 0.03 μM, corresponding to a free energy change ($\Delta G_r°$) of −8.7 ± 0.1 kcal/mol, an enthalpic change ($\Delta H_r°$) of –4.5 ± 0.2 kcal/mol, and an entropic change ($\Delta S_r°$) of 13.9 ± 0.7 cal/K mol ($-T\Delta S_r° = -4.2 \pm 0.2$ kcal/mol) (Table 3). The K_d for the binding between ChiA-R172A and $(GlcNAc)_6$ equals 0.61 ± 0.02 μM with a $\Delta G_r° = -8.6 \pm 0.1$ kcal/mol, Table 3). The reaction is accompanied by a $\Delta H_r° = -4.8 \pm 0.2$ kcal/mol and a $\Delta S_r°$ = 12.5 ± 0.7 cal/K mol ($-T\Delta S_r° = -3.8 \pm 0.2$ kcal/mol). For ChiA-T276A, the binding has a K_d = 1.2 ± 0.2 μM ($\Delta G_r° = -8.2 \pm 0.1$ kcal/mol) and a $\Delta H_r°$ and $\Delta S_r°$ of −1.9 ± 0.2 kcal/mol and 20.8 ± 0.7 cal/K mol ($-T\Delta S_r° = -6.3 \pm 0.2$ kcal/mol), respectively.

The binding of allosamidin to ChiA-WT has previously been measured at pH 6.0 (20 mM potassium phosphate buffer) and 30 °C using ITC (65) (Table 3). In our study, the binding to ChiA-R172A and ChiA-T276A was studied under the same conditions for direct comparison. Figure 4 shows typical ITC thermograms and theoretical fits to the experimental data for each enzyme. For ChiA-R172A, the binding has a K_d = 0.067 ± 0.008 μM ($\Delta G_r° = -9.9 \pm 0.1$ kcal/mol, Table 3). The reaction is accompanied by a $\Delta H_r°$ of –7.1 ± 0.1 kcal/mol and a $\Delta S_r°$ of 9.2 ± 0.3 cal/K mol ($-T\Delta S_r° = -2.8 \pm 0.1$ kcal/mol). The binding between ChiA-T276A and $(GlcNAc)_6$ has a K_d = 1.0 ± 0.1 μM ($\Delta G_r° = -8.3 \pm 0.1$ kcal/mol) and a $\Delta H_r°$ and $\Delta S_r°$ of –3.7 ± 0.2 kcal/mol and 15.2 ± 0.7 cal/K mol ($-T\Delta S_r° = -4.6 \pm 0.2$ kcal/mol), respectively (Table 3).

Interestingly, the binding affinity of both $(GlcNAc)_6$ and allosamidin to ChiA-WT and ChiA-R172A is virtually identical, while ligand binding affinity to ChiA-T276A is significantly weaker. Moreover, the reduced affinity of $(GlcNAc)_6$ and allosamidin for ChiA-T276A is due to less favorable enthalpy changes (2.6 and 3.8 kcal/mol, respectively) signifying a weaker binding interaction between the protein and the ligand when a threonine is substituted with an alanine.

Molecular Dynamics

Molecular dynamics simulations were performed to obtain molecular-level insight into the experimental observations of binding free energy and apparent processivity measurements. From the 250-ns MD trajectories of ChiA-WT, ChiA-R172A, and ChiA-T276A, we calculated three different quantities related to physical behavior in the active site. First, we calculated the root mean square fluctuation (RMSF) of the hexamer ligand on a per-binding-site basis (Figure 5A). This value represents the degree to which the ligand fluctuates in its binding site, as referenced against the average structure. Uncertainty was estimated using block averaging; the standard deviation of 2.5 ns blocks of data is shown in the figure. The ligand bound to ChiA-R172A behaves similarly to ChiA-WT. By comparison, the ChiA-T276A ligand fluctuates significantly more than either ChiA-WT or ChiA-R172A along the length of the active site.

In a similar fashion, the RMSF of the catalytic tetrad, Asp^{313}, Glu^{315}, Tyr^{390}, and Asp^{391}, reveals that the ChiA-T276A catalytic center exhibits a greater degree of freedom (Figure 5B). The tetrad of residues selected are either directly involved in catalysis or are known to play a key role in stabilization of the catalytically active conformation of the ligand, in which the −1 pyranose ring displays a $^{1,4}B$ boat conformation (26). The RMSF value here again represents the average degree of fluctuation of these four residues alone, as compared to the average structure. Block averaging of 2.5 ns data blocks was used to determine uncertainty. The ChiA-R172A catalytic center fluctuates to the same extent as ChiA-WT. As we will discuss below, the prior two simulation observations are indicative of processive ability or lack thereof (66).

The effect of the R172A and T276A mutations on the conformation of the ligand in the active site was also evaluated. Specifically, we were interested in the effect each mutation had on the ability of the enzyme to maintain the energetically unfavorable skew conformation in the −1 binding site. Ring distortion in the −1 binding site is a notable requirement of glycoside hydrolases, where the catalytic itinerary invariably passes through a skew, boat,

envelope or otherwise distorted conformation to effect catalysis (67,68). ChiA-WT initially exhibits a $^{1,4}B$ conformation in the −1 binding site. Unless catalysis takes place, relieving distortion, the $^{1,4}B$ conformation should be maintained throughout the simulations. Periodic jumps to other conformations can be expected, but prolonged occupation of the relaxed chair conformation is suggestive of a fundamental change in the active site behavior, though not necessarily inactivation. To determine this conformation, we measured the Cremer-Pople ring pucker amplitude, which is a geometric measure of a ring's conformation, over the course of the 250-ns simulation (Figure 5C) (69). A boat conformation will have an amplitude of 0.73 Å, while a chair conformation will have an amplitude of 0.57 Å (70). Both ChiA-WT and ChiA-R172A maintain the $^{1,4}B$ conformation of the −1 pyranose ring over the entire 250-ns simulation. At approximately 130 ns, the ChiA-T276A ligand relaxes to the chair conformation and never recovers the distortion. The latter behavior suggests that the T276A mutation affords the ligand a lower degree of affinity and more flexibility for relaxation; the length of time required to relax the −1 sugar conformation reflects the distance of the T276A mutation from the catalytic center (−1/+1 binding sites).

Discussion

The possibility that GH binding affinity and degree of processivity is correlated was recently described in a computational study of five processive Family 7 cellulases (10). Using thermodynamics of chemical equilibrium and a previously defined statistical definition of processivity (63), intrinsic processivity (P^{Intr}), Payne *et al.* defined a mathematical relationship between ligand binding free energy and intrinsic processivity (Equation 1),

$$\Delta G_b^\circ / RT = \ln (P^{\mathrm{Intr}} * k_{on} / k_{cat}) \qquad (1)$$

where R is the universal gas constant, T is the temperature, P^{Intr} is intrinsic processivity, k_{on} is the association rate coefficient, and k_{cat} is the catalytic rate coefficient. The relationship in Equation 1 is thought to be general to processive GHs; though, this has not been explicitly demonstrated. Further, the difficulties associated with validating the relationship in cellulases are multitude. Until recently, the free energy of binding a cello-oligomer to the entire processive cellulase active site had not been reported (71). Even now, this information is available for only a single *T. Reesei* cellobiohydrolase. Degree of processivity is also difficult to accurately quantify, particularly for cellulases, as they do not make use of a substrate-assisted mechanism (62), and the values vary significantly by laboratory. Accordingly, Payne *et al.* used an enhanced sampling free energy methodology to calculate the binding free energies of five Family 7 GHs. Of these five enzymes, self-consistent processivity measurements were available for two cellulases, which served as the basis for substantiating a link between calculated binding free energies and processivity (63). Thus far, additional experimental evidence has not been made available by which to quantitatively or qualitatively confirm the relationship in Equation 1.

To describe how our results pertain to Equation 1, we must address the terms 'apparent' and 'intrinsic' processivity. The degree of processivity reported here are measurements of apparent processivity, a value that includes contributions from variables such as substrate heterogeneity and environmental conditions. Intrinsic processivity can be thought of as the theoretical limit of processive ability, under ideal conditions. While Equation 1 was developed with respect to intrinsic processivity, apparent processivity can be used to confirm a qualitative relationship. The experiments performed here have been conducted under the same conditions, and thus, confounding environmental variables will contribute equally to each measurement.

The ligand binding free energies of ChiA-WT, ChiA-R172A, and ChiA-T276A alongside measurements of apparent processivity provide the first complete experimental data set illustrating qualitative agreement with Equation 1. This relationship implies that the stronger an enzyme binds to the substrate the more processive ability it will have, up to a maximum value, after which the enzyme becomes inhibited by the substrate. We therefore set out to examine the relationship between binding free energy and processivity using a model chitinase system, in which measurements of binding affinity and processivity are more straightforward than for cellulase systems. The

mutations R172A and T276A were selected such that the effects of polar residues on binding free energy and processivity could also be assessed. Initial [$(GlcNAc)_2$/(GlcNAc)] ratios show that exchange of Arg^{172} to Ala only slightly alters the initial degree of processivity (P^{app} of 25.9 ± 0.9 vs. 30.1 ± 1.5). The impact is significantly larger when Thr^{276} is exchanged to Ala with a reduction in P^{app} to 17.1 ± 0.4. The T276A mutation effectively renders this variant non-processive, as evidenced by prior apparent processivity measurements of the non-processive endo-chitinase ChiC (P^{app} = 14.3 ± 1.4), also from *S. marcescens* (38). The free energy changes for binding $(GlcNAc)_6$ to ChiA-WT, ChiA-R172A, and ChiA-T276A indeed reveal a correlation between the degree of processivity and binding strength. ChiA-WT and ChiA-R172A bind $(GlcNAc)_6$ with approximately the same affinity, and the processive ability of ChiA-R172A is only moderately lower than the wild-type. The reduced affinity of ChiA-T276A is reflected in its reduced processive ability. This relationship is even clearer in examining the binding affinity of the allosamidin inhibitor to the three enzymes. The slightly reduced affinity of ChiA-R172A for allosamidin, compared to wild-type, reflects the slightly lower processive ability. This phenomenon, inhibitor binding more closely trending with processivity, is likely related to the use of inactive variants in the $(GlcNAc)_6$ ITC measurements. It is suggestive of an experimental design approach, should binding affinity-based predictions of processive ability become a standard tool.

The changes in enthalpic and entropic components of binding free energy resulting from the T276A mutation indicate Thr^{276} plays a significant role in hydrogen bonding and maintaining the rigidity of the bound ligand. The less processive ChiA-T276A exhibits significantly reduced binding free energy change towards both $(GlcNAc)_6$ and allosamidin compared to the wild-type (0.5 kcal/mol and 2.2 kcal/mol, respectively). In general, $\Delta H_r°$ reflect changes in weak interactions (i.e. hydrogen bonds, electrostatic and polar interactions) between the ligand and the enzyme compared to those with the solvent. The differences in $\Delta H_r°$ for $(GlcNAc)_6$ and allosamidin binding to ChiA-T276A vs. the wild type are even more pronounced than the $\Delta G_r°$ values with a decrease of 2.6 and 3.8 kcal/mol respectively. An enthalpy-entropy compensation, where removal of a strong binding interaction may allow for a gain in entropy through more flexibility of the protein backbone, negates a full conversion of the reduced enthalpy change into free energy change (72).

Molecular dynamics simulations support the observation that the active sites of ChiA-WT and ChiA-R172A behave similarly and that ChiA-T276A is a clear outlier. Three characteristic measurements of active site dynamics were determined from 250-ns MD simulations of the three enzymes: the RMSF of the bound $(GlcNAc)_6$ ligand, the RMSF of the protein catalytic center, and the −1 pyranose ring pucker amplitude. Each of these measurements indirectly reflects binding affinity and was expected to illustrate the above-described trend, namely that enzymes with more flexible/dynamic active sites will have a lower binding affinity and lower processive ability. The RMSF of the ligand is perhaps most closely related to the binding affinity; a ligand able to fluctuate to any significant degree in an enzyme binding site is unlikely to be strongly bound. In the case of the T276A variant, the $(GlcNAc)_6$ ligand fluctuates significantly more across the length of the cleft than ChiA-WT, while the ChiA-R172A ligand behaves roughly the same as ChiA-WT (Figure 5A). The results align with experimental measurements of binding affinity. The R172A mutation has little effect on the overall stability of the ligand, which indicates that the hydrogen bonds formed with the substrate in the −3 and −4 binding sites are not critical to binding. Rather, the remaining hydrogen bond with Glu^{473} is sufficient to maintain stable binding. On the other hand, the broken hydrogen bond in subsite −3 resulting from the T276A mutation cannot be compensated by the surrounding protein, and the localized range of freedom translates across the length of the active site. It is interesting to observe that the effect on T276A likely only depends on hydrogen bonding to subsite −2, since the hydrogen bond to subsite −3 via the backbone of the protein is likely similar to that of the wild-type.

The RMSF of the protein catalytic center, residues Asp^{313}, Glu^{315}, Tyr^{390}, and Asp^{391}, also indicates that protein fluctuation correlates with binding affinity, wherein increased fluctuation corresponds to lower binding affinity. These

catalytic residues are responsible for maintaining a suitable reactive ligand conformation in the −1/+1 binding site (73,74). We observe that the fluctuation of the catalytic tetrad in ChiA-R172A is within error of ChiA-WT, but that ChiA-T276A fluctuates significantly more in this critical region of the active site (Figure 5B). Previously, we hypothesized that both RMSF of the ligand and the catalytic center is a molecular "hallmark" of processivity (66). This prior study focused on the delineation between processive and non-processive chitinases rather than variations as a result of mutagenesis. The results we present here confirm the observed relationship between active site dynamics and processive ability and extend its relevance to mutations of the same enzyme. The link between catalytic center flexibility and processivity is likely a result of the need, either evolutionarily or engineered, to associate and dissociate quickly from the substrate. Flexibility in the active site affords the enzyme with momentum to escape chemical attraction.

Related to the dynamics of the catalytic center, the conformation of the pyranose sugar in the −1 binding site illustrates the new dynamics imposed by the R172A and T276A mutations. The Cremer-Pople ring puckering amplitude of the −1 site pyranose ring was calculated over the 250-ns MD simulations for all three enzymes (Figure 5C) (69). Structural studies indicate that the ChiA ligand forms an approximate boat conformation along the catalytic itinerary of the substrate-assisted mechanism (73). Both ChiA-WT and ChiA-R172A maintain the structural conformation of the ring in the −1 binding site over the length of the simulation. However, ChiA-T276A allows the −1 pyranose to relax to the chair conformation after approximately 130 ns. The catalytic conformation is never recovered indicating that the active site does not maintain as close an association with the substrate in the −1 binding site. This is particularly suggestive of the role T276A indirectly plays in catalysis. As previously mentioned, T276A primarily interacts with the substrate in the −2 and −3 binding subsites, yet clearly affects the dynamics of the entire binding site.

Chitosan degradation experiments suggest that Arg^{172} is responsible in part for the recognition and positioning of the oligomer in the active site and that Thr^{276} does not determine the location of acetyl groups along the cleft. Chitosan with a degree of acetylation of 65 % was degraded before the reducing ends were labeled and the pentameric fraction was analyzed by MALDI-TOF-TOF-MS/MS. In the case of ChiA-R172A, the results imply no strong preferences for either acetylated or deacetylated units in subsites other than −1. This result is particularly interesting, as Arg^{172} interacts with as many as three different sugar moieties (−2, −3, and −4). Thus, Arg^{172} is central in the recognition and positioning of the substrate into the active site. Interestingly, the strong interacting ChiA-T276 that mainly binds with the −2 sugar does not appear to affect the positioning of the substrate.

Finally, degree of processivity correlates with the extent of chitin degradation. The enzymes with a higher initial degree of processivity are more efficient degraders of *β*-chitin (Figure 3). Drastic reduction in efficiency combined with reduction in processivity has previously been shown for aromatic residues in both ChiA and ChiB from *S. marcescens* (18,19). This result supports the notion that overall substrate turnover is improved by processivity, which results from the ability to maintain proximity with the substrate after each catalytic event.

From both simulation results and experimental evidence, we suggest that T276A is critical to formation of a stable, processive chitinase, while R172A does not play a significant role in processive action. Prior studies have suggested that both hydrophobic stacking interactions and hydrogen bonding are important for a smooth processive cycle (21), and our results indicate that beyond that canonical carbohydrate-aromatic stacking interactions, polar residues can play a key role in this process. In particular, Thr^{276} in the ChiA active site is important to processive function. The fact that Arg^{172} does not participate in processive function indicates that replacement could be beneficial for enhanced processive action. Furthermore, our findings provide the first qualitative experimental characterization of the hypothesized relationship of binding affinity to GH processive action (10). The free energy of binding chito-oligosaccharides and allosamidin are indicative of processive ability. Perhaps the most interesting finding was that the inhibitor binding provided a more sensitive characterization of the relationship between

binding and processivity. On the whole, our results provide new and valuable insight into the role polar residues along the length of a GH active site contributes to molecular interactions, substrate binding, and processivity in chitinases. More broadly, we suggest our results represent an important first step toward validating a hypothesized relationship that potentially describes the action of an entire class of GHs and greatly compliments our understanding of how GHs are able to depolymerize recalcitrant polysaccharides.

Reference List

1. Gardner, K. H., and Blackwell, J. (1975) Refinement of the structure of β-chitin. *Biopolymers* **14**, 1581-1595
2. Kim, J., Yun, S., and Ounaies, Z. (2006) Discovery of cellulose as a smart material. *Macromolecules* **39**, 4202-4206
3. Tharanathan, R. N., and Kittur, F. S. (2003) Chitin-the undisputed biomolecule of great potential. *Crit. Rev. Food Sci. Nutr.* **43**, 61-87
4. Lombard, V., Golaconda Ramulu, H., Drula, E., Coutinho, P. M., and Henrissat, B. (2014) The carbohydrate-active enzymes database (CAZy) in 2013. *Nucleic Acids Res.* **42**, D490-495
5. Sinnott, M. L. (1990) Catalytic mechanisms of enzymatic glycosyl transfer. *Chem Rev* **90**, 1171-1202
6. Davies, G., and Henrissat, B. (1995) Structures and mechanisms of glycosyl hydrolases. *Structure* **3**, 853-859
7. Teeri, T. T. (1997) Crystalline cellulose degradation: New insight into the function of cellobiohydrolases. *Trends Biotechnol* **15**, 160-167
8. von Ossowski, I., Ståhlberg, J., Koivula, A., Piens, K., Becker, D., Boer, H., Harle, R., Harris, M., Divne, C., Mahdi, S., Zhao, Y. X., Driguez, H., Claeyssens, M., Sinnott, M. L., and Teeri, T. T. (2003) Engineering the exo-loop of *Trichoderma reesei* cellobiohydrolase, Ce17A. A comparison with *Phanerochaete chrysosporium* Cel7D. *J. Mol. Biol.* **333**, 817-829
9. Beckham, G. T., Ståhlberg, J., Knott, B. C., Himmel, M. E., Crowley, M. F., Sandgren, M., Sørlie, M., and Payne, C. M. (2014) Towards a molecular-level theory of carbohydrate processivity in glycoside hydrolases. *Curr. Opin. Biotechnol.* **27C**, 96-106
10. Payne, C. M., Jiang, W., Shirts, M. R., Himmel, M. E., Crowley, M. F., and Beckham, G. T. (2013) Glycoside hydrolase processivity is directly related to oligosaccharide binding free energy. *J. Am. Chem. Soc.* **135**, 18831-18839
11. Zolotnitsky, G., Cogan, U., Adir, N., Solomon, V., Shoham, G., and Shoham, Y. (2004) Mapping glycoside hydrolase substrate subsites by isothermal titration calorimetry. *Proc. Natl. Acad. Sci. U. S. A.* **101**, 11275-11280
12. Vyas, N. K. (1991) Atomic features of protein-carbohydrate interactions. *Curr. Opin. Struct. Biol.* **1**, 732-740
13. Rouvinen, J., Bergfors, T., Teeri, T., Knowles, J. K., and Jones, T. A. (1990) Three-dimensional structure of cellobiohydrolase II from *Trichoderma reesei*. *Science* **249**, 380-386
14. Varrot, A., Frandsen, T. P., von Ossowski, I., Boyer, V., Cottaz, S., Driguez, H., Schulein, M., and Davies, G. J. (2003) Structural basis for ligand binding and processivity in cellobiohydrolase Cel6A from *Humicola insolens*. *Structure* **11**, 855-864
15. Uchiyama, T., Katouno, F., Nikaidou, N., Nonaka, T., Sugiyama, J., and Watanabe, T. (2001) Roles of the exposed aromatic residues in crystalline chitin hydrolysis by chitinase A from *Serratia marcescens* 2170. *J. Biol. Chem.* **276**, 41343-41349
16. Watanabe, T., Ariga, Y., Sato, U., Toratani, T., Hashimoto, M., Nikaidou, N., Kezuka, Y., Nonaka, T., and Sugiyama, J. (2003) Aromatic residues within the substrate-binding cleft of *Bacillus circulans* chitinase A1 are essential for hydrolysis of crystalline chitin. *Biochem. J.* **376**, 237-244
17. Zhou, W., Irwin, D. C., Escovar-Kousen, J., and Wilson, D. B. (2004) Kinetic studies of *Thermobifida fusca* Cel9A active site mutant enzymes. *Biochemistry* **43**, 9655-9663
18. Horn, S. J., Sikorski, P., Cederkvist, J. B., Vaaje-Kolstad, G., Sørlie, M., Synstad, B., Vriend, G., Vårum, K. M., and Eijsink, V. G. (2006) Costs and benefits of processivity in enzymatic degradation of recalcitrant polysaccharides. *Proc. Natl. Acad. Sci. U. S. A.* **103**, 18089-18094
19. Zakariassen, H., Aam, B. B., Horn, S. J., Vårum, K. M., Sørlie, M., and Eijsink, V. G. (2009) Aromatic residues in the catalytic center of chitinase A from *Serratia marcescens*

affect processivity, enzyme activity, and biomass converting efficiency. *J. Biol. Chem.* **284**, 10610-10617
20. Bu, L., Beckham, G. T., Shirts, M. R., Nimlos, M. R., Adney, W. S., Himmel, M. E., and Crowley, M. F. (2011) Probing carbohydrate product expulsion from a processive cellulase with multiple absolute binding free energy methods. *J. Biol. Chem.* **286**, 18161-18169
21. Meyer, J. E., and Schulz, G. E. (1997) Energy profile of maltooligosaccharide permeation through maltoporin as derived from the structure and from a statistical analysis of saccharide-protein interactions. *Protein Sci.* **6**, 1084-1091
22. Fuchs, R. L., McPherson, S. A., and Drahos, D. J. (1986) Cloning of a *Serratia marcescens* Gene Encoding Chitinase. *Appl. Environ. Microbiol.* **51**, 504-509
23. Vaaje-Kolstad, G., Horn, S. J., Sørlie, M., and Eijsink, V. G. (2013) The chitinolytic machinery of *Serratia marcescens*--a model system for enzymatic degradation of recalcitrant polysaccharides. *FEBS J.* **280**, 3028-3049
24. Igarashi, K., Uchihashi, T., Uchiyama, T., Sugimoto, H., Wada, M., Suzuki, K., Sakuda, S., Ando, T., Watanabe, T., and Samejima, M. (2014) Two-way traffic of glycoside hydrolase family 18 processive chitinases on crystalline chitin. *Nat. Commun.* **5**, 3975
25. Monreal, J., and Reese, E. T. (1969) The chitinase of *Serratia marcescens*. *Can. J. Microbiol.* **15**, 689-696
26. Papanikolau, Y., Prag, G., Tavlas, G., Vorgias, C. E., Oppenheim, A. B., and Petratos, K. (2001) High resolution structural analyses of mutant chitinase A complexes with substrates provide new insight into the mechanism of catalysis. *Biochemistry* **40**, 11338-11343
27. Hult, E. L., Katouno, F., Uchiyama, T., Watanabe, T., and Sugiyama, J. (2005) Molecular directionality in crystalline β-chitin: hydrolysis by chitinases A and B from *Serratia marcescens* 2170. *Biochem. J.* **388**, 851-856
28. Horn, S. J., Sørbotten, A., Synstad, B., Sikorski, P., Sørlie, M., Vårum, K. M., and Eijsink, V. G. (2006) Endo/exo mechanism and processivity of family 18 chitinases produced by *Serratia marcescens*. *FEBS J.* **273**, 491-503
29. Norberg, A. L., Dybvik, A. I., Zakariassen, H., Mormann, M., Peter-Katalinic, J., Eijsink, V. G., and Sørlie, M. (2011) Substrate positioning in chitinase A, a processive chito-biohydrolase from *Serratia marcescens*. *FEBS Lett.* **585**, 2339-2344
30. Sakuda, S., Isogai, A., Matsumoto, S., and Suzuki, A. (1987) Search for microbial insect growth regulators. II. Allosamidin, a novel insect chitinase inhibitor. *J. Antibiot. (Tokyo)* **40**, 296-300
31. Sakuda, S., Isogai, A., Matsumoto, S., Suzuki, A., and Koseki, K. (1986) The structure of allosamidin, a novel insect chitinase inhibitor, produced by *Streptomyces Sp*. *Tetrahedron Lett.* **27**, 2475-2478
32. Brurberg, M. B., Eijsink, V. G., and Nes, I. F. (1994) Characterization of a chitinase gene (chiA) from *Serratia marcescens* BJL200 and one-step purification of the gene product. *FEMS Microbiol. Lett.* **124**, 399-404
33. Brurberg, M. B., Nes, I. F., and Eijsink, V. G. (1996) Comparative studies of chitinases A and B from *Serratia marcescens*. *Microbiology* **142 (Pt 7)**, 1581-1589
34. Norberg, A. L., Karlsen, V., Hoell, I. A., Bakke, I., Eijsink, V. G. H., and Sørlie, M. (2010) Determination of substrate binding energies in individual subsites of a family 18 chitinase. *FEBS Lett.* **584**, 4581-4585
35. Sørbotten, A., Horn, S. J., Eijsink, V. G., and Vårum, K. M. (2005) Degradation of chitosans with chitinase B from *Serratia marcescens*. Production of chito-oligosaccharides and insight into enzyme processivity. *FEBS J.* **272**, 538-549
36. Cederkvist, F. H., Parmer, M. P., Vårum, K. M., Eijsink, V. G. H., and Sørlie, M. (2008) Inhibition of a family 18 chitinase by chitooligosaccharides. *Carbohyd. Polym.* **74**, 41-49
37. Bahrke, S., Einarsson, J. M., Gislason, J., Haebel, S., Letzel, M. C., Peter-Katalinic, J., and Peter, M. G. (2002) Sequence analysis of chitooligosaccharides by matrix-assisted laser desorption ionization postsource decay mass spectrometry. *Biomacromolecules* **3**, 696-704
38. Hamre, A. G., Lorentzen, S. B., Väljamäe, P., and Sørlie, M. (2014) Enzyme processivity changes with the extent of recalcitrant polysaccharide degradation. *FEBS Lett.* **588**, 4620-4624

39. Wiseman, T., Williston, S., Brandts, J. F., and Lin, L. N. (1989) Rapid measurement of binding constants and heats of binding using a new titration calorimeter. *Anal. Biochem.* **179**, 131-137
40. van Aalten, D. M., Komander, D., Synstad, B., Gåseidnes, S., Peter, M. G., and Eijsink, V. G. (2001) Structural insights into the catalytic mechanism of a family 18 exo-chitinase. *Proc. Natl. Acad. Sci. U. S. A.* **98**, 8979-8984
41. Anandakrishnan, R., Aguilar, B., and Onufriev, A. V. (2012) H++ 3.0: automating pK prediction and the preparation of biomolecular structures for atomistic molecular modeling and simulations. *Nucleic Acids Res.* **40**, W537-541
42. Myers, J., Grothaus, G., Narayanan, S., and Onufriev, A. (2006) A simple clustering algorithm can be accurate enough for use in calculations of pKs in macromolecules. *Proteins* **63**, 928-938
43. Gordon, J. C., Myers, J. B., Folta, T., Shoja, V., Heath, L. S., and Onufriev, A. (2005) H++: a server for estimating pKas and adding missing hydrogens to macromolecules. *Nucleic Acids Res.* **33**, W368-371
44. Brooks, B. R., Brooks, C. L., 3rd, Mackerell, A. D., Jr., Nilsson, L., Petrella, R. J., Roux, B., Won, Y., Archontis, G., Bartels, C., Boresch, S., Caflisch, A., Caves, L., Cui, Q., Dinner, A. R., Feig, M., Fischer, S., Gao, J., Hodoscek, M., Im, W., Kuczera, K., Lazaridis, T., Ma, J., Ovchinnikov, V., Paci, E., Pastor, R. W., Post, C. B., Pu, J. Z., Schaefer, M., Tidor, B., Venable, R. M., Woodcock, H. L., Wu, X., Yang, W., York, D. M., and Karplus, M. (2009) CHARMM: the biomolecular simulation program. *J. Comput. Chem.* **30**, 1545-1614
45. Mackerell, A. D., Feig, M., and Brooks, C. L. (2004) Extending the treatment of backbone energetics in protein force fields: Limitations of gas-phase quantum mechanics in reproducing protein conformational distributions in molecular dynamics simulations. *J. Comput. Chem.* **25**, 1400-1415
46. MacKerell, A. D., Bashford, D., Bellott, M., Dunbrack, R. L., Evanseck, J. D., Field, M. J., Fischer, S., Gao, J., Guo, H., Ha, S., Joseph-McCarthy, D., Kuchnir, L., Kuczera, K., Lau, F. T., Mattos, C., Michnick, S., Ngo, T., Nguyen, D. T., Prodhom, B., Reiher, W. E., Roux, B., Schlenkrich, M., Smith, J. C., Stote, R., Straub, J., Watanabe, M., Wiorkiewicz-Kuczera, J., Yin, D., and Karplus, M. (1998) All-atom empirical potential for molecular modeling and dynamics studies of proteins. *The journal of physical chemistry. B* **102**, 3586-3616
47. Durell, S. R., Brooks, B. R., and Bennaim, A. (1994) Solvent-induced forces between 2 hydrophilic groups. *J. Phys. Chem.* **98**, 2198-2202
48. Jørgensen, W. L., Chandrasekhar, J., Madura, J. D., Impey, R. W., and Klein, M. L. (1983) Comparison of simple potential functions for simulating liquid water. *J Chem Phys* **79**, 926-935
49. Hoover, W. G. (1985) Canonical dynamics: Equilibrium phase-space distributions. *Phys. Rev. A* **31**, 1695-1697
50. Nose, S., and Klein, M. L. (1983) Constant pressure molecular-dynamics for molecular-systems. *Mol. Phys.* **50**, 1055-1076
51. Phillips, J. C., Braun, R., Wang, W., Gumbart, J., Tajkhorshid, E., Villa, E., Chipot, C., Skeel, R. D., Kalé, L., and Schulten, K. (2005) Scalable molecular dynamics with NAMD. *J. Comput. Chem.* **26**, 1781-1802
52. Essmann, U., Perera, L., Berkowitz, M. L., Darden, T., Lee, H., and Pedersen, L. G. (1995) A smooth particle mesh ewald method. *The Journal of chemical physics* **103**, 8577-8593
53. Ryckaert, J. P., Ciccotti, G., and Berendsen, H. J. C. (1977) Numerical-integration of cartesian equations of motion of a system with constraints - molecular-dynamics of N-alkanes. *J. Comput. Phys.* **23**, 327-341
54. Humphrey, W., Dalke, A., and Schulten, K. (1996) VMD: visual molecular dynamics. *J. Mol. Graph.* **14**, 33-38, 27-38
55. Hackman, R. H. (1954) Studies on chitin. I. Enzymic degradation of chitin and chitin esters. *Aust. J. Biol. Sci.* **7**, 168-178
56. Sannan, T., Kurita, K., and Iwakura, Y. (1976) Studies on chitin, 2. Effect of deacetylation on solubility. *Macromol. Chem.* **177**, 3589-3600

57. Vårum, K. M., Anthonsen, M. W., Grasdalen, H., and Smidsrød, O. (1991) 13C-n.m.r. studies of the acetylation sequences in partially N-deacetylated chitins (chitosans). *Carbohydr. Res.* **217**, 19-27
58. Vårum, K. M., Anthonsen, M. W., Grasdalen, H., and Smidsrød, O. (1991) Determination of the degree of N-acetylation and the distribution of N-acetyl groups in partially N-deacetylated chitins (chitosans) by high-field n.m.r. spectroscopy. *Carbohydr. Res.* **211**, 17-23
59. Synstad, B., Gåseidnes, S., Van Aalten, D. M., Vriend, G., Nielsen, J. E., and Eijsink, V. G. (2004) Mutational and computational analysis of the role of conserved residues in the active site of a family 18 chitinase. *Eur. J. Biochem.* **271**, 253-262
60. Terwisscha van Scheltinga, A. C., Armand, S., Kalk, K. H., Isogai, A., Henrissat, B., and Dijkstra, B. W. (1995) Stereochemistry of chitin hydrolysis by a plant chitinase/lysozyme and X-ray structure of a complex with allosamidin: evidence for substrate assisted catalysis. *Biochemistry* **34**, 15619-15623
61. Tews, I., Terwisscha van Scheltinga, A. C., Perrakis, A., Wilson, K. S., and Dijkstra, B. W. (1997) Substrate-assisted catalysis unifies two families of chitinolytic enzymes. *J. Am. Chem. Soc.* **119**, 7954-7959
62. Horn, S. J., Sørlie, M., Vårum, K. M., Väljamäe, P., and Eijsink, V. G. (2012) Measuring processivity. *Methods Enzymol.* **510**, 69-95
63. Kurasin, M., and Väljamäe, P. (2011) Processivity of cellobiohydrolases is limited by the substrate. *J. Biol. Chem.* **286**, 169-177
64. Igarashi, K., Uchihashi, T., Koivula, A., Wada, M., Kimura, S., Okamoto, T., Penttila, M., Ando, T., and Samejima, M. (2011) Traffic jams reduce hydrolytic efficiency of cellulase on cellulose surface. *Science* **333**, 1279-1282
65. Baban, J., Fjeld, S., Sakuda, S., Eijsink, V. G. H., and Sørlie, M. (2010) The roles of three *Serratia marcescens* chitinases in chitin conversion are reflected in different thermodynamic signatures of allosamidin binding. *The journal of physical chemistry. B* **114**, 6144-6149
66. Payne, C. M., Baban, J., Horn, S. J., Backe, P. H., Arvai, A. S., Dalhus, B., Bjørås, M., Eijsink, V. G., Sørlie, M., Beckham, G. T., and Vaaje-Kolstad, G. (2012) Hallmarks of processivity in glycoside hydrolases from crystallographic and computational studies of the *Serratia marcescens* chitinases. *J. Biol. Chem.* **287**, 36322-36330
67. Blake, C. C., Johnson, L. N., Mair, G. A., North, A. C., Phillips, D. C., and Sarma, V. R. (1967) Crystallographic studies of the activity of hen egg-white lysozyme. *Proc. R. Soc. Lond. B. Biol. Sci.* **167**, 378-388
68. Phillips, D. C. (1966) The three-dimensional structure of an enzyme molecule. *Sci. Am.* **215**, 78-90
69. Cremer, D., and Pople, J. A. (1975) General definition of ring puckering coordinates. *J. Am. Chem. Soc.* **97**, 1354-1358
70. Hill, A. D., and Reilly, P. J. (2007) Puckering coordinates of monocyclic rings by triangular decomposition. *J. Chem. Inf. Model.* **47**, 1031-1035
71. Colussi, F., Sørensen, T. H., Alasepp, K., Kari, J., Cruys-Bagger, N., Windahl, M. S., Olsen, J. P., Borch, K., and Westh, P. (2015) Probing substrate interactions in the active tunnel of a catalytically deficient cellobiohydrolase (cel7). *J. Biol. Chem.* **290**, 2444-2454
72. Cooper, A., Johnson, C. M., Lakey, J. H., and Nöllmann, M. (2001) Heat does not come in different colours: entropy-enthalpy compensation, free energy windows, quantum confinement, pressure perturbation calorimetry, solvation and the multiple causes of heat capacity effects in biomolecular interactions. *Biophys. Chem.* **93**, 215-230
73. Brameld, K. A., and Goddard, W. A. (1998) Substrate distortion to a boat conformation at subsite −1 is critical in the mechanism of family 18 chitinases. *J. Am. Chem. Soc.* **120**, 3571-3580
74. Aronson, N. N., Halloran, B. A., Alexeyev, M. F., Zhou, X. E., Wang, Y., Meehan, E. J., and Chen, L. (2006) Mutation of a conserved tryptophan in the chitin-binding cleft of *Serratia marcescens* chitinase A enhances transglycosylation. *Biosci. Biotech. Biochem.* **70**, 243-251

75. Towns, J., Cockerill, T., Dahan, M., Foster, I., Gaither, K., Grimshaw, A., Hazlewood, V., Lathrop, S., Lifka, D., Peterson, G. D., Roskies, R., Scott, J. R., and Wilkins-Diehr, N. (2014) XSEDE: Accelerating scientific discovery. *Comput. Sci. Eng.* **16**, 62-74
76. Dybvik, A. I., Norberg, A. L., Schute, V., Soltwisch, J., Peter-Katalinic, J., Vårum, K. M., Eijsink, V. G., Dreisewerd, K., Mormann, M., and Sørlie, M. (2011) Analysis of noncovalent chitinase-chito-oligosaccharide complexes by infrared-matrix assisted laser desorption ionization and nanoelectrospray ionization mass spectrometry. *Anal. Chem.* **83**, 4030-4036

ACKNOWLEDGEMENTS

This work was supported by Grants 209335/F20 from the Norwegian Research Council (MS), and the Oak Ridge Associated Universities Ralph E. Powe Junior Faculty Award (FY2014_419) (CMP). The computational work primarily used the Extreme Science and Engineering Discovery Environment (XSEDE), which is supported by National Science Foundation grant number ACI-1053575 (75). The University of Kentucky Information Technology department and Center for Computational Sciences provided additional computational support.

FOOTNOTES

[1]A. G. Hamre and S. Jana contributed equally to this work.

[2]To whom correspondence should be addressed: E-mail address: morten.sorlie@nmbu.no and christy.payne@uky.edu Tel.: +47-67232562 and Fax: +47-64965901 (MS); Tel.: + 859-257-2902 and Fax: + 859-323-1929 (CMP).

[3] The abbreviations used are: $\Delta G_r°$, reaction free energy change; $\Delta H°_r$, the reaction enthalpy change; $\Delta S_r°$, reaction entropy change; **A**, *N*-acetyl-glucosamine; ABNR, adopted basis Newton-Raphson; AMAC, 2-aminoacridone; ChiA, Chitinase A; CHOS, chito-oligosaccharides; **D**, *N*-glucosamine; DHB, 2,5-dihydroxybenzoic acid; DP, degree of polymerization; F_A, fraction of *N*-acetylated units; GH, glycoside hydrolase; GlcNAc, *N*-acetyl-glucosamine; GlcN, *N*-glucosamine; ITC, isotherm titration calorimetry; K_a, the equilibrium binding association constant; K_d, the equilibrium binding dissociation constant; MD, molecular dynamics; *n*, the stoichiometry; P^{app}, apparent processivity; RMSF, the root mean square fluctuation; SD, steepest descent; TB, terrific broth

FIGURE LEGENDS

Figure 1. Crystal structures of the active site of ChiA in the presence of $(GlcNAc)_6$ (A, colored grey) and allosamidin (B, colored yellow). Highlighted in green are the two residues investigated in this study (Thr^{276} and Arg^{172}). Other important substrate binding residues (Trp^{167}, Glu^{473}, Asp^{313} and Glu^{315}) are highlighted in orange while product binding residues (Trp^{275}, Tyr^{390} and Asp^{391}) are shown in cyan.

Figure 2. Comparison of initial $[(GlcNAc)_2/(GlcNAc)]$ ratios for ChiA wt (■), ChiA-R172A (●) and ChiA-T276A (▲). Hydrolysis was undertaken with 2.5 μM enzyme, pH 6.1 sodium acetate buffer at t = 37 °C with 2.0 mg/ml chitin. Error bars represent standard deviation of duplicate experiments.

Figure 3. Relationship of the $[(GlcNAc)_2/(GlcNAc)]$ ratio for ChiA wt (■), ChiA-R172A (●) and ChiA-T276A (▲) with extent of degradation. Hydrolysis was undertaken with 2.5 μM enzyme, pH 6.1 sodium acetate buffer at t = 37 °C with 2.0 mg/ml chitin. Error bars represent standard deviation of duplicate experiments.

Figure 4. Top: Thermograms (upper panels) and binding isotherms with theoretical fits (lower panels) obtained for the binding of allosamidin to ChiA-WT (left), ChiA-T276A (middle), and ChiA-R172A (right) at t = 30 °C in 20 mM potassium phosphate at pH 6.0.
Bottom: Thermograms (upper panels) and binding isotherms with theoretical fits (lower panels) obtained for the binding of $(GlcNAc)_6$ to Chi-WT (left), ChiA-T276A (middle), and ChiA-R172A (right) at t = 30 °C in 20 mM potassium phosphate at pH 6.0.

Figure 5. Dynamics of the ChiA-WT, ChiA-R172A, and ChiA-T276A active sites as determined from 250-ns MD simulations. (A) Root mean square fluctuation (RMSF) of the chito-oligosaccharide $(GlcNAc)_6$ given on a per-binding-site basis. (B) RMSF of the four residues implicated in catalysis, either directly or indirectly: Asp^{313}, Glu^{315}, Tyr^{390}, and Asp^{391}. In both panels (A) and (B) uncertainty of the RMSF value was obtained through block averaging (2.5 ns blocks). (C) Cremer-Pople ring pucker amplitude of the -1 site pyranose sugar ring over the entire 250-ns simulation. The boat conformation is represented by 0.73 Å, and chair conformation is represented by 0.57 Å (70)

Table 1. Primers used for site-directed mutagenesis

Mutant	DNA template	Primer	Sequence
ChiA-R172A	ChiA-WT	Forward	5'- GGGGCGTTTACGGGGCCAATTTCACCGTCG-3'
		Reverse	5'- CGACGGTGAATTGGCCCCTAAACGCCCC-3'
ChiA-T276A	ChiA-WT	Forward	5'- TCGGCGGCTGGGCGCTGTCCGAC-3'
		Reverse	5'- GTCGGACAGCGCCCAGCCGCCGA-3'
ChiA-E315Q-R172A	ChiA-E315Q[a]	Forward	5'- GGGGCGTTTACGGGGCCAATTTCACCGTCG-3'
		Reverse	5'- CGACGGTGAATTGGCCCCTAAACGCCCC-3'
ChiA-E315Q-T276A	ChiA-E315Q[a]	Forward	5'- TCGGCGGCTGGGCGCTGTCCGAC-3'
		Reverse	5'- GTCGGACAGCGCCCAGCCGCCGA-3'

[a] (76)

Table 2. Sequence determination of CHOS of DP = 5 obtained after hydrolysis of chitosan (F_A = 0.65) with ChiA-WT, ChiA-T267A, ChiA-R172A to a maximum degree of scission.

m/*z*	CHOS	Sequence		
		WT [a)]	T276A	R172A
1124.252		-	-	DDADA-▲
1166.265	D2A3	DADAA-▲	-	DDAAA-▲
				DAADA-▲
				DADAA-▲
				ADADA-▲
				ADDAA-▲
1208.269	D1A4	AADAA-▲	DAAAA-▲	AAADA-▲
			AAADA-▲	ADAAA-▲

▲ represents the reducing end tag.
[a)] (29)

Table 3. Thermodynamic Parameters for $(GlcNAc)_6$ and allosamidin binding to ChiA-WT, ChiA-T276A, ChiA-R172A from *Serratia marcescens* at t = 30 °C, pH = 6.0.

Enzyme	K_d [a]	ΔG_r° [b]	ΔH_r° [b]	$-T\Delta S_r^{\circ}$ [b]
		$(GlcNAc)_6$		
ChiA-WT[c]	0.56 ± 0.03	−8.7 ± 0.1	–4.5 ± 0.2	−4.2 ± 0.2
ChiA-T276A[c]	1.2 ± 0.2	−8.2 ± 0.1	−1.9 ± 0.2	−6.3 ± 0.2
ChiA-R172R[c]	0.61 ± 0.02	−8.6 ± 0.1	−4.8 ± 0.2	−3.8 ± 0.2
		Allosamidin		
ChiA-WT[d]	0.027 ± 0.002	–10.5 ± 0.1	–7.5 ± 0.3	–2.8 ± 0.3
ChiA-T276A	1.0 ± 0.1	–8.3 ± 0.1	–3.7 ± 0.2	–4.6 ± 0.2
ChiA-R172A	0.067 ± 0.008	–9.9 ± 0.1	–7.1 ± 0.1	–2.8 ± 0.1

[a] μM, [b] kcal/mol, [c] the catalytic acid Glu^{315} have been exchanged to Gln, [d] (65)

Figure 1

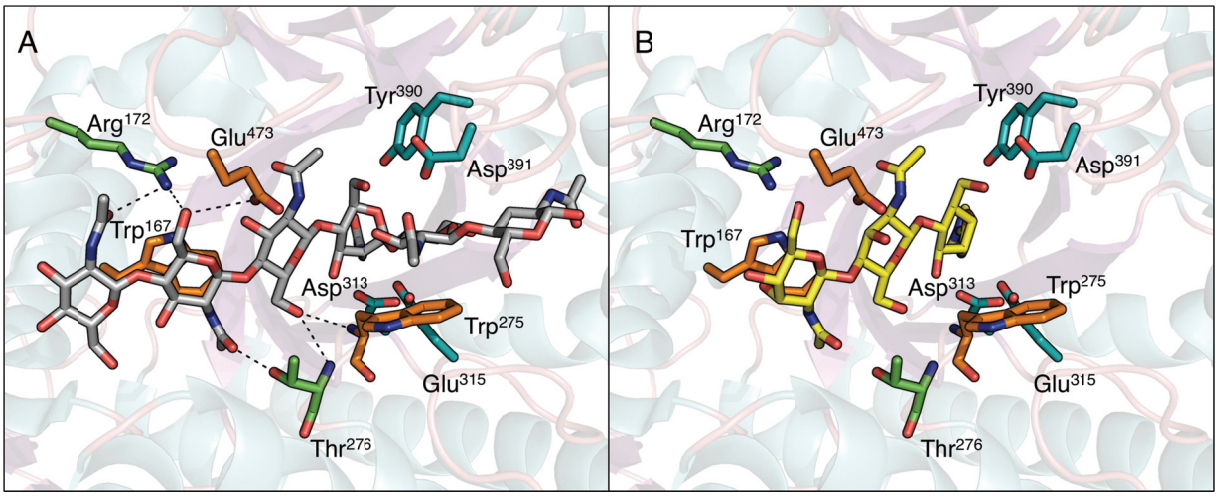
A
Arg172
Glu473
Tyr390
Asp391
Trp167
Asp313
Trp275
Glu315
Thr275
B
Arg172
Glu473
Tyr390
Asp391
Trp167
Asp313
Trp275
Glu315
Thr276

Figure 2

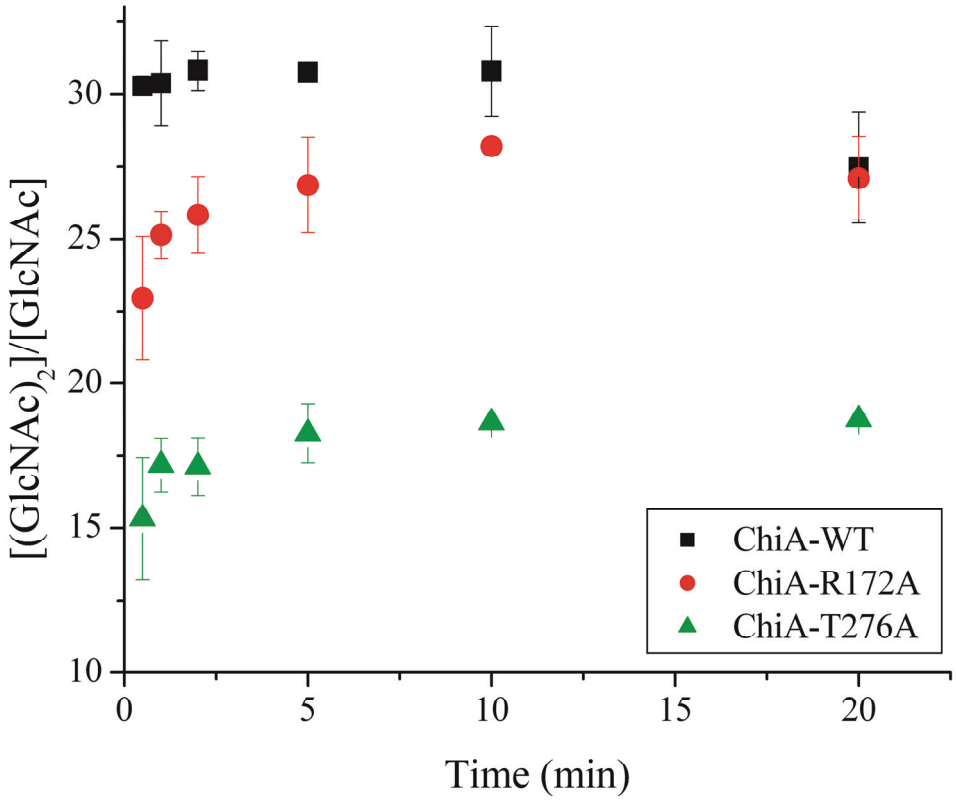
[(GlcNAc)2]/[GlcNAc]
30
25
20
15
10
0
5
10
15
20
Time (min)
ChiA-WT
ChiA-R172A
ChiA-T276A

Figure 3

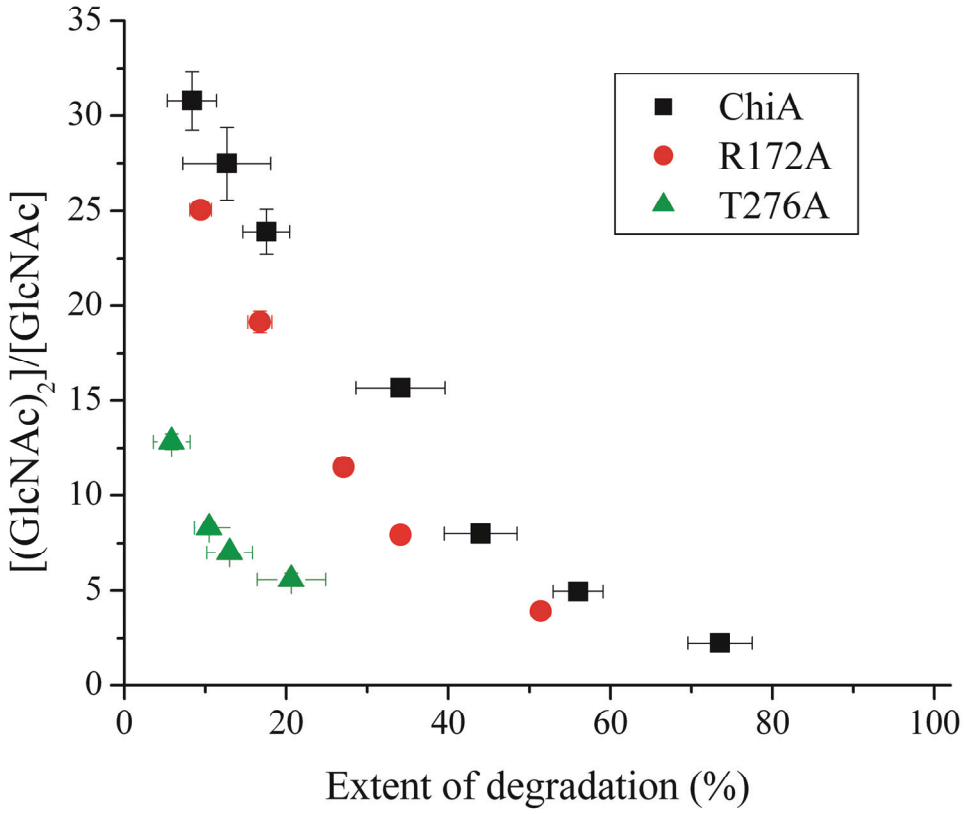
35
30
25
20
15
10
5
0
0
20
40
60
80
100
[(GlcNAc)2]/[GlcNAc]
Extent of degradation (%)
ChiA
R172A
T276A

Figure 4

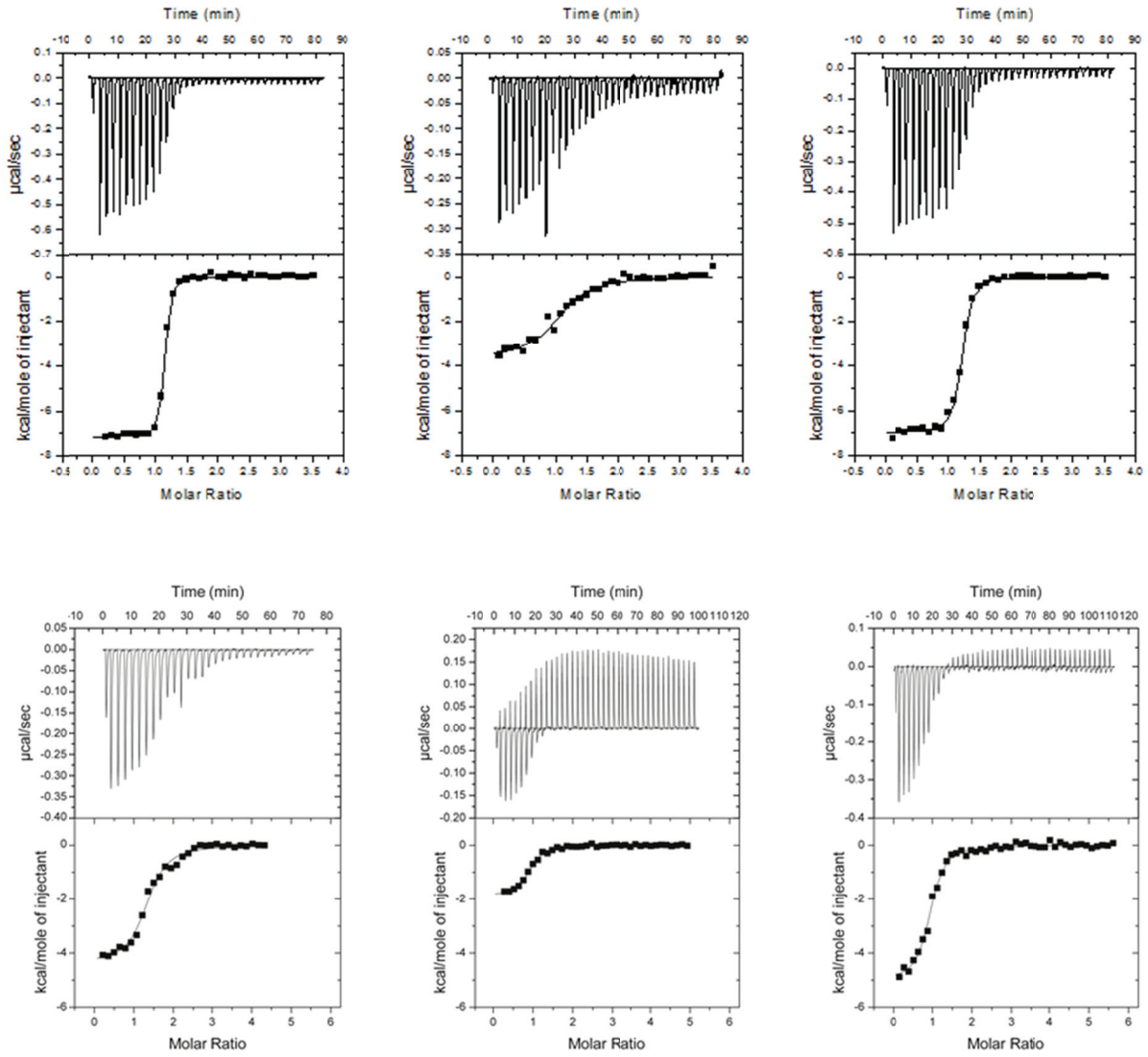

Figure 5

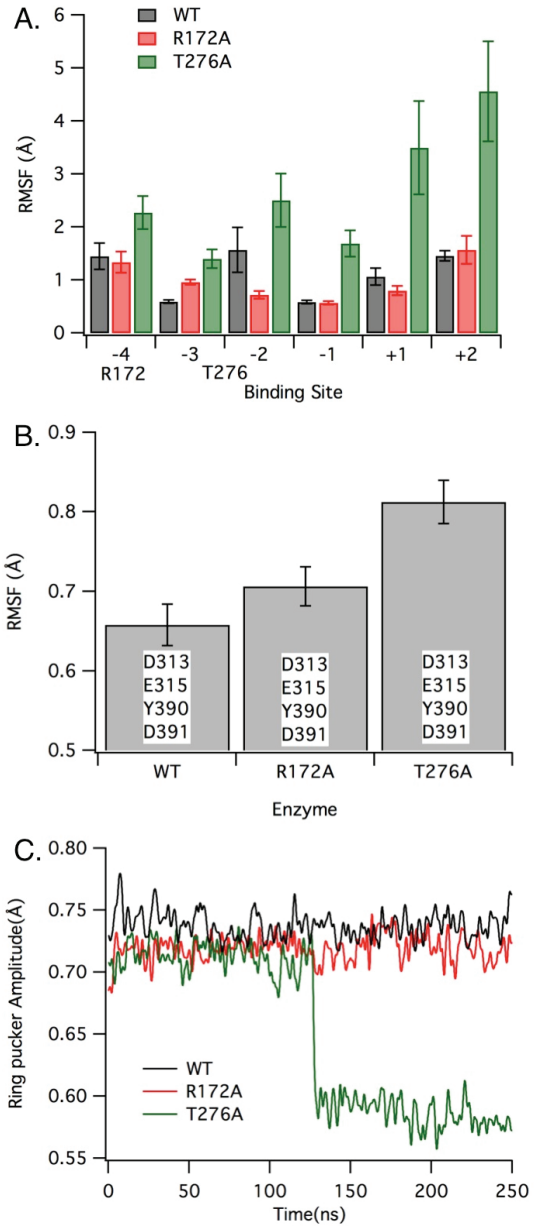
A.
WT
R172A
T276A
RMSF (Å)
0
1
2
3
4
5
6
-4
-3
-2
-1
+1
+2
R172
T276
Binding Site
B.
RMSF (Å)
0.5
0.6
0.7
0.8
0.9
D313
E315
Y390
D391
WT
R172A
T276A
Enzyme
C.
Ring pucker Amplitude(Å)
0.55
0.60
0.65
0.70
0.75
0.80
WT
R172A
T276A
0
50
100
150
200
250
Time(ns)

Paper V

Aromatic-mediated Carbohydrate Recognition in Processive *Serratia marcescens* Chitinases

Suvamay Jana,[1,†] *Anne Grethe Hamre,*[2,†] *Patricia Wildberger,*[2] *Matilde Menkrog Holen,*[2] *Vincent G. H. Eijsink,*[2] *Gregg T. Beckham,*[3] *Morten Sørlie,*[2,*] *and Christina M. Payne*[1,*]

[1]Department of Chemical and Materials Engineering, University of Kentucky, Lexington, KY, USA

[2]Department of Chemistry, Biotechnology, and Food Science, Norwegian University of Life Sciences, Ås, Norway

[3]National Bioenergy Center, National Renewable Energy Laboratory, Golden, CO, USA

[†] These authors contributed equally to this work.

[*] To whom correspondence should be addressed. E-mail: morten.sorlie@nmbu.no, Tel.: +47-67232562 and Fax: +47-64965901 or christy.payne@uky.edu, Tel.: + 859-257-2902 and Fax: + 859-323-1929

Abstract

Microorganisms use a host of enzymes, including processive glycoside hydrolases, to hydrolytically deconstruct recalcitrant polysaccharides. Processive glycoside hydrolases closely associate with polymer chains and repeatedly cleave glycosidic linkages without dissociating from the crystalline surface. A notable feature of processive glycoside hydrolases is the ubiquity of aromatic residues lining the enzyme catalytic tunnels and clefts. We hypothesize these aromatic residues have uniquely defined roles according to their local environment and position relative to the substrate. We have chosen *Serratia marcescens* Family 18 processive chitinases ChiA and ChiB as model systems in which to investigate our hypothesis. The roles of six aromatic residues Trp-167, Trp-275 and Phe-396 in ChiA and Trp-97, Trp-220 and Phe-190 in ChiB catalytic active sites have been examined. We see that point mutation of the tryptophan residues to alanine have high unfavorable relative free energy of binding implying critical role of these aromatic residues in ligand binding and likely processivity. Interestingly we see that phenylalanine mutations in ChiA and ChiB have little or no effect at all on chitin binding. These insights are directly compared to experimental characterizations of free energy of binding and degree of processive action to understand how active site topology affects function.

Keywords: Cellulose, Cellulase, Chitin, Chitinase, Glycoside hydrolase, Processivity, Ligand binding free energy, Molecular dynamics, Thermodynamic integration

1. Introduction

Polysaccharides are fundamental components of many of nature's most important structures, including plant and fungal cell walls and arthropod exoskeletons. Crystalline homo-polysaccharides, such as cellulose and chitin, are formed of vast polymeric networks of covalently bonded carbohydrates secured in well-packed layers through hydrogen bonding interactions; these molecular interactions, contributing both strength and insolubility, slow or preclude microbial and animal attacks.[1]

Nevertheless, the carbon-rich, monomeric carbohydrate units are ideal sources of energy, and to take advantage of this, microorganisms have evolved to secrete synergistic glycoside hydrolase (GH) enzyme cocktails capable of reducing these recalcitrant polysaccharides to monomeric and dimeric sugars.[2] The cocktails consist of multiple classes of processive, non-processive, and accessory enzymes. Non-processive enzymes attack the amorphous regions of polymer crystals and cleave glycosidic linkage once or sparingly few times, creating accessible polymeric chain ends; whereas, processive enzymes typically attach to polymer chain ends (in exo-mode) or generate a new end (in endo-mode) and sequentially hydrolyze many glycosidic linkages to produce disaccharide products prior to dissociation.[3,4] Accessory enzymes aid in substrate accessibility and reduce product inhibition by further degrading disaccharides to monosaccharides. By virtue of their ability to maintain association with the polysaccharide substrate, processive enzymes are responsible for the majority of hydrolytic bond cleavages, and hence, are of great interest as logical targets for activity improvements towards efficient and economical biomass conversion.[5,6,7,8]

Historically, the ability of a GH to be processive has been attributed to global structural features of the active site geometry.[9] For example, the structures of processive cellulases exhibit tunnel-like active sites with loops on either side: these loops are flexible,

having both an open and closed conformation allowing for endo-initiated hydrolysis and processive behavior.[10] Homologous, non-processive cellulases lack the loops forming the active site tunnels resulting in a more open cleft.[11] Similarly, processive chitinases possess deep substrate binding clefts, while non-processive chitinases have a shallow, open binding cleft.[12,13,14] Critically, biochemical studies have demonstrated that processivity can be changed dramatically by point mutations or deletions of only a few amino acids within active site loops.[5,6,,15,16] Furthermore, examples from nature such as the *Thermobifida fusca* cellulase, E4, exhibit processive behavior while having an open and shallow active site.[17] Thus, while it may seem straightforward to identify an enzyme as processive or not based on these coarse structural features, such an assignment is not always possible.

Alternatively, critical examination of the chemical and dynamic composition of processive GH active sites is anticipated to elucidate the governing features responsible for processive function. A notable feature in processive Family 18 chitinases is the ubiquity of aromatic residues lining the enzyme tunnels and clefts, similar to other 130 families of GHs, and it is assumed that these aromatic residues are mainly responsible for substrate chain acquisition and binding in the catalytic tunnel via carbohydrate-π stacking interactions.[18,19,20,21,22,23,24] The non-specific nature and the large interaction surface of the hydrophobic stacking interactions usually facilitate the processive mechanism whereby the enzyme must maintain attachment to the substrate while still allowing forward processive motion.

Given the prevalence of aromatic residues along GH active sites and the remaining question of how, if feasible, to generalize aromatic-carbohydrate mediated binding in GHs, we set out to study the aromatic/chito-oligosaccharide interactions that occur in processive chitinases, which are frequently used as a model system for understanding cellulase function.[25] Family 18 chitinases from *S. marcescens* include three types – processive

chitinases A (ChiA), processive chitinases B (ChiB), and non-processive chitinases C (ChiC).[26,27] These enzymes act synergistically to degrade crystalline chitin to disaccharides. From structural data and analysis of reaction products, it has been shown that ChiA and ChiB are exo-acting enzymes (ChiA reducing end-specific and ChiB non-reducing end-specific) while ChiC is an endo-acting, non-processive enzyme.[28,29]

To date, studies addressing the role of aromatic residues in GH tunnels primarily investigate the extent to which the residue abolishes either activity or processive ability on crystalline and amorphous substrates. In ChiA, two active site residues, Trp-245 and Phe-232, were mutated to alanine.[30] These individual mutations resulted in a significant reduction in the ability of ChiA to hydrolyze chitin but had little effect on conversion of soluble substrate, suggesting the catalytic mechanism remained intact but that processivity was affected. A more recent study of ChiB, individually mutating both Trp-97 and Trp-220 to alanine, found that mutating aromatic residues to alanine in the catalytic domain increased processivity on soluble chitosan substrate but drastically decreased processivity on crystalline chitin substrates.[5] Similarly, Zakariassen et al. compared the degree of processivity between wild-type ChiA and the W167A, W275A, F396A, and W167A/W275A double mutants, again observing that processivity on crystalline substrates was slowed while throughput of soluble substrate was increased.[6]

Recent computational investigations of the role aromatic residues play in processive cellulase carbohydrate binding reveal a given aromatic residue's function is specific to its position within the tunnel. In the processive cellulase *Trichoderma reesei* Cel6A, we demonstrated that mutation of aromatic residues near the catalytic center had little impact on ligand binding free energy, but mutation of aromatic residues at the entrance and exit of the Cel6A tunnel dramatically impacted binding affinity.[31] Along with molecular dynamic simulation and prior experimental literature describing how these aromatic residues affected

processive ability, we were able to ascribe roles, such as, substrate chain acquisition and product stabilization. In a later study investigating key industrial cellulases, processive *T. reesei* Cel7A and non-processive Cel7B cellulase, Taylor, et al. determined that removal of aromatic residues near the catalytic center resulted in higher relative binding free energies than tunnel entrance residues.[32] Taken together, it is clear that an aromatic residue's role may be different based on its position along the length of the GH active site. Moreover, these prior studies reveal that aromatic residues in similar binding sites across different GH families are not required to have similar functional roles, even while maintaining identical hydrolytic mechanisms.

Here, we explore the aromatic-mediated interactions of processive chitinases ChiA and ChiB with chito-oligosaccharides with the intent of defining the roles of each residue. As these chitinases are frequently compared to processive cellulases, it is important to understand the similarities and differences between the two. Further, we anticipate that detailed studies such as this will eventually help to illustrate a general interaction mechanism across various carbohydrate active enzyme families. We integrate computational and experimental methods to define the roles of Trp-167, Trp-275, and Phe-396 in the cleft of ChiA, and Trp-97, Trp-220 and Phe-190 in the cleft of ChiB (Figure 1), which were selected on the basis of interaction energies from wild-type molecular dynamics (MD) simulations. Molecular dynamics simulations of wild-type and variant ChiA and ChiB enzymes bound to a hexameric oligomer of *N*-acetylglucosamine, $(GlcNAc)_6$, were performed to understand dynamic contributions to carbohydrate binding and processive ability. Free energy calculations, using thermodynamic integration (TI), and experimental determinations of ligand binding free energy, from isothermal titration calorimetry (ITC), reveal the various thermodynamic contributions. Apparent processivity of wild-type ChiA and ChiB and several of the variants has been previously reported in the literature;[5,6,33] as in

our prior studies, we build on this literature, defining the roles of each active site aromatic residue.

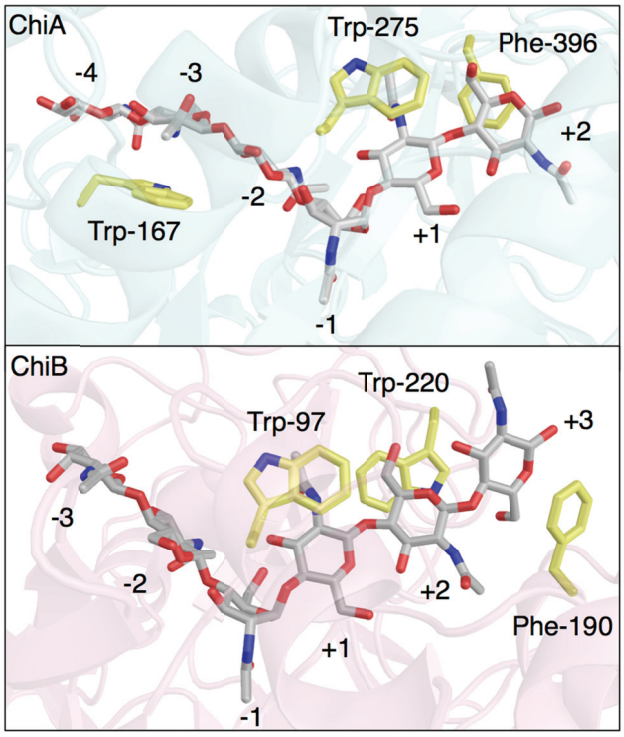

Figure 1. Aromatic residues along the catalytic active sites of *S. marcescens* processive chitinases ChiA and ChiB. ChiA is shown in transparent cyan cartoon, and ChiB is shown in transparent pink cartoon. The $(GlcNAc)_6$ ligand is shown in stick, with grey carbons. The aromatic residues are shown in stick with yellow carbons. The ChiA and ChiB binding sites are labeled according to standard nomenclature from -4 to +2 and -3 to +3, respectively. Hydrolysis occurs between the +1 and -1 binding sites of all GHs.

2. Experimental Materials and Methods

2.1 Chemicals

Hexa-*N*-acetylglucosamine was purchased from Megazyme (Wicklow, Ireland). All other chemicals were purchased from standard manufacturers.

2.2 Enzymes

Site directed mutagenesis

Mutation of Trp-167, Trp-275, Phe-396 (catalytically inactivated ChiA-E315Q template), and Phe-190 (catalytically inactivated ChiB-E144Q template) to alanine were performed using the QuikChange™ site directed mutagenesis kit from Stratagene (La Jolla, CA, USA), as described by the manufacturer. The primers and templates used for the mutagenesis are listed in Table 1. Primers were purchased from Life Technologies (Carlsbad, CA, USA). To confirm that the genes contained the desired mutations and to check for the occurrence of nondesirable mutations, the mutated genes were sequenced using GATC Biotech's (Constance, Germany) LIGHTrun sequencing service before they were transformed into *Escherichia coli* BL21Star (DE3) cells (Life Technologies).

The ChiB mutations, W220A (His_{10}-ChiB E144Q template) and E144Q (His_{10}-ChiB W97A template), were introduced using a two-stage PCR protocol.[34] The primers and templates used for the mutagenesis are listed in Table 1 and were purchased from Life Technologies (Carlsbad, CA, USA). In the first step of the two-stage protocol, two separate PCR reactions were completed with the forward and reverse primer. These reactions consisted of a preheating step at 98 °C for 30 s followed by 6 reaction cycles of 15 s at 98 °C, 20 s at 49.6 °C and 4 min at 72 °C, and a final extension step of 7 min at 72 °C. In the second step, PCR reactions were combined and continued for 30 reaction cycles of 15 s at 98 °C, 20 s at 63 °C, and 4 min at 72 °C. The amplification products were subjected to parental template digest by DpnI and transformed into *E. coli* BL21Star (DE3) cells (Life Technologies). *Phusion* High-Fidelity Polymerase (Thermo Scientific, Waltham, USA) was used for amplification. The mutated genes were sequenced using GATC Biotech's LIGHTrun sequencing service in order to verify the introduction of the desired mutations.

Table 1. Primers used for site directed mutagenesis

mutant	DNA template	primer	sequence
ChiA-E315Q/W167A	ChiA-E315Q [35]	W167A fw	5'TTCTTATTTCGTCGAGGCGGGCGTTTACGG'3
		W167A rev	5'CGCCCGTAAACGCCCGCCTCGACGAAATA'3
ChiA-E315Q/W275A	ChiA-E315Q [35]	W275A fw	5'GTCGATCGGCGGCGCGACGCTGTCCGAC'3
		W275A rev	5'GTCGGACAGCGTCGCGCCGCCGATCGAC'3
ChiA-E315Q/F396A	His_{10}-ChiA E315Q	F396A fw	5'ACGACTTCTATGGCGGCCGCCGATCTGAAGAACCTGG '3
		F396A rev	5'CCAGGTTCTTCAGATCGGCGGCGCCATTAGAAGTCGT '3
ChiB-E144Q/W220A	His_{10}-ChiB-E144Q [36]	W220A fw	5'TGGCCGGCCCCGCGGAGAAG-'3
		W220A rev	5'CTTCTCCGCGGGGCCGGCCA-'3
ChiB-E144Q/F190A	ChiB-E144Q [37]	F190A fw	5'GCCGGCGGCGCCGCCTTCCTGTCGCG'3
		F190A rev	5'CGCGACAGGAAGGCGGCGCCGCCGGC'3
ChiB-E144Q/W97A	His_{10}-ChiB-W97A[a]	E144Q fw	5'GGACATCGACTGGCAGTACCCGCAAGC'3
		E144Q rev	5'GCTTGCGGGTACTGCCAGTCGATGTCC'3

[a] ChiB-W97A has previously been constructed. [5]

Construction of His_{10}-tagged mutants

To subclone ChiA and ChiB mutants into the vector pET16b (Novagen, Madison, WI, USA), the chitinase fragments were amplified by PCR using primers (Life Technologies) listed in Table 2. PCR reactions were conducted with Q5® High-Fidelity 2X Master Mix (New England Biolabs, Ipswich, MA). The amplification protocol consisted of an initial denaturation cycle of 30 s at 98 °C, followed by 30 cycles of 5 s at 98 °C, 30 s at 55 °C, and 30 s at 72 °C, and a final step of 2 min at 72 °C. All PCR fragments were clone into an NdeI/XhoI digested pET16b by using the In-Fusion HD Cloning kit (Clontech Laboratories, Kyoto, Japan). The resulting pET16b constructs were sequenced using GATC Biotech's (Constance, Germany) LIGHTrun sequencing service to confirm the correct insert

before transformation into *E. coli* BL21Star (DE3) cells (Life Technologies, Carlsbad, CA, USA).

Table 2. Primers used for PCR amplification

Chitinase	primer	sequence
ChiA	Forward	5' TCGAAGGTCGTCATATGGCCGCGCCGGGC '3
	Reverse	5' CAGCCGGATCCTCGAGTTATTGAACGCCGGCGC '3
ChiB	Forward	5' TCGAAGGTCGTCATATGTCCACACGCAAAGCCGTT '3
	Reverse	5' AGCCGGATCCTCGAGTTACGCTACGCGGCCCA '3

Protein expression

For protein expression, *E. coli* BL21 (DE3) cells containing the appropriate plasmid were inoculated into 25 mL LB-Amp (Luria broth medium containing 115 μg / mL ampicillin) medium and grown at 37 °C and 200 rpm for 16 h. Cell culture were then inoculated into 250 mL LB-Amp medium to an OD_{600} of 0.1. This culture was cultivated until the OD_{600} reached 0.8-1.0. The temperature was decreased to 22°C, and gene expression was induced with 1 mM isopropyl-β-D-thiogalactopyranoside for 20 h. The cells were harvested by centrifugation (8000 rpm, 20 min at 4 °C). Periplasmic fractions were prepared by osmotic shocking as described elsewhere.[36] A cytoplasmic protein extraction was also performed by re-suspending the spheroplasts in lysis buffer (0.1 mg / mL lysozyme, 50 mM Tris-HCl, 50 mM NaCl, 4 mM $MgCl_2$, 1 mM EDTA, 0.1 mM PMSF pH 8.0) and incubating it at 37 °C for 30 min. Cell debris was removed by centrifugation (8000 rpm, 20 min at 4 °C). The resulting supernatant was used for further enzyme purification. Both the periplasmic and cytoplasmic extracts were sterilized by filtration (0.2 μm) prior to protein purification.

Protein purification

Proteins were purified on a column packed with Ni-NTA Agarose matix (Qiagen, Venlo, Netherlands) (1.5 cm in diameter, 5 ml stationary phase in total). The column was pre-equilibrated in a buffer containing 20 mM Tris-HCl, 20 mM imidazole, and 500 mM NaCl at pH 8.0 before the periplasmic and cytoplasmic extracts were applied. After washing with a buffer containing 20 mM Tris-HCl and 500 mM NaCl at pH 8.0, fractions containing the enzyme were eluted with a buffer containing 20 mM Tris-HCl, 250 mM imidazole, and 500 mM NaCl at pH 8.0. A flow rate of 2.5 ml / min was used at all times. Enzyme purity was verified by SDS-PAGE, and fractions containing purified enzyme were concentrated and transferred (Macrosep Advance Centrifugal Device, 10 kDa cutoff, Pall corporation, Port Washington, USA) to 20 mM potassium phosphate buffer pH 6.0. Protein concentrations were determined by using the Bradford Protein Assay from Bio-Rad (Hercules, CA, USA).

2.3 Isothermal Titration Calorimetry Experiments

ITC experiments were performed with a VP-ITC system from Microcal, Inc. (Northampton, MA, USA).[38] Solutions were thoroughly degassed prior to experiments to avoid air bubbles in the calorimeter. For experiments with ChiA-W275A and ChiA-F396A, 500 μM of $(GlcNAc)_6$ was placed in the syringe and 15 μM of enzyme was placed in the reaction cell with a volume of 1.42 ml. For ChiA-W167A, 3 mM $(GlcNAc)_6$ and 15 μM enzyme were used; for ChiB W220A, 2 mM of $GlcNAc_6$ and 20 μM of enzyme was used; for ChiB F190A, 500 μM of $GlcNAc_6$ and 20 μM of enzyme was used; and for ChiB W97A, 2 mM of $GlcNAc_6$ and 80 μM of enzyme was used. Both enzyme and ligand were diluted in 20 mM potassium phosphate buffer pH 6.0. The heat of ionization of this buffer is 1.22 kcal/mol.[39] Typically, 40 to 60 injections of 4-8 μl $GlcNAc_6$ were injected into the

reaction cell at 180 s intervals at 30 °C with a stirring speed of 260 rpm. Due to instability of ChiB W97A at 30 °C, experiments at 10, 12.5, 15, and 17.5 °C were performed, and the values for 30 °C were extrapolated with this as basis. At least two independent titrations were performed for each binding reaction.

2.4 Analysis of Calorimetric Data.

The shape of the ITC binding curve is determined by the Wiseman c-value expressed as in Equation 1:[38]

$$c = nK_a[M]_t \tag{1}$$

where n is the stoichiometry of the reaction, K_a is the equilibrium binding association constant, and $[M]_t$ is the protein concentration. When the c value is in the range of $10 < c < 1000$, K_a can be determined from the Wiseman binding isotherm. When the c value is in the range of $0.01 < c < 10$, as was the case for ChiA W167A, ChiB W220A, and ChiB W97A, the binding thermodynamics can be determined if a sufficient portion of the binding isotherm is used for analysis.[40] This can be achieved by ensuring a high molar ratio of ligand to protein at the end of the titration, accurate knowledge of the concentrations of both ligand and receptor, an adequate level of signal-to-noise in the data and known stoichiometry.

ITC data were collected automatically using the Microcal Origin v.7.0 software accompanying the VP-ITC system.[38] Prior to further analysis, data were corrected for heat dilution by subtracting the heat remaining after saturation of binding sites on the enzyme. Data were fit with a single-site binding model using a non-linear least-squares algorithm available in Origin. All data from the binding reactions were well-represented by the single site binding model, yielding the stoichiometry (n), equilibrium binding association constant (K_a), and the reaction enthalpy change ($\Delta H_r°$) of the reaction. The equilibrium binding

dissociation constant (K_d), reaction free energy change ($\Delta G_r°$) and the reaction entropy change ($\Delta S_r°$) were calculated as in Equation 2.

$$\Delta G_r^\circ = -RT \ln K_a = RT \ln K_d = \Delta H_r^\circ - T\Delta S_r^\circ \quad (2)$$

Errors are reported as standard deviations of at least two experiments at each temperature. A description of how the entropic term is parameterized has been described previously.[40,41]

3. Computational Methods

3.1 Molecular Dynamics Simulations

Models of ChiA and ChiB were constructed from crystal structures obtained from the Protein Data Bank (PDB), PDB 1EHN for ChiA[12] and PDBs 1E6N and 1OGG for ChiB.[13,42] As ChiA is a reducing end-specific enzyme,[28,29] substrate bound in the ChiA active site is numbered −4 to +2 from cleft entrance to exit (Figure 1).[43] Similarly, ChiB is a non-reducing end-specific enzyme in which the binding sites are numbered +3 to −3 from the entrance to exit (Figure 1).[27,44] Hydrolysis occurs between −1 and +1 site, catalyzed by a glutamic acid. Rotation of an aspartic acid in the −1 binding site forms a hydrogen bond with the catalytic glutamic acid and the *N*-acetyl group of −1 bound sugar. This residue orientation in the active site enables nucleophilic attack by the *N*-acetyl oxygen on the anomeric carbon of the −1 binding site pyranose.[13,45,46,47] Model construction included manual manipulation of the glutamic acid and *N*-acetyl side chains from their initial crystal structure orientations, such that they mimic the catalytically competent complexes. Additionally, the catalytic Glu to Gln mutations in the PDB structures were reversed. A total of 10 MD simulations were constructed including: a ligand-free and ligand-bound version of wild-type ChiA and ChiB; ligand-bound simulations of W167A, W275A, and F396A ChiA variants; and ligand-bound simulations of W97A, W220A, and F190A ChiB variants. The

$(GlcNAc)_6$ ligand was bound as shown in Figure 1. Explicit details of the system construction, including the steps involved in manipulation of the catalytic residues and the construction of a hexameric ligand in the active sites of ChiA and ChiB, are provided in the Supporting Information.

After the systems were constructed, the enzymes and ligands were solvated with water and sodium ions were added using CHARMM.[48] The solvated ChiA and ChiB systems contained approximately 175,000 atoms and 52,000 atoms, respectively. ChiA was simulated with the fused carbohydrate binding module (CBM). The ChiB catalytic domain is stable and active in absence of its catalytic domain (unpublished observations), and thus, we simulated only ChiB without the CBM for computational efficiency. Using CHARMM, the solvated systems were (1) minimized using an extensive step-wise procedure, (2) heated from 100 K to 300 K in 4 ps increments over 20 ps, and finally, (3) the systems were density equilibrated in the *NPT* ensemble for 0.1 ns. After equilibration, the data collection MD simulations were performed using NAMD in the *NVT* ensemble for 250 ns.[49] For all MD simulations and the free energy calculations below, the CHARMM36 all atom force field with CMAP[48,50,51] corrections was used to model the enzyme. The CHARMM 36 carbohydrate force field was used to model the $(GlcNAc)_6$ ligands, and water was modeled with the modified TIP3P force field.[52,53] VMD was used for visualization of trajectories.[54]

3.2 Thermodynamic Integration

Relative ligand binding free energies were determined from TI calculations performed using NAMD with the dual-topology methodology.[49,55,56,57] The simulations were started from an equilibrated 25 ns snapshot obtained from the MD simulations. The TI methodology entails the additional equilibration of single system containing a "hybrid" residue at the mutation site. The hybrid residue contained atoms from both the wild-type

aromatic residue and the mutant alanine residues; the wild-type and mutant atoms did not interact with one another. The hybrid residue atoms interacted with the rest of the system via standard bonded and non-bonded interactions scaled by λ from the reactant (wild-type) to the product state (mutant) in windows over λ. Electrostatic and van der Waals calculations were decoupled into two separate process, and soft-core potentials were used to overcome endpoint singularities.[58] The electrostatic and van der Waals calculations included 15 windows ranging from λ values of 0 to 1 for a total of 30 simulations per mutation. The windows were divided so as to use more closely coupled window near the endpoints, improving accuracy. The electrostatics and van der Waals calculations were equilibrated for 0.5 ns prior to collecting 14.5 ns of TI data. The potential energy was calculated over the range of the coupling parameter.

The change in free energy, ΔG, for each set of simulations was determined by numerical integration with Cubic Spline Gaussian Quadrature numerical method, integrating $dU/d\lambda$ over $\lambda = 0$ to 1. We compared the numerical integration method against both trapezoidal with unequal step sizes and cubic spline integrations for verification. The electrostatic and van der Waals terms were combined to obtain ΔG for the bound and ligand-free states of each point mutation. The binding free energy of each mutant relative to wild-type, ΔΔG, was determined from Equation 3, where "M" refers to the mutant and "WT" refers to the wild-type. The thermodynamic cycle used in these calculations is shown in Figure 2.

$$\Delta\Delta G = \left(\Delta G_{M(Bound \rightarrow Free)} - \Delta G_{WT(Bound \rightarrow Free)}\right)_{\text{Experimental}} = \left(\Delta G_{Bound(M \rightarrow WT)} - \Delta G_{Free(M \rightarrow WT)}\right)_{\text{Calculated}} \quad (3)$$

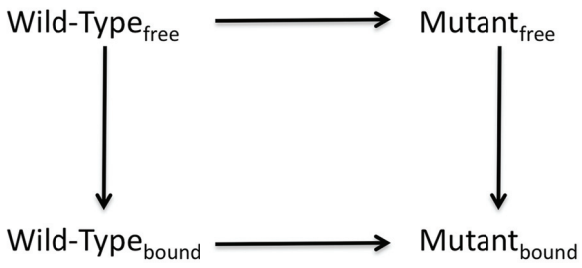

Figure 2. Thermodynamic cycle for measuring ΔΔG with TI. Free and bound refer to the absence and presence of the ligand, respectively.

Sufficient sampling was visually confirmed by plotting the $dU/d\lambda$ histograms from each λ window. The autocorrelation time was determined for each window, which was then used as input for error analysis. Error analysis was performed following the method of Steinbrecher et al.[59] Additional details and example simulation convergence analysis is provided in the Supporting Information (Figure S1).

4. Results

Ligand binding free energies obtained experimentally from ITC and computationally from TI are reported in Table 3. The dissociation constant has been directly determined from experiment, and the free energy of binding, ΔG_{ITC}, was calculated from K_d as in Equation 2. Enthalpic and entropic contributions to binding free energy are also reported (Table 3). For direct comparison with computational results, ligand binding free energy relative to wild-type, $\Delta\Delta G_{ITC}$, was determined by subtracting the free energy of binding $(GlcNAc)_6$ to the wild-type from the free energy of binding $(GlcNAc)_6$ to the variant. Error was propagated using standard rules for combining error. The calculated relative ligand binding free energy, $\Delta\Delta G_{TI}$, was determined from the sum of the electrostatic and van der Waals

components, as described in the Methods. The individual components are reported in Table S1.

Table 3. Absolute and relative free energies of binding $(GlcNAc)_6$ to ChiA and ChiB wild-type and variants. The dissociation constant and free energies denoted with the "ITC" subscript were obtained experimentally from ITC. The calculated relative ligand binding free energies are denoted with the "TI" subscript. ITC experiments were performed at t = 30 °C and pH = 6.0.

chitinase	mutation	binding site	Isothermal Titration Calorimetry					Thermodynamic Integration
			K_d [a]	ΔG_{ITC}° [b]	ΔH_r° [b]	$-T\Delta S_r^\circ$ [b]	$\Delta\Delta G_{ITC}$ [b]	$\Delta\Delta G_{TI}$ [b]
ChiA	WT	------	0.56 ± 0.03	−8.7 ± 0.1	−4.5 ± 0.2	−4.2 ± 0.2	------	------
	W167A	-3	134 ± 13	−5.4 ± 0.1	−4.5 ± 0.3	−0.9 ± 0.2	3.3 ± 0.1	5.0 ± 0.4
	W275A	+1	2.1 ± 0.3	−7.9 ± 0.1	−6.7 ± 0.7	−1.2 ± 0.6	0.8 ± 0.1	3.6 ± 0.4
	F396A	+2	1.2 ± 0.1	−8.2 ± 0.1	−3.3 ± 0.03	−4.9 ± 0.1	0.5 ± 0.1	-0.2 ± 0.2
ChiB	WT	------	0.20 ± 0.03[c]	−9.3 ± 0.1	−0.1 ± 0.3	−9.2 ± 0.3	------	------
	W97A	+1	0.87 ± 0.14[d]	−8.4 ± 0.1	−1.2 ± 0.1	−7.2 ± 0.2	0.9 ± 0.1	2.8 ± 0.4
	W220A	+2	57 ± 0.04[c]	−5.9 ± 0.1	−1.9 ± 0.1	−4.0 ± 0.2	3.4 ± 0.1	3.5 ± 0.3
	F190A	+3	0.55 ± 0.12	−8.7 ± 0.2	−0.7 ± 0.1	−7.5 ± 0.2	0.6 ± 0.1	-0.3 ± 0.2

[a] μM, [b] kcal/mol, [c] interpolated from values above and below t = 30 °C, [d] extrapolated from values below t = 30 °C

The computational and experimental results are generally well aligned within the capabilities of each technique. The notable outlier in comparing the computational and experimental relative ligand binding free energies is the ChiA W275A variant, which differs by more than 2 kcal/mol. As we will discuss below, we expect this is a result of the uncertainty involved in experimental determination of ligand binding free energies (i.e., experimentally, we cannot be certain that the ligand binds in precisely the same binding sites as those investigated computationally). This illustrates the importance of using computational methods to understand the dynamics of ligand binding in GHs.

The relative binding free energies of W167A and W275A along the cleft of ChiA are quite unfavorable, suggesting aromatic residues in these positions play important roles in tight binding. The free energy change associated with mutating Phe-396, on the product side of the ChiA cleft, is relatively inconsequential. It is unlikely this residue has much influence in direct ligand binding. The relative ligand binding free energies of W97A and W220A, closer to the catalytic center of ChiB, are unfavorable, indicating a clear preference for aromatic residues in these positions. The change in binding free energy associated with mutating the tunnel entrance Phe-190 of ChiB to alanine is negligible by comparison to W97A and W220A variants, suggesting a more indirect role in carbohydrate binding. As we will discuss below, experimental evidence suggests Phe-190 may not be required for processive catalytic function.

To understand the role of aromatic residues in the catalytic clefts of processive chitinases, we performed 250-ns MD simulations of ChiA and ChiB wild-types and variants. From these simulations, we have calculated the root mean square fluctuation (RMSF) of the catalytic residues involved in hydrolysis and the RMSF of ligand on binding site basis (Figure 3). These dynamic measures provide additional insights as to how point mutations affect stabilization of the ligand in the clefts and potentially how this affects processivity.

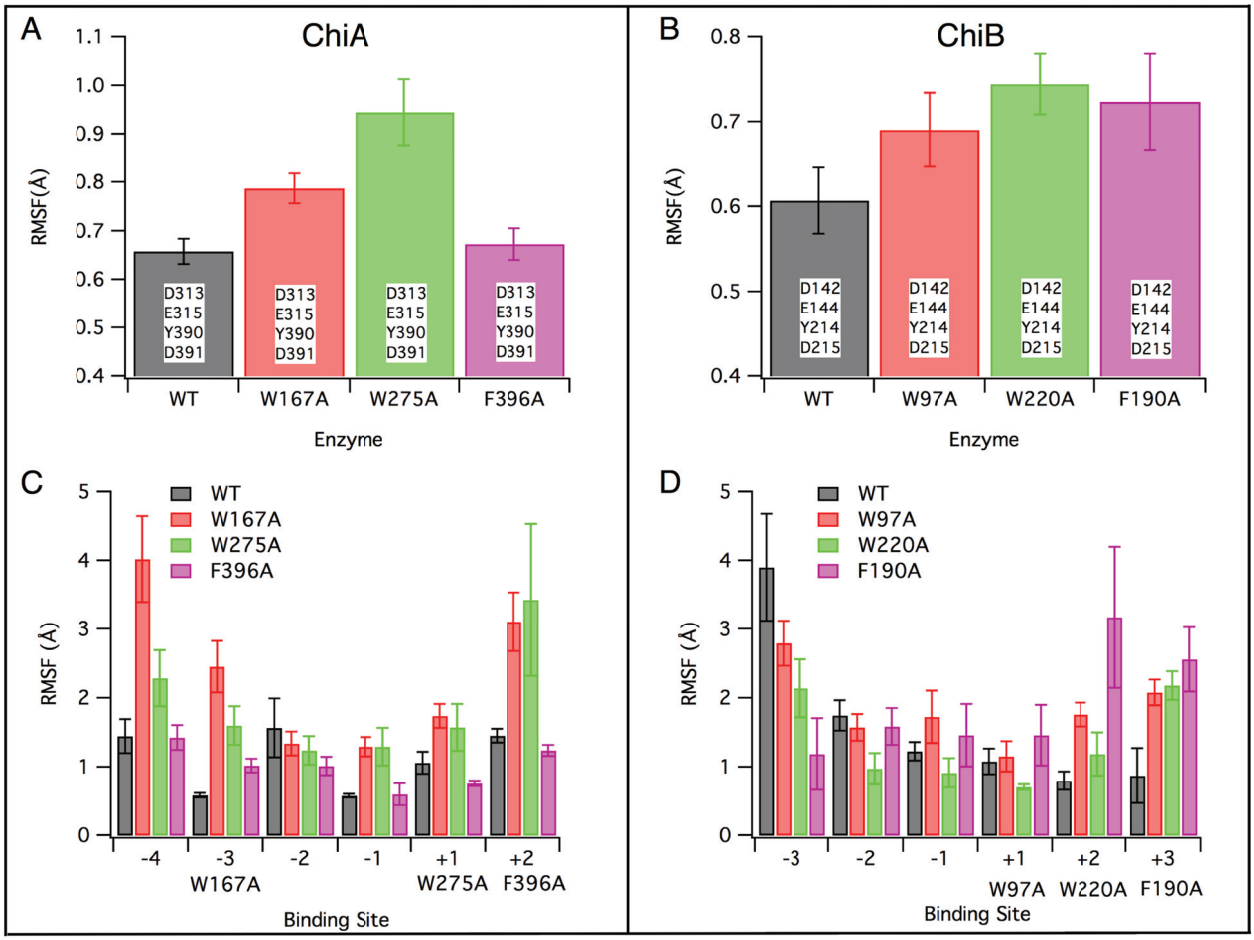

Figure 3. Dynamic characterizations of processive chitinases ChiA and ChiB and chitinase variants from MD simulations. Root mean square fluctuation (RMSF) of the catalytic tetrad for wild-type and mutants of processive ChiA (A) and ChiB (B). RMSF of the $(GlcNAc)_6$ ligand across the binding sites of processive chitinases ChiA (C) and ChiB (D). Labels below x-axis indicate the position of the aromatic residues relative to the binding site. Error bars have been obtained through 2.5 ns block averaging.

In both ChiA and ChiB, four residues have been implicated as participants in the substrate-assisted catalytic mechanism.[13,45,46,47] During catalysis, these residues facilitate the hydrolytic reaction through hydrogen bonding and steric effects that encourage distortion of the -1 pyranose ring. We have previously suggested that the flexibility of the catalytic

center, as measured by the RMSF of the catalytic tetrad, may be associated with reduced substrate chain association (k_{on}) and likely reduced processivity.[14] Thus, we examine this measure of active site dynamics, comparing to both binding free energy and literature assessments of processive ability, where available. In ChiA, this tetrad includes Asp-313, Glu-315, Tyr-390, and Asp-391.[45,47] The ChiB catalytic tetrad includes Asp-142, Glu-144, Asp-215 and Tyr-214. In general, the RMSF of the mutants chitinases is higher than that of wild-type ChiA and ChiB (Figures 3A and 3B). The exception to this is the F396A ChiA variant, whose catalytic center is unaffected by the mutation. As we discuss below, literature indicates this residue has little impact on processivity or hydrolysis despite its location in the active site (Figure 1),[6] which is evidenced by the minimal impact on dynamics. The flexibility of the ChiA and ChiB catalytic tetrad is roughly the same, within error.

The RMSF of carbohydrate ligands bound in the active sites of GHs has also been linked to processive function. To understand the relationship of this measure of active site dynamics with binding free energy and processive ability, we have determined the RMSF of the $(GlcNAc)_6$ ligands of wild-type ChiA, ChiB, and the six variants over the course of the 250-ns MD simulations. As with the RMSF of catalytic residues, the RMSF of the $(GlcNAc)_6$ ligand is a measure of the degree to which the ligand fluctuates about an average position; higher RMSF values correspond to ligands with a higher degree of freedom. In ChiA, both the ligands bound to W167A and W275A variants fluctuate significantly more than wild-type across the length of the binding cleft (Figure 3C). The ligand of the F396A ChiA variant is equally as flexible as that of wild-type ChiA. In ChiB, the effect of mutation on $(GlcNAc)_6$ is more localized, primarily affecting the substrate binding sites +2 and +3; in these two sites, the flexibility of $(GlcNAc)_6$ is significantly higher than that of wild-type (Figure 3D). Interestingly, the ChiB W220A ligand appears marginally stabilized in the

product binding sites as a result of mutation. In the -3 binding site, wild-type ChiB displays the highest degree of ligand flexibility.

5. Discussion

Relative Binding Free Energies

Experimental and computational determinations of relative binding free energies are generally within good agreement of each other. Though, as mentioned above, the ChiA W275A variant differs by more than a 2 kcal/mol between the computational and experimental values. Further, the computational and experimental relative binding free energies of ChiA W167A and ChiB W97A variants are not within error of each other, though to a lesser extent than ChiA W275A. A number of factors may contribute to these discrepancies, which we expect have more to do with location and binding conformation of $(GlcNAc)_6$ than error in either method.

As with any computational assessment of binding free energy, the starting configuration of the bound ligand relies on structural input from crystallographic studies or docking calculations. Here, we have initiated simulations using crystallographic structures representative of thermodynamically stable configurations of the $(GlcNAc)_6$ ligand within the ChiA and ChiB active site.[12,13,42] These crystallographic structures display single point mutations of the catalytic acids, such that a non-hydrolyzed ligand can be bound across the length of the cleft. In each case, the distorted -1 pyranose conformation has been captured in the crystallographic structure; though computationally, the side chains associated with the wild-type catalytically active conformation were rotated such that the actual distorted Michaelis complex was represented. This *in silico* rotation of the side chains represents a potential deviation from the conformation experimentally observed during ITC experiments.

As in structural studies, ITC makes use of catalytically inactivated variants, such that the free energy associated with formation of the Michaelis complex may be underestimated. The free energy of forming this complete distorted complex, a $^{1,4}B$ conformation, is quite significant overall. The free energy landscape associated with a β-glucopyranose traversing from the solution equilibrium $^{1,4}C$ conformation to the boat conformation is approximate 8 kcal/mol.[60] While the distortion of the pyranose ring may be almost completely formed, as visualized through crystallography, it is possible the additional rotation of the *N*-acetyl side chain and that of the catalytic residues at least partially contributes to the any discrepancy between computational and experimental determinations of relative ligand binding free energies.

ChiA and ChiB each have multiple binding subsites beyond those examined here, where ChiA can bind ligands from −3 to +3 binding sites, and ChiB can bind ligands from −2 to +4 binding sites. Kinetic studies have shown both ChiA and ChiB are capable of binding shorter oligomers, such as $(GlcNAc)_6$ in different locations along the cleft. These prior studies suggest that ChiA will bind $(GlcNAc)_6$ in either the −4 to +2 binding sites or the −3 to +3 binding sites with approximately equal favorability.[61] ChiB favors binding $(GlcNAc)_6$ in the −2 to +4 binding sites over the −3 to +3 binding sites (80% vs. 20%).[27] The kinetic studies were conducted on wild-type ChiA and ChiB, and it is unknown what effect mutation of active site residues will have on this balance of occupancy. Assuming favorable occupancy does not change at all, ITC measurements of ChiA have approximately a 50/50 chance of binding in the same fashion represented computationally. Further, our computational investigation considers the less favorable ChiB occupancy, so as to determine the role of Phe-190 in the ChiB +3 binding site. In all cases, there is uncertainty that the ITC values exactly represent the computational ligand binding configuration. That is not to say that either is incorrect. Rather, the ITC values more likely represent a mean of ligand

binding conformations, while computational results examine a single, catalytically active conformation. Thus, for the purposes of examining roles of aromatic residues in the chitinase active sites, we primarily consider the computational relative binding free energy results, as we can control both the position of the ligand across the active site as well as assure the Michaelis complex is fully formed at the start of the thermodynamic assessment.

ChiA Aromatic Residues

Aromatic residues Trp-167 and Trp-275 of ChiA appear to play significant roles in ligand stabilization and tight binding. The change in binding free energy associated with mutating these tryptophans to alanines is very unfavorable, significantly reducing the ability of the ligand to bind somewhat rigidly in the cleft (Table 3). This is illustrated dynamically in both the enhanced flexibility of the ChiA W167A and W275A active sites and the flexibility of the $(GlcNAc)_6$ ligands across the cleft (Figures 3A and 3C). Trp-167 is largely responsible for maintaining the shape of the substrate-side of the ChiA cleft. The $(GlcNAc)_6$ ligand face opposite Trp-167 is otherwise quite solvent exposed. Replacement of Trp-167 with alanine greatly reduces ligand contact with the protein, and the normally strained ligand relaxes into the newly opened protein space to maintain protein interactions. In doing so, the ligand has a significantly greater degree of freedom, seen in the level to which the ligand fluctuates across the entire W167A active site in comparison to wild-type (Figure 3C). Interestingly, W167A is known to induce transglycosylation in ChiA in lieu of hydrolysis.[47,62.] The added flexibility and reduced affinity driving hydrolysis likely enables transglycosylation.

Trp-275 and Phe-396 are the only two aromatic residues in the product side of the ChiA binding cleft with the ability to form stacking interaction with $(GlcNAc)_6$. The significant reduction in affinity by mutation to alanine indicates the binding platform created by the bulk of the Trp-275 hydrophobic side chain plays an important role in ligand binding.

As with W167A, removal of Trp-275 destabilized the ligand across the length of the active site. The catalytic residues fluctuate significantly, indicating $(GlcNAc)_6$ is no longer productively bound. In addition to overall ligand stability, Trp-275 occupies an important position in the +1 product binding site. The large change in affinity and destabilization of the ligand implicates Trp-275 in product stability. After hydrolysis of the ligand, we hypothesize that the favorability of Trp-275 for the dimeric product may even contribute to inhibition. ChiA is moderately inhibited by its products,[63] and mutation of Trp-275 to a slightly less favorable aromatic, such as phenylalanine, might alleviate inhibition, while maintaining overall ligand binding affinity.

The product side phenylalanine, Phe-396, appears to have little or no role in ligand binding. Both experimental and computational estimates of change in binding free energy associated with mutating Phe-396 to alanine indicate the residue does not tight bind with the ligand. Further, the mutation has relatively little effect on the dynamics of either the protein or the ligand (Figures 3A and 3C). Despite what appears to hydrophobic stacking interaction observed in the crystal structure (Figure 1), Phe-396 can be removed from the active site with apparently little consequence. This is consistent with the slight reduction of processivity determined by Zakariassen et al. [6] Moreover, replacement of Phe-396 with a hydrogen-bonding residue, perhaps tyrosine, would increase binding affinity and possibly processivity.[64] Of course, this increase in affinity in the product subsite would have to be balance against the adverse effect of enhancing product inhibition.

ChiB Aromatic Residues

At first glance, each of the ChiB aromatic residues investigated here, Trp-97, Trp-220, and Phe-190, appear responsible for formation of the hydrophobic stacking platform enabling the sliding processive motion. Structurally, the large side chains nicely overlap

with the +1, +2, and +3 substrate-side pyranose rings.[13] However, relative binding free energies upon mutation to alanine and dynamics tell a different story. Notably, that only Trp-97 and Trp-220 are key to tight binding. These two residues are closer to the catalytic center, at the +1 and +2 binding sites, respectively, and mutation to alanine reduces ligand affinity by nearly 3 kcal/mol (Table 3). In contrast with aromatic mutations in ChiA, the ChiB W97A and W220A variants result in localized ligand destabilization, primarily affecting the stability of the ligand in the +2 and +3 substrate binding sites (Figure 3D). Interestingly, though the W97A and W220A ligands are as stable as the wild-type ChiB ligand, the catalytic residues fluctuate more than wild-type (Figure 3B). This finding corresponds with our prior hypothesis that increased flexibility of the catalytic residues corresponds with a decreased ability to processively hydrolyze crystalline substrates.[14] Horn et al. previously investigated the impact of the W97A and W220A mutation on processive ability, finding that indeed processivity is reduced on crystalline β-chitin.[5] These variants remain capable of hydrolysis on soluble chitosan substrates and reportedly do so with enhanced processive turnover relative to wild-type on crystalline substrates. The roles of these two residues is then to tightly bind with the substrate, enabling the enzyme to maintain it association with crystalline substrate throughout processive action. This is in line with general hypotheses for GH action suggesting that increased binding affinity correlates with increased processivity,[64] and furthermore, that substrate-side tight binding may have the highest impact on processive ability.[29]

Despite what appears to be an important stacking interaction, according to structural studies, Phe-190 seems to play a minor role in ligand binding. Both experimental and computational measures of the binding free energy change associated with mutating Phe-190 to alanine are low (Table 3), indicating that the much smaller alanine side chain maintains approximately the same degree affinity. Despite the relatively low affinity change,

the F190A mutation in ChiB has a profound localized effect on ligand dynamics. The ligand in the +2 and +3 binding site fluctuates a great deal more that the wild-type ligand (Figure 3D), and the catalytic residues appear to be affected by the distal mutation as well (Figure 3C).

To investigate why the F190A variant exhibits an increased degree of freedom without an apparent effect on binding affinity, we examined the local dynamics of Phe-190 and Trp-220 relative to the +3 pyranose ring. The removal of Phe-190 in the ChiB cleft enhances the interactions between Trp-220 and the +3 sugar (Figure 4). In wild-type ChiB, Phe-190 and Trp-220 are on the opposite sides of the cleft, sandwiching the ligand through carbohydrate/π-stacking interactions. This affords the ligand stability in the ChiB cleft. Removal of Phe-190 initiates a local shift of the +3 sugar towards Trp-220, as the stacking interaction with Phe-190 is abolished and +3 subsite interaction with Trp-220 is maintained. This is quantitatively illustrated with the distance between the Trp-220 and Phe-190 (or Ala-190) α carbons and the +3 pyranose ring atoms (Figure 4). In wild-type ChiB, the α carbon of Phe-190 is generally situated within 4 Å of the +3 pyranose. On the opposite side of the cleft, one binding site removed, Trp-220 maintains a steady 8-Å distance from the sugar. When Phe-190 is mutated to alanine, the ligand wildly fluctuates in the +3 binding site, but the proximity of the +3 sugar to Trp-220 is significantly increased. This effect is not entirely surprising given the reduced volumetric constraints imposed by the alanine residue with respect to the larger phenylalanine side chain. Nevertheless, one would think this would be manifested in the binding affinity. Based on these observations, we suggest Phe-190 plays a role in substrate recruitment; though at sufficient substrate concentrations, this residue's function could be deemed unnecessary. Along those lines, Katouno et al. observed that mutation of Phe-190 has little impact on processive chitin hydrolysis.[65] Though, the substrate concentration in this study was quite high at 1 mg chitin per 750 μL of reaction

mixture. Thus, the reduced ability to recruit substrate to the active site upon mutation to alanine could go undetected.

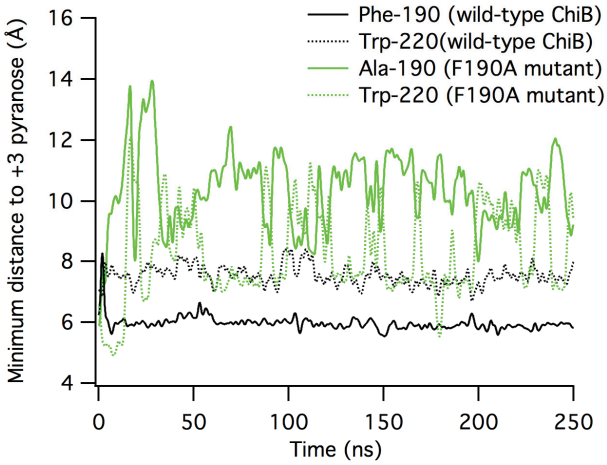

Figure 4. Minimum distance between the backbone α carbon of ChiB residues to the +3 pyranose over 250-ns MD simulations. The distance between wild-type residues Phe-190 and Trp-220 to the +3 pyranose is shown as black firm and dash lines, respectively. The distance between F190A variant residues Ala-190 and Trp-220 and the +3 pyranose is shown as green firm and dash lines, respectively.

Phe-190 is not strictly conserved among homologous chitinases, supporting the suggestion that ChiB has not developed a function requiring a bulky, hydrophobic residue in this position. From a multiple sequence alignment of 20 family 18 chitinases (Table S2), we determined only six enzymes exhibit a phenylalanine in this location. More frequently, polar and charged residues (Asn, Arg, and Thr) appear at this site. This lack of conservation of an aromatic residue at the center of a carbohydrate active enzyme domain is quite surprising, given the abundance and relative utility of this class of amino acids in carbohydrate binding. Comparatively, Trp-97 and Trp-220 are strictly conserved, appearing as Trp in each of the 20 enzymes. This conservation is illustrated in Figure 5, where much of the ChiB core is

well conserved, and Phe-190 appears as a variable outlier. Portions of the multiple sequence alignment are provided in the Supporting Information.

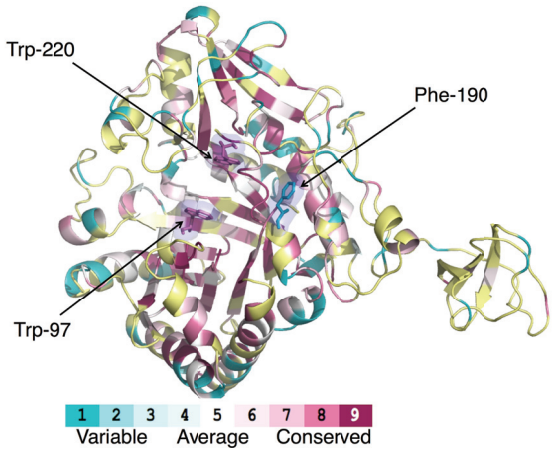

Figure 5. Cartoon illustration of the ChiB three-dimensional structure colored by sequence conservation. The most highly conserved residues are colored in increasingly darker shades of magenta. Residues with significant flexibility in chemical nature are colored in increasing darker shades of turquoise. Yellow regions indicate insufficient data is available to accurately predict conservation. The aromatic residues of the ChiB active site cleft are shown in stick. Trp-220 and Trp-97 are well conserved aromatic residues, while Phe-190 is quite variable. The sequences used to generate the multiple sequence alignment are provided in the Supporting Information (Table S2). The multiple sequence alignment was generated with Clustal Omega.[66,67,68] The conservation analysis was obtained using the ConSurf Server,[69,70] and PyMOL was used to render the structure.[71]

Trends Across Glycoside Hydrolase Families

In this study, we find the residues at the entrance and exits of the ChiA and ChiB clefts have the least direct involvement in ligand binding and binding affinity, where the ChiA F396A variant and ChiB F190A variant minimally impact affinity and dynamics. A prior study of the *T. reesei* cellobiohydrolase Cel6A active site suggests the opposite is true,

where, counterintuitively, aromatic residues closer to the −1 binding site had lower binding affinity compared to tunnel entrance and exit residues.[31] Considering ChiB and *T. reesei* Cel6A are both non-reducing end-specific processive GHs, one might expect that the substrate entrance residues would exhibit similar functional roles. However, Trp-272 of *T. reesei* Cel6A, which sits at the very entrance of the cellulase tunnel, clearly plays a role in crystalline substrate acquisition, such that mutation to alanine negates activity on insoluble cellulosic substrates.

A tight binding aromatic residue in the product binding site immediately following the cleavage location appears generally indicative of product inhibition in GHs. The relative binding free energies of ChiA W275A (+1 binding site) and *T. reesei* cellobiohydrolase Cel7A W367A (+1 binding site), both reducing end-specific processive GHs, are approximately equal, where the *T. reesei* Cel7A W376A variant affinity was reduced by 3.6 ± 0.4 kcal/mol.[32] Taylor et al. also reported unfavorable relative binding energy resulting from mutation of Trp-329 to alanine in the +1 product binding site of *T. reesei* Cel7B.[32] All three of these enzymes exhibit some degree of product inhibition that could likely be alleviated through mutation of this aromatic residue.[63,72] Selection of the replacement would need to provide a similar degree of steric hindrance, as the proximity of this tryptophan to the −1 pyranose is likely to affect formation of the distorted ring conformation necessary for hydrolysis.

Comparison of the secondary product binding sites of several GHs does not immediately reveal a trend. The relative free energy of binding associated with mutation of Phe-396 indicatess this aromatic residue does not tightly bind and has no role in product stability, as one would expect. Alternatively, mutation of Trp-135 in *T. reesei* Cel6A, near the −2 product binding site, results in a remarkably large, unfavorable change in binding affinity, 9.4 ± 0.4 kcal/mole, where this residue plays a critical role in product stabilization

and inhibition.[31] We suspect that the minimal affinity Phe-396 affords $(GlcNAc)_6$ binding may partially justify observations of higher processive velocity relative to ChiB.[29] Aronson et al. previously reported that Phe-396 significantly interacts with the ligand at the +2 site and mutation of Phe-396 initiates the local shifting of the entire ligand towards the non-reducing end to make up for lost interactions.[43] We do not observe this phenomenon throughout our simulations. We suggest the phenomenon observed by Aronson et al. is a direct result of the use of pentameric GlcNAc substrate and the strong affinity of Trp-167 for the ligand. In fact, Trp-167 is likely the driving force between the split ligand occupancy between the −4 to +2 sites and the −3 to +3 sites.

Finally, binding free energy alone is not sufficient to describe aromatic residue function. A great example of this is the residues at the catalytic center if *T. reesei* Cel6A, Trp-269 and Trp-376.[31] Each of these residues had relatively little impact on ligand binding affinity upon mutation; though, their mutation is detrimental to hydrolytic function.[73] Further, MD simulation reveals the roles of these residues as physically maintaining the -1 ring distortion through bulkiness. Similarily, the endoglucanase *T. reesei* Cel7B exhibits similar magnitude changes to binding free energy as a result of aromatic residue mutation in comparison to *T. reesei* Cel7A, though Cel7B has an wide, solvent exposed binding cleft.[32] Thus, generalization of aromatic residue function from free energy alone only partially tells the story of a given residue. MD simulation coupled with free energy calculations or measurements and activity measurements enables the description of additional factors to define the roles of aromatic residues. With these approaches, we capture dominant effects including: hydrophobic stacking interactions; active site architecture, such as the availability of long, asymmetric substrate binding sites and the flexibility of tunnel forming loops; and variations in substrate conformation.[29,74] Further detailed evaluations of GH active sites, such as in this study, will provide the necessary information to catalogue variations in

behavior, enabling generalization of function in GH active sites.

6. Conclusions

Using experimental binding free energy techniques alongside MD simulations and calculated binding free energies, we have explored aromatic-mediated carbohydrate interactions in Family 18 *S. marcescens* processive chitinases ChiA and ChiB, aiming to ascribe explicit roles to each of the aromatic residues directly interacting with a bound $(GlcNAc)_6$ ligand. We find that ChiA aromatic residues Trp-167 and Trp-275 contribute greatly to ligand binding and stability of the active site by virtue of their location near the catalytic center. The ChiA residue at the exterior product-binding site, Phe-396, appears to have little to no role in ligand binding, and replacement by a tighter binding residue may facilitate enhanced processive ability. ChiB residues near the catalytic center, Trp-97 and Trp-220, play critical roles in stabilizing ligand binding, while Phe-190, at the substrate entrance, plays a minimal role, likely in substrate acquisition at low concentrations. Generally, the presence of an aromatic residue in the product binding site immediately following the hydrolytic cleavage site appears to be associated with product inhibition in GHs. Otherwise, generalization across GH families is difficult, with the relatively limited data explicitly describing aromatic residue function. Similar studies across a variety of GH families would enable generalization of aromatic residue function. With the abundance of the carbohydrate active enzymes across all kingdoms of life, such a generalization greatly benefits a broad variety of scientific fields.

.

References

1. Himmel, M. E.; Ding, S. Y.; Johnson, D. K.; Adney, W. S.; Nimlos, M. R.; Brady, J. W.; Foust, T. D., Biomass recalcitrance: engineering plants and enzymes for biofuels production. *Science* **2007,** *315* (5813), 804-7.

2. Payne, C. M.; Knott, B. C.; Mayes, H. B.; Hansson, H.; Himmel, M. E.; Sandgren, M.; Stahlberg, J.; Beckham, G. T., Fungal Cellulases. *Chem. Rev.* **2015,** *115* (3), 1308-1448.

3. Stern, R.; Jedrzejas, M. J., Carbohydrate Polymers at the Center of Life's Origins: The Importance of Molecular Processivity. *Chem. Rev.* **2008,** *108* (12), 5061-5085.

4. Divne, C.; Stahlberg, J.; Reinikainen, T.; Ruohonen, L.; Pettersson, G.; Knowles, J. K. C.; Teeri, T. T.; Jones, T. A., The 3-Dimensional Crystal-Structure of the Catalytic Core of Cellobiohydrolase-I from *Trichoderma reesei*. *Science* **1994,** *265* (5171), 524-528.

5. Horn, S. J.; Sikorski, P.; Cederkvist, J. B.; Vaaje-Kolstad, G.; Sorlie, M.; Synstad, B.; Vriend, G.; Varum, K. M.; Eijsink, V. G. H., Costs and Benefits of Processivity in Enzymatic Degradation of Recalcitrant Polysaccharides. *Proc. Natl. Acad. Sci. U. S. A.* **2006,** *103* (48), 18089-18094.

6. Zakariassen, H.; Aam, B. B.; Horn, S. J.; Varum, K. M.; Sorlie, M.; Eijsink, V. G. H., Aromatic Residues in the Catalytic Center of Chitinase A from *Serratia marcescens* Affect Processivity, Enzyme Activity, and Biomass Converting Efficiency. *J. Biol. Chem.* **2009,** *284* (16), 10610-10617.

7. Levine, S. E.; Fox, J. M.; Blanch, H. W.; Clark, D. S., A Mechanistic Model of the Enzymatic Hydrolysis of Cellulose. *Biotechnol. Bioeng.* **2010,** *107* (1), 37-51.

8. Beckham, G. T.; Bomble, Y. J.; Bayer, E. A.; Himmel, M. E.; Crowley, M. F., Applications of Computational Science for Understanding Enzymatic Deconstruction of Cellulose. *Curr. Opin. Biotechnol.* **2011,** *22* (2), 231-238.

9. Davies, G.; Henrissat, B., Structures and mechanisms of glycosyl hydrolases. *Structure* **1995,** *3* (9), 853-9.

10. Zou, J. Y.; Kleywegt, G. J.; Stahlberg, J.; Driguez, H.; Nerinckx, W.; Claeyssens, M.; Koivula, A.; Teerii, T. T.; Jones, T. A., Crystallographic Evidence for Substrate Ring Distortion and Protein Conformational Changes During Catalysis in Cellobiohydrolase Cel6A from *Trichoderma reesei*. *Structure Fold. Des.* **1999,** *7* (9), 1035-1045.

11. Spezio, M.; Wilson, D. B.; Karplus, P. A., Crystal-Structure of the Catalytic Domain of a *Thermophilic endocellulase*. *Biochemistry* **1993,** *32* (38), 9906-9916.

12. Papanikolau, Y.; Prag, G.; Tavlas, G.; Vorgias, C. E.; Oppenheim, A. B.; Petratos, K., High resolution structural analyses of mutant chitinase A complexes with substrates provide new insight into the mechanism of catalysis. *Biochemistry* **2001,** *40* (38), 11338-43.

13. van Aalten, D. M. F.; Komander, D.; Synstad, B.; Gaseidnes, S.; Peter, M. G.; Eijsink, V. G. H., Structural Insights into the Catalytic Mechanism of a Family 18 Exo-Chitinase. *Proc. Natl. Acad. Sci. U. S. A.* **2001,** *98* (16), 8979-8984.

14. Payne, C. M.; Baban, J.; Horn, S. J.; Backe, P. H.; Arvai, A. S.; Dalhus, B.; Bjoras, M.; Eijsink, V. G. H.; Sorlie, M.; Beckham, G. T.; Vaaje-Kolstad, G., Hallmarks of Processivity in Glycoside Hydrolases from Crystallographic and Computational Studies of the *Serratia marcescens* Chitinases. *J. Biol. Chem.* **2012,** *287* (43), 36322-36330.

15. Davies, G. J.; Brzozowski, A. M.; Dauter, M.; Varrot, A.; Schulein, M., Structure and Function of *Humicola insolens* Family 6 Cellulases: Structure of the Endoglucanase, Cel6B, at 1.6 Å Resolution. *Biochem. J.* **2000,** *348*, 201-207.

16. von Ossowski, I.; Stahlberg, J.; Koivula, A.; Piens, K.; Becker, D.; Boer, H.; Harle, R.; Harris, M.; Divne, C.; Mahdi, S.; Zhao, Y. X.; Driguez, H.; Claeyssens, M.; Sinnott, M. L.; Teeri, T. T., Engineering the Exo-Loop of *Trichoderma reesei* Cellobiohydrolase, Cel7A. A Comparison with *Phanerochaete chrysosporium* Cel7D. *J. Mol. Biol.* **2003,** *333* (4), 817-829.

17. Li, Y. C.; Irwin, D. C.; Wilson, D. B., Processivity, Substrate Binding, and Mechanism of Cellulose Hydrolysis by *Thermobifida fusca* Cel9A. *Appl. Environ. Microbiol.* **2007,** *73* (10), 3165-3172.

18. Asensio, J. L.; Arda, A.; Canada, F. J.; Jimenez-Barbero, J., Carbohydrate-Aromatic Interactions. *Acc. Chem. Res.* **2013,** *46* (4), 946-954.

19. McGaughey, G. B.; Gagne, M.; Rappe, A. K., π-Stacking Interactions - Alive and Well in Proteins. *J. Biol. Chem.* **1998,** *273* (25), 15458-15463.

20. Santana, A. G.; Jimenez-Moreno, E.; Gomez, A. M.; Corzana, F.; Gonzalez, C.; Jimenez-Oses, G.; Jimenez-Barbero, J.; Asensio, J. L., A Dynamic Combinatorial Approach for the Analysis of Weak Carbohydrate/Aromatic Complexes: Dissecting Facial Selectivity in CH/π Stacking Interactions. *J. Am. Chem. Soc.* **2013,** *135* (9), 3347-3350.

21. Ramirez-Gualito, K.; Alonso-Rios, R.; Quiroz-Garcia, B.; Rojas-Aguilar, A.; Diaz, D.; Jimenez-Barbero, J.; Cuevas, G., Enthalpic Nature of the CH/π Interaction Involved in the Recognition of Carbohydrates by Aromatic Compounds, Confirmed by a Novel

Interplay of NMR, Calorimetry, and Theoretical Calculations. *J. Am. Chem. Soc.* **2009,** *131* (50), 18129-18138.

22. Pace, C. J.; Kim, D.; Gao, J. M., Experimental Evaluation of CH-π Interactions in a Protein Core. *Chemistry-a European Journal* **2012,** *18* (19), 5832-5836.

23. Wimmerova, M.; Kozmon, S.; Necasova, I.; Mishra, S. K.; Komarek, J.; Koca, J., Stacking Interactions between Carbohydrate and Protein Quantified by Combination of Theoretical and Experimental Methods. *PLoS One* **2012,** *7* (10).

24. Kiehna, S. E.; Laughrey, Z. R.; Waters, M. L., Evaluation of a Carbohydrate-π Interaction in a Peptide Model System. *Chem. Commun.* **2007,** (39), 4026-4028.

25. Vaaje-Kolstad, G.; Horn, S. J.; Sorlie, M.; Eijsink, V. G., The Chitinolytic Machinery of *Serratia marcescens* - A Model System for Enzymatic Degradation of Recalcitrant Polysaccharides. *FEBS J.* **2013,** *280* (13), 3028-3049.

26. Horn, S. J.; Sorbotten, A.; Synstad, B.; Sikorski, P.; Sorlie, M.; Varum, K. M.; Eijsink, V. G. H., Endo/Exo Mechanism and Processivity of Family 18 Chitinases Produced by *Serratia marcescens*. *FEBS J.* **2006,** *273* (3), 491-503.

27. Horn, S. J.; Sorlie, M.; Vaaje-Kolstad, G.; Norberg, A. L.; Synstad, B.; Varum, K. M.; Eijsink, V. G. H., Comparative Studies of Chitinases A, B and C from *Serratia marcescens*. *Biocatal. Biotransform.* **2006,** *24* (1-2), 39-53.

28. Hult, E. L.; Katouno, F.; Uchiyama, T.; Watanabe, T.; Sugiyama, J., Molecular Directionality in Crystalline β-Chitin: Hydrolysis by Chitinases A and B from *Serratia marcescens* 2170. *Biochem. J.* **2005,** *388* (Pt 3), 851-856.

29. Igarashi, K.; Uchihashi, T.; Uchiyama, T.; Sugimoto, H.; Wada, M.; Suzuki, K.; Sakuda, S.; Ando, T.; Watanabe, T.; Samejima, M., Two-Way Traffic of Glycoside Hydrolase Family 18 Processive Chitinases on Crystalline Chitin. *Nat. Commun.* **2014,** *5*, 3975.

30. Uchiyama, T.; Katouno, F.; Nikaidou, N.; Nonaka, T.; Sugiyama, J.; Watanabe, T., Roles of the Exposed Aromatic Residues in Crystalline Chitin Hydrolysis by Chitinase A from *Serratia marcescens* 2170. *J. Biol. Chem.* **2001,** *276* (44), 41343-41349.

31. Payne, C. M.; Bomble, Y.; Taylor, C. B.; McCabe, C.; Himmel, M. E.; Crowley, M. F.; Beckham, G. T., Multiple Functions of Aromatic-Carbohydrate Interactions in a Processive Cellulase Examined with Molecular Simulation. *J. Biol. Chem.* **2011,** *286* (47), 41028-41035.

32. Taylor, C. B.; Payne, C. M.; Himmel, M. E.; Crowley, M. F.; McCabe, C.; Beckham, G. T., Binding Site Dynamics and Aromatic-Carbohydrate Interactions in Processive and Non-Processive Family 7 Glycoside Hydrolases. *J. Phys. Chem. B* **2013,** *117* (17), 4924-4933.

33. Hamre, A. G.; Lorentzen, S. B.; Valjamae, P.; Sorlie, M., Enzyme Processivity Changes with the Extent of Recalcitrant Polysaccharide Degradation. *FEBS Lett.* **2014,** *588* (24), 4620-4624.

34. Wang, W. Y.; Malcolm, B. A., Two-Stage PCR Protocol Allowing Introduction of Multiple Mutations, Deletions and Insertions Using QuikChange (TM) Site-Directed Mutagenesis. *BioTechniques* **1999,** *26* (4), 680-682.

35. Dybvik, A. I.; Norberg, A. L.; Schute, V.; Soltwisch, J.; Peter-Katalinic, J.; Varum, K. M.; Eijsink, V. G. H.; Dreisewerd, K.; Mormann, M.; Sorlie, M., Analysis of Noncovalent Chitinase-Chito-Oligosaccharide Complexes by Infrared-Matrix Assisted Laser Desorption Ionization and Nanoelectrospray Ionization Mass Spectrometry. *Anal. Chem.* **2011,** *83* (11), 4030-4036.

36. Norberg, A. L.; Karlsen, V.; Hoell, I. A.; Bakke, I.; Eijsink, V. G. H.; Sorlie, M., Determination of Substrate Binding Energies in Individual Subsites of a Family 18 Chitinase. *FEBS Lett.* **2010,** *584* (22), 4581-4585.

37. Synstad, B.; Gaseidnes, S.; van Aalten, D. M. F.; Vriend, G.; Nielsen, J. E.; Eijsink, V. G. H., Mutational and Computational Analysis of the Role of Conserved Residues in the Active Site of a Family 18 Chitinase. *Eur. J. Biochem.* **2004,** *271* (2), 253-262.

38. Wiseman, T.; Williston, S.; Brandts, J. F.; Lin, L. N., Rapid Measurement of Binding Constants and Heats of Binding Using a New Titration Calorimeter. *Anal. Biochem.* **1989,** *179* (1), 131-137.

39. Fukada, H.; Takahashi, K., Enthalpy and heat capacity changes for the proton dissociation of various buffer components in 0.1 M potassium chloride. *Proteins* **1998,** *33* (2), 159-66.

40. Turnbull, W. B.; Daranas, A. H., On the Value of C: Can Low Affinity Systems be Studied by Isothermal Titration Calorimetry? *J. Am. Chem. Soc.* **2003,** *125* (48), 14859-14866.

41. Zakariassen, H.; Sorlie, M., Heat Capacity Changes in Heme Protein-Ligand Interactions. *Thermochim. Acta* **2007,** *464* (1-2), 24-28.

42. Vaaje-Kolstad, G.; Houston, D. R.; Rao, F. V.; Peter, M. G.; Synstad, B.; van Aalten, D. M. F.; Eijsink, V. G. H., Structure of the D142N Mutant of the Family 18 Chitinase ChiB from *Serratia marcescens* and its Complex with Allosamidin. *Biochimica Et Biophysica Acta-Proteins and Proteomics* **2004,** *1696* (1), 103-111.

43. Aronson, N. N.; Halloran, B. A.; Alexyev, M. F.; Amable, L.; Madura, J. D.; Pasupulati, L.; Worth, C.; Van Roey, P., Family 18 Chitinase-Oligosaccharide Substrate Interaction: Subsite Preference and Anomer Selectivity of *Serratia marcescens* Chitinase A. *Biochem. J.* **2003,** *376*, 87-95.

44. van Aalten, D. M. F.; Synstad, B.; Brurberg, M. B.; Hough, E.; Riise, B. W.; Eijsink, V. G. H.; Wierenga, R. K., Structure of a Two-Domain Chitotriosidase From *Serratia marcescens* at 1.9-Å Resolution. *Proceedings of the National Academy of Sciences* **2000,** *97* (11), 5842-5847.

45. Brameld, K. A.; Goddard, W. A., Substrate Distortion to a Boat Conformation at Subsite-1 is Critical in the Mechanism of Family 18 Chitinases. *J. Am. Chem. Soc.* **1998,** *120* (15), 3571-3580.

46. Tews, I.; vanScheltinga, A. C. T.; Perrakis, A.; Wilson, K. S.; Dijkstra, B. W., Substrate-Assisted Catalysis Unifies Two Families of Chitinolytic Enzymes. *J. Am. Chem. Soc.* **1997,** *119* (34), 7954-7959.

47. Aronson, N. N.; Halloran, B. A.; Alexeyev, M. F.; Zhou, X. E.; Wang, Y. J.; Meehan, E. J.; Chen, L. Q., Mutation of a Conserved Tryptophan in the Chitin-Binding Cleft of *Serratia marcescens* Chitinase A Enhances Transglycosylation. *Biosci. Biotechnol. Biochem.* **2006,** *70* (1), 243-251.

48. Brooks, B. R.; Brooks, C. L.; Mackerell, A. D.; Nilsson, L.; Petrella, R. J.; Roux, B.; Won, Y.; Archontis, G.; Bartels, C.; Boresch, S.; Caflisch, A.; Caves, L.; Cui, Q.; Dinner, A. R.; Feig, M.; Fischer, S.; Gao, J.; Hodoscek, M.; Im, W.; Kuczera, K.; Lazaridis, T.; Ma, J.; Ovchinnikov, V.; Paci, E.; Pastor, R. W.; Post, C. B.; Pu, J. Z.; Schaefer, M.; Tidor, B.; Venable, R. M.; Woodcock, H. L.; Wu, X.; Yang, W.; York, D. M.; Karplus, M., CHARMM: The Biomolecular Simulation Program. *J. Comput. Chem.* **2009,** *30* (10), 1545-1614.

49. Phillips, J. C.; Braun, R.; Wang, W.; Gumbart, J.; Tajkhorshid, E.; Villa, E.; Chipot, C.; Skeel, R. D.; Kale, L.; Schulten, K., Scalable Molecular Dynamics with NAMD. *J. Comput. Chem.* **2005,** *26* (16), 1781-1802.

50. MacKerell, A. D.; Bashford, D.; Bellott, M.; Dunbrack, R. L.; Evanseck, J. D.; Field, M. J.; Fischer, S.; Gao, J.; Guo, H.; Ha, S.; Joseph-McCarthy, D.; Kuchnir, L.; Kuczera, K.; Lau, F. T. K.; Mattos, C.; Michnick, S.; Ngo, T.; Nguyen, D. T.; Prodhom, B.; Reiher, W. E.; Roux, B.; Schlenkrich, M.; Smith, J. C.; Stote, R.; Straub, J.; Watanabe, M.; Wiorkiewicz-Kuczera, J.; Yin, D.; Karplus, M., All-Atom Empirical Potential for Molecular Modeling and Dynamics Studies of Proteins. *J. Phys. Chem. B* **1998,** *102* (18), 3586-3616.

51. Mackerell, A. D.; Feig, M.; Brooks, C. L., Extending the Treatment of Backbone Energetics in Protein Force Fields: Limitations of Gas-Phase Quantum Mechanics in Reproducing Protein Conformational Distributions in Molecular Dynamics Simulations. *J. Comput. Chem.* **2004,** *25* (11), 1400-1415.

52. Durell, S. R.; Brooks, B. R.; Bennaim, A., Solvent-Induced Forces between 2 Hydrophilic Groups. *J. Phys. Chem.* **1994,** *98* (8), 2198-2202.

53. Jorgensen, W. L.; Chandrasekhar, J.; Madura, J. D.; Impey, R. W.; Klein, M. L., Comparison of Simple Potential Functions for Simulating Liquid Water. *J. Chem. Phys.* **1983,** *79* (2), 926-935.

54. Humphrey, W.; Dalke, A.; Schulten, K., VMD: Visual Molecular Dynamics. *J. Mol. Graph. Model.* **1996,** *14* (1), 33-38.

55. Kirkwood, J. G., Statistical Mechanics of Fluid Mixtures. *J. Chem. Phys.* **1935,** *3* (5), 300-313.

56. Frenkel, D., and Smit, B., *Understanding Molecular Simulations: From Algorithms to Applications*. 2nd ed.; Academic Press: 2002.

57. Straatsma, T. P.; Mccammon, J. A., Multiconfiguration Thermodynamic Integration. *J. Chem. Phys.* **1991,** *95* (2), 1175-1188.

58. Pohorille, A.; Jarzynski, C.; Chipot, C., Good Practices in Free-Energy Calculations. *J. Phys. Chem. B* **2010,** *114* (32), 10235-10253.

59. Steinbrecher, T.; Mobley, D. L.; Case, D. A., Nonlinear Scaling Schemes for Lennard-Jones Interactions in Free Energy Calculations. *J. Chem. Phys.* **2007,** *127* (21).

60. Biarnes, X.; Ardevol, A.; Planas, A.; Rovira, C.; Laio, A.; Parrinello, M., The Conformational Free Energy Landscape of β-D-Glucopyranose. Implications for Substrate Preactivation in β-Glucoside Hydrolases. *J. Am. Chem. Soc.* **2007,** *129* (35), 10686-10693.

61. Norberg, A. L.; Dybvik, A. I.; Zakariassen, H.; Mormann, M.; Peter-Katalinic, J.; Eijsink, V. G. H.; Sorlie, M., Substrate Positioning in Chitinase A, A Processive Chito-Biohydrolase from *Serratia marcescens*. *FEBS Lett.* **2011,** *585* (14), 2339-2344.

62. Zakariassen, H.; Hansen, M. C.; Joranli, M.; Eijsink, V. G. H.; Sorlie, M., Mutational Effects on Transglycosylating Activity of Family 18 Chitinases and Construction of a Hypertransglycosylating Mutant. *Biochemistry* **2011,** *50* (25), 5693-5703.

63. Kuusk, S.; Sorlie, M.; Valjamae, P., The Predominant Molecular State of Bound Enzyme Determines the Strength and Type of Product Inhibition in the Hydrolysis of Recalcitrant Polysaccharides by Processive Enzymes. *J. Biol. Chem.* **2015**.

64. Payne, C. M.; Jiang, W.; Shirts, M. R.; Himmel, M. E.; Crowley, M. F.; Beckham, G. T., Glycoside Hydrolase Processivity Is Directly Related to Oligosaccharide Binding Free Energy. *J. Am. Chem. Soc.* **2013,** *135* (50), 18831-18839.

65. Katouno, F.; Taguchi, M.; Sakurai, K.; Uchiyama, T.; Nikaidou, N.; Nonaka, T.; Sugiyama, J.; Watanabe, T., Importance of Exposed Aromatic Residues in Chitinase B from *Serratia marcescens* 2170 for Crystalline Chitin Hydrolysis. *J. Biochem. (Tokyo)* **2004,** *136* (2), 163-168.

66. Sievers, F.; Wilm, A.; Dineen, D.; Gibson, T. J.; Karplus, K.; Li, W. Z.; Lopez, R.; McWilliam, H.; Remmert, M.; Soding, J.; Thompson, J. D.; Higgins, D. G., Fast, Scalable Generation of High-Quality Protein Multiple Sequence Alignments Using Clustal Omega. *Mol. Syst. Biol.* **2011,** *7*, 539.

67. Goujon, M.; McWilliam, H.; Li, W. Z.; Valentin, F.; Squizzato, S.; Paern, J.; Lopez, R., A New Bioinformatics Analysis Tools Framework at EMBL-EBI. *Nucleic Acids Res.* **2010,** *38*, W695-W699.

68. McWilliam, H.; Li, W. Z.; Uludag, M.; Squizzato, S.; Park, Y. M.; Buso, N.; Cowley, A. P.; Lopez, R., Analysis Tool Web Services from the EMBL-EBI. *Nucleic Acids Res.* **2013,** *41* (W1), W597-W600.

69. Celniker, G.; Nimrod, G.; Ashkenazy, H.; Glaser, F.; Martz, E.; Mayrose, I.; Pupko, T.; Ben-Tal, N., ConSurf: Using Evolutionary Data to Raise Testable Hypotheses about Protein Function. *Isr. J. Chem.* **2013,** *53* (3-4), 199-206.

70. Ashkenazy, H.; Erez, E.; Martz, E.; Pupko, T.; Ben-Tal, N., ConSurf 2010: Calculating Evolutionary Conservation in Sequence and Structure of Proteins and Nucleic Acids. *Nucleic Acids Res.* **2010,** *38*, W529-W533.

71. Schrödinger, L. *The PyMOL Molecular Graphics System*, 1.5.0.4; 2010.

72. Murphy, L.; Bohlin, C.; Baumann, M. J.; Olsen, S. N.; Sorensen, T. H.; Anderson, L.; Borch, K.; Westh, P., Product Inhibition of Five *Hypocrea jecorina* Cellulases. *Enzyme. Microb. Technol.* **2013,** *52* (3), 163-169.

73. Vuong, T. V.; Wilson, D. B., Processivity, Synergism, and Substrate Specificity of *Thermobifida fusca* Cel6B. *Appl. Environ. Microbiol.* **2009,** *75* (21), 6655-6661.

74. Nakamura, A.; Watanabe, H.; Ishida, T.; Uchihashi, T.; Wada, M.; Ando, T.; Igarashi, K.; Samejima, M., Trade-off between Processivity and Hydrolytic Velocity of Cellobiohydrolases at the Surface of Crystalline Cellulose. *J. Am. Chem. Soc.* **2014,** *136* (12), 4584-4592.

Supporting Information

Aromatic-mediated Carbohydrate Recognition in Processive Serratia marcescens Chitinases

Suvamay Jana,[1,†] Anne Grethe Hamre,[2,†] Patricia Wildberger,[2] Matilde Menkrog Holen,[2] Vincent G. H. Eijsink,[2] Gregg T. Beckham,[3] Morten Sørlie,[2,] and Christina M. Payne[1,*]*

[1]Department of Chemical and Materials Engineering, University of Kentucky, Lexington, KY, USA

[2]Department of Chemistry, Biotechnology, and Food Science, Norwegian University of Life Sciences, Ås, Norway

[3]National Bioenergy Center, National Renewable Energy Laboratory, Golden, CO, USA

[†] These authors contributed equally to this work.

[*] To whom correspondence should be addressed. E-mail: morten.sorlie@nmbu.no; christy.payne@uky.edu

1. Computational Methods

Initial System Preparation

The crystal structures from PDB entries 1EHN and 1OGG were used as input for construction of the ChiA and ChiB models, respectively.[1,2] In total, 10 separate MD simulations were constructed: ChiA and ChiB wild-types with and without a bound $(GlcNAc)_6$ ligand state, and ChiA-W167A, ChiA-W275A, ChiA-F396A, ChiB-W97A, ChiB-W220A, and ChiB-F190A with a bound $(GlcNAc)_6$ ligand state.

The ChiA wild-type simulations were constructed from PDB 1EHN entry by reversing the E315Q mutation. The entire catalytic domain and fused carbohydrate binding module (CBM) ChiA structure was used in these models, as cleaving the from the catalytic domain has been shown to adversely impact the stability of the catalytic domain fold. Aromatic to alanine variants, W167A, W275A, and F396A, were constructed by simply removing the aromatic residue side chain atoms. In the simulations where the $(GlcNAc)_6$ ligand was bound to ChiA, the pyranose rings bound to the -4 through +2 subsites of 1EHN were retained, and the remaining two pyranose rings (in the solvent exposed -5 and -6 sites) were deleted. The ligand-free ChiA models were constructed by removing all the 1EHN pyranose rings from the cleft.

The wild-type ChiB model was constructed from the PDB 1OGG entry by reversing the D142N mutation. Here, we cleaved the CBM from the ChiB catalytic domain for the purposes of modeling. The stability of the catalytic domain in the absence of the attached CBM has been experimentally established (unpublished observations). Again, ChiB variants, W97A, W220A, and F190A, were constructed from wild-type by removing the aromatic side chain atoms. The $(GlcNAc)_6$ ligand bound in the -3 to +3 subsites of the ChiB cleft was modeled from the ligands of two different chitinase structures. The protein backbones of PDBs 1E6N and 1OGG were aligned in PyMOL.[3,4] The pyranose ring in the -

2 through +3 binding sites were retained from the 1E6N structures, while the -3 binding site sugar originated from the 1OGG structure.

In both ChiA and ChiB ligand-bound simulations, the catalytically competent active site conformation was constructed by manually rotating the *N*-acetyl group of the -1 site pyranose ring and the side chains of the catalytic residues (Asp-313 and Glu-315 in ChiA and Asp-142 and Glu-144 in ChiB) in PyMOL to ensure that the catalytic residues and the -1 sugar reflected the distorted Michaelis complex of Family 18 chitinases.[3] The manual rotation of the -1 pyranose and catalytic residues followed additional stepwise minimization (100 steps of steepest descent minimization followed by 100 steps of adopted basis Newton Raphson minimization) to make sure the rotation did not adversely affect stability of the protein and the remaining 5 pyranose rings.

CHARMM was used to build and solvate the wild-type and aromatic variants of ChiA and ChiB.[5] The input protonation states of the systems were determined using H++ at pH 6 and internal and external dielectric constant of 10 and 80, respectively.[6,7,8] The disulfide bonds, between Cys115-Cys120 and Cys195-Cys218 for ChiA, and Cys328-Cys331 for ChiB, were specified based on crystal structure. The constructed systems were solvated with TIP3P water molecules, and sodium counterions were used to make the systems charge neutral. For ChiA, the final system size was approximately 120 Å x 120 Å x 120 Å, totaling roughly 175,000 atoms. The ChiB final system was 80 Å x 80 Å x 80 Å, for a total of approximately 52,000 atoms.

MD Simulations Protocols

The solvated systems were minimized, heated, and equilibrated using CHARMM. The minimization of the systems was conducted in a step-wise manner. First, the water molecules were minimized for 10,000 steps with the protein and ligand (if present) held

rigid. The harmonic restraints on the ligand were then released, and the protein and water molecules were minimized for 10,000 steps. Finally, all restraints were removed, and the entire system was minimized for 10,000 steps. The minimized system was heated from 100 K to 300 K in steps of 4 ps with 50 K increments. The system density was equilibrated in the *NPT* ensemble at 1 atm and 300K with the Nosé-Hoover thermostat and barostat for 100 ps using a 2-fs time step.[9,10] For all MD simulations conducted as part of this study, the CHARMM force field with the CMAP correction was used to describe the protein.[5,11,12] The chitin oligomer was described with the CHARMM C36 carbohydrate force field,[13,14] and water was described with the modified TIP3P model.[15,16]

The equilibrated systems were then simulated for 250 ns in the *NVT* ensemble using NAMD.[17] A 2-fs time step was used in the velocity Verlet integration scheme. The Langevin thermostat was used for temperature control in the 250-ns MD simulations.[18] The SHAKE algorithm was used to fix all hydrogen distances for computational efficiency.[19] Non-bonded interactions used the following cutoffs: a non-bonded cutoff distance of 10 Å, a switching distance of 9 Å, and a non-bonded pair list distance of 12 Å. The Particle Mesh Ewald method was used to calculate the long-range electrostatics.[20] The PME grid spacing was 1 Å, and a 6^{th} order b-spline and Gaussian distribution width of 0.320 Å was used.

Thermodynamic Integration (TI) Protocols

An equilibrated 25-ns snapshot from MD simulations was used as the input coordinates for the TI calculations. We used the dual-topology method with NAMD to determine the relative change in free energy.[21,22,23] The electrostatic and van der Waals calculations were decoupled in separate processes, each of which included 15 λ-windows ranging from λ values of 0 to 1 (total of 30 simulations per mutation). The windows were divided as follows: 0.0, 0.05, 0.1, 0.15, 0.2, 0.3, 0.4, 0.5, 0.6, 0.7, 0.8, 0.85, 0.9, 0.95, 1.0,

using more closely coupled windows near the endpoints to improve accuracy.[24] The electrostatics and van der Waals calculations were equilibrated for 0.5 ns prior to collection of 14.5 ns of TI data. The change in free energy, ΔG, for each set of simulations was determined using Cubic Spline Gaussian Quadrature numerical method to integrate dU/dλ over λ = 0 to 1. Error calculations were performed as described by Steinbrecher et al.[25]

Convergence Analysis

The simulations comprising the TI calculations were evaluated for appropriate window overlap and convergence as described by Pohorille et al. For each van der Waals and electrostatic calculation of each variant evaluated, we plotted histograms of $dU/d\lambda$ for each λ window (Figure S1A). Window overlap was considered sufficient when at least 25% of neighboring windows overlapped. The autocorrelation function (ACF) of each dataset was also determined, as required for error analysis. An example is provided in Figure S1B. The convergence analysis illustrated in Figure S1 for the ChiB F190A system is representative of the trends observed for the thermodynamic data collected in this study.

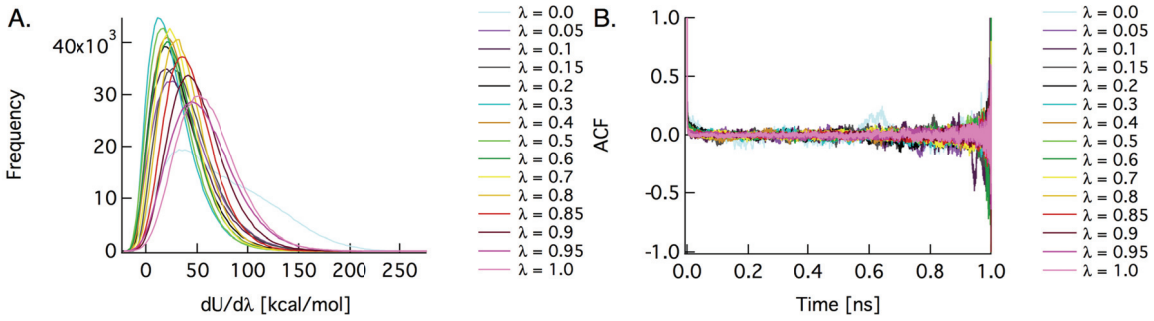

Figure S1: An example of window overlap (A) and autocorrelation function analysis (B). Data are taken from the reactant state during van der Waals calculations from the bound F190A simulation.

2. Additional Results

The individual electrostatic and van der Waals components of the calculated relative ligand binding free energies are provided in Table S1.

Table S1. Detailed ligand binding free energies calculated from TI

ChiA	Energy	Bound		Free	
		Energy (kcal/mol)	Error (kcal/mol)	Energy (kcal/mol)	Error (kcal/mol)
W167A	Electrostatics	9.3	± 0.1	5.7	± 0.0
	VDW	3.5	± 0.4	2.1	± 0.1
	ΔG	12.8	± 0.4	7.8	± 0.1
	ΔΔG (kcal/mol)		5.0 ± 0.4		
W275A	Electrostatics	8.5	± 0.1	5.2	± 0.0
	VDW	2.5	± 0.3	2.2	± 0.1
	ΔG	11.0	± 0.3	7.4	± 0.1
	ΔΔG (kcal/mol)		3.6 ± 0.4		
F396A	Electrostatics	4.3	± 0.0	3.5	± 0.0
	VDW	-2.8	± 0.1	-1.8	± 0.1
	ΔG	1.5	± 0.1	1.7	± 0.1
	ΔΔG (kcal/mol)		-0.2 ± 0.2		
ChiB	Energy	Bound		Free	
		Energy (kcal/mol)	Error (kcal/mol)	Energy (kcal/mol)	Error (kcal/mol)
W97A	Electrostatics	8.4	± 0.1	6.8	± 0.1
	VDW	2.4	± 0.4	1.2	± 0.2
	ΔG	10.8	± 0.4	8.0	± 0.2
	ΔΔG (kcal/mol)		2.8 ± 0.4		
W220A	Electrostatics	9.6	± 0.1	7.8	± 0.0
	VDW	2.9	± 0.3	1.2	± 0.1
	ΔG	12.5	± 0.3	9.0	± 0.1
	ΔΔG (kcal/mol)		3.5 ± 0.4		
F190A	Electrostatics	-8.5	± 0.0	-7.7	± 0.0
	VDW	6.3	± 0.1	5.9	± 0.1
	ΔG	-2.2	± 0.1	-1.8	± 0.1
	ΔΔG (kcal/mol)		-0.4 ± 0.2		

Table S2. Multiple sequence alignment table

ChiB	**GenBank Accession number**	**Trp-97**	**Phe-190**	**Trp-220**
Serratia marcescens	gi|48425130|	W	F	W
Pseudomonas sp.	gi|321173846|	W	F	W
Serratia plymuthica	gi|518650018|	W	F	W
Serratia proteamaculans	gi|157371713|	W	F	W
Serratia liquefaciens	gi|22652066|	W	F	W
Bacillus halodurans	gi|15613479|	W	G	W
Bacillus clausii	gi|56962420|	W	E	W
Kurthia zopfii	gi|927653|	W	T	W
Paenibacillus sanguinis	gi|517582257|	W	A	W
Bacillus toyonensis	gi|557622580|	W	R	W
Bacillus cereus	gi|376264400|	W	R	W
Bacillus weihenstephanensis	gi|163938376|	W	R	W
Bacillus thuringiensis serovar kurstaki	gi|259558661|	W	R	W
Geobacillus stearothermophilus	gi|345548065|	W	R	W
Bacillus circulans	gi|20150306|	W	T	W
Saccharophagus degradans	gi|89953110|	W	F	W
Laceyella putida	gi|573461615|	W	N	W
Laceyella sacchari	gi|550993861|	W	S	W
Desmospora sp.	gi|497397203|	W	N	W
Paenibacillus elgii	gi|498185052|	W	N	W

References

1. Papanikolau, Y.; Prag, G.; Tavlas, G.; Vorgias, C. E.; Oppenheim, A. B.; Petratos, K., High Resolution Structural Analyses of Mutant Chitinase A Complexes with Substrates Provide New Insight into the Mechanism of Catalysis. *Biochemistry* **2001,** *40* (38), 11338-11343.

2. Vaaje-Kolstad, G.; Houston, D. R.; Rao, F. V.; Peter, M. G.; Synstad, B.; van Aalten, D. M. F.; Eijsink, V. G. H., Structure of the D142N Mutant of the Family 18 Chitinase ChiB from *Serratia marcescens* and its Complex with Allosamidin. *Biochim. Biophys. Acta* **2004,** *1696* (1), 103-111.

3. van Aalten, D. M. F.; Komander, D.; Synstad, B.; Gaseidnes, S.; Peter, M. G.; Eijsink, V. G. H., Structural Insights into the Catalytic Mechanism of a Family 18 Exo-Chitinase. *Proc. Natl. Acad. Sci. U. S. A.* **2001,** *98* (16), 8979-8984.

4. Schrödinger, L. *The PyMOL Molecular Graphics System*, 1.5.0.4; 2010.

5. Brooks, B. R.; Brooks, C. L.; Mackerell, A. D.; Nilsson, L.; Petrella, R. J.; Roux, B.; Won, Y.; Archontis, G.; Bartels, C.; Boresch, S., et al., CHARMM: The Biomolecular Simulation Program. *J. Comput. Chem.* **2009,** *30* (10), 1545-1614.

6. Anandakrishnan, R.; Aguilar, B.; Onufriev, A. V., H++3.0: Automating pK Prediction and the Preparation of Biomolecular Structures for Atomistic Molecular Modeling and Simulations. *Nucleic Acids Res.* **2012,** *40* (W1), W537-W541.

7. Myers, J.; Grothaus, G.; Narayanan, S.; Onufriev, A., A Simple Clustering Algorithm can be Accurate Enough for Use in Calculations of pKs in Macromolecules. *Proteins: Struct. Funct. Bioinf.* **2006,** *63* (4), 928-938.

8. Gordon, J. C.; Myers, J. B.; Folta, T.; Shoja, V.; Heath, L. S.; Onufriev, A., H++: A Server for Estimating pK(a)s and Adding Missing Hydrogens to Macromolecules. *Nucleic Acids Res.* **2005,** *33*, W368-W371.

9. Hoover, W. G., Canonical Dynamics: Equilibrium Phase-Space Distributions. *Phys. Rev. A* **1985,** *31* (3), 1695-1697.

10. Nosé, S., and Klein, M. L., Constant Pressure Molecular Dynamics for Molecular Systems. *Mol. Phys.* **1983,** *50* (5), 1055-1076.

11. MacKerell, A. D.; Bashford, D.; Bellott, M.; Dunbrack, R. L.; Evanseck, J. D.; Field, M. J.; Fischer, S.; Gao, J.; Guo, H.; Ha, S., et al., All-Atom Empirical Potential for Molecular Modeling and Dynamics Studies of Proteins. *J. Phys. Chem. B* **1998,** *102* (18), 3586-3616.

12. Mackerell, A. D.; Feig, M.; Brooks, C. L., Extending the Treatment of Backbone Energetics in Protein Force Fields: Limitations of Gas-Phase Quantum Mechanics in Reproducing Protein Conformational Distributions in Molecular Dynamics Simulations. *J. Comput. Chem.* **2004,** *25* (11), 1400-1415.

13. Guvench, O.; Greene, S. N.; Kamath, G.; Brady, J. W.; Venable, R. M.; Pastor, R. W.; Mackerell, A. D., Additive Empirical Force Field for Hexopyranose Monosaccharides. *J. Comput. Chem.* **2008,** *29* (15), 2543-2564.

14. Guvench, O.; Hatcher, E.; Venable, R. M.; Pastor, R. W.; MacKerell, A. D., CHARMM Additive All-Atom Force Field for Glycosidic Linkages between Hexopyranoses. *J. Chem. Theory Comput.* **2009,** *5* (9), 2353-2370.

15. Durell, S. R.; Brooks, B. R.; Bennaim, A., Solvent-Induced Forces between 2 Hydrophilic Groups. *J. Phys. Chem.* **1994,** *98* (8), 2198-2202.

16. Jorgensen, W. L.; Chandrasekhar, J.; Madura, J. D.; Impey, R. W.; Klein, M. L., Comparison of Simple Potential Functions for Simulating Liquid Water. *J. Chem. Phys.* **1983,** *79* (2), 926-935.

17. Phillips, J. C.; Braun, R.; Wang, W.; Gumbart, J.; Tajkhorshid, E.; Villa, E.; Chipot, C.; Skeel, R. D.; Kale, L.; Schulten, K., Scalable Molecular Dynamics with NAMD. *J. Comput. Chem.* **2005,** *26* (16), 1781-1802.

18. Grest, G. S.; Kremer, K., Molecular Dynamics Simulation for Polymers in the Presence of a Heat Bath. *Phys. Rev. A* **1986,** *33* (5), 3628-3631.

19. Ryckaert, J. P.; Ciccotti, G.; Berendsen, H. J. C., Numerical Integration of Cartesian Equations of Motion of a System with Constraints - Molecular Dynamics of n-Alkanes. *J. Comput. Phys.* **1977,** *23* (3), 327-341.

20. Essmann, U.; Perera, L.; Berkowitz, M. L.; Darden, T.; Lee, H.; Pedersen, L. G., A Smooth Particle Mesh Ewald Method. *J. Chem. Phys.* **1995,** *103* (19), 8577-8593.

21. Kirkwood, J. G., Statistical Mechanics of Fluid Mixtures. *J. Chem. Phys.* **1935,** *3* (5), 300-313.

22. Straatsma, T. P.; Mccammon, J. A., Multiconfiguration Thermodynamic Integration. *J. Chem. Phys.* **1991,** *95* (2), 1175-1188.

23. Frenkel, D., and Smit, B., *Understanding Molecular Simulations: From Algorithms to Applications*. 2nd ed.; Academic Press: 2002.

24. Pohorille, A.; Jarzynski, C.; Chipot, C., Good Practices in Free-Energy Calculations. *J. Phys. Chem. B* **2010,** *114* (32), 10235-10253.

25. Steinbrecher, T.; Mobley, D. L.; Case, D. A., Nonlinear Scaling Schemes for Lennard-Jones Interactions in Free Energy Calculations. *J. Chem. Phys.* **2007,** *127* (21).

Paper VI

The directionality of processive enzymes acting on recalcitrant polysaccharides is reflected in the kinetic signatures of oligomer degradation

Anne Grethe Hamre, Daniel Schaupp, Vincent G.H. Eijsink, and Morten Sørlie*

Department of Chemistry, Biotechnology and Food Science, Norwegian University of Life Sciences, PO 5003, N-1432 Ås, Norway.

* To whom correspondence should be addressed, Morten Sørlie (morten.sorlie@nmbu.no)

ABSTRACT

The enzymatic degradation of the closely related insoluble polysaccharides cellulose (β(1–4)-linked glucose) by cellulases and chitin (β(1–4)-linked *N*-acetylglucosamine) by chitinases is of large biological and economical importance. Processive enzymes with different inherent directionalities, i.e. attacking the polysaccharide chains from opposite ends, are crucial for the efficiency of this degradation process. While processive cellulases with complementary functions differ in structure and catalytic mechanism, processive chitinases belong to one single protein family with similar active site architectures. Using the unique model system of *Serratia marcescens* with two processive chitinases attacking opposite ends of the substrate, we here show that different directionalities of processivity are correlated to distinct differences in the kinetic signatures for hydrolysis of oligomeric tetra-*N*-acetyl chitotetraose.

Keywords: Processivity; kinetics; glycoside hydrolases; recalcitrant polysaccharides.

1. Introduction

Chitin, a β-1,4-linked linear polymer of N-acetyl glucosamine (GlcNAc), and cellulose, comprised of β-1,4-linked glucose, are the two most abundant biopolymers in Nature with an annual production amounting to 100 billion and one trillion tons respectively [1,2]. Thus, these polymers are an almost unlimited source of raw material for environmentally friendly and biocompatible products. The enzymatic degradation of these recalcitrant polysaccharides is therefore of great biological and economical importance.

Enzymes catalyzing the hydrolysis of *O*-glycosidic bonds between two or more carbohydrates or between a carbohydrate and a non-carbohydrate moiety are called glycoside hydrolases (GHs) (www.cazy.org; [3]). The enzymatic hydrolysis of glycosidic bonds requires a proton donor and a nucleophile/base and leads to either retention or inversion of the stereochemistry on the anomeric oxygen at C1 [4-6]. Moreover, enzymes acting on polysaccharides can have different modes of action. Endo-acting enzymes randomly cleave the polymer chains, whereas exo-acting enzymes have a preference for acting from either the reducing or the non-reducing chain end [4]. Both endo and exo mechanisms can be combined with processive action meaning that the enzyme hydrolyzes a series of glycosidic linkages along the same polymer chain producing dimeric products before dissociation. In order to bind to and guide the insoluble substrate through the active site cleft, many GHs have a path of solvent exposed aromatic residues leading from a carbohydrate binding domain to the active site cleft [7-12]. It has been suggested that these residues function as a flexible and hydrophobic sheath along which the polymer chain can slide during the processive mode of action [13,14].

There are 21 different GH families that contain one or more cellulose degrading enzymes. Most of these cellulases are classified into GH family 5, 6, 7, 8, 9, 12, 44, 45 and 48 [3,15]. Processive exo-acting cellulases are found in families 6, 7, and 48 [16]. Families

7 and 48 contain exocellulases moving from the reducing end all use the retaining mechanism. Exocellulases moving in the opposite direction are found in family 6 and use the inverting mechanism [3,17]. Some processive endo-cellulases belonging to families 5 and 9 have recently been discovered [18,19].

Chitinases occur in GH families 18 and 19, and family 18 chitinases are thought to be Nature's primary instrument for degradation of recalcitrant chitinous biomass. Interestingly, while all GH18 enzymes use the same retaining substrate-assisted catalytic mechanism [20-22], members of the GH18 family differ in terms of endo versus exo activity, processive versus non-processive action, and the directionality of processivity [7,23-26]. A specific example is the chitinolytic machinery of *Serratia marcescens* that includes three well-characterized GH18 chitinases [24]. Chitinase A (ChiA) is processive and moves towards the non-reducing end, while chitinase B (ChiB) also is processive but moves towards the reducing end (Fig. 1) [26]. Chitinase C (ChiC) is a less processive endo-acting enzyme [27,28]. The two processive chitinases have aromatic residues in their +1 and +2 subsites. In ChiB, these subsites interact with the substrate during processive hydrolysis while in ChiA the product of a processive hydrolysis, chitobiose, is displaced from these subsites (Fig. 1). In this study, we show, by kinetic analyses of site-directed mutants in subsite +1 and +2 in ChiA and ChiB, that different directionalities of processivity are correlated to distinct differences in the kinetic signatures for hydrolysis of oligomeric tetra-*N*-acetyl chitotetraose.

2. Materials and Methods

2.1 Chemicals.

Chitooligosaccharides were obtained from Megazyme (Wicklow, Ireland). All other chemicals were of analytical grade.

2.2 Protein expression and purification.

The chitinases used were from *S. marcescens* strain BJL200 [29,30], ChiA-F396A and ChiA-W275A genes were expressed in *Escherichia coli* as described previously [25]. For protein purification, periplasmic extracts were loaded on a column packed with chitin beads (New England Biolabs) equilibrated in 50 mM Tris-HCl pH 8.0. After washing the column with the same buffer, the enzymes were eluted with 20 mM acetic acid. The buffer was then changed to 100 mM Tris-HCl pH 8.0 using Amicon Ultra- Centrifugal filters (Millipore). Enzyme purity was verified by SDS-PAGE and estimated to be > 95 %. Protein concentrations were determined by using the Bradford Protein Assay from Bio-Rad.

2.3 Kinetic analysis

The kinetic constants k_{cat} and K_m of the ChiA mutants were determined essentially as described previously [31,32]. In each experiment, 8-10 different $(GlcNAc)_4$ concentrations varying from 2 – 200 µM in 20 mM sodium acetate buffer, pH 6.1 and 0.1 mg/ml BSA were pre-incubated in 10 minutes at 37 °C in an Eppendorf thermo mixer at 800 rpm before the reactions were started by adding purified enzyme to the reactions. Final enzyme concentrations were 1 nM for ChiA-W275A and 0.5 nM for ChiA-F396A. Seven samples of 75 µl were withdrawn at regular time intervals up to 20 minutes, and the enzyme was inactivated by adding 75 µl 20 mM H_2SO_4. At such mildly acidic conditions and short time

intervals before analysis, there are no significant acid catalyzed hydrolysis in line with the work of Einbu and Vårum where such rate constant has been found to be 1.5×10^{-4} s^{-1} in concentrated acid (12 M) [33]. Prior to HPLC analysis, all samples were filtrated through a 0.45 μm Duapore membrane (Millipore) to remove denaturated protein. All samples were stored at –20 °C until HPLC analysis.

2.4 High performance liquid chromatography (HPLC) of chito-oligosaccharides

Concentrations of chito-oligosaccharides were determined using HPLC with a Rezex Fast fruit H^+ column (100 mm length and 7.8 mm inner diameter) (Phenomonex). An 8 μl sample was injected on the column, and the oligosaccharides were eluted isocratically at 1 ml/min with 5 mM H_2SO_4 at 85 °C. The chito-oligosaccharides were monitored by measuring absorbance at 210 nm, and the amounts were quantified by measuring peak areas. Peak areas were transferred to concentrations using standard samples with known concentrations of chitooligosaccharides.

2.5 Data analysis

Reaction conditions were such that the rate of hydrolysis of $(GlcNAc)_4$ was essentially constant over time, with the $(GlcNAc)_4$ concentration always staying above 80 % of the starting concentration. Data points were only discarded if more than 20 % of the initial $(GlcNAc)_4$ were hydrolyzed (to ensure initial rates only). If, for any reason, more than two data points, out of the seven, had to be removed, the whole set was discarded. The slopes of plots of 0.5 times the $(GlcNAc)_2$ concentration versus time were taken as the hydrolysis rate. The rates were plotted versus substrate concentration in a Michaelis-Menten plot, and the experimental data were fitted to either the Michaelis-Menten equation (Eq. 1) or the Michaelis-Menten equation with substrate inhibition (Eq. 2) [34] by nonlinear

regression using Origin v7.0 (OriginLab Corp., Northampton, MA). Three independent measurements were performed for each mutant, and obtained parameters are presented as an average of these three measurements and their standard deviations.

$$v_0 = V_{\max} \frac{[\mathrm{S}]}{K_\mathrm{m} + [\mathrm{S}]} \quad (1)$$

$$v_0 = V_{\max} \frac{[\mathrm{S}]}{K_\mathrm{m} + \left(1 + \frac{[\mathrm{S}]}{K_\mathrm{i}}\right)[\mathrm{S}]} \quad (2)$$

3. Results and Discussion

Kinetic data have previously been obtained for ChiA-WT, ChiB-WT, ChiB-W97A (subsite +1), and ChiB-W220A (subsite +2) using $(GlcNAc)_4$ as the substrate (Table 1) [31]. In this work, we have obtained kinetic data for ChiA-W275A (subsite +1) and ChiA-F396A (subsite +2) allowing comparative analyses of effects on the same mutations in ChiB to address the connection between directionality and structural features of the +1 and +2 subsites (Fig. 1). Note that, due to the difference in directionality [23,26], the +1 and +2 subsites are *product* binding sites in ChiA, whereas they are *substrate* binding sites in ChiB. In other words, in ChiB, these subsites bind to the polymeric part of the chitin molecule that is being processively degraded.

Hydrolysis of $(GlcNAc)_4$ always yielded two $(GlcNAc)_2$ molecules showing that productive binding exclusively takes place at −2 to +2 subsites. Moreover, in the substrate concentration range studied, all enzymes with the exception of ChiA-W275A showed straightforward Michaelis-Menten kinetics, and the experimental data were therefore fitted to the standard Michaelis-Menten equation (Eq. 1; Fig. 2). ChiA-W275A, however, displayed substrate inhibition necessitating the use of a version of the Michaelis-Menten

equation (Eq. 2) that is adapted to this situation (Fig. 2) [34]. Upon removal of Trp^{275}, less binding energy is available to overcome the free energy penalty of the conformational changes that accompany substrate binding (see below), and it is conceivable that, consequently, other, non-productive binding modes become more prominent. Notably, ChiA has an extended substrate-binding cleft and surface, displaying considerable substrate affinities in many subsites [35-37]. MacDonald *et al*. observed from a crystal structure the binding of two chitotriose thiazolines in ChiA, one molecule binding in the −3 to −1 subsites (as expected), and a second molecule in the "leaving-group subsites" +1 and +2 (with the third moiety of the ligand disordered in solvent) [36]. It may therefore be that for a fraction of available ChiA-W275A two molecules of $(GlcNAc)_4$ bind of either side of the catalytic acid in the same manner as the chitotriose thiazolines causing the substrate inhibition. Other substrate inhibition binding modes cannot of course be completely ruled out. It is unlikely that we observe product inhibition since our data are obtained at initial rates (always between 0 to 20 % of the substrate being consumed), and that product inhibition by and binding of $(GlcNAc)_2$ to ChiA has been found to be 0.45 mM (K_i) and 0.4 mM (K_d). respectively [38]. Fitting of the data to Eq. 2 yielded a substrate inhibition constant, K_i, of 25 μM.

The kinetic data (Table 1) show that while the wild type enzymes have similar k_{cat} and K_m values, the kinetic effects of mutations in their quite conserved +1 and +2 subsites are different. K_m values increase for both enzymes, but the increase is much more pronounced in ChiB (200-fold and 18-fold for W97A and W220A, respectively) than in ChiA (17-fold and 2.3-fold for W275A and F396A, respectively). Furthermore, in ChiB the mutations lead to an increase in $k_{cat,}$ (from 28 s^{-1} to 126 s^{-1} and 45 s^{-1} for W97A and W220A, respectively), whereas in ChiA the mutations resulted in decreased k_{cat} values (from 33 s^{-1} to

8 s^{-1} and 13 s^{-1} for W275A and F396A, respectively). For both enzymes, the effects of mutating the +1 subsite were more prominent than the effects of mutating the +2 subsite.

A previous study on the temperature-dependency of catalytic rate for ChiA led to the conclusion that the rate-determining step is substrate association when the substrate is insoluble while it is product release when the substrate is soluble [39]. Generally, product release should be considered when analyzing the catalytic properties of polysaccharide degrading enzymes, as exemplified by product inhibition issues encountered in the industrial saccharification of cellulose [40]. Including product release as a potentially rate-limiting factor, the equations for Michaelis-Menten kinetics look as follows [41]:

$$E + S \underset{k_{-1}}{\overset{k_1}{\rightleftarrows}} E\text{-}S \xrightarrow{k_2} E\text{-}P \xrightarrow{k_3} E + P \tag{3}$$

$$K_{\mathrm{m}} = \frac{k_3}{k_2 + k_3} \cdot \frac{k_2 + k_{-1}}{k_1} \tag{4}$$

$$k_{\mathrm{cat}} = \frac{k_2 k_3}{k_2 + k_3} \tag{5}$$

Notably, Eq. 5 shows that the rate constant for product displacement, k_3, is part of k_{cat} and may even dominate the term if it is much lower than the rate of the catalysis of the chemical reaction, k_2 [41].

It is likely that mutations in the +1 and +2 subsites affect the rate constant for product formation, k_2. Productive binding of $(GlcNAc)_4$ involves that the sugar moiety in the −1 subsite undergoes a conformational change with a considerable free energy penalty [42]. Classical work of lysozyme [43] has shown that in such cases, catalysis depends on this energy penalty being compensated by binding energy resulting from interactions

between other sugar moieties and the enzyme. Weakening enzyme-substrate interactions in the +1 and +2 subsites is likely to reduce this binding energy (carbohydrate-aromate stacking interactions in GHs typically yield ~2 kcal/mol in favorable free energy change [35,44]). In addition to affecting binding energies, changes in the +1 and +2 subsites may affect the stereochemistry of the enzyme-substrate complex, with possible additional consequences on k_2. Importantly, ChiA and ChiB have very similar catalytic centers, including a fully conserved −1 subsite. Structural data for their Michaelis complexes [22,45] show almost identical enzyme-substrate interactions in subsites near the catalytic center, including similar stacking interactions of the Trp (Trp97/Trp275) in subsite +1 and the aromate (Trp220/Phe396) in subsite 2 (Fig. 1). Thus, it seems reasonable to assume that the effects of the mutations on k_2 are similar for the two enzymes.

Removal of aromatic side chains in the +1 and +2 subsites is likely to reduce the substrate association rate, k_1, increase the substrate dissociation rate, k_{-1}, and increase the rate of product release, k_3. All these possible effects lead to an increase in K_m, as is indeed observed. The key difference between the two enzymes lies in the effect of the mutations on k_{cat}, which, considering Eq. 5 and the assumption that changes in k_2 are similar for both enzymes, must imply a difference in the effect on k_3 and/or in the overall importance of k_3. Notably, the only alternative explanation would imply that the mutations have a positive effect on k_2 in ChiB, which is highly unlikely, for reasons explained above. In ChiA, the mutations reduce k_{cat}, which must be due to a negative effect on k_2 that, apparently, is not compensated by an increase in k_3. In ChiB, however, the presumed similar effect on k_2 is more than compensated for by a positive effect of k_3, leading to an overall increase in k_{cat} (Table 1). Since the mutational effects in terms of lost binding energy should be similar in both enzymes, the only logic explanation for these observations is that k_3 is a rate-limiting factor in ChiB only. This explanation is in accordance with the observation that K_m effects

are larger in ChiB than in ChiA, since Eq. 4 shows that the effect of changes in k_3 on K_m becomes larger as the relative magnitude of k_3 increases.

Previous studies have shown that surface exposed tryptophans close to the catalytic center are important for the degree of processivity in chitinases [7,25]. In ChiB, Trp^{97} is the most important residue for processivity [7] while Trp^{167}, in the – 3 subsite, has the same importance in ChiA [25]. Mutation of the Trp^{275} in ChiA, the equivalent of Trp^{97} in ChiB, hardly affects processivity. These existing data show that tryptophans interacting with the polymeric part of the substrate, i.e. in the – subsites in ChiA and the + subsites in ChiB determine the degree of processivity. The present comparative analysis shows that the tailoring of the enzymes to opposite directionalities is reflected in the kinetics of $(GlcNAc)_4$ degradation. The + subsites in ChiA are likely to be optimized for rapid release of dimeric products during processive action, which may explain why expected beneficial effects of the W275A and F396A mutations on k_3 are not noticeable in the catalytic performance (k_{cat}) on $(GlcNAc)_4$. On the other hand the + subsites in ChiB are optimized to stay attached to the (normally polymeric) substrate in between catalytic steps, hence k_3 is rate-limiting and mutational effects on k_3 are noticeable in the overall catalytic performance on $(GlcNAc)_4$.

Inspection of the structures of ChiA and ChiB in complex with substrate shows that the +1 and +2 sites in ChiA are more open than in ChiB (Fig. 3) [22,45]. This is in line with our conclusion that product release from the +1 and +2 subsites is more restricted and rate-limiting in ChiB compared to ChiA.

In conclusion, the present study provides further insight into how chitinases of the same glycoside hydrolase family are fine-tuned to the directionality of processivity. We show that relatively simple kinetic studies with oligomeric substrates reveal differences between such enzymes that are in accordance with the directionality of their processivity. In particular, we show that the +1 and +2 subsites in ChiB are tailored to remain attached to

the product after catalysis, as one might expect for a processive enzyme moving towards the polymers reducing end.

Acknowledgements

This work was supported by Grant 209335/F20 from the Norwegian Research Council.

Reference List

[1] Kim, J., Yun, S. and Ounaies, Z. (2006). Discovery of cellulose as a smart material. Macromolecules 39, 5583-5583.

[2] Tharanathan, R.N. and Kittur, F.S. (2003). Chitin - The undisputed biomolecule of great potential. Crit. Rev. Food Sci. Nutr. 43, 61-87.

[3] Lombard, V., Ramulu, H.G., Drula, E., Coutinho, P.M. and Henrissat, B. (2014). The carbohydrate-active enzymes database (CAZy) in 2013. Nucleic Acids Res. 42, D490-D495.

[4] Davies, G. and Henrissat, B. (1995). Structures and mechanisms of glycosyl hydrolases. Structure 3, 853-9.

[5] Koshland, D.E. (1953). Stereochemistry and the Mechanism of Enzymatic Reactions. Biological Reviews of the Cambridge Philosophical Society 28, 416-436.

[6] Sinnott, M.L. (1990). Catalytic Mechanisms of Enzymatic Glycosyl Transfer. Chemical Reviews 90, 1171-1202.

[7] Horn, S.J. et al. (2006). Costs and benefits of processivity in enzymatic degradation of recalcitrant polysaccharides. Proc. Natl. Acad. Sci U.S.A 103, 18089-18094.

[8] Katouno, F., Taguchi, M., Sakurai, K., Uchiyama, T., Nikaidou, N., Nonaka, T., Sugiyama, J. and Watanabe, T. (2004). Importance of exposed aromatic residues in chitinase B from Serratia marcescens 2170 for crystalline chitin hydrolysis. J Biochem. 136, 163-168.

[9] Perrakis, A., Tews, I., Dauter, Z., Oppenheim, A.B., Chet, I., Wilson, K.S. and Vorgias, C.E. (1994). Crystal structure of a bacterial chitinase at 2.3 A resolution. Structure. 2, 1169-1180.

[10] van Aalten, D.M.F., Synstad, B., Brurberg, M.B., Hough, E., Riise, B.W., Eijsink, V.G.H. and Wierenga, R.K. (2000). Structure of a two-domain chitotriosidase from Serratia marcescens at 1.9-angstrom resolution. Proc.Natl.Acad.Sci.U.S.A 97, 5842-5847.

[11] Watanabe, T. et al. (2003). Aromatic residues within the substrate-binding cleft of Bacillus circulans chitinase A1 are essential for hydrolysis of crystalline chitin. Biochem. J. 376, 237-244.

[12] Rouvinen, J., Bergfors, T., Teeri, T., Knowles, J.K. and Jones, T.A. (1990). Three-dimensional structure of cellobiohydrolase II from Trichoderma reesei. Science 249, 380-6.

[13] Divne, C., Stahlberg, J., Teeri, T.T. and Jones, T.A. (1998). High-resolution crystal structures reveal how a cellulose chain is bound in the 50 angstrom long tunnel of

cellobiohydrolase I from Trichoderma reesei. Journal of Molecular Biology 275, 309-325.
[14] Varrot, A., Frandsen, T.P., von Ossowski, I., Boyer, V., Cottaz, S., Driguez, H., Schulein, M. and Davies, G.J. (2003). Structural Basis for Ligand Binding and Processivity in Cellobiohydrolase Cel6A from Humicola insolens. Structure 11, 855-864.
[15] Lee, J.W. (2013) Advanced Biofuels and Bioproducts, Springer New York. New York, NY.
[16] Wilson, D.B. and Kostylev, M. (2012). Cellulase processivity. Methods Mol Biol 908, 93-9.
[17] Barr, B.K., Hsieh, Y.L., Ganem, B. and Wilson, D.B. (1996). Identification of two functionally different classes of exocellulases. Biochemistry 35, 586-592.
[18] Sakon, J., Irwin, D., Wilson, D.B. and Karplus, P.A. (1997). Structure and mechanism of endo/exocellulase E4 from *Thermomonospora fusca*. Nat. Struct. Mol. Biol. 4, 810-818.
[19] Watson, B.J., Zhang, H.T., Longmire, A.G., Moon, Y.H. and Hutcheson, S.W. (2009). Processive endoglucanases mediate degradation of cellulose by *Saccharophagus degradans*. J. Bacteriol. 191, 5697-5705.
[20] Terwisscha van Scheltinga, A.C., Armand, S., Kalk, K.H., Isogai, A., Henrissat, B. and Dijkstra, B.W. (1995). Stereochemistry of chitin hydrolysis by a plant chitinase/lysozyme and X-ray structure of a complex with allosamidin: evidence for substrate assisted catalysis. Biochemistry 34, 15619-15623.
[21] Tews, I., Terwisscha van Scheltinga, A.C., Perrakis, A., Wilson, K.S. and Dijkstra, B.W. (1997). Substrate-assisted catalysis unifies two families of chitinolytic enzymes. J. Am. Chem. Soc. 119, 7954-7959.
[22] van Aalten, D.M.F., Komander, D., Synstad, B., Gåseidnes, S., Peter, M.G. and Eijsink, V.G.H. (2001). Structural insights into the catalytic mechanism of a family 18 exo-chitinase. Proc. Natl. Acad. Sci. U.S.A 98, 8979-8984.
[23] Hult, E.L., Katouno, F., Uchiyama, T., Watanabe, T. and Sugiyama, J. (2005). Molecular directionality in crystalline beta-chitin: hydrolysis by chitinases A and B from Serratia marcescens 2170. Biochem. J. 388, 851-856.
[24] Vaaje-Kolstad, G., Horn, S.J., Sørlie, M. and Eijsink, V.G.H. (2013). The chitinolytic machinery of Serratia marcescens – a model system for enzymatic degradation of recalcitrant polysaccharides. FEBS J. 280, 3028-3049.
[25] Zakariassen, H., Aam, B.B., Horn, S.J., Vårum, K.M., Sørlie, M. and Eijsink, V.G.H. (2009). Aromatic residues in the catalytic center of chitinase A from *Serratia marcescens* affect processivity, enzyme activity, and biomass converting efficiency. J. Biol. Chem. 284, 10610-10617.
[26] Igarashi, K. et al. (2014). Two-way traffic of glycoside hydrolase family 18 processive chitinases on crystalline chitin. Nat. Commun. 5
[27] Hamre, A.G., Lorentzen, S.B., Väljamäe, P. and Sørlie, M. (2014). Enzyme processivity changes with the extent of recalcitrant polysaccharide degradation. FEBS Lett. 588, 4620-4624.
[28] Horn, S.J., Sørbotten, A., Synstad, B., Sikorski, P., Sørlie, M., Vårum, K.M. and Eijsink, V.G.H. (2006). Endo/exo mechanism and processivity of family 18 chitinases produced by Serratia marcescens. FEBS J. 273, 491-503.
[29] Brurberg, M.B., Eijsink, V.G.H., Haandrikman, A.J., Venema, G. and Nes, I.F. (1995). Chitinase B from Serratia marcescens BJL200 is exported to the periplasm without processing. Microbiology 141, 123-131.

[30] Brurberg, M.B., Eijsink, V.G.H. and Nes, I.F. (1994). Characterization of a chitinase gene (chiA) from Serratia marcescens BJL200 and one-step purification of the gene product. FEMS Microbiol. Lett. 124, 399-404.
[31] Krokeide, I.M., Synstad, B., Gåseidnes, S., Horn, S.J., Eijsink, V.G.H. and Sørlie, M. (2007). Natural substrate assay for chitinases using high-performance liquid chromatography: A comparison with existing assays. Anal. Biochem. 363, 128-134.
[32] Zakariassen, H., Hansen, M.C., Jøranli, M., Eijsink, V.G.H. and Sørlie, M. (2011). Mutational effects on transglycosylating activity of family 18 chitinases and construction of a hypertransglycosylating mutant. Biochemistry 50, 5693-5703.
[33] Einbu, A. and Vårum, K.M. (2008). Characterization of Chitin and Its Hydrolysis to GlcNAc and GlcN. Biomacromol. 9, 1870-1875.
[34] Papežová, K., Němec, T., Chaloupková, R. and Glatz, Z. (2007). Study of substrate inhibition by electrophoretically mediated microanalysis in partially filled capillary. J. Chromatogr. A 1150, 327-331.
[35] Baban, J., Fjeld, S., Sakuda, S., Eijsink, V.G.H. and Sørlie, M. (2010). The Roles of Three Serratia marcescens Chitinases in Chitin Conversion Are Reflected in Different Thermodynamic Signatures of Allosamidin Binding. J. Phys. Chem. B 114, 6144-6149.
[36] Macdonald, J.M., Tarling, C.A., Taylor, E.J., Dennis, R.J., Myers, D.S., Knapp, S., Davies, G.J. and Withers, S.G. (2010). Chitinase inhibition by chitobiose and chitotriose thiazolines. Angew. Chem. Int. Ed. Engl. 49, 2599-2602.
[37] Norberg, A.L., Dybvik, A.I., Zakariassen, H., Mormann, M., Peter-Katalinic´, J., Eijsink, V.G.H. and Sørlie, M. (2011). Substrate positioning in chitinase A, a processive chito-biohydrolase from *Serratia marcescens*. FEBS Lett. 585, 2339-2344.
[38] Kuusk, S., Sørlie, M. and Väljamäe, P. (2015). The predominant molecular state of bound enzyme determines the strength and type of product inhibition in the hydrolysis of recalcitrant polysaccharides by processive enzymes. J. Biol. Chem.
[39] Zakariassen, H., Eijsink, V.G.H. and Sørlie, M. (2010). Signatures of activation parameters reveal substrate-dependent rate determining steps in polysaccharide turnover by a family 18 chitinase. Carbohyd.Polym. 81, 14-20.
[40] Teugjas, H. and Valjamae, P. (2013). Product inhibition of cellulases studied with C-14-labeled cellulose substrates. Biotechnol. Biofuels 6, 14.
[41] Fersht, A. (1999) Structure and mechanism in protein science: a guide to enzyme catalysis and protein folding, Freeman. New York.
[42] Biarnes, X., Ardevol, A., Planas, A., Rovira, C., Laio, A. and Parrinello, M. (2007). The Conformational Free Energy Landscape of β-D-Glucopyranose. Implications for Substrate Preactivation in β-Glucoside Hydrolases. J. Am. Chem. Soc. 129, 10686-10693.
[43] Honda, Y. and Fukamizo, T. (1998). Substrate binding subsites of chitinase from barley seeds and lysozyme from goose egg white. Biochim.Biophys.Acta 1388, 53-65.
[44] Zolotnitsky, G., Cogan, U., Adir, N., Solomon, V., Shoham, G. and Shoham, Y. (2004). Mapping glycoside hydrolase substrate subsites by isothermal titration calorimetry. Proc. Natl. Acad. Sci. U.S.A 101, 11275-11280.
[45] Papanikolau, Y., Prag, G., Tavlas, G., Vorgias, C.E., Oppenheim, A.B. and Petratos, K. (2001). High resolution structural analyses of mutant chitinase A complexes with substrates provide new insight into the mechanism of catalysis. Biochemistry 40, 11338-11343.

Table 1. Kinetic parameters of wild-type and mutant ChiA and ChiB for the hydrolysis of $(GlcNAc)_4$ at pH 6.1 and 37 °C.

	k_{cat} (s^{-1})[a]	K_m (μM)[a]	k_{cat}/K_m ($s^{-1}\mu M^{-1}$)
ChiA-WT[b]	33 ±1	9 ± 1	4
ChiA-W275A[c]	8 ± 1	157 ± 8	0.1
ChiA-F396A	13 ± 2	21 ± 8	0.6
ChiB-WT[b]	28 ± 2	4 ± 2	7
ChiB-W97A[b]	126 ± 4	807 ± 40	0.2
ChiB-W220A[b]	45 ± 2	71± 3	0.6

[a] Average of three measurements. [b] Data from Krokeide *et al*. [31]. [c] The kinetic parameters were calculated with respect to the Michaelis-Menten equation for substrate inhibition; see text for details.

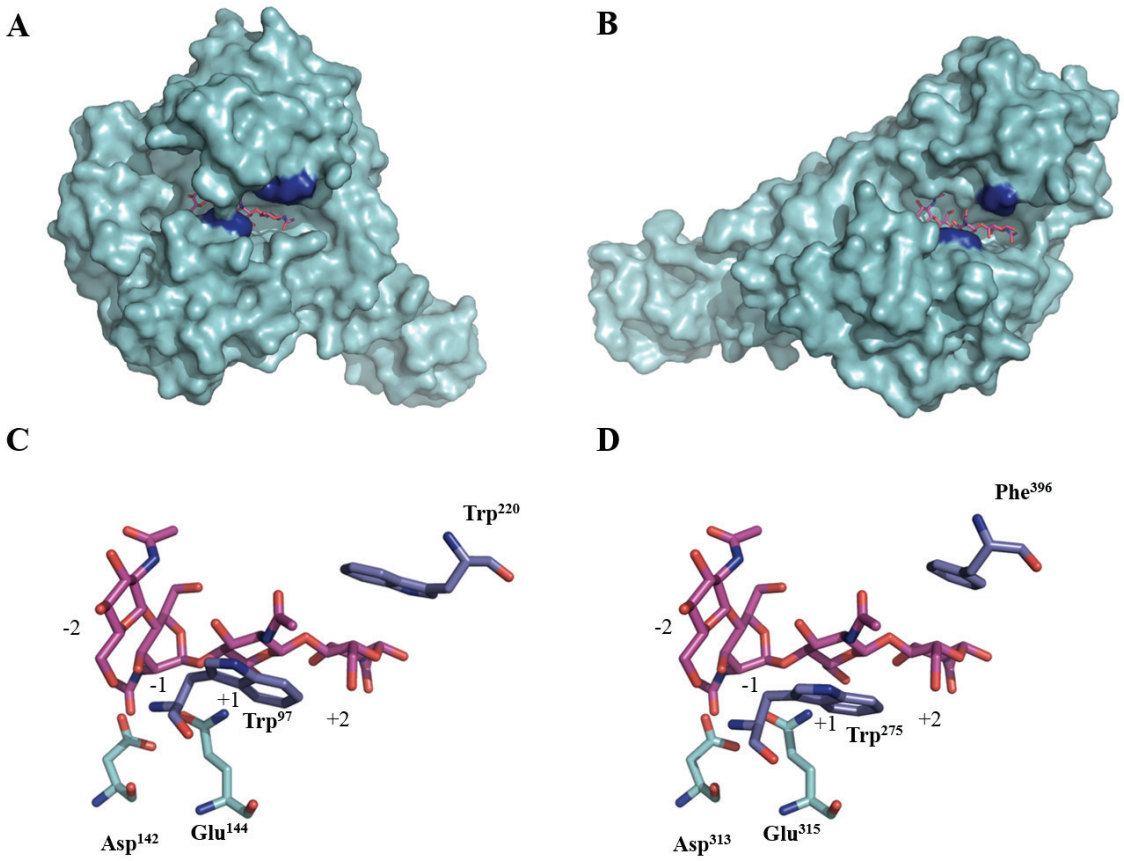

Fig. 1. Enzyme-substrate interactions for ChiA and ChiB. Panel A and C show the structure of exo-processive ChiB (PDB ID code 1e6n, [22]) that degrades chitin from the non-reducing end. Panels B and D show the structure of exo-processive ChiA (PDB ID code 1ehn, [45]) that degrades chitin from the reducing end. Panels A and C show surface representations of the complete protein; the surface-exposed aromatic amino acids in subsites +1 and +2 are highlighted in blue, whereas crystallographically observed substrate molecules are shown in magenta. Bothe chitinases contain a carbohydrate-binding module, a CBM5/12 pointing to the right in ChiB and and FnIII domain pointing to the left in ChiA (for more details, see Vaaje-Kolstad et al., 2013 [24]) (C) Close up of the active site of ChiB. Asp^{142} and Glu^{144} are part of the diagnostic DXDXE motif containing the catalytic acid/base (Glu144). (D) Close up of the active site of ChiA.

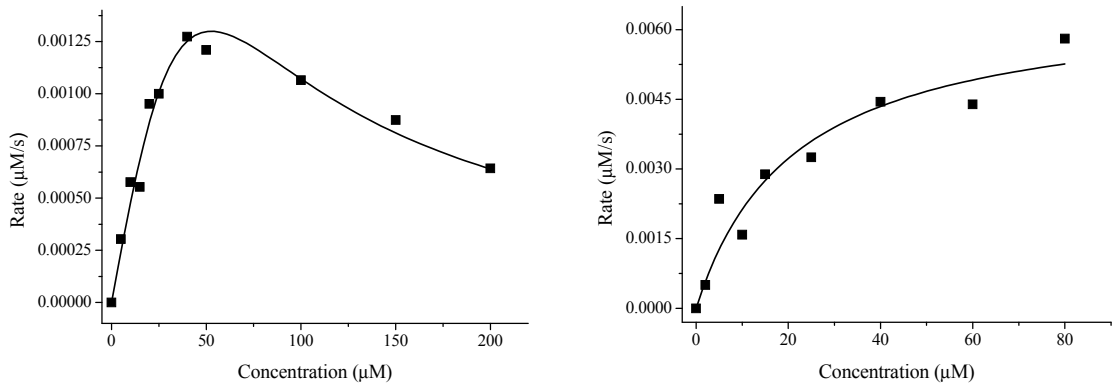

Fig. 2. Examples of Michaelis-Menten plots for degradation of $(GlcNAc)_4$ by ChiA-W275A (left) and ChiA-F396A (right). The left plot shows substrate inhibition; see text for details.

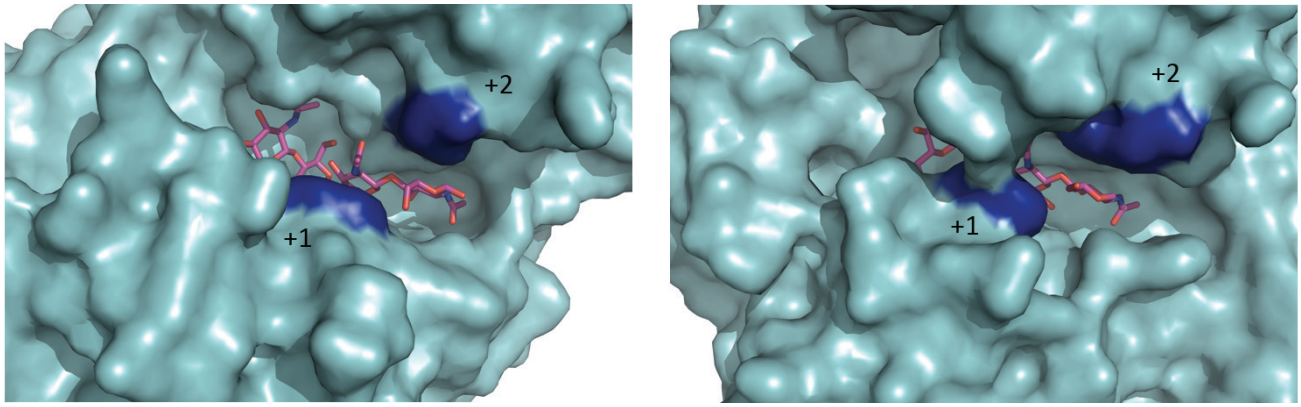

Fig. 3. A close-up of a surface presentation of the +1 and +2 subsites of ChiA (left; PDB ID code 1ehn, [45]) with Trp^{275} and Phe^{396} colored blue and ChiB (right; PDB ID code 1e6n, [22]) with Trp^{97} and Trp^{220} colored blue, respectively. The structures show that ChiA has a more open active site cleft compared to ChiB; in ChiB, part of the cleft has a tunnel-like shape.